

# **Novel Microwave Devices Based on Multi-Port Filtering Networks**

By

**Eugene Amobichukwu Ogbodo**

*Submitted in Partial Fulfilment of the  
Requirements for the Degree of*

**Doctor of Philosophy**



**Engineering Science  
Faculty of Engineering and Science**

20 December 2017

# Declaration

I certify that the work contained in this thesis, or any part of it, has not been accepted in substance for any previous degree awarded to me, and is not concurrently being submitted for any degree other than that of Doctor of Philosophy being studied at the University of Greenwich. I also declare that this work is the result of my own investigations, except where otherwise identified by references and that the contents are not the outcome of any form of research misconduct.

**SIGNED:**

\_\_\_\_\_  
Student Date

\_\_\_\_\_  
First Supervisor Date

\_\_\_\_\_  
Second Supervisor Date

\_\_\_\_\_  
Third Supervisor Date

# Abstract

This thesis is based on the novel device concept of Multi-Port Filtering Networks (MPFNs). This is a concept derived from conventional two-port filters to link two or more filters in communication systems. It is interesting to the microwave filtering component designers as it reduces the footprint, cost and structural size. One potential application of this concept is diplexers/multiplexers. The conventional structure of joining two or more filters using the transmission based line junctions or circulators is eliminated. It is replaced by a common resonant junction which also contributes to the resonant poles of filtering network.

In this thesis, the methodology for MPFNs is developed and a number of microwave filtering components are designed and results presented. It starts with a comparative study between the conventional diplexer and a resonant junction diplexer in terms of performance, size, and power handling capabilities. It was found that the resonant junction diplexer is more compact with slightly higher power handling capability.

Some number of diplexers were presented using the MPFNs technique. Various dual-mode resonators such as the patch, the split-ring-resonator and the asynchronously-coupled-junction were implemented as the junction of the diplexers. All demonstrated the signal distribution and combining functions. The demonstrated techniques resulted in a more compact diplexer circuitry without sacrificing the selectivity of the channel filters.

As the building block of a diplexer or a multiplexer, this thesis also proposed and demonstrated several single-band or dual-band filters. In particular, the mixed use of single and dual-mode resonators has shown the capability and flexibility to improve the frequency selectivity by controlling the transmission zeros. Dual mode resonators were also used to split and combine the signals in dual-band designs as in the diplexers.

This thesis has started exploring and examining the new idea of multi-input and multi-output filters in the framework of MPFNs. Several four-port filtering networks were investigated. And finally, as an extension and slightly diversion of the work, the integration of a duplexer and an antenna based on an all-resonator structure was studied using the co-design approach essentially based on filter designs.

# Acknowledgements

My deepest acknowledgement goes to my first supervisor Dr Yi Wang, for his support, patience, and guidance throughout my research and in difficult times. His understanding of this topic and his resilience towards life and academic in general made my journey with him a memorable one.

To my second and third supervisors, Dr Peter Callaghan and Prof Peter Kyberd, for their guidance and support towards my research and development.

My sincerest gratitude goes to Dr Yun Wu for his advice, support, and numerous inspiring discussions over the projects.

Thanks to the staff of the school of Science and Engineering, University of Greenwich, for their immediate assistance whenever the need arises.

My wonderful parents Chief Alexander Ogbodo and Lolo Caroline Ogbodo, my siblings; Nathaniel, Nelly, Sandra, Alex and Emmanuel Ogbodo for their support, encouragement, and advice throughout my studies.

And finally, to my family, Patience, Alvin and Lexie Ogbodo for their inspiration, encouragement and immense understanding of the difficulties that go with research work.



# Table of Contents

<b>DECLARATION</b> .....	<b>I</b>
<b>ABSTRACT</b> .....	<b>II</b>
<b>ACKNOWLEDGEMENTS</b> .....	<b>III</b>
<b>TABLE OF CONTENTS</b> .....	<b>IV</b>
<b>LIST OF ACRONYMS</b> .....	<b>VII</b>
<b>LIST OF FIGURES</b> .....	<b>VIII</b>
<b>CHAPTER 1: INTRODUCTION</b> .....	<b>1</b>
1.1 MULTI-PORT FILTERING NETWORKS (MPFN) .....	1
1.2 DIPLEXERS/MULTIPLEXERS AND THEIR APPLICATIONS .....	3
1.3 THESIS MOTIVATION .....	3
1.4 MAIN CONTRIBUTIONS TO KNOWLEDGE .....	4
1.5 THESIS OVERVIEW .....	5
<b>CHAPTER 2: LITERATURE REVIEW</b> .....	<b>8</b>
2.1. BACKGROUND OVERVIEW.....	8
2.2 CONVENTIONAL DIPLEXERS AND MULTIPLEXERS .....	8
2.2.1 T-Junction and Y-Junction.....	9
2.2.2 Manifolds and Circulators .....	10
2.2.3 Miniaturisation Technique .....	11
2.3 ALL-RESONATOR BASED DIPLEXERS AND MULTIPLEXERS.....	11
2.3.1 Different Types of Junction Resonators .....	12
2.3.2 Comparison of Junction Resonator Diplexers with Conventional Diplexers .....	13
2.4 DUAL-MODE RESONATORS.....	14
2.4.1 Patch Resonators.....	14
2.4.2 Split-Ring Resonator (SRR) .....	17
2.4.3 Stepped-Impedance Resonator (SIR).....	18
2.4.4 Stub-Loaded Resonator (SLR).....	21
2.5 DUAL-MODE RESONATORS IN DIPLEXERS AND FILTERS.....	22

2.6 SUMMARY .....	28
<b>CHAPTER 3: THEORY OF TWO-PORT FILTER SYNTHESIS .....</b>	<b>29</b>
3.1 MICROSTRIP LINE.....	29
3.2 COUPLING MATRIX .....	30
3.3 BANDPASS FILTER DESIGN OVERVIEW .....	33
3.4 DUAL-BAND FILTER DESIGN THEORY .....	35
3.5 A MICROSTRIP IMPLEMENTATION EXAMPLE.....	40
SUMMARY.....	42
<b>CHAPTER 4: TRANSMISSION LINE JUNCTION VERSUS RESONATOR</b>	
<b>JUNCTION IN DIPLEXERS – A COMPARATIVE STUDY.....</b>	<b>44</b>
4.1 DESIGN OF THE CONVENTIONAL DIPLEXER.....	44
4.2 DESIGN OF THE RESONANT JUNCTION DIPLEXER .....	45
4.3 COMPARISON .....	47
4.3.1 Size.....	47
4.3.2 Rejection and Isolation .....	48
4.3.3 Current Density Distribution and Implication on Power Handling .....	50
4.4 SUMMARY .....	52
<b>CHAPTER 5: DIPLEXERS AND FILTERS USING PATCH RESONATORS.....</b>	<b>53</b>
5.1 PROPERTIES OF A PATCH RESONATOR.....	53
5.2 BANDPASS FILTER WITH TRANSMISSION ZERO (DESIGN-1) .....	58
5.3 DIPLEXER WITH A PATCH RESONATOR AS ITS JUNCTION (DESIGN-2).....	64
5.4 DUAL-BAND BPF (DESIGN-3) .....	69
5.5 SUMMARY .....	76
<b>CHAPTER 6: DIPLEXERS WITH A SPLIT-RING RESONANT JUNCTION .....</b>	<b>77</b>
6.1 SPLIT-RING RESONATOR (SRR) AS THE JUNCTION RESONATOR .....	78
6.2 BANDPASS FILTERS USING OPEN-LOOP AND SRR .....	79
6.3 DIPLEXER IMPLEMENTATION USING SRR AS THE COMMON RESONANT JUNCTION .....	82
6.3.1 Design .....	83
6.3.2 Coupling.....	84
6.3.3 Simulation Results .....	86

6.3.4 Fabrication and Measurements .....	88
6.4 COMPACT DUAL-BAND BANDPASS FILTER USING SRR.....	88
6.5 SUMMARY .....	91
<b>CHAPTER 7: INTEGRATED FILTERING ANTENNA.....</b>	<b>92</b>
7.1 INTRODUCTION.....	92
7.2 DUPLEXER-ANTENNA .....	94
7.2.1 Design Specifications .....	94
7.2.2 Filtering Antenna .....	95
7.2.3 Duplexing Antenna Design.....	98
7.3 DUAL-BAND BANDPASS FILTERING ANTENNA .....	100
7.4 SUMMARY .....	105
<b>CHAPTER 8: FOUR-PORT FILTER NETWORK.....</b>	<b>107</b>
8.1 MULTI-INPUT MULTI-OUTPUT (MIMO) FILTER AND DIPLEXER.....	107
8.2 MASTHEAD COMBINER (MHC) .....	112
8.3 SUMMARY .....	118
<b>CHAPTER 9: CONCLUSIONS AND FUTURE WORK .....</b>	<b>119</b>
9.1 CONCLUSIONS .....	119
9.2 FUTURE WORK.....	124
REFERENCES .....	125
PUBLICATIONS .....	138

# List of Acronyms

ASSR	Asymmetrical Separated Spirals resonator
BW	Bandwidth
BPF	Bandpass Filter
CHR	Compact Hybrid Resonators
DSPSL	Double-Sided Parallel-Strip Line
DS-UWB	Direct Sequence Ultra-Wideband
DBR	Dual Behaviour Resonator
EDA tools	Electronic design automation tool
EM	Electromagnetic
FBW	Fractional Bandwidth
HTSC	High-temperature Superconductor
MHC	Mast Head Combiners
MMICs	Monolithic Microwave Integrated Circuits
MICs	Microwaves Integrated Circuits
MIMO	Multi-input Multi-output
MPFNs	Multi-port filtering networks
NBCSSR	Non-Bi-anisotropic Complementary Split-Ring Resonator
RF	Radio Frequency
RX	Receive
RL	Return Loss
SCMRC	Spiral Compact Microstrip Resonant Cell
SIR	Stepped Impedance Resonators
SLR	Stub-Loaded Resonator
TX	Transmit
TEM mode	Transverse electro-magnetic mode

# List of Figures

Figure 1.1 Concept of a MPFN.....	1
Figure 1.2 Example topology: (a) a three-port diplexer; (b) a five-port multiplexer .....	2
Figure 1.3 Block diagram of a diplexer .....	3
Figure 2.1 Current distribution of the orthogonal mode square patch resonator. (a) 2.45 GHz; (b) 2.60 GHz.....	16
Figure 2.2 Asynchronous coupled SRR: (a) Current distribution; (b) response with an inset of the physical and coupling topology .....	18
Figure 2.3 Half-wavelength SIR: (a) $K = Z_2 / Z_1 < 1$ ; (b) $K = Z_2 / Z_1 > 1$ .....	19
Figure 2.4 An SIR resonator; (a) Current distribution: (b) Frequency response .....	20
Figure 2.5 Dual-mode SLR resonator: (a) Current distribution (b) S-parameter response .....	22
Figure 3.1 Microstrip line .....	30
Figure 3.2 Circuit models for coupled resonator filters: (a) Magnetic coupling; (b) Electric coupling .....	31
Figure 3.3 Normalised third-order low pass prototype filter .....	33
Figure 3.4 Lowpass prototype to bandpass transformation .....	34
Figure 3.5 Third-order single mode Band Pass Filter.....	35
Figure 3.6 Normalised third-order low pass prototype filter .....	36
Figure 3.7 Normalised low pass filter with only shunt reactive components.....	36
Figure 3.8 Low-pass to dual-band bandpass transformation .....	36
Figure 3.9 Dual-band BPF with shunt LC resonators.....	37
Figure 3.10 Dual-band BPF coupled resonator pair circuit model transformation.....	38
Figure 3.11 (a) Dual-band circuit model; (b) Dual-band coupling path .....	39
Figure 3.12 Dual-band BPF responses from the circuit models and EM simulations.....	39
Figure 3.13 (a) Coupling of $M_{1,1}$ against spacing (S); Coupling of $M_{1,2}$ against spacing (S1).....	40
Figure 3.14 Resonator arrangement for extracting $Q_{ex}$ .....	41
Figure 3.15. Dual-band microstrip filter layout. $L = 17.2$ mm, $L_1 = 6.8$ mm, $W = 1.126$ mm, $X = 17$ mm, $S = 2.4$ mm, $S_1 = 0.35$ mm, $Y = 12$ mm.....	41
Figure 3.16. Simulated and measured responses. ....	42
Figure 3.17. Fabricated microstrip dual-band filter. ....	42

Figure 4.1 Coupling topology of a diplexer with a transmission-line T-junction .....	44
Figure 4.2 Conventional T-junction diplexer. $F = 10\text{mm}$ , $F1 = 13.7\text{mm}$ , $X1 = 13.8\text{mm}$ , $X2 = 17.6\text{mm}$ , $T = 0.3\text{mm}$ , $T1 = 0.4\text{mm}$ , $W = 1.2\text{mm}$ , $W1 = 0.6\text{mm}$ , $W2 =$ $0.6\text{mm}$ , $L = 11.5\text{mm}$ , $L1 = 9.95\text{mm}$ , $LL = 11\text{mm}$ , $LL1 = 6.59\text{mm}$ , $d_{1,2} =$ $1.77\text{mm}$ , $d_{2,3} = 1.77\text{mm}$ , $d_{4,5} = 1.75\text{mm}$ , $d_{5,6} = 1.75\text{mm}$ , $TH = 25.2\text{mm}$ , $TL$ $= 124.28\text{mm}$ . .....	45
Figure 4.3 Coupling topology of a diplexer with an asynchronously coupled resonant junction (ACJ).....	45
Figure 4.4 Resonant frequencies of the ACJ with an inset of topology used .....	46
Figure 4.5 (a) Simulated typical response of the configuration used to extract the $Q_{\text{ext}}$ ; (b) Current distribution.....	47
Figure 4.6 Resonant junction diplexer. $F = 10\text{mm}$ , $T = 0.4\text{mm}$ , $T1 = 0.2\text{mm}$ , $W = 1.2\text{mm}$ , $W1 = 0.4\text{mm}$ , $W2 = 0.6\text{mm}$ , $W3 = 0.6\text{mm}$ , $L = 9.6\text{mm}$ , $L1 = 11.5\text{mm}$ , $LL =$ $6.6\text{mm}$ , $LL1 = 11\text{mm}$ , $d_{1,2} = 1.7\text{mm}$ , $d_{1,4} = 0.2\text{mm}$ , $d_{2,3} = 1.7\text{mm}$ , $d_{4,5} =$ $1.65\text{mm}$ , $d_{5,6} = 1.7\text{mm}$ , $TH = 65\text{mm}$ , $TL = 61.5\text{mm}$ .....	48
Figure 4.7 Simulated response of the conventional diplexer and resonant junction diplexer .....	49
Figure 4.8 Simulated isolation response of the conventional diplexer and resonant junction diplexer .....	49
Figure 4.9 Fabricated designs: (a) Conventional T-junction diplexer; (b) Coupled resonant Junction diplexer .....	50
Figure 4.10 Measured frequency responses of the two diplexers.....	50
Figure 4.11 Simulated current distribution of the two diplexers, plotted using the same current density scale.....	51
Figure 4.12 Simulated current density distribution across the microstrip lines at the circled areas of Fig. 4.11: (a) 1.8 GHz; (b) 2.1 GHz. The range of the X-axis is proportional to the width of the microstrip line. ....	52
Figure 5.1 Simulation response with an inset of the layout used.....	54
Figure 5.2 Simulated current distribution .....	55
Figure 5.3 Simulation response of the dual-mode patch resonator.....	56
Figure 5.4 Simulated current distribution at both modes.....	56
Figure 5.5 Coupling coefficient between the two modes of a perturbed patch as a function of X .....	57
Figure 5.6 Simulation layout used for $Q_{\text{ex}}$ extraction .....	58
Figure 5.7 Typical simulated responses of the layout shown in Fig. 5.6.....	58

Figure 5.8. Circuit layouts of (a) the hairpin filter and (b) the hairpin-patch filter; $F = 10$ , $F1 = 8.73$ , $L = 5.07$ , $L1 = 4.96$ , $S = 1.24$ , $S1 = 0.26$ , $S0 = 0.68$ , $X = 5$ , $H = 9.73$ , $D_X = D_Y = 17.59$ ; unit: mm. (c) The simulated responses of the mixed hairpin-patch filter in comparison with a conventional hairpin filter of the same order.....	60
Figure 5.9 Simulated current distribution of the hairpin-patch filter at 2.6 GHz. ....	60
Figure 5.10 Parameter studies. (a) Layout; (b) The change of $S_{21}$ with $X$ ; (c) The change of $S_{21}$ with $X_c$ . ....	62
Figure 5.11 Photo of the fabricated filter with its box lid removed.....	63
Figure 5.12 Simulated and measured responses of the hairpin-patch filter.....	63
Figure 5.13 Coupling topology of duplexers: (a) Conventional technique; (b) Proposed technique.....	64
Figure 5.14(a) Coupling coefficient $M_{1a,2}$ against $ZS$ ; (b) Coupling coefficient $M_{1b,4}$ against $S$ ; (c) Simulated resonance curves from the assembled resonator 1, 2 and 4. The inset shows the layout used in the simulation.....	66
Figure 5.15 Design curve used to extract $Q_{ex1a}$ and $Q_{ex1b}$ .....	67
Figure 5.16 (a) Design layout (unit: mm); $ZL = 5.4$ , $ZL1 = 3.9$ , $ZS = 1$ , $ZS1 = 1.4$ , $ZS11 = 0.2$ , $L = 5$ , $L1 = 3.4$ , $S = 0.84$ , $S1 = 1.26$ , $S11 = 0.2$ , $D = 10.9$ , $X = 4.6$ , $F = 6$ , $F1 = 5$ , $F2 = 10$ , $W = 1.1$ , $W1 = 0.9$ , $W2 = 0.6$ , $W3 = 0.9$ , $y = 0.5$ , $y1 = 1.6$ ; (b) Measured responses in comparison with full-wave simulations.....	68
Figure 5.17 (a) Current distribution at 3.99 GHz (b) current distribution at 4.39 GHz.....	68
Figure 5.18 Photograph of the fabricated diplexer with the dual-mode patch junction. ....	69
Figure 5.19 Dual-band bandpass filter coupling topology.....	70
Figure 5.20 Arrangement for external Q-factor extraction and the typical responses.....	70
Figure 5.21 (a) Coupling topology; (b) Simulated response of the low passband.....	71
Figure 5.22 (a) Simulated response of the high passband; (b) Coupling topology with a $\lambda$ line resonator.....	72
Figure 5.23 High passband topology and response with a $\lambda/2$ line resonator.....	73
Figure 5.24 Simulated and measured responses of the filter in Fig. 5.19 with the inset showing the fabricated design.....	74
Figure 5.25 Simulated and measured responses of the filter in Fig. 5.25(a) with the inset showing the fabricated design.....	74
Figure 5.26 (a) Circuit layout dual-band BPF with $\lambda$ resonator: $F = 10$ mm, $F1 = 6$ mm, $S = 0.7$ mm, $S1 = 0.2$ mm, $L = 11.3$ mm, $L1 = 10.1$ mm, $LL = 53.2$ mm, $D = 25.2$ mm, $X = 12.4$ mm, $W = 1.2$ mm, $W1 = 2.8$ mm .....	75

Figure 5.27 (b) Circuit layout dual-band BPF with $\lambda/2$ resonator: $F = 10$ mm, $F1 = 6$ mm, $S = 0.7$ mm, $S1 = 0.2$ mm, $L = 11.3$ mm, $L1 = 10.1$ mm, $LL = 26.2$ mm, $D = 25.2$ mm, $X = 12.4$ mm, $W = 1.2$ mm, $W1 = 2.8$ mm. ....	75
Figure 6.1 Topology and typical response used to extract external Q-factors.....	79
Figure 6.2 BPF at 2 GHz.....	80
Figure 6.3 BPF at 3 GHz.....	80
Figure 6.4 Simulated current distribution of the 2 GHz and 3 GHz filters.....	81
Figure 6.5 Simulated and measured response of the 2 GHz filter with the SRR.....	81
Figure 6.6 Simulated and measured response of the 3 GHz filter with the SRR.....	82
Figure 6.7 Topology of a diplexer using SRR as resonant junction .....	83
Figure 6.8 Diplexer layout. $F1 = 7.9$ mm, $F2 = 9.3$ mm, $F3 = 7.9$ mm, $Ta = 8.1$ mm, $Tb = 5.3$ mm, $Tc = 8.3$ mm, $La1 = 10.2$ mm, $La2 = 8$ mm, $La3 = 4.5$ mm, $Laa3 = 4.6$ mm, $Lb1 = 7.5$ mm, $Lb2 = 5.2$ mm, $Lb3 = 3.3$ mm, $Lcc3 = 2.9$ mm, $Lc1 = 7.6$ mm, $Lc2 = 5.2$ mm, $Lc3 = 3.3$ mm, $Lc4 = 3.1$ mm, $d2,3 = 0.5$ mm, $d3,4 = 0.8$ mm, $d2,5 = 0.7$ mm, $d5,6 = 0.8$ mm, $W = 1.2$ mm, $W1 = 2.1$ mm.....	83
Figure 6.9 (a). $M_{2,3}$ against $d_{2,3}$ with the inset of topology and typical response; (b) $M_{1,5}$ against $d_{2,5}$ with the inset of topology and typical response; (c) Coupling response of Fig. 6.9 (a) without resonator 1; (d) Coupling of Fig. 6.9 (b) without resonator 2. ....	85
Figure 6.10. Eigen-mode response and topology.....	86
Figure 6.11 Simulated and measured responses of the diplexer.....	87
Figure 6.12 Simulated current distribution of the diplexer at 2 and 3 GHz.....	87
Figure 6.13 Photo of the fabricated diplexer .....	88
Figure 6.14 Dual-band BPF coupling topology.....	89
Figure 6.15 Dual-band BPF simulated response.....	90
Figure 6.16 Layout of the dual-band BPF. $F = 7.9$ mm, $L = 8$ mm, $L1 = 3$ mm, $L2 = 2.5$ mm, $L3 = 5.2$ mm, $L4 = 5.2$ mm, $L5 = 3.2$ mm, $L6 = 3.2$ mm, $W = 1.1$ mm, $W1 = 3.2$ mm, $T = 5.3$ mm, $T1 = 1.7$ mm, $S = 0.2$ mm.....	90
Figure 7.1 Duplexer and antenna (a) Conventional cascaded subsystem (b) Integrated duplexer-antenna.....	93
Figure 7.2 (a) 1.8 GHz hairpin filter layout; (b) 1.8 GHz hairpin and patch filtering antenna layout .....	96
Figure 7.3 Extracting the coupling coefficient (a) layout; (b) response .....	96
Figure 7.4 Simulated 1.8 GHz hairpin and patch filtering antenna response .....	97



Figure 7.5 2.4 GHz filtering antenna (a) layout ;(b) response .....	97
Figure 7.6 Coupling topology (a) conventional; (b) proposed .....	98
Figure 7.7 Designed duplexer antenna layout with parameters. $D_x = 52.5$ mm, $D_y = 43$ mm, $S_1 = 1.05$ mm, $S_2 = 2.1$ mm, $S_3 = 0.3$ mm, $S_4 = 0.25$ , $S_5 = 2$ mm, $S_6 = 0.3$ mm, $F_1 = 15$ mm, $F_2 = 20$ mm, $H = 15.5$ mm, $H_1 = 17.9$ mm .....	99
Figure 7.8 Simulated duplexer antenna isolation between two channels (ports) and the frequency responses .....	100
Figure 7.9 Dual-band bandpass filtering antenna (a) front view; (b) side view; (c) back view.....	101
Figure 7.10 Dual band bandpass filtering antenna coupling topology .....	101
Figure 7.11 Simulated S-parameter response – impedance matching .....	102
Figure 7.12 Simulated farfield radiation pattern at 1.8 GHz .....	103
Figure 7.13 Measured Fairfield radiation patterns on the E-plane at 1.8 GHz (cross-polarisation) and 2.1 GHz (co-polarisation) .....	103
Figure 7.14 Simulated farfield radiation pattern at 2.1 GHz .....	104
Figure 7.15 Measured Fairfield radiation patterns on the H-plane at 1.8 GHz (co-polarisation) and 2.1 GHz (cross-polarisation).....	105
Figure 8.1 Multi-input multi-output filter and diplexer coupling topology.....	108
Figure 8.2 (a) Proposed design layout; (b) Circuit block diagram. $F = 10$ mm, $F_1 = 15$ mm, $F_2 = 15$ mm, $T = 0.4$ mm, $T_1 = 0.2$ mm, $T_2 = 0.38$ mm, $T_3 = 1$ mm, $T_4 = 0.4$ mm, $W = 1.2$ mm, $W_1 = 0.4$ mm, $W_2 = 0.6$ mm, $W_3 = 0.6$ mm, $L = 9.6$ mm, $L_1 = 11.5$ mm, $LL = 6.6$ mm, $LL_1 = 11$ mm, $d_{1,2} = d_{2,3} = 1.46$ mm, $d_{1,4} = d_{3,7} = 0.22$ mm, $d_{4,5} = 1.65$ mm, $d_{5,6} = 1.7$ mm, $d_{7,8} = 1.84$ mm, $d_{8,9} = 1.82$ mm ....	108
Figure 8.3 The duplexing responses when Port-1 is excited as the common port.....	109
Figure 8.4 The duplexing responses when Port-2 is excited as the common port.....	109
Figure 8.5 Dual filter operation mode.....	110
Figure 8.6 Measured and simulated isolation responses.....	111
Figure 8.7 Prototyped multi-input multi-output filter and diplexer.....	111
Figure 8.8 Current density distribution of the MIMO filtering network .....	112
Figure 8.9 Classical connection in an antenna and transceiver module .....	113
Figure 8.10 Masthead combiner allowing the introduction of an LNA at the antenna output .....	113
Figure 8.11 Masthead combiner coupling topology with an LNA connected.....	114

Figure 8.12 Proposed microstrip MHC: (a) design layout (b) coupling topology. $F = 10\text{mm}$ , $T = 0.4\text{mm}$ , $T1 = 0.2\text{mm}$ , $T3 = 0.4\text{mm}$ , $W = 1.2\text{mm}$ , $W1 = 0.4\text{mm}$ , $W3 = 0.6\text{mm}$ , $L = 9.85\text{mm}$ , $L1 = 11.5\text{mm}$ , $LL = 6.6\text{mm}$ , $LL1 = 11\text{mm}$ , $d1,2 = 1.7\text{mm}$ , $d1,4 = 0.2\text{mm}$ , $d4,5 = 1.6\text{mm}$ , $d5,6 = 1.6\text{mm}$ .....	115
Figure 8.13 Simulated response of MHC showing RX channel, TX channel and isolation response.....	116
Figure 8.14 Current density distribution at TX, and RX1 channels .....	117
Figure 8.15 Prototyped MHC circuit .....	117

# Chapter 1: Introduction

This chapter presents the overview of what the Multi-Port Filtering Networks (MPFNs) is and where it can be applied in the mobile base station communication systems. It also considered the thesis motivation and the contribution to knowledge acquired through the research process. The overview of what to expect at the individual stages of this thesis are also presented.

## 1.1 Multi-Port Filtering Networks (MPFN)

Multi-Port Filtering Network (MPFN) is a concept derived from conventional two-port filters and applied to the design of multi-port networks such as diplexers, multiplexers, power dividers, and couplers, which can then form even more complicated microwave signal distribution networks [1 - 8]. Fig. 1.1 shows the concept of a MPFN. The coupling-matrix-based synthesis method for two-port filters has been successfully applied to the synthesis of a multi-port filtering network [9 - 12]. Such a network, formed entirely of resonators or resonant structures, removes the requirement of part or all the transmission line based circuitry. This brings the advantage of the potentially reduced footprint of the complex microwave circuits. Also, new configurations of multi-port devices can be implemented.

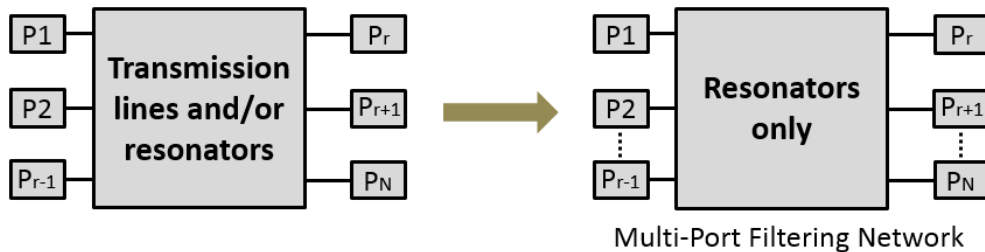


Figure 1.1 Concept of a MPFN

A MPFN uses junction resonator(s) instead of a transmission-line junction to route the signal to different ports; this is the main difference it has with a two-port filter. This junction resonator(s) acts as signal splitter(s) or combiner(s). It also normally provides a pole in the filtering response. One of the microwaves circuits that benefit most from the MPFN concept is the diplexer and multiplexer, which is also known as a combiner or a filter bank. Fig. 1.2(a) and Fig. 1.2(b) illustrates the coupling topology of a MPFN-based diplexer and a multiplexer

respectively. It mostly contains multiple interconnected filters. The multiplexer is used to combine multiple channels and feed to a common antenna for transmission or reception purposes. It is one of the most complex passive circuits in wireless base stations and satellite payloads. In the conventional design of a multiplexer, all the employed channel filters are connected to a common port using a signal distribution network based on transmission lines, couplers or circulators [13 - 19]. The drawback with conventional multiplexers is the fact that it involves complicated signal distribution networks that often occupies extra circuit area. By applying MPFN concept, two or more filters can be joined into a diplexer or multiplexer without extra signal distribution network [1, 3, 9, 11, 21 - 24]. The coupling topology presented in Fig. 1.2(a) and Fig. 1.2(b) represents two basic topologies and can be changed if a different coupling topology is required for further miniaturisation or improved frequency selective response.

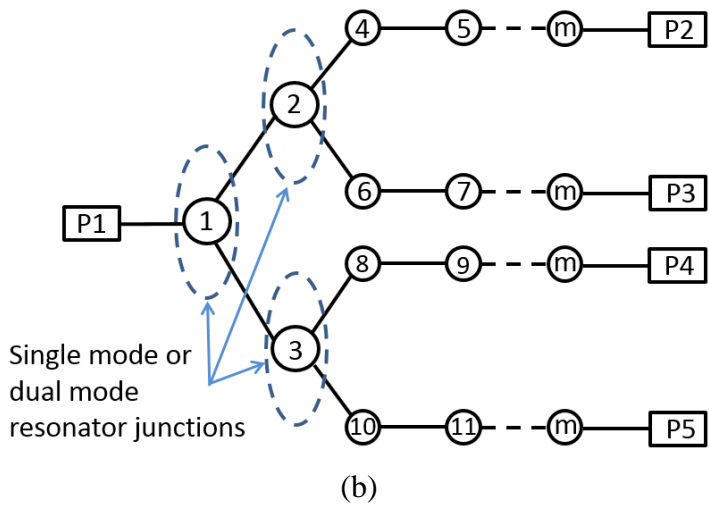
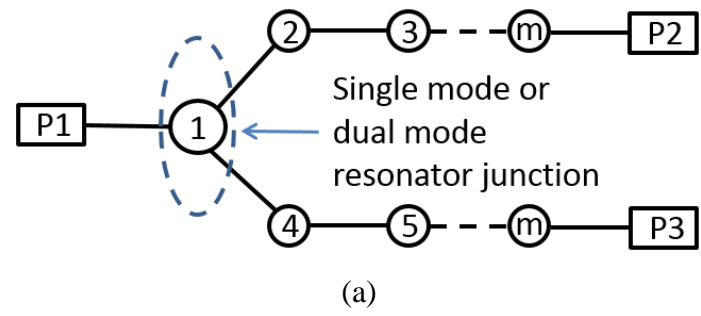


Figure 1.2 Example topology: (a) a three-port diplexer; (b) a five-port multiplexer

## 1.2 Diplexers/Multiplexers and their Applications

A diplexer is usually made up of two individually designed filters known as channel filters. If properly configured, a diplexer can combine or separate two networks operating at different frequencies. A block diagram of a diplexer is shown in Fig. 1.3. In the case of a diplexer, these individual channel filters will serve as the receiving channel and transmitting channel in frequency division duplex (FDD) RF and microwave applications for broadband, satellite and mobile communications.

In order to create a miniaturised diplexer, the transmission line based geometry can be avoided and then replaced with a common resonator whose role is to distribute signals to the channel filters. In some cases, this common resonator also takes the place of a resonant pole in the channel filters.

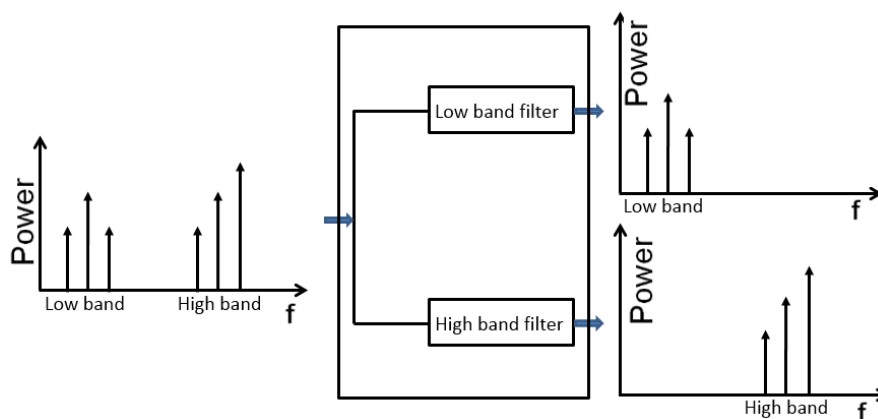


Figure 1.3 Block diagram of a diplexer

The design of a multiplexer follows the steps of diplexer design, but instead of using two channel filters, three or more numbers of filters are used and connected to a signal distribution network. A diplexer is the simplest version of a multiplexer.

## 1.3 Thesis Motivation

With the ever-growing congestion in the communication system and the on-going introduction of more communication channels, multi-port filtering network based components play a significant role in reducing the footprints and costs in the communication infrastructures. This

technology is most useful in the design of diplexers and multiplexers through the employment of channel filters [25 - 28] that separate wanted signals from the unwanted signals.

The primary focus of this research is to develop new diplexers and multiplexers based on the MPFNs concept mentioned in Section 1.1. This is focused on improved frequency selectivity, isolation and miniaturisation. Some novel approaches are also considered in the design of channel filters with improved selectivity. Both single mode and dual-mode resonators will be investigated and utilised. The use of resonators to replace the transmission line base network is a paramount task in this study. The innovation aims to a reduction in size and mass of the designs without sacrificing the performance. This, will potentially reduce the cost of base stations infrastructures significantly.

## **1.4 Main Contributions to Knowledge**

- A systematic comparison study has been performed between a conventional diplexer based on the transmission-line junction and an all-resonator diplexer based on the MPFN concept. While the big advantage of a compact footprint of the latter was clearly demonstrated, the challenge in maintaining good isolation and rejection was also highlighted to guide future designs. The simulation-based comparison of the current density distribution of the two diplexers showed comparable peak current density. The current study implies no degradation in the power handling capability of the all-resonator based diplexer. Further investigation using a more accurate modelling approach and simulation tool, which is not readily available to this work, is needed.
- A number of diplexers were presented using the MPFNs technique which comprises of all resonant structures. Various dual-mode resonators such as the patch, the split-ring-resonator and the asynchronously-coupled-junction were implemented as the junctions of the diplexers and were presented. All demonstrated the signal distribution and combining functions, as well as contributing to the resonant poles to the filtering channels. The demonstrated techniques resulted in a more compact diplexer circuitry without sacrificing the selectivity of the channel filters.
- Several single-band or dual-band filters were proposed and demonstrated as the building block of diplexers and multiplexers. In particular, the mixed use of single and dual-mode

resonators has shown the capability and flexibility to improve the frequency selectivity by controlling the transmission zeros. Dual-mode resonators were also used to split and combine the signals in dual-band designs as in the diplexers.

- This thesis has started the exploration of the new idea of multi-input and multi-output filters in the framework of MPFNs. Several four-port filtering networks were investigated. One design demonstrated the capability of selecting discrete operation frequencies depending on the excitation ports, which makes it a great utility when multiple operation modes are to be used by the same receiver. A Masthead Combiner (MHC) was presented as another example. Both designs contained an all resonant structure while the signal splitting and combining was made possible using an Asynchronously Coupled Junction.
- Finally, as an extension of the work, the integration of a diplexer and an antenna based on an all-resonator structure was studied using the co-design approach essentially based on filter designs. Using a direct coupling method, the need for an additional feedline or balun circuitry to the antenna is avoided. A novel dual-band filtering antenna was also demonstrated using a similar design approach.

## 1.5 Thesis Overview

The work carried out in this research relies on the synthesis and implementation of coupled resonator circuits. It concentrated on extending the two-ports design technique used for coupled resonator filters towards multi-port resonator circuits. The review of other works of literature is presented in Chapter 2. It covers different methods of diplexer designs from the conventional technique to the multiport filtering networks technique based on all resonant structures. Techniques on how to realise dual-mode resonators are also presented. Chapter 3 presents the theoretical background and design methods in single-band and dual-band filters. It also covers the coupling matrix synthesis of the MPFNs.

Chapter 4 presents a comparison between a diplexer with a non-resonant transmission-line T-junction (conventional diplexer) and a diplexer with an Asynchronously-Coupled-resonant Junction (ACJ). The diplexer with an ACJ is designed by asynchronously coupling the first resonators of two channel filters of different frequencies together to create a common resonant

junction for both channel filters. The technique used in obtaining the ACJ is explained in detail and its implementation is applied to other designs in Chapter 4 and 8.

Chapter 5 presents several designs using patch resonators. It included the use of a dual-mode patch resonator to generate a transmission zero for a highly selective frequency response for a bandpass filter. Also, a patch resonator is used as a common resonant junction in a diplexer design. The conventional diplexer design technique was avoided by using a dual-mode patch resonator instead of a transmission line for signal splitting and combining. To further miniaturise the diplexer, the orthogonal mode of the patch resonator was each made to serve as a resonant pole for the channel filters. This led to a reduction of one resonant structure from each of the channel filters. A dual band filter with dual coupling paths were also presented using two dual-mode patch resonators.

Chapter 6 focuses on implementing a split-ring resonator (SRR) as a resonant junction in joining two Chebyshev BPFs in a diplexer design. The SRR was designed by nesting a higher resonant open-loop resonator into a lower resonant open-loop resonator. In this case, an asynchronously tuned technique was used again in realising the resonant poles of the SRR. The SRR implementation in this design resulted in an improved frequency selectivity of the passband and a reduced diplexer circuit size.

Chapter 7 concentrates on the integration of filters and antenna. It explores the integration of two filters and one antenna to create a duplexing antenna. The duplexing antenna utilised the antenna as the common resonant and radiating junction. For the antenna to perform these functions, it was designed to resonate/radiate orthogonally at the centre frequencies of the two channel filters. This allowed the antenna to function as a signal splitter/combiner, and a resonant pole for each channel. The configuration resulted in a compact structural size which is a product of integrating two microwave components. A miniaturised dual-band filtering antenna is also presented. The design utilised two dual-mode resonant structures of which one is a patch resonator and the other a patch antenna. The resonator and the antenna were coupled to each other using a slot coupling method with a common ground between them. The antenna contributed to the resonant poles of the filtering response while functioning as the radiating element.



Chapter 8 presents several four-port filtering devices which comprise a Masthead Combiner (MHC) and a Multi-Input Multi-Output (MIMO) filters/diplexer using all resonant structures. The MIMO filter/diplexer allows the selection of different channel(s) that suit an application of purpose depending on the port of excitation. The summaries, contributions and conclusions drawn from the whole work are then presented in Chapter 9.

# Chapter 2: Literature Review

This chapter reviews relevant literature and previous works published on microwave diplexers and multiplexers. It compares different techniques used in the diplexer and multiplexer implementation which ranges from the conventional technique to all resonator based technique. As a key constituent component of the designs in this thesis, different types of dual-mode resonators are also discussed.

## 2.1. Background Overview

In communication systems, microwave diplexers are used to connect two networks operating at different frequencies to a common port or antenna, allowing simultaneously transmit and receive functions. In a more complicated network configuration, three or more filters can be joined in a single unit to form the so-called multiplexer. During the design of diplexers/multiplexers, attention is paid in achieving a good frequency response in terms of frequency selectivity, isolations, matching, etc.

Recently, more attention is being paid to the type of junction used during the diplexer and multiplexer implementation, as the junction used can contribute to the frequency selectivity as well as the size and other performance. There are different types of junction techniques which can be applied in joining the channel filters, which are;

- T-Junction technique
- Manifolds and circulators technique
- MPFN technique (all resonator based)

## 2.2 Conventional Diplexers and Multiplexers

Conventional diplexers/multiplexers are frequently referred to the earlier techniques used in joining the channel filters. This technique involves connecting the channel filters to an energy distribution network such as T-junction [13, 29], Y-junction [30, 31], hybrid couplers [32, 33], waveguide manifold [11, 34], or circulator [35, 36]. They are usually big, due to the type of

junction technique used for their implementation when compared to the MPFNs technique which is a current trend. When design simplicity is the main drive, diplexers can just use lowpass and highpass filters with low insertion loss and low cost [37]. However, in applications requiring higher selectivity, the use of narrow bandpass filters is necessary. This may result in device size increase and spurious coupling effects between the two channels. A trade-off is often needed between the isolation and the size of a diplexer in conventional implementations. Different techniques used in the conventional diplexer/multiplexer implementations are reviewed below.

### **2.2.1 T-Junction and Y-Junction**

The T-Junction technique uses a transmission line in a T-shape to join two filters. The T-shape junction functions as the signal splitter and combiner for both operating frequencies. Its operation is by using a  $\lambda/4$  electrical length section of the low band channel filter to feed the high band channel filter and vice versa. Both  $\lambda/4$  line sections are then joined together at the input feed point. This simple technique works well, but it occupies more space with increased footprint. In [13], a high isolation and compact diplexer design was proposed and achieved using Compact Hybrid Resonators (CHR), with its capability to introduce transmission zeros. The proposed design operated at 1.82 GHz and 2.5 GHz with 5% fractional bandwidth each. It was evident that a good isolation of about 55 dB was achieved.

The Spiral Compact Microstrip Resonant Cell (SCMRC) was adopted in the design of a diplexer in [38]. The SCMRC was transformed into a Dual Behaviour Resonator (DBR) and was used in the design of a bandpass filter with high rejection in the upper stopband. The adopted SCMRC operates as a slow-wave transmission line. The SCMRC was introduced into the RX filter to improve rejection in the upper stopband to over 60 dB. The Tx-filter is designed without the SCMRC and linked to the Rx-filter via a T-junction.

In [39, 40], diplexers were proposed to have a good rejection. Two filters with oversized stubs were designed and integrated using a T-junction. These diplexers were designed to operate on the Ku-Band and explored the idea of Dual Behaviour Resonator (DBR). In [29], modified Stepped Impedance Resonators (SIRs) in the form of an open-loop SIR was used in the design of two bandpass filters of which one is for the GPS and the other is for WLAN. The filters

achieved wide stopband and two transmission zeros near the passband edges; these were used in the design of a diplexer. With the location of the transmission zeros, an improved passband selectivity, as well as band isolation was achieved.

A miniaturised planar diplexer using spiral-based resonators was proposed in [41]. The resonators were asymmetrically separated from each other, thus the name; Asymmetrical Separated Spirals resonator (ASSR). The two-individual channel filters were joined using a T-junction technology to achieve the diplexer. A compact and high isolation microstrip diplexer were also presented in [42]. It was achieved using two four-pole cross-coupled bandpass filters placed side by side and joined using T-junction. The diplexer in [43] shows a very low port-to-port insertion loss and provides high isolation. With the topology used, a straightforward integration of other planar elements with the diplexer on the same substrate can be achieved.

The Y-junction uses the same technique as the T-junction, but it has been shown that the Y-junction introduces fewer losses in the circuit than the T-junction [44]. Using a direct synthesis approach for Chebyshev filters with real load impedance, a set of polynomial functions was formulated [45]. A validation of this approach was implemented in a diplexer with Y-junction. [46] reported a non-contiguous waveguide diplexer with Y-junction. [31] provides an analytical criterion for the design of optimum Y-junctions for the realisation of diplexers. It concentrated on providing the parameters for the location of the channel filters which resulted in a simplification of the overall synthesis as well as reduced optimisation time. A diplexer consisting of two bandpass filters using folded hairpin resonators with SIR was designed in [47] and joined using a Y-junction. The response has no spurious up to the second harmonic frequencies, thanks to the  $\theta^\circ$  feed scheme.

## **2.2.2 Manifolds and Circulators**

A multiplexer based on the sequential connection of channel filters to a wide-band manifold was presented in [34]. Without the use of stubs, the attachment of the filters resulted in a minimised effect of spurious resonances. The interconnection elements, the manifold, and the remaining filters are all seen as the first inverter for each subsequent new filter that is attached. [19] presented a manifold diplexer without tuning elements. A procedure that consists of decomposing the complex design task into four simpler tasks was used, which only involves

the soft tuning of a limited number of physical parameters. The procedure used substantially reduced design time and cost.

Two edge-coupled microstrip filters were employed in the design of a diplexer by joining them together using a circulator device [35]. The channel filters can be tuned or exchanged without affecting the opposite channel. The worst-case isolation of the diplexer was estimated to be 20 dB. [36] it consists of a multiplexer which is composed of two branches joined by a circulator, with each branch containing straight waveguide manifold shorted at one end with bandpass filters distanced from the short.

### **2.2.3 Miniaturisation Technique**

In order to achieve diplexer miniaturisation, a technique that allows the channel filters to share one input feed line can be used. Two folded cavity filters are joined using one coaxial input [48]. A diplexer operating at Direct Sequence Ultra-Wideband (DS-UWB) was reported in [49], using the hairpin line resonators for the lower and higher channels and joined at a common feed line. In [50] a compact diplexer was presented with each channel having dual bands. For compactness, the channel filters were designed using stepped impedance resonators. The joining of the two channel filters was done by directly connecting them to a common port.

Other ways in which diplexer miniaturisation is possible is by using miniaturised resonators, dual-mode resonators or multi-layered circuits. This has been shown in [51, 52], where a dual-band BPF and a diplexer based on the Double-Sided Parallel-Strip Line (DPSL) were reported. Two transmission paths for RF signals were provided by the isolation feature of the inserted conductor plane. In [53], a compact size tuneable diplexer using dual-mode stepped-impedance microstrip resonators (SIRs) was presented.

## **2.3 All-resonator Based Diplexers and Multiplexers**

This section presents literature on diplexers and multiplexers based on coupled resonators circuits theory. Without the involvement of the transmission-line based power distribution network, the designs are thus smaller than the conventional multiplexers. The structures

presented have diverse properties of channels and different filtering responses due to the direct coupling and cross-coupling which existed in the different structures and topologies used.

### **2.3.1 Different Types of Junction Resonators**

A compact diplexer using three dual-mode stub-loaded resonators is presented [54]. One stub-loaded resonator in the form of a T-shape served as the common resonator. The T-shaped resonator had its two resonant frequencies set for the operating frequencies of the channels. In [1], a diplexer was designed using a T-shaped dual-mode resonator and two open-loop resonators of different frequencies for the high and low passband. The T-shaped resonator was made to resonate at the centre frequencies of the two passbands and used in linking the two open-loop resonators. The technique used in [1, 54] was further extended to the creation of a multiplexer and switchable diplexer in [3]. The multiplexer made use of four channel filters combined using two T-shaped resonators. Each T-shaped resonator has two open-loop resonators coupled to it, making it an independent diplexer [1, 54] with two channels of different frequencies. The two separate diplexers were then coupled together to a common feed line making them a complete multiplexer with five ports.

There are other published works using a common resonant junction as expressed in [15] where a diplexer with a resonant Y-junction was designed using an elliptic ridge resonator. The Y-junction behaves like a common dual-mode resonator and functions as a resonant pole for both channel filters. [55] presented a design where the location of SIR's fundamental and the first spurious resonant frequencies are achieved and shared by both filter channels. In [56], a diplexer was designed by using a dual-mode Split-Ring Resonator (SRR) as a common resonator. By synchronously nesting an open loop resonator into another, the SRR was tuned to generate a dual-mode for the two channels of the diplexer.

The work in [10] described a method for coupling matrix synthesis of a symmetric or asymmetric diplexer with a common resonator junction. The method is based on the evaluation of the characteristic polynomials of the channel filters and optimisations. An objective error function was constructed using the transmission and reflection zeros obtained from the polynomials of the TX and RX filters. The frequency selectivity was improved by introducing cross couplings in the channel filters. A second design was achieved by using parallel coupling

method in the channel filters. Using the synthesis of coupling matrix of a 3-port coupled resonator circuit presented in [57], a diplexer was designed. The design does not need separate junction for its distribution of signal contrary to the conventional counterpart. By using a waveguide cavity with its resonator coupled together, the diplexer achieved a miniaturisation.

Using dual-mode cavities, two topologies for realising compact microwave diplexers were presented in [58]. Two multiplexer topologies based on all-resonator structures were reported in [59]. The first topology was a diplexer with transmission zeros in the guard band, shared by both channels. These transmission zeros are generated by introducing a cross coupling in a quadruplet in resonators common to both channels. The second topology is a multiplexer with a bifurcated structure that limits the connections to any resonator to three or less, regardless of the number of output channels. Both topologies were demonstrated at X-band using waveguide technology. The technique used in [59] was extended in [23, 60]. The synthesis of the designed multiplexers was performed using an optimisation technique. The technique presented allows the possibility of dividing the multiplexer into diplexers and optimising each diplexer individually. In [61, 62], the diplexers were designed to have various topologies by altering the number of resonators on the stem and branches. It was noticed that the higher isolation and lower bandwidths occur with increasing numbers of resonators in the branches.

A method for the polynomial synthesis of microwave star-junction multiplexers with a resonating junction was presented in [63, 64]. The channel filters used in this method can be arbitrarily specified, including the assignment of transmission zeros. To evaluate the characteristic polynomials of the multiplexer, an iterative procedure was developed and used for computing the polynomials associated with the channel filters. The design approach was used in the design and implementation of a triplexer. [12] presented a technique that utilises the synthesis of two port filters and three port diplexers to develop a synthesis for N port multiplexers.

### **2.3.2 Comparison of Junction Resonator Diplexers with Conventional Diplexers**

Conventionally, the design of microwave multiplexer networks involves four steps: firstly, the filters serving the channels are independently designed to specification. Secondly, junction or

manifold network is designed, allowing the filters to be minimally affected by integration. Thirdly, the junction or manifold network is used in joining the channel filters [34]. Usually, these networks are formed of transmission lines [13]. After the joining of the channel filters, disruptive interaction is very likely to occur. Finally, an optimisation step is carried out to further improve the response of the channels. However, in the designs comprising all-resonator based diplexers and multiplexers, a different approach is followed. The complete network is formed exclusively of coupled resonators [47]. A single generalised coupling matrix can be used to represent the whole network [12]. In some diplexer designs, a dual-mode resonator can be implemented as the junction connecting the channel filters [54]. In this instance, the dual-mode resonator will function as a signal splitting and combining circuit as well as contributing to the resonant pole(s) of the channel filters. This is contrary to the conventional counterpart where the junction does not contribute to the pole(s) of the channel filters.

## **2.4 Dual-mode Resonators**

Dual-mode resonators are resonant structures that are capable of resonating in two different modes. They play a major role in the design of miniaturized RF and microwave components [65]. In the microstrip technology, these types of resonators come in different shapes/structures. Some examples of dual-mode resonators are patch resonators, SRR, SIR and SLR which will be discussed below. In this thesis, dual-mode patch resonators and SRR are used.

### **2.4.1 Patch Resonators**

To increase the power-handling capability [66 - 68], patch resonators were employed in the design of microstrip filters/diplexers. A significant advantage of microstrip patch resonators is their lower conductor losses when compared with the narrow microstrip line resonators. Although patch resonators tend to have a stronger radiation, they are normally enclosed in a metal housing for filter applications so that the radiation loss can be minimised. Patch resonators usually have a relatively large size. Patches may take different shapes, such as triangular [69 - 72], square [73 - 78], circular [79 - 81], hexagonal [82 - 84] and octagonal [85], etc.



Patch resonators are advantageous in terms of its orthogonal modes. The dual-mode features have found its way in the design of diplexers [86, 87]. Orthogonal mode square patch resonator has also been used in a design of mixed resonator three-pole BPF [26], where one of its orthogonal modes was coupled to the transmission path and the other used to generate a transmission zero with improved frequency selectivity. It was also used in a dual-band BPF and multiplexer where a supposedly eight-resonator structure was reduced to a four-resonator one [88].

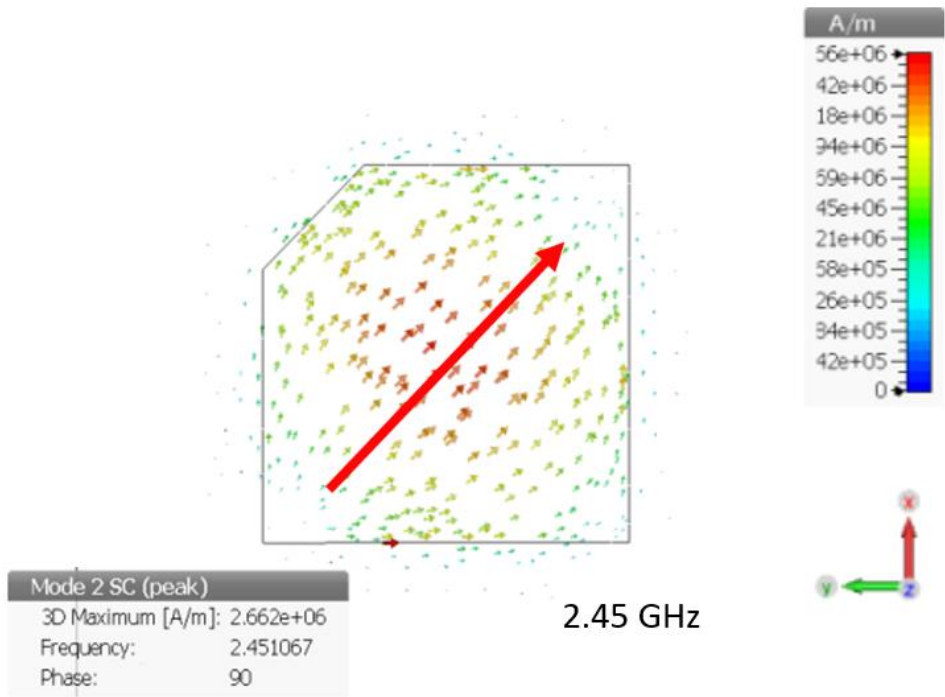
To design an orthogonal mode square patch resonator, the length  $D$  of the patch can be calculated using (2.1).

$$D = \frac{\lambda_{0g}}{2} \quad (2.1 a)$$

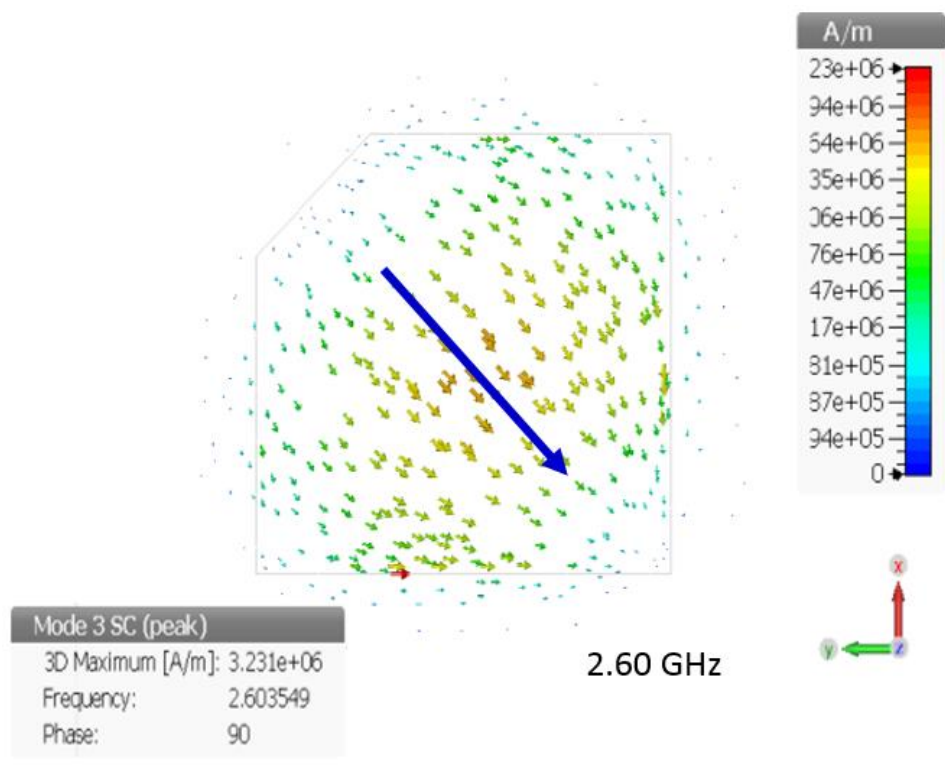
$$\lambda_{0g} = \frac{c_0}{f_0 \sqrt{\epsilon_r}} \quad (2.1 b)$$

Where  $\lambda_{0g}$  is the guided wavelength,  $c_0$  is the speed of light in free space,  $\epsilon_r$  is the relative permittivity, and  $f_0$  is the centre frequency between the orthogonal modes [65]. To generate a dual-mode from the square resonator, a perturbation or slot can be introduced to one corner or in the middle of the square resonator. By varying the perturbation/slot length, the coupling coefficient between the dual-modes can be adjusted, thereby increasing or reducing the dual-mode frequencies.

To clearly understand the orthogonal capability of a square patch resonator, a look into its current distribution is advised. Fig. 2.1(a) and (b) illustrates a patch resonator resonating at 2.45 GHz and 2.60 GHz. Using Computer Simulation Technology Electromagnetic and Multiphysics (CST EM) simulator, it is seen that the current heads in two different directions, one in the longer diagonal length is the 2.45 GHz while the one in the shorter diagonal is the 2.6 GHz.



(a)

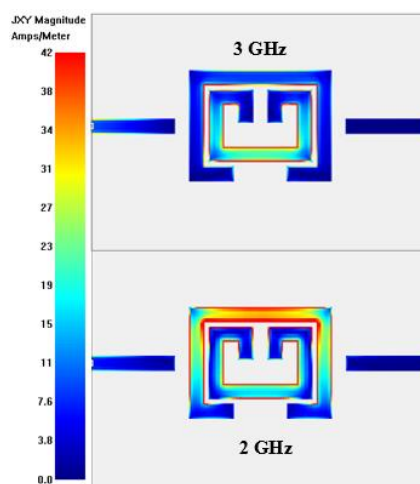


(b)

Figure 2.1 Current distribution of the orthogonal mode square patch resonator. (a) 2.45 GHz; (b) 2.60 GHz.

## 2.4.2 Split-Ring Resonator (SRR)

The Split-Ring Resonator (SRR) is another resonator with a dual-mode function. It is designed by nesting and coupling one resonator into another. These two coupled resonators can come in different shapes, such as circular open-loop resonators [89, 90], triangular [91], or square open-loop resonators [92]. The coupling between the resonators can be synchronously or asynchronously achieved, giving this type of resonator an opportunity to be used in an application that requires both widely separated frequencies and narrowly separated frequencies. To design a synchronously coupled SRR, two resonators with the same electrical lengths are folded into required shape. For an asynchronously coupled SRR, the electrical lengths of the two resonators are not the same. The resonator with the higher frequency is usually the inner core while that of the lower frequency is the outer. This type of resonator is very useful in the design of compact duplexers [93], and dual-band filters [94]. Fig. 2.2(a) shows the current distribution at both frequencies and Fig. 2.2(b) the frequency response of an asynchronously coupled SRR with an inset of the physical structure and the coupling topology. The colour indicates the current densities at different locations in the resonator structure. This asynchronously coupled SRR is made up of two open loop resonators of 2 GHz and 3 GHz. As shown in the Fig. 2.2(b), the SRR produced an inter-band transmission zero, making it very useful in the design of an improved selective frequency response. The difficulty working with this resonator is that only the outer core can be easily coupled with adjacent resonators or the feed lines.



(a)

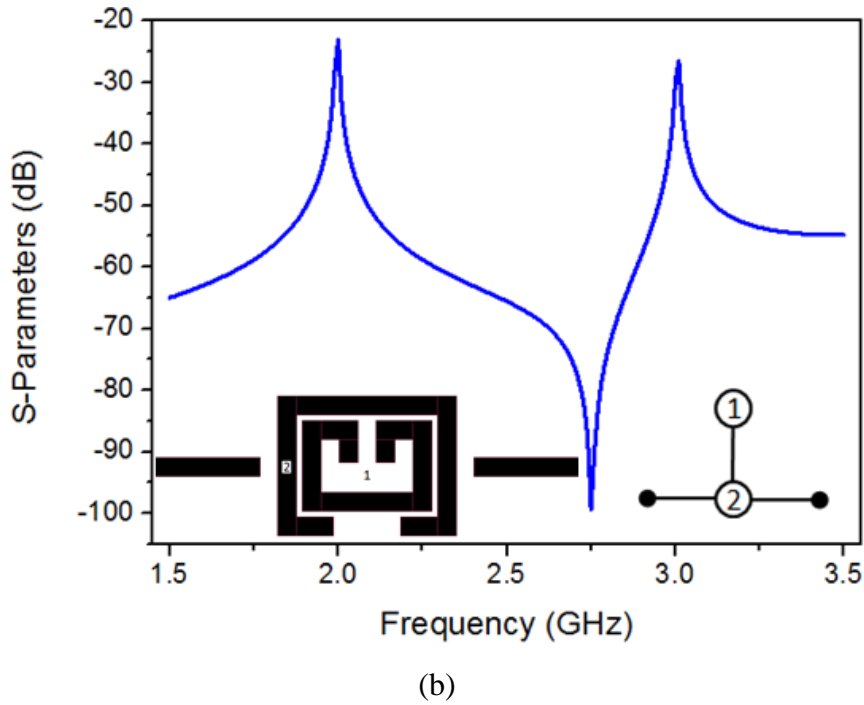


Figure 2.2 Asynchronous coupled SRR: (a) Current distribution; (b) response with an inset of the physical and coupling topology

There is also a modified SRR structure – the so-called Non-Bianisotropic Complementary Split-Ring Resonator (NBCSSR) [95]. The difference between a SRR and a NBCSSR is that while the SRR have an inner and outer core rings, the NBCSSR's half ring swap their disposition by crossing through the gap of the opposite ring. This facilitates the coupling between adjacent NBCSSRs. In the response wise, the NBCSSR has a simple second order response with one band and no transmission zeros. This type of resonator has been used in the design of filtering devices like bandstop filters [95] and dualband filters [96].

### 2.4.3 Stepped-Impedance Resonator (SIR)

A microstrip stepped-impedance resonator (SIR) is formed by joining two microstrip transmission lines with different characteristic impedance  $Z_1$  and  $Z_2$ , with  $Y_1$  and  $Y_2$ ,  $\theta_1$  and  $\theta_2$  being the corresponding characteristic admittances and the electrical lengths [97, 98]. The use of SIR in different types of RF and microwaves components is evident in the designs of diplexers [99 - 101], dual-band filters [102 - 104], multiband bandpass filter [105, 106] and bandpass filters [107, 108].

In Fig. 2.3(a) and (b), a typical structure of the half-wavelength SIR for the cases of  $K < 1$  and  $K > 1$  is presented, where  $K$  is the impedance ratio defined in (2.2). The resonant conditions are described in (2.3) and (2.4) which corresponds to the resonance of the odd and even mode respectively.

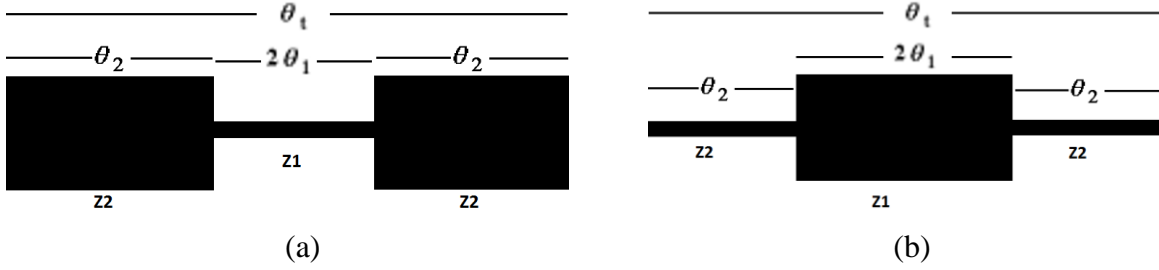


Figure 2.3 Half-wavelength SIR: (a)  $K = Z_2 / Z_1 < 1$ ; (b)  $K = Z_2 / Z_1 > 1$

$$K = \frac{Z_2}{Z_1} \quad (2.2)$$

$$\text{Odd mode: } K \cdot \cot\theta_2 = \tan\theta_1 \quad (2.3)$$

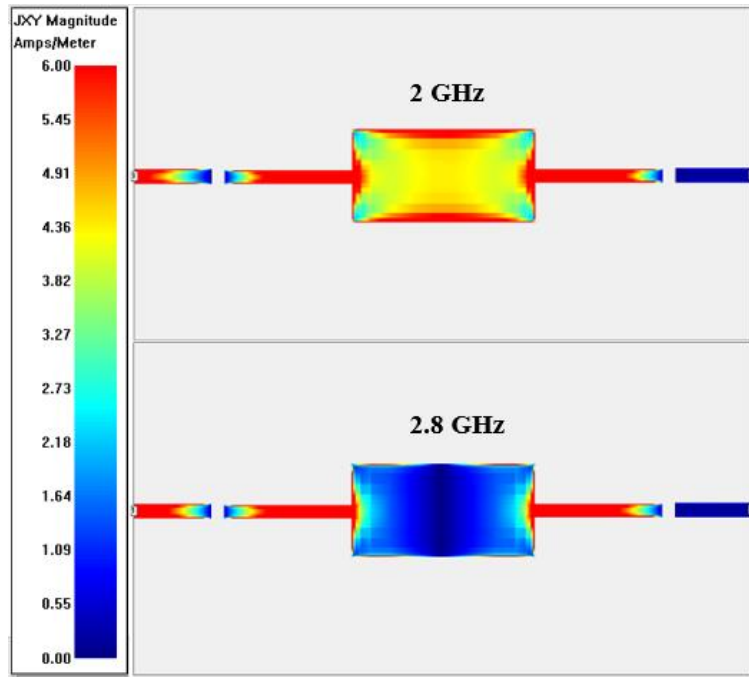
$$\text{Even mode: } K \cdot \cot\theta_2 = -\cot\theta_1 \quad (2.4)$$

By substituting the length ratio  $\alpha$  of the SIR as defined in (2.5) into (2.3) and (2.4), the electrical length of the odd mode and the even mode can be found by (2.6) and (2.7) respectively [55]. If a suitable combination of the impedance and length ratios is chosen, the frequencies of the fundamental and the higher order mode can be determined. Fig. 2.4 illustrates a SIR at 2 GHz and 2.8 GHz with Fig. 2.4(a) showing the simulated current distribution and (b) the frequency response.

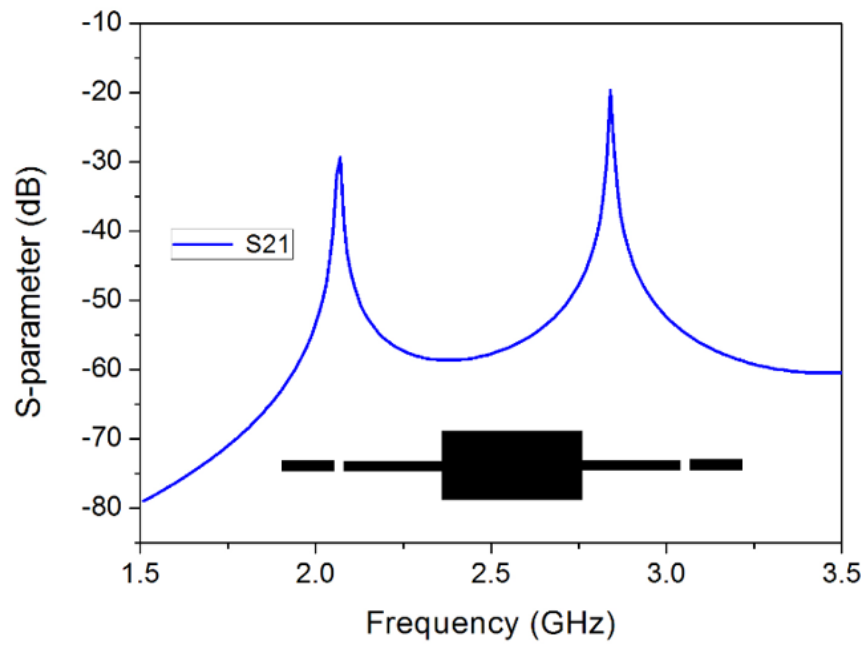
$$\alpha = \frac{\theta_2}{\theta_1 + \theta_2} = \frac{2\theta_2}{\theta_t} \quad (2.5)$$

$$\text{Odd mode: } K \cdot \cot\left(\frac{1}{2}\alpha\theta_t\right) = \tan\left[\frac{1}{2}(1 - \alpha)\theta_t\right] \quad (2.6)$$

$$\text{Even mode: } K \cdot \cot\left(\frac{1}{2}\alpha\theta_t\right) = -\cot\left[\frac{1}{2}(1 - \alpha)\theta_t\right] \quad (2.7)$$



(a)



(b)

Figure 2.4 An SIR resonator; (a) Current distribution: (b) Frequency response

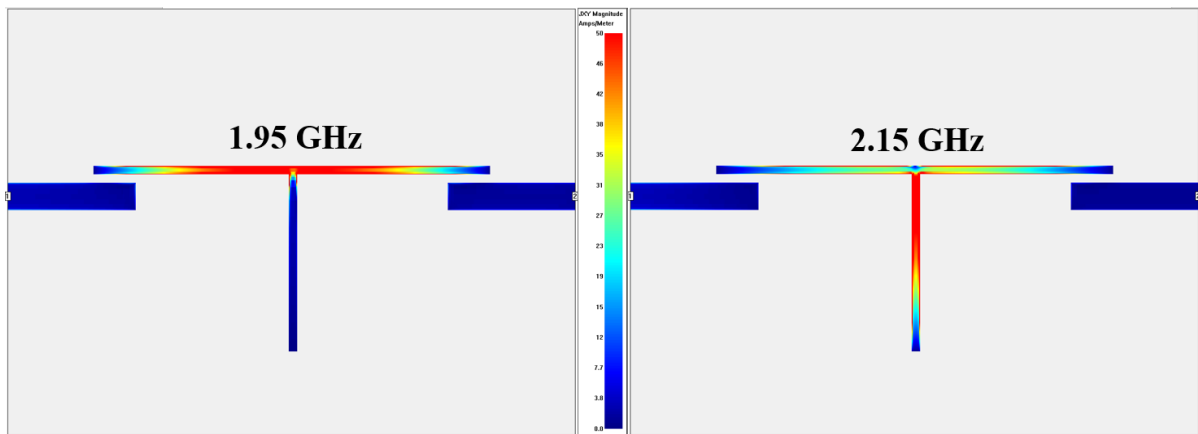
## 2.4.4 Stub-Loaded Resonator (SLR)

A T-shaped resonator also regarded as a Stub-Loaded Resonator (SLR) is a dual-mode resonator that assumes the shape of a transmission line based T-junction. To determine the resonant frequencies, the even-odd mode theory as presented in (2.8) and (2.9) can be used. Fig. 2.5(a) presents the current distribution of a dual-mode SLR, resonating at 1.95 GHz and 2.15 GHz. Fig. 2.5(b) presents the resonant frequency with an inset of the topology.

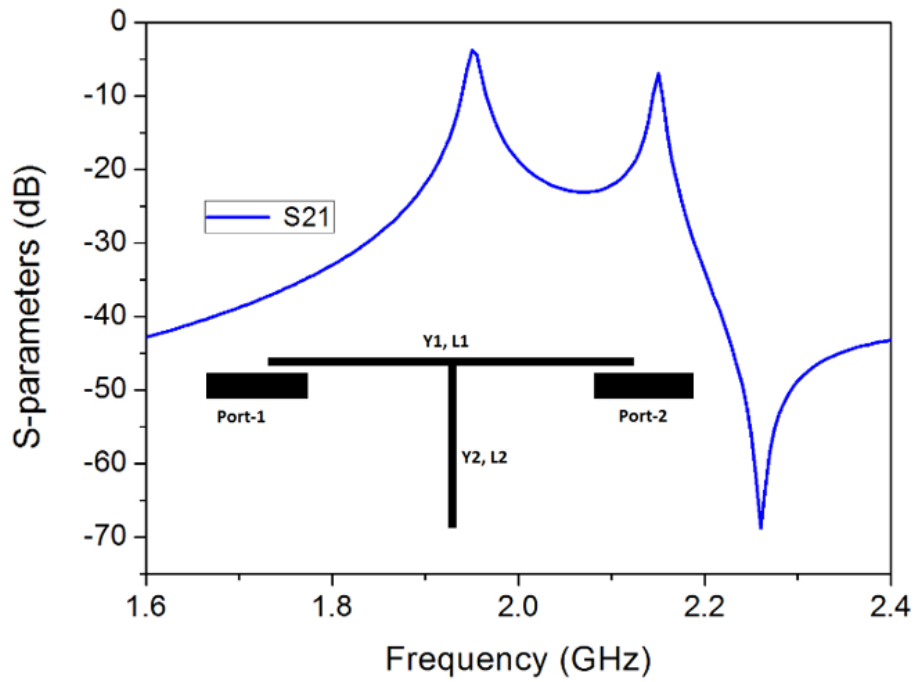
$$f_{even} = \frac{nc_0}{(L_1 + 2L_2)\sqrt{\epsilon_{eff}}} \quad (2.8)$$

$$f_{odd} = \frac{(2n - 1)c_0}{2L_1\sqrt{\epsilon_{eff}}} \quad (2.9)$$

where  $n = 1, 2, 3 \dots$ ,  $c_0$  is the speed of light in free space and  $\epsilon_{eff}$  is the effective dielectric constant of microstrip line. The even-mode resonant frequency can be varied as a function of the open stub length. The  $Y_1$  and  $Y_2$  as labeled in Fig. 2.5 are the characteristic admittances for the horizontal and open-circuited stub sections with lengths  $L_1$  and  $L_2$  respectively. If length  $L_2$  is adjusted to near one-quarter guided-wavelength, the two resonant frequencies in the stub-loaded resonator can be set to be close to each other [54, 109].



(a)



(b)

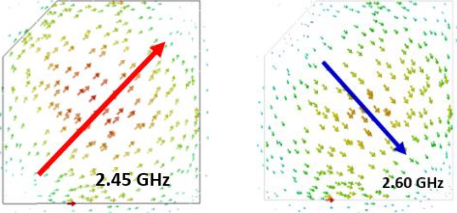
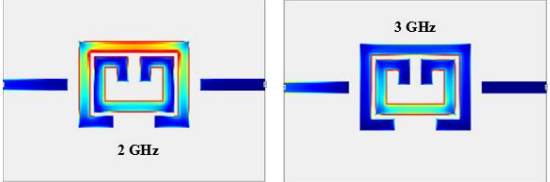
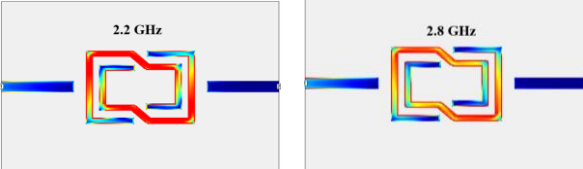
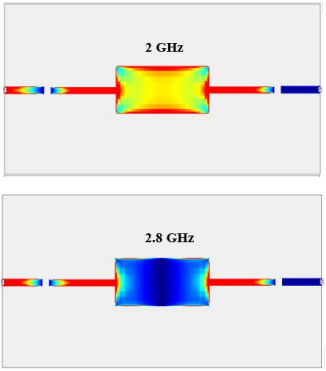
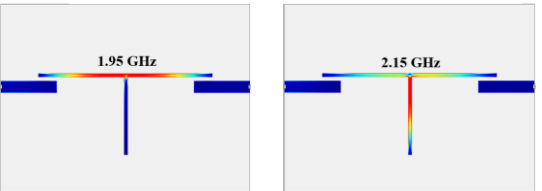
Figure 2.5 Dual-mode SLR resonator: (a) Current distribution (b) S-parameter response

## 2.5 Dual-mode Resonators in Diplexers and Filters

The use of dual-mode resonators in the design of microwave components are evident in several published works of literature. Its application, in most cases, leads to more compact devices as they perform the task of two single-mode resonators. It has been used in the implementation of bandpass filters [110, 111], dual-bandpass filters [112 - 115], diplexers [116, 117], etc. A few other applications of dual-mode resonators can be found in this thesis. Table 2.1 compares several types of dual mode resonators, their responses, features and sizes. Table 2.2 presents a summary of features/parameters of some of the diplexers/multiplexers reviewed in this chapter.



Table 2-1 Comparison of different dual mode resonators

Dual mode resonators	Size (mm)	Frequency (GHz)	Features
	$17.6 \times 17.6$	2.45, 2.6	Outer-band transmission zero
	$10.2 \times 8$	2, 3	Inter-band transmission zero
	$9.1 \times 7.2$	2.2, 2.8	One outer-band transmission zero
	$34.3 \times 7$	2, 2.8	No transmission zero
	$46.7 \times 21.8$	1.95, 2.15	One outer-band transmission zero

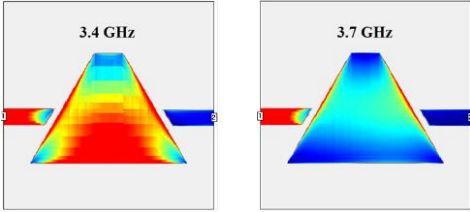
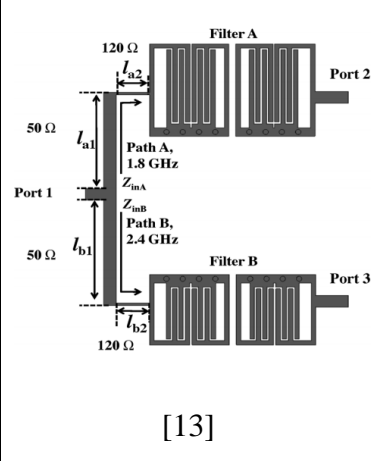
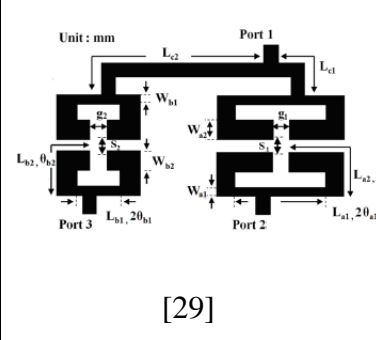
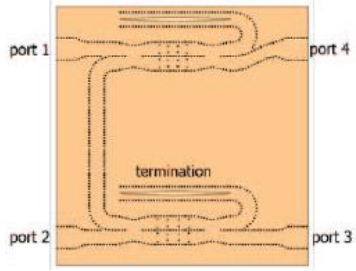
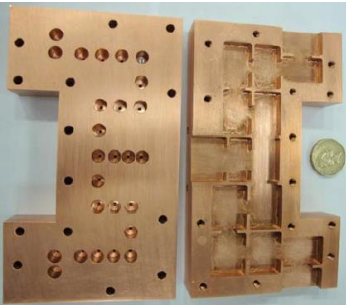
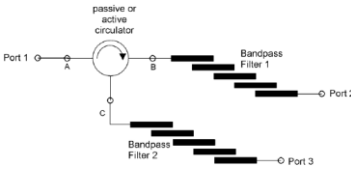
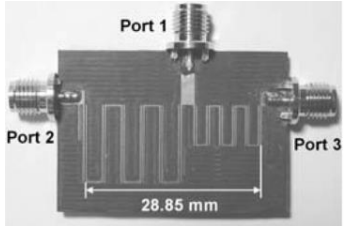
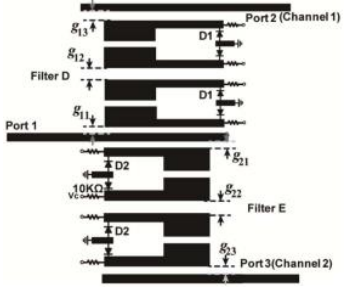
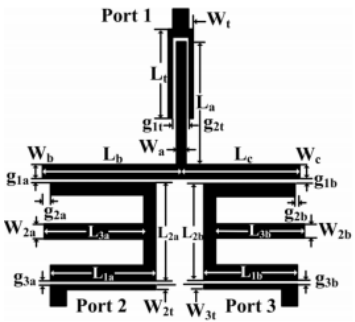
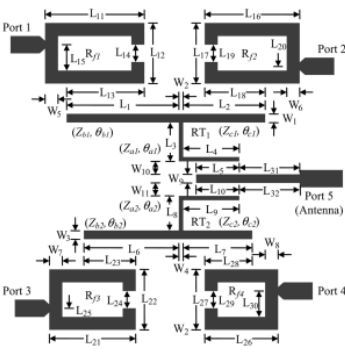
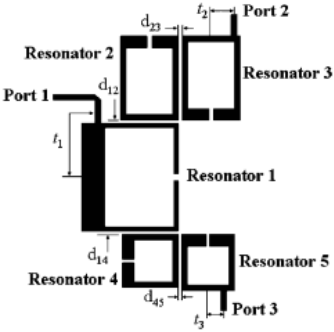
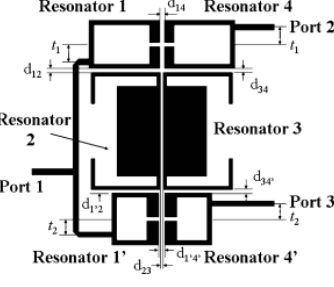
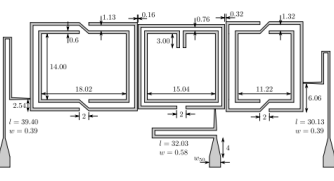
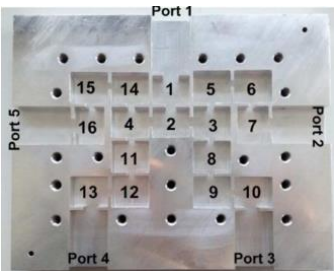
	$30.2 \times$ $21.2$	$3.4, 3.7$	One outer-band transmission zero
---	-------------------------	------------	-------------------------------------

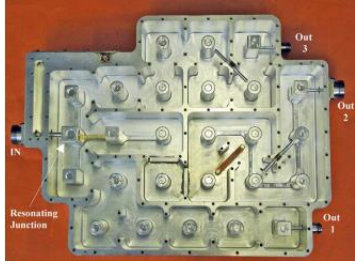
Table 2-2 Some reviewed diplexers/multiplexers and their features

Layout	Design	Junction type	Size	Frequency (GHz)	Isolation (dB)
 <p>[13]</p>	Diplexer	T-junction	$0.113\lambda_0 * 0.2\lambda_0$	1.8, 2.45	55
 <p>[29]</p>	Diplexer	T-junction	$0.67\lambda_0 * 0.35\lambda_0$	1.575, 2.4	30

 <p>[32]</p>	Diplexer	Hybrid couplers	Not shown	84, 93	Not shown
 <p>[11]</p>	Diplexer	Resonant T-junction	Not shown	10, 11.35	60
 <p>[35]</p>	Diplexer	Circulator	Not shown	2.85, 3.15	32
 <p>[49]</p>	Diplexer	Direct feed	$0.04\lambda_0$ $* 0.095\lambda_0$	4, 8	Not shown

 <p>[53]</p>	diplexer	Direct feed	$0.04\lambda_0$ $* 0.158\lambda_0$	Tunable frequencies and bandwidths	35
 <p>[54]</p>	Diplexer	Resonant T-junction	$0.36\lambda_0 * 0.38\lambda_0$	1.95, 2.14	30
 <p>[3]</p>	Multiplexer (4 channels)	Resonant T-junction	$0.16\lambda_0$ $* 0.154\lambda_0$	2, 2.2, 2.4, 2.6	Not shown

 <p>[55]</p>	Diplexer	Common resonant junction	$0.04\lambda_0$ $* 0.059\lambda_0$	1.5, 2.0	40
 <p>[55]</p>	Diplexer	Non-resonant T-junction	Not shown	1.5, 1.76	30
 <p>[56]</p>	Diplexer	Resonant T-junction	$0.234\lambda_0$ $* 0.09\lambda_0$	1.575, 1.925	Not shown
 <p>[59]</p>	Multiplexer (4 channels)	Resonant junction	Not shown	9.895, 9.965, 10.035, 10.105	Not shown

 <p>[64]</p>	Triplexer	Resonant junction	Not shown	0.707, 0.748, 0.787	Not shown
---	-----------	-------------------	-----------	---------------------------	-----------

## 2.6 Summary

In this chapter, a review of different types of diplexer implementation is presented, ranging from the conventional implementation to the MPFN (all resonator based) technique. It also covered different types of dual-mode resonators, expressing its application in microwave devices using microstrip technology. The application of dual-mode resonator as a resonant junction in the design of diplexers are also reviewed.

In the work presented in this thesis, dual-mode resonators were used for several purposes, for example: dual-mode resonator junctions in diplexers; a dual-mode resonant antenna junction in the duplexing antenna design; and dual-band filters.

# Chapter 3: Theory of Two-Port Filter Synthesis

This chapter presents the theoretical background and design methods used for the implementation of single-band and dual-band filters. It describes and derives the general filter synthesis, which can be applied to the implementation of coupled-resonator filters and the all-resonator based duplexers to be investigated in this thesis. This chapter will introduce the  $g$ -values of the lowpass prototype and coupling coefficients. The microstrip technology will also be briefly discussed. These are fundamental to the designs presented in the rest of this thesis.

## 3.1 Microstrip Line

A transmission line can be referred to as anything be it material or structure that has the capabilities of transferring energy from one point source to another point. The energy here may be electrical (power) energy, electromagnetic wave or acoustic wave. In electromagnetic or communications engineering, it is specialised cables or other medium designed for transferring electromagnetic wave and alternating currents of radio frequencies. The transmission line is an excellent example used in describing a distributed model, as the length of a transmission line often affects the operating frequency.

Transmission lines contribute a lot to RF circuit design due to the ease of manufacture, low cost and relatively small size. A few examples of transmission lines are the coplanar waveguide, coplanar strip, stripline, slotline, and microstrip line. The microstrip line is one of the most widely used. The microstrip technology is adopted in all the designs carried out in this thesis.

A microstrip is a conducting line (strip) with a width,  $w$  and a thickness,  $t$  which is attached to a dielectric material with the height,  $h$  and resting on a ground plane. A microstrip is illustrated in Fig. 3.1. It is well known and the most popular, particularly in the Microwaves Integrated Circuits (MICs) as well as in the Monolithic Microwave Integrated Circuits (MMICs). Its principal drawback is unintended radiation loss.

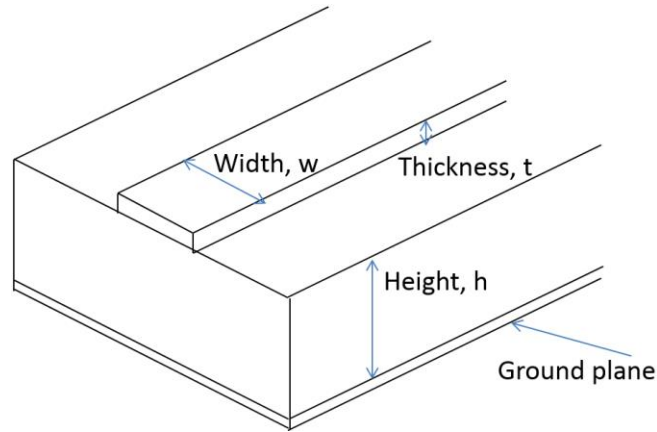


**Figure 3.1 Microstrip line**

In the implementation of a microstrip transmission line, it is vital to control the characteristic impedance ( $Z_0$ ) of the microstrip.

Provided that the height,  $h$  and dielectric constant  $\epsilon_r$  of a microstrip are known, the characteristic impedance  $Z_0$ , the line width corresponding to a specified  $Z_0$ , and the length of a full or half-wavelength microstrip resonator can be mathematically obtained [65].

The resonator may be folded into different shapes like hairpin to suit the purpose of use, such as compactness or access to coupling.

## 3.2 Coupling Matrix

The coupled resonator theorem has been widely presented in different works of literature for many applications. In filter design, a general technique can be applied to any resonator regardless of its physical structure [65]. This technique is based on the coupling matrix for coupled resonators which are arranged in a two-port network. In the works presented in this thesis, the coupled resonator filter theories are applied.

The general coupling matrix of a coupled resonator filter has been derived in [65, 118, 119]. A generalised solution has been provided for the electric and magnetic coupling even though they were separately considered during the derivation. If Kirchoff's voltage law is applied to magnetically coupled resonators, as shown in Fig. 3.2(a), its loop equations can be derived and presented in the impedance matrix form. In the case of electrically coupled resonators as shown



in Fig. 3.2(b), the Kirchoff's current law applies, node equations can be derived and presented in the admittance matrix form. It has been shown that both derivations have the identical form and a normalised matrix  $[A]$  regarding the coupling coefficients and external quality factors can be derived as presented in (3.1) [65].

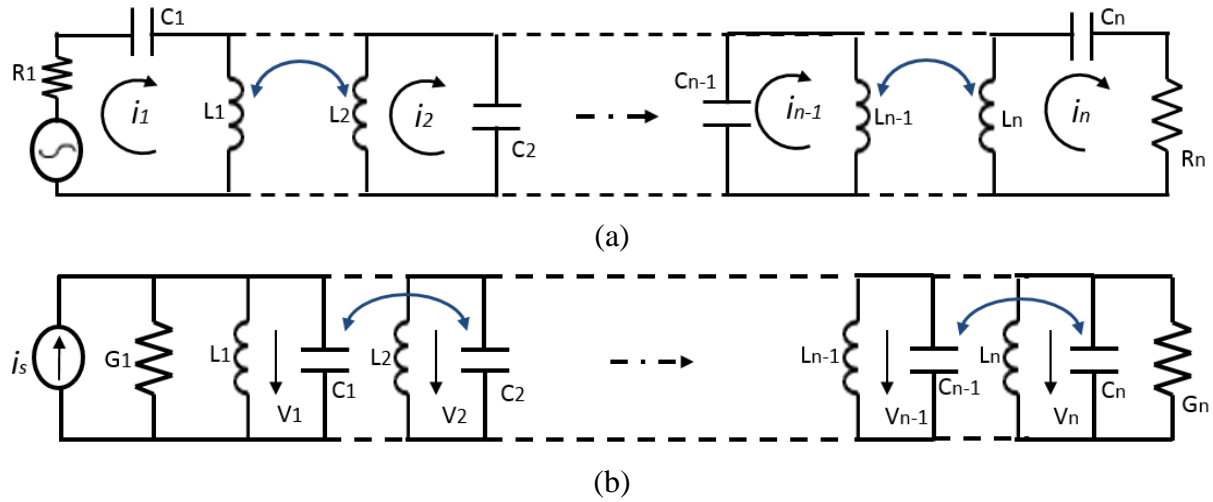


Figure 3.2 Circuit models for coupled resonator filters: (a) Magnetic coupling; (b) Electric coupling

$$[A] = \begin{bmatrix} \frac{1}{q_{e1}} & 0 & \cdots & \\ 0 & \ddots & & \vdots \\ \vdots & & 0 & \\ 0 & \cdots & \frac{1}{q_{en}} & \end{bmatrix} + p \begin{bmatrix} 1 & 0 & \cdots & \\ & 1 & & \vdots \\ \vdots & & \ddots & \\ 0 & \cdots & & 1 \end{bmatrix} - j \begin{bmatrix} m_{11} & m_{12} & \cdots & \\ & \ddots & & \vdots \\ \vdots & & & \\ m_{n1} & \cdots & & m_{nn} \end{bmatrix} \quad (3.1)$$

where  $q_{ei}$  is the scaled external quality factor ( $q_{ei} = Q_{ei} \cdot FBW$ ) for resonator  $i$ ,  $p$  is the complex low-frequency variable,  $m_{ij}$  is the normalised coupling coefficient ( $m_{ij} = M_{ij}/FBW$ ),  $m_{ii}$  represents the self coupling which allows the resonators to have different resonant frequencies.  $Q_{ei}$  is the quality external factor for the input and output ports and  $M_{ij}$  is the coupling coefficient between two resonators.

The transmission as well as the reflection scattering parameters can be expressed using the coupling matrix and the external quality factors as presented in (3.2).

$$S_{21} = \frac{2}{\sqrt{q_{e1} \cdot q_{en}}} [A]_{n1}^{-1} \quad (3.2 a)$$

$$S_{11} = \pm \left( 1 - \frac{2}{q_{e1}} [A]_{11}^{-1} \right) \quad (3.5 b)$$

The coupling matrix for coupled-resonator filters can be linked to the low-pass prototype. The lumped-element circuits with the cut-off frequency of 1 Rad/s with an input/output impedance of  $1 \Omega$  which represents the low-pass prototype filters have been widely reported [120]. The  $g$ -values which represent the inductance, capacitance, resistance and conductance of the circuit elements of the lowpass prototype filter, can be used in calculating the coupling coefficients and the external quality factors for coupled resonator bandpass filters. For an  $N^{\text{th}}$  order Chebyshev lowpass prototype filter having a passband ripple of  $L_{Ar}$  dB, its  $g$ -values may be extracted using the formulae (3.3) [65].

$$g_0 = 1$$

$$g_1 = \frac{2}{\gamma} \sin\left(\frac{\pi}{2N}\right)$$

$$g_i = \frac{1}{g_{i-1}} \frac{4 \sin\left[\frac{(2i-1)\pi}{2N}\right] \cdot \sin\left[\frac{(2i-3)\pi}{2N}\right]}{\gamma^2 + \sin^2\left[\frac{(i-1)\pi}{N}\right]} \quad \text{for } i = 2, 3, \dots, N \quad (3.3)$$

$$g_{N+1} = \begin{cases} 1 & \text{for } N \text{ odd} \\ \coth^2\left(\frac{\beta}{4}\right) & \text{for } N \text{ even} \end{cases}$$

where

$$\beta = \ln \left[ \coth \left( \frac{L_{Ar}}{17.37} \right) \right]$$

$$\gamma = \sinh \left( \frac{\beta}{2N} \right)$$

After obtaining the  $g$ -values of the lowpass prototype filter, the coupling matrix values and the external quality factors for a coupled resonator bandpass filter with a centre frequency of  $\omega_0$  and passband edges of  $\omega_1$  and  $\omega_2$  can be found as follows.

$$m_{i,i+1} = \frac{FBW}{\sqrt{g_i g_{i+1}}}, \text{ for } i = 1, 2 \dots N - 1 \quad (3.4)$$

$$Q_{e1} = \frac{g_0 g_1}{FBW}, \quad Q_{eN} = \frac{g_N g_{N+1}}{FBW} \quad (3.5)$$

where  $FBW$  is the fractional bandwidth and can be expressed as,

$$FBW = \frac{\omega_2 - \omega_1}{\omega_0}$$

### 3.3 Bandpass Filter Design Overview

A bandpass filter (BPF) is a microwave device which allows a wanted frequency to pass through it while rejecting the unwanted frequencies. A BPF can be designed from the lowpass filter parameters. By using a normalised third-order low-pass prototype filter (LPF) [121] as an example in Fig. 3.3, a BPF can be designed.

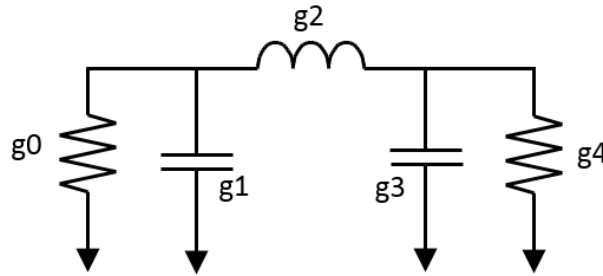


Figure 3.3 Normalised third-order low pass prototype filter

To transform a lowpass prototype response into a bandpass response having a passband-edge angular frequency of  $\omega_2 - \omega_1$ . The frequency transformation can be represented using (3.6) [65].

$$\Omega = \frac{\Omega_c}{FBW} \left( \frac{\omega}{\omega_0} - \frac{\omega_0}{\omega} \right) \quad (3.6)$$

where

$$\Omega_c = 1 \text{ rad/s}$$

$$\omega_0 = \sqrt{\omega_1 \omega_2}$$

$\omega_0$  is the centre angular frequency. When applied to the g-reactive element of the normalised lowpass prototype, we have an expression as described in (3.7).  $\Omega_c$  is a radian frequency variable of a lowpass prototype with a cut off frequency at  $\Omega = \Omega_c$  for  $\Omega_c = 1$ .

$$j\Omega g \rightarrow j\omega \frac{\Omega_c g}{FBW \omega_0} + \frac{1}{j\omega} \frac{\Omega_c \omega_0 g}{FBW} \quad (3.7)$$

This shows that an inductive/capacitive element  $g$  of the lowpass prototype can be transformed into a series/parallel LC resonant circuit of the bandpass filter. The essential element transformation can be performed using (3.8) and the transformation illustrated in Fig. 3.4. The final achieved circuit is displayed in Fig. 3.5.

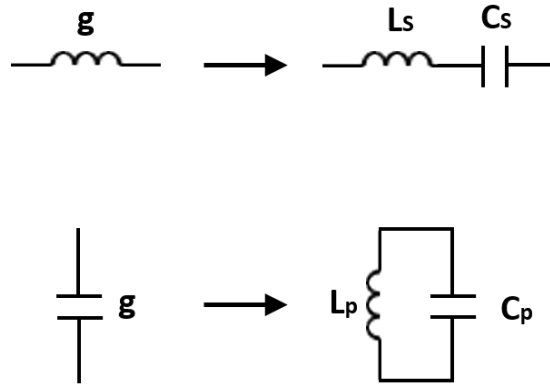


Figure 3.4 Lowpass prototype to bandpass transformation

$$L_S = \left( \frac{\Omega_c}{FBW \omega_0} \right) Y_0 g \quad (3.8 a)$$

$$C_S = \frac{1}{\omega_0^2 L_S} \quad (3.8 b)$$

$$C_P = \left( \frac{\Omega_c}{FBW \omega_0} \right) \frac{g}{Y_0} \quad (3.8 c)$$

$$L_P = \frac{1}{\omega_0^2 C_P} \quad (3.8 d)$$

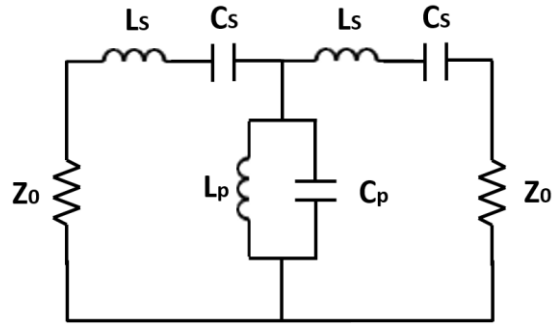


Figure 3.5 Third-order single mode Band Pass Filter

### 3.4 Dual-band Filter Design Theory

The dual-band BPF is a microwave filtering device that can pass two wanted frequencies while rejecting the unwanted ones. It performs the same function of two single bandpass filters which makes it more desirable to be used in a congested network system as it reduces the number of required filters. Different work has demonstrated different ways of achieving a dual-band bandpass filter. It normally starts from a normalised lowpass filter, then to a bandpass filter and finally to a dual-band BPF [122]. It can also be achieved by integrating one wideband filter and one notch band filter [123].

The transformation steps taken to achieve a dual-band BPF from a normalised lowpass filter is presented below. Using a normalised third-order low-pass prototype filter (LPF) [124], as shown in Fig. 3.6 as an example, with a ripple factor of 0.043 dB having  $g_0 = g_4 = 1.0$ ,  $g_1 = g_3 = 0.8516$  and  $g_2 = 1.1032$ . The dual-band BPF is designed to have centre frequency of lower and upper passbands of 1747 MHz and 1879 MHz with FBW of 4.3% each and passband return loss of 20 dB. By applying admittance inverters (J-inverter) using (3.9) to the normalised LPF, the circuit is made to contain only shunt reactive components. This process allows all the low pass filter parameters to be equal to  $g_1$  as shown in Fig. 3.7.

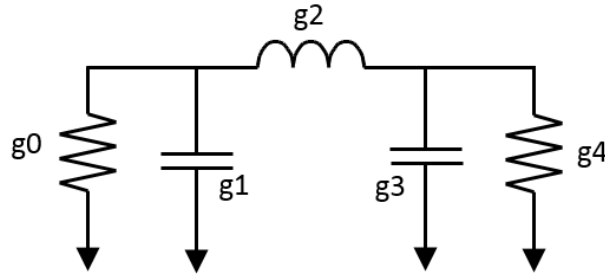


Figure 3.6 Normalised third-order low pass prototype filter

$$J_{01} = J_{n,n+1} = 1 \quad (3.9 a)$$

where  $n$  is the order of the low pass filter.  $n = 3$ . For  $1 \leq m < n$ ,

$$J_{m,m+1} = \sqrt{\frac{g_1^2}{g_m g_{m+1}}} \quad (3.9 b)$$

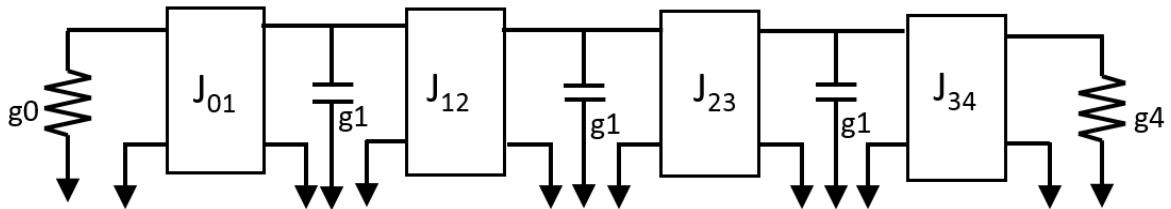


Figure 3.7 Normalised low pass filter with only shunt reactive components

The shunt reactive components (capacitor) are at this stage transformed into a dual-band BPF component by transforming each of the capacitors into two shunt LC resonators with one being a series type and the other a parallel type. The transformation step is presented in Fig. 3.8, while its capacitance and inductance values can be obtained using (3.10).

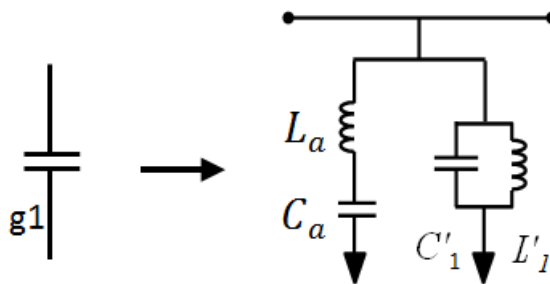


Figure 3.8 Low-pass to dual-band bandpass transformation

$$L_a = \frac{FBW_0 Z_0}{g_1 \omega_c (\omega_2 - \omega_1)} \quad (3.10 a)$$

$$C_a = \frac{1}{L_a \omega_0^2} \quad (3.10 b)$$

$$L'_1 = \frac{FBW_0(\omega_2 - \omega_1)Z_0}{g_1 \omega_c \omega_0^2} \quad (3.10 c)$$

$$C'_1 = \frac{1}{L'_1 \omega_0^2} \quad (3.10 d)$$

where  $\omega_c = 1$  rad/s and represents the cut-off angular frequency of the prototype low-pass filter,  $\omega_0$  is the centre angular frequency  $\omega_0 = \sqrt{\omega_1 \omega_2}$ ,  $\omega_1$  is the centre angular frequency of the first passband,  $\omega_2$  is the centre angular frequency of the second passband,  $FBW_1$  is the fractional bandwidth for each of the passbands and  $FBW_0$  is defined as the dual-band BPF fractional bandwidth, and it can be obtained as follows for narrow bands (that is:  $FBW_0 < 0.1$ ).

$$FBW_0 = FBW_1 \left( \frac{\omega_2 + \omega_1}{\omega_2 - \omega_1} \right) \quad (3.13 e)$$

The impedance scaling can be achieved using (3.11), where  $Z_0$  is the system impedance measured in ohms ( $\Omega$ ). The completed dual-band BPF circuit is presented in Fig. 3.9.

$$J'_{m,m+1} = \frac{J_{m,m+1}}{Z_0} \quad (3.11)$$

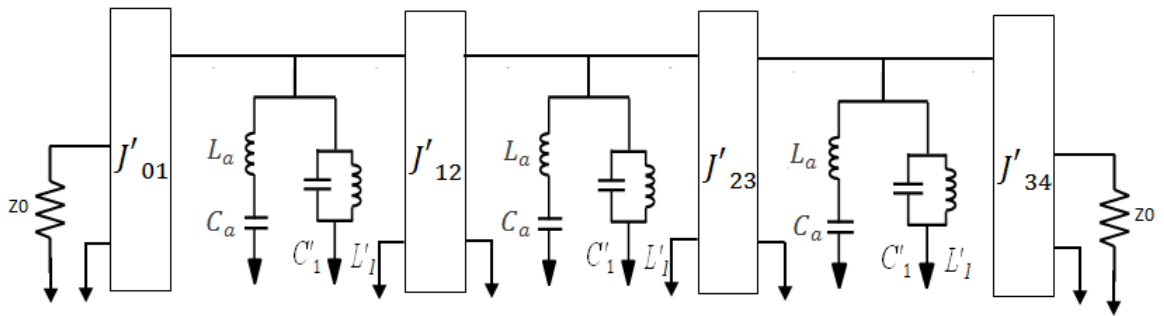


Figure 3.9 Dual-band BPF with shunt LC resonators

The dual-band BPF presented in Fig. 3.9 can be transformed into a dual-band BPF circuit model with coupled resonators if needed. The transformation can be achieved if the mixed series-parallel dual-resonator circuit is transformed into two resonators of the same type (parallel

type) coupled through a unity J-inverter ( $J = 1 \text{ S}$ ) [122]. Fig. 3.10 presents the transformation pattern used and the final circuit model is shown in Fig. 3.11(a). Fig. 3.11(b) illustrates the coupling path of the dual-band BPF. At this stage, it is noted that Fig. 3.9 can be used for dual resonator implementation whereas Fig. 3.11(a) is used for coupled resonator pair implementation. The coupling coefficients and the external quality factors can be calculated from the circuit model using (3.12), (3.13) and (3.14) [119]. Table 3.1 shows the calculated values used for the design and Fig. 3.12 shows the calculated response of the dual-band BPF in thick lines and the simulated response in dashed lines.

$$M_{1,1'} = M_{2,2'} = M_{3,3'} = J \sqrt[4]{\frac{L'_1 L_a}{C'_1 C_a}} \quad (3.12)$$

$$M_{1,2} = M_{2,3} = J'_{12} \sqrt{\frac{L'_1}{C'_1}} \quad (3.13)$$

$$Q_{ex} = \frac{\omega_0 C'_1}{J'_{01}} \quad (3.14)$$

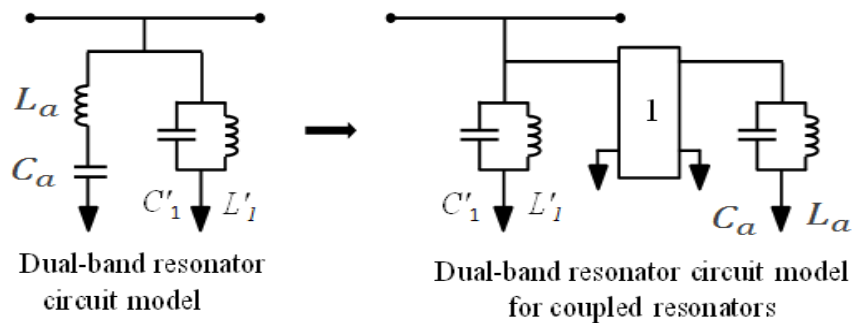
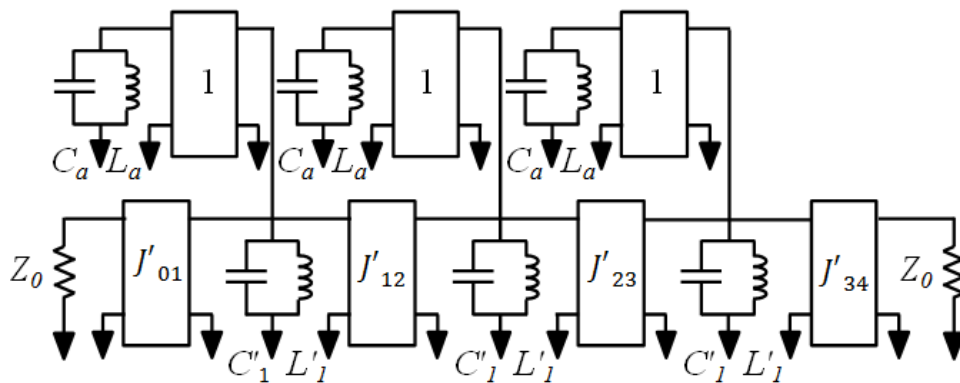


Figure 3.10 Dual-band BPF coupled resonator pair circuit model transformation



(a)



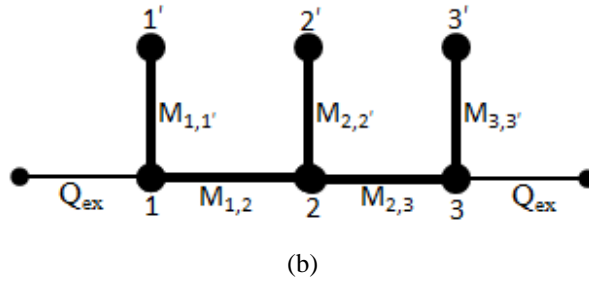


Figure 3.11 (a) Dual-band circuit model; (b) Dual-band coupling path

Table 3-1 Circuit model parameters

$L'_1/\text{nH}$	0.4435		$L_a/\text{nH}$	0.093
$C'_1/\text{pF}$	17.3932		$C_a/\text{pF}$	82.659
$J_{01} = J_{34}$	0.02		$M_{11}$	0.073
$J_{12} = J_{23}$	0.018		$M_{12}$	0.089
$J_{119}$	1		$Q_{ex}$	9.902

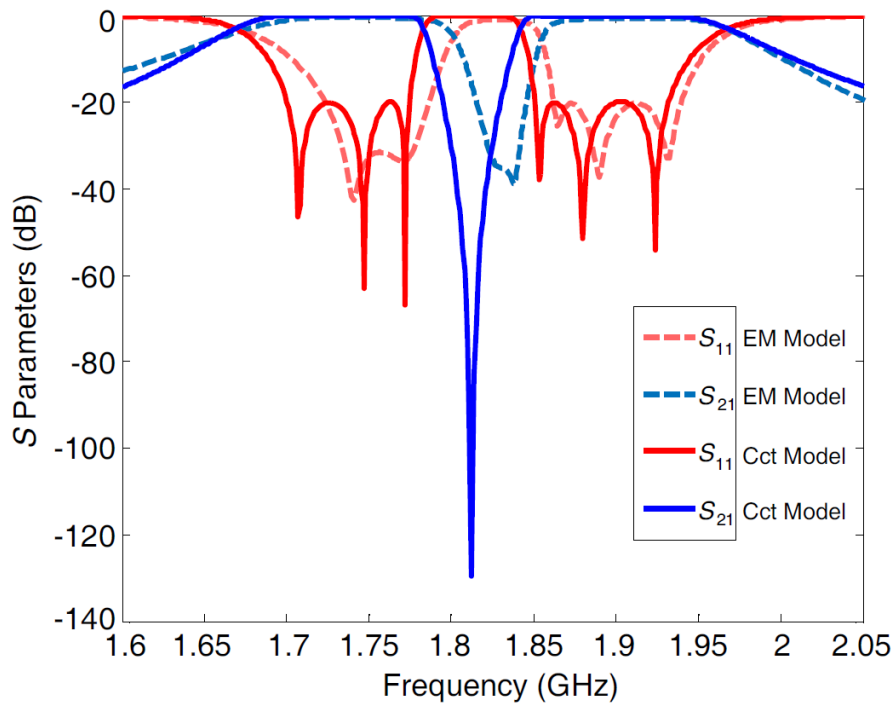


Figure 3.12 Dual-band BPF responses from the circuit models and EM simulations

### 3.5 A Microstrip Implementation Example

The circuit layout of Fig. 3.11(a) can be realised using the microstrip technology in a coupled resonator pair configuration. Here, the U-shaped microstrip resonators were used in a parallel configuration. The coupling coefficients of the resonator configuration were first extracted using the arrangements of two U-shaped resonators as shown in Fig. 3.13(a) and (b). The coupled resonators resemble one dual-mode ‘cluster’ resonator which can be considered as a dual-band resonator. The coupling coefficients of  $M_{1,1'}$ ,  $M_{2,2'}$  and  $M_{3,3'}$  were extracted by varying the spacing ( $S$ ) between the two U-shaped resonators. A graph of the coupling coefficient against  $S$  was plotted in Fig 3.13(a) with an inset of the topology used. To determine the coupling coefficients of  $M_{1,2}$  and  $M_{2,3}$ , the configuration in Fig. 3.13(b) was simulated. The coupling coefficient against the spacing  $S_1$  is also illustrated.

To obtain the external quality factor at the input and output (I/O), an arrangement was set up as shown in Fig. 3.14. At Port-1, a 50 Ohm feed line is tapped to the first resonator whereas Port-2 is weakly coupled to the resonator to remove the external coupling at Port-2. The tapping point of the feeder line as defined by  $Y$  on the resonator was adjusted. The length  $X$  of the resonator was reduced; this is to compensate the loading effect from the tapped feeder.

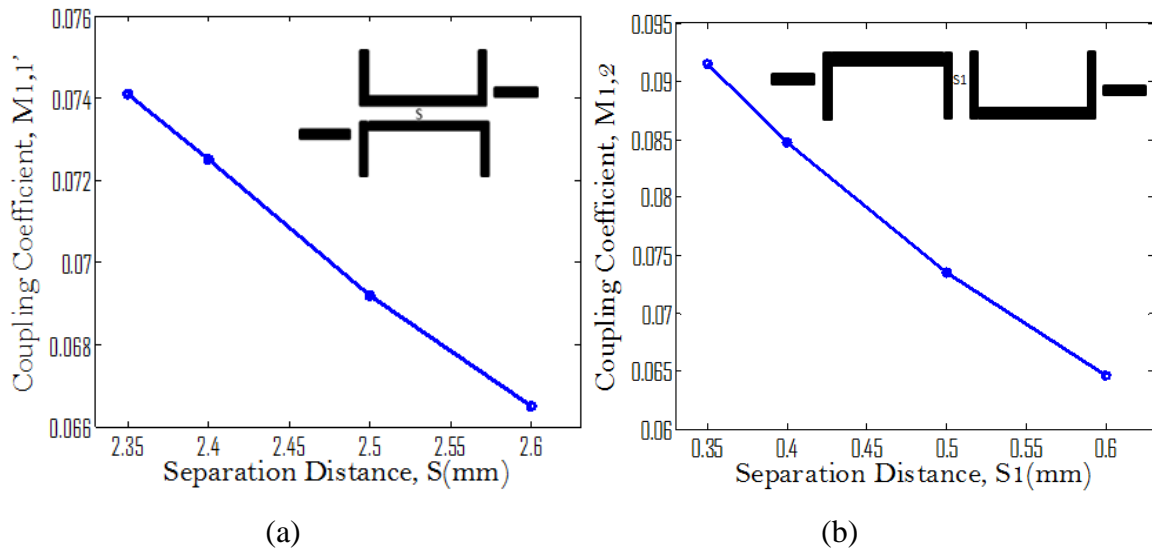


Figure 3.13 (a) Coupling of  $M_{1,1'}$  against spacing ( $S$ ); Coupling of  $M_{12}$  against spacing ( $S_1$ )

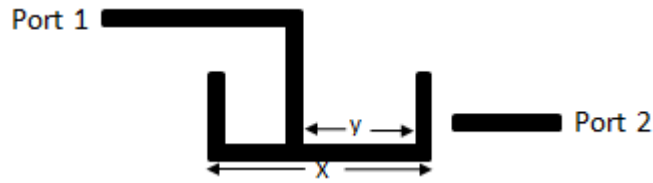


Figure 3.14 Resonator arrangement for extracting  $Q_{ex}$

After extracting and satisfying the parameters needed for the design of the dual-band bandpass filter, the entire layout was put together as shown in Fig. 3.15. After optimisation, the simulated responses of the EM model were presented using dashed lines as shown in Fig. 3.16 as well as in Fig. 3.12.

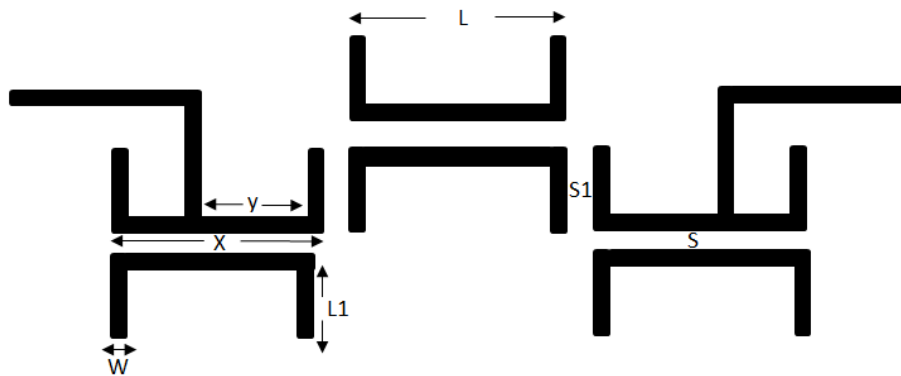


Figure 3.15. Dual-band microstrip filter layout.  $L = 17.2$  mm,  $L_1 = 6.8$  mm,  $W = 1.126$  mm,  $X = 17$  mm,  $S = 2.4$  mm,  $S_1 = 0.35$  mm,  $Y = 12$  mm.

RT/Duroid 6010LM substrate from Rogers® was used for the fabrication. The dielectric constant of the material is 10.2 with a loss tangent of 0.0035 and a thickness of 1.27 mm. Fig. 3.17 shows the fabricated prototype with input and output port connected and in comparison with one pound coin. A comparison of the simulated and measured response is shown in Fig. 3.16. A reasonably good agreement is achieved at both passbands with a return loss close to 20 dB. Due to the machining tolerance, the measured responses can be seen shifted to the higher frequency by 40 MHz. The minimum measured insertion loss in the passband is less than 2 dB.

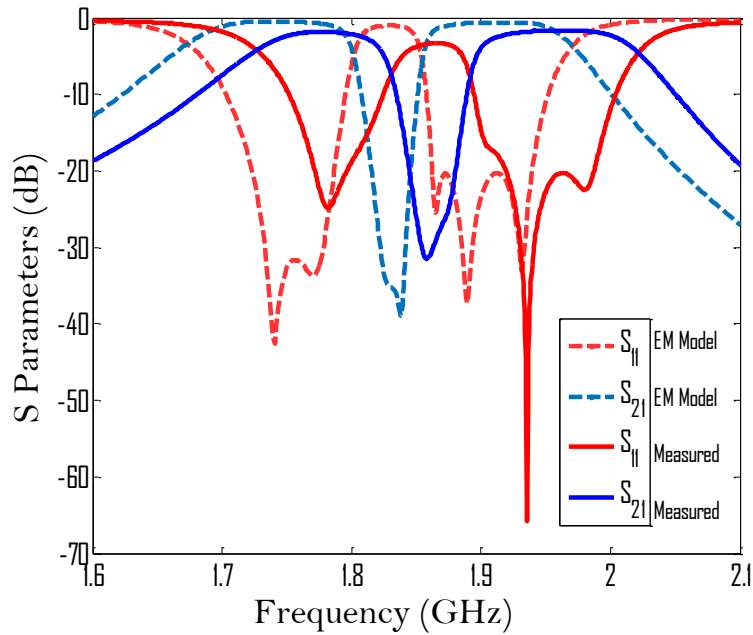


Figure 3.16. Simulated and measured responses.

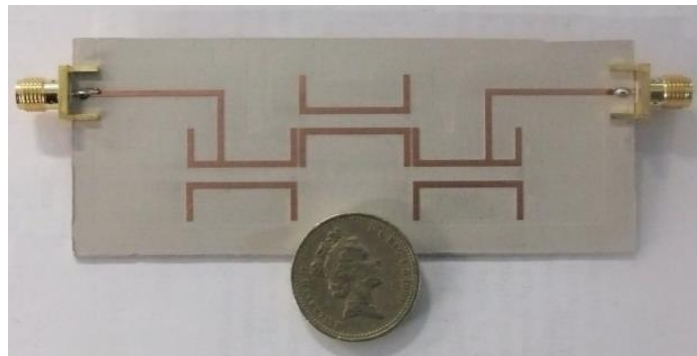


Figure 3.17. Fabricated microstrip dual-band filter.

The method to extract the coupling coefficients and external quality factor as well as the general microstrip implementation technique, as demonstrated in this section, will also be applied to the other designs in this thesis.

## Summary

This chapter has demonstrated the theoretical background of two-port filter network. The realisation of the coupling matrix and the quality external factor that can be applied in the design of two-port filters are derived. The realisation of  $g$ -values of normalised low pass filters of Chebyshev response is also presented. These parameters are the fundamental bedrock of the

conventional lumped element two-port filters. The lumped elements of the normalised low pass filter are used to derive the theoretical background and design methods used for the implementation of single-band and dual-band filters. As an extension, this theory extended the lumped element dual-band bandpass filter to the all coupled-resonator technology which is to be investigated in this thesis.

# Chapter 4: Transmission Line Junction versus Resonator Junction in Diplexers – A Comparative Study

In this chapter, a comparison of a diplexer with a conventional transmission line junction and a diplexer with a resonant junction based on the multi-port filtering network (MPFN) concept is presented. The comparison between the two diplexers is drawn between their topology, sizes, rejection, isolation and current density distribution.

## 4.1 Design of the Conventional Diplexer

A conventional non-resonant T-junction diplexer [125, 126] and a diplexer with a resonant junction [63, 127, 128] is designed and compared. Both diplexers are designed to operate at 1.8 GHz and 2.1 GHz with 4% fractional bandwidth and 20 dB return loss. To achieve the designs, two channel filters operating at 1.8 GHz and 2.1 GHz were first separately designed to specifications using hairpin resonators. For the conventional diplexer, the two channel filters were joined using a T-junction transmission line followed by optimisation to meet the required specifications. Fig. 4.1 presents the coupling topology used for the design.

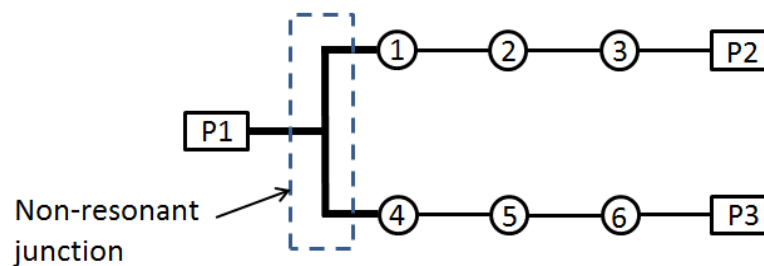


Figure 4.1 Coupling topology of a diplexer with a transmission-line T-junction

To design the non-resonant T-junction transmission line, two asymmetric line sections are used. The line section connected to one channel filter is around quarter-wavelength long at the centre frequency of the opposite channel and vice versa. The T-junction is essentially an impedance matching network. Fig. 4.2 shows the layout and dimensions of the T-junction and the diplexer after optimization.

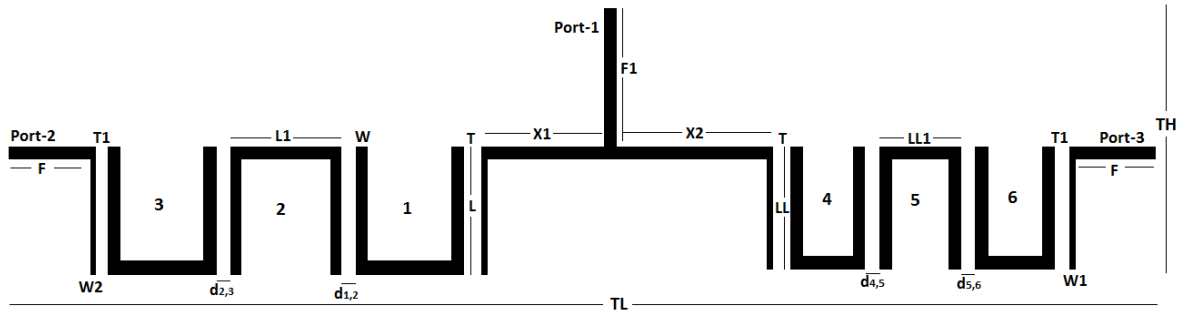


Figure 4.2 Conventional T-junction diplexer.  $F = 10\text{mm}$ ,  $F1 = 13.7\text{mm}$ ,  $X1 = 13.8\text{mm}$ ,  $X2 = 17.6\text{mm}$ ,  $T = 0.3\text{mm}$ ,  $T1 = 0.4\text{mm}$ ,  $W = 1.2\text{mm}$ ,  $W1 = 0.6\text{mm}$ ,  $W2 = 0.6\text{mm}$ ,  $L = 11.5\text{mm}$ ,  $L1 = 9.95\text{mm}$ ,  $LL = 11\text{mm}$ ,  $LL1 = 6.59\text{mm}$ ,  $d_{1,2} = 1.77\text{mm}$ ,  $d_{2,3} = 1.77\text{mm}$ ,  $d_{4,5} = 1.75\text{mm}$ ,  $d_{5,6} = 1.75\text{mm}$ ,  $TH = 25.2\text{mm}$ ,  $TL = 124.28\text{mm}$ .

## 4.2 Design of the Resonant Junction Diplexer

To achieve the diplexer with a resonant junction, the two individually designed channel filters were asynchronously coupled together using the first resonators of each channel filter, and their external Q factor was determined using the general filter synthesis. In the process, one feed line was removed to allow both channel filters share one input feed line for receiving and transmitting functions. The technique used resulted in a compact circuit topology and the diplexer having an all-resonant structure as presented in Fig. 4.3.

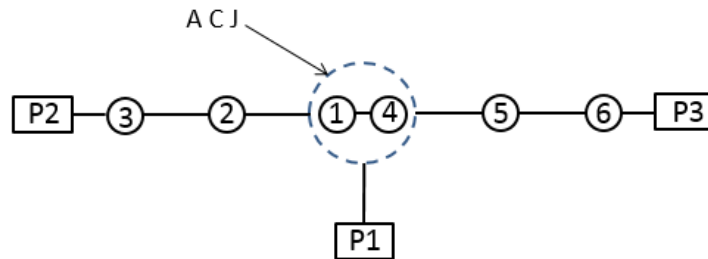


Figure 4.3 Coupling topology of a diplexer with an asynchronously coupled resonant junction (ACJ)

The dashed circle marks out the asynchronously coupled junction (ACJ) which comprises the first resonators of both channel filters. The ‘asynchronous’ in the name refers to the two coupled resonators with different inherent resonant frequencies, corresponding to the two channels respectively. The ACJ does the signal splitting and combining in the diplexer circuitry. Fig. 4.4 presents the frequency responses of the two coupled resonators against their separation,  $d_{1,4}$ .

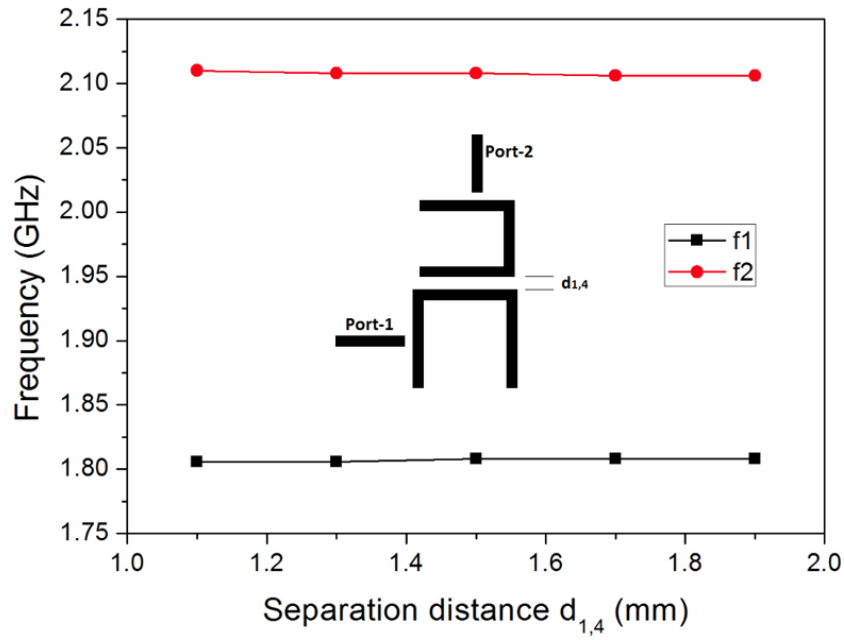
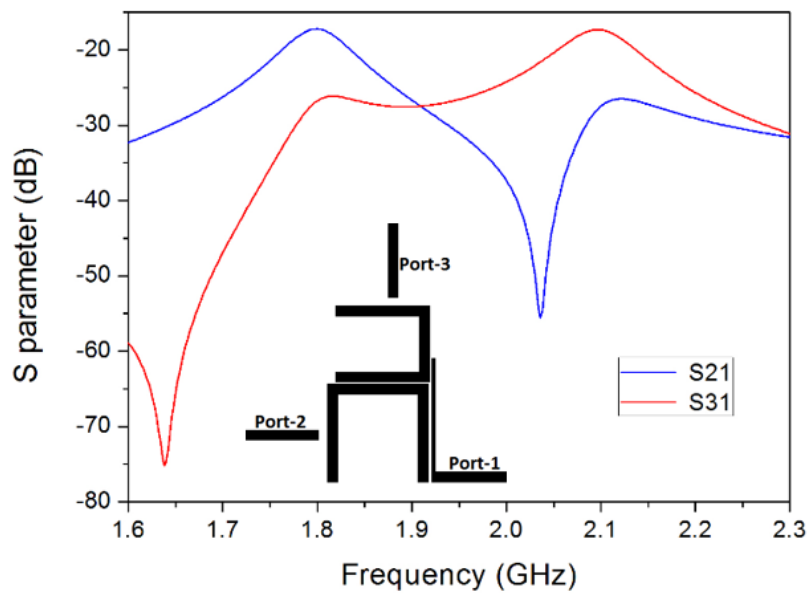


Figure 4.4 Resonant frequencies of the ACJ with an inset of topology used

To achieve the  $Q_{\text{ext}}$  factor for the ACJ, a coupled feed line technique [86, 129, 130] was used to feed the resonators at port-1 as shown in Fig. 4.5. Port-2 and port-3 were weakly coupled to the resonators while the coupling gaps, width and length at port-1 were adjusted. Fig. 4.5(a) presents the typical frequency response. Fig. 4.5(b) presents the simulated current distribution of the ACJ at 1.8 GHz and 2.1 GHz. It is evident that at the operating frequencies, the ACJ directed the signal to different channels.



(a)



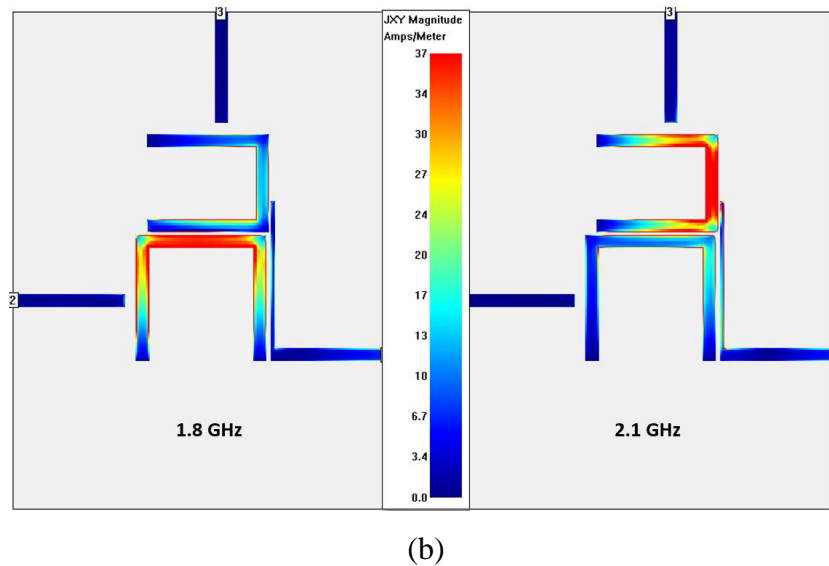


Figure 4.5 (a) Simulated typical response of the configuration used to extract the  $Q_{ext}$ ; (b) Current distribution

At this point, the corresponding channel filters are coupled to their associated resonant pole of the ACJ. Layout optimisation is performed to meet the design specifications.

## 4.3 Comparison

### 4.3.1 Size

After matching the simulated responses of the non-resonant T-junction diplexer and the resonant junction diplexer, a comparison between them can be drawn. Fig. 4.2 and Fig. 4.6 present the two diplexer layouts respectively. The physical dimensions achieved after optimisation are given in the caption. It can be seen that the diplexer with the resonant junction is more compact than the diplexer with a non-resonant T-junction. This is due to the elimination of the non-resonant T-junction.

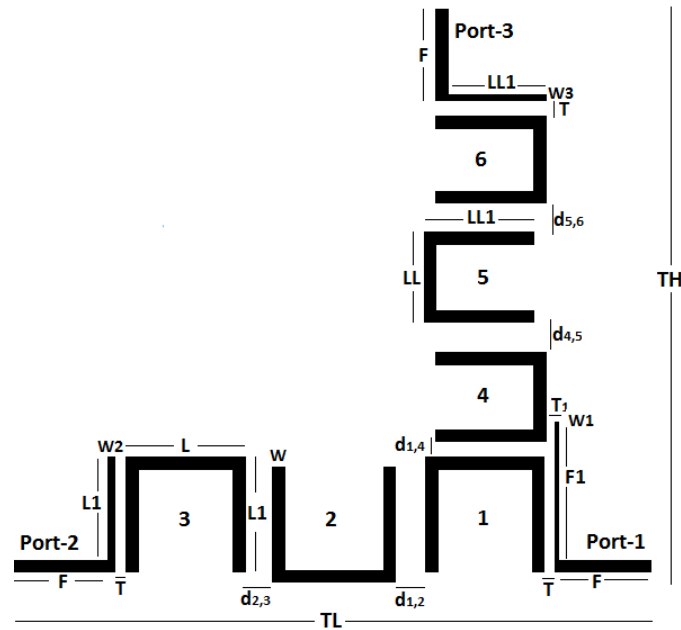


Figure 4.6 Resonant junction diplexer.  $F = 10\text{mm}$ ,  $T = 0.4\text{mm}$ ,  $T1 = 0.2\text{mm}$ ,  $W = 1.2\text{mm}$ ,  $W1 = 0.4\text{mm}$ ,  $W2 = 0.6\text{mm}$ ,  $W3 = 0.6\text{mm}$ ,  $L = 9.6\text{mm}$ ,  $L1 = 11.5\text{mm}$ ,  $LL = 6.6\text{mm}$ ,  $LL1 = 11\text{mm}$ ,  $d1,2 = 1.7\text{mm}$ ,  $d1,4 = 0.2\text{mm}$ ,  $d2,3 = 1.7\text{mm}$ ,  $d4,5 = 1.65\text{mm}$ ,  $d5,6 = 1.7\text{mm}$ ,  $TH = 65\text{mm}$ ,  $TL = 61.5\text{mm}$ .

### 4.3.2 Rejection and Isolation

The simulated frequency response of the conventional diplexer is shown in Fig. 4.7 in comparison with the simulated frequency response of the diplexer using the resonant ACJ. The bandwidths are seen to match each other. The insertion losses are the same while the return losses meet the 20 dB mark.

The rejections at the high passband frequency in both diplexers are very similar. The ACJ offers slightly higher rejection due to a transmission zero at 2.02 GHz. At the low passband frequency, the T-junction offers better rejection mainly due to a transmission zero generated at 1.85 GHz.

Fig. 4.8 presents the isolation  $S_{32}$  for both diplexers. It indicates that both isolations are better than 43 dB. At the low pass band, the conventional diplexer is at about 55 dB while the resonant ACJ has a lower isolation of 43 dB.

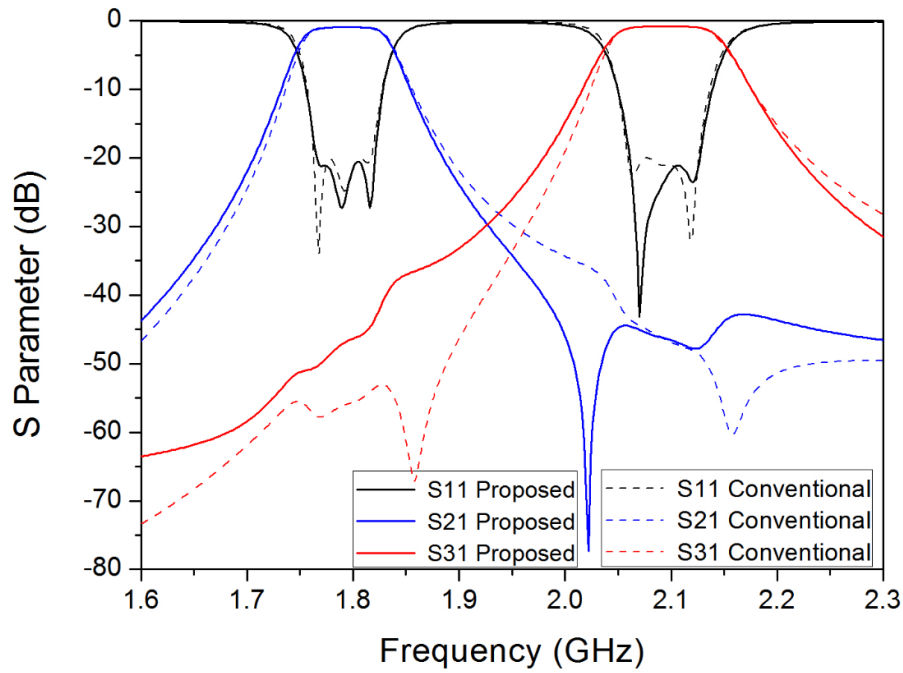


Figure 4.7 Simulated response of the conventional diplexer and resonant junction diplexer

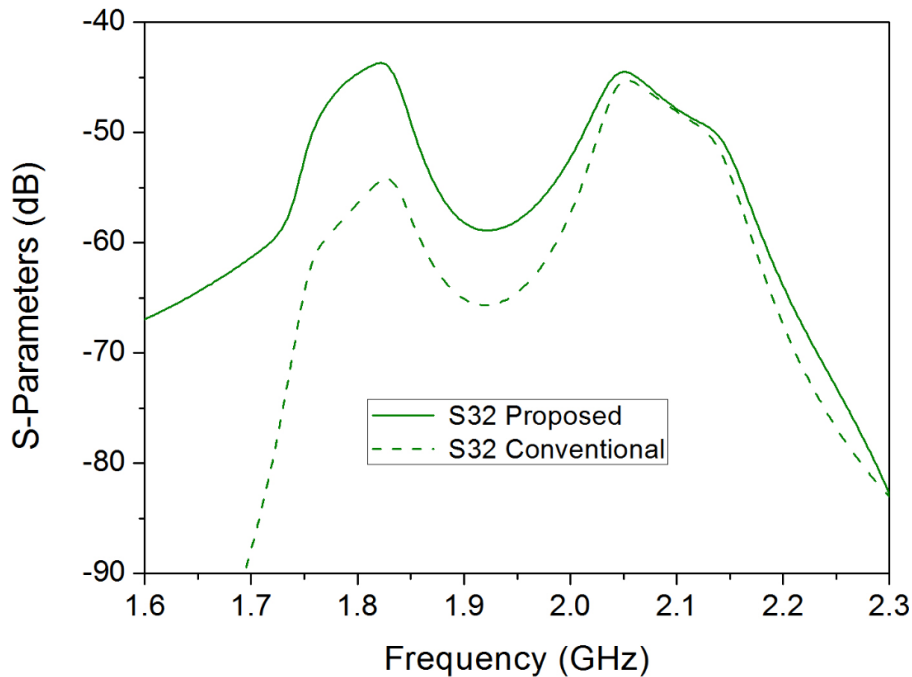


Figure 4.8 Simulated isolation response of the conventional diplexer and resonant junction diplexer

To realise the design, both diplexers were fabricated using the Rogers 3010 substrate with a thickness of 1.27mm, a relative permittivity of 10.8 and a loss tangent of 0.0022 and are presented in Fig. 4.9. Measurements were taken using the Agilent Network Analyser N5230A and compared with each other. Fig. 4.10 presents the measured responses. It can be noticed

that a good agreement is achieved between the two diplexers. Measurements also agree well with the simulations. The frequency shifts between the measured and simulated responses are due to fabrication errors and the variation of the dielectric constant.

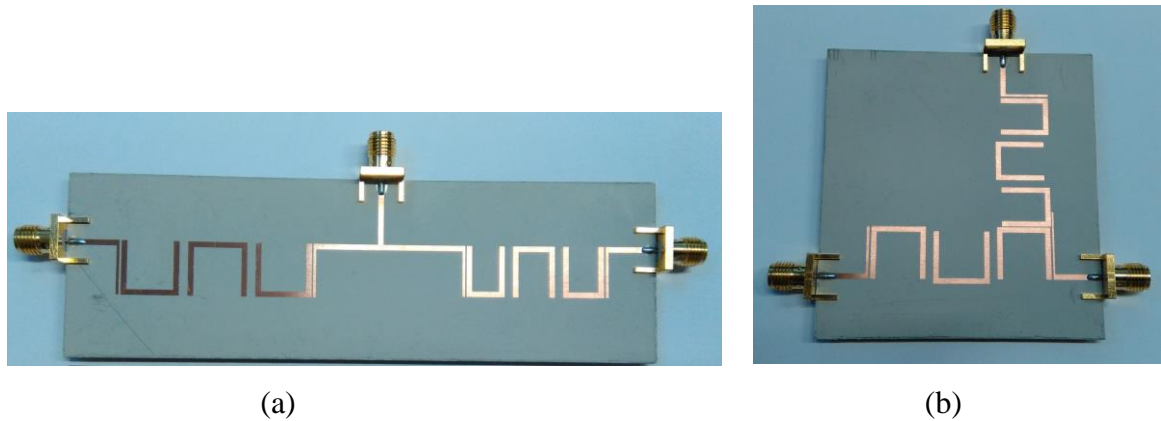


Figure 4.9 Fabricated designs: (a) Conventional T-junction diplexer; (b) Coupled resonant Junction diplexer

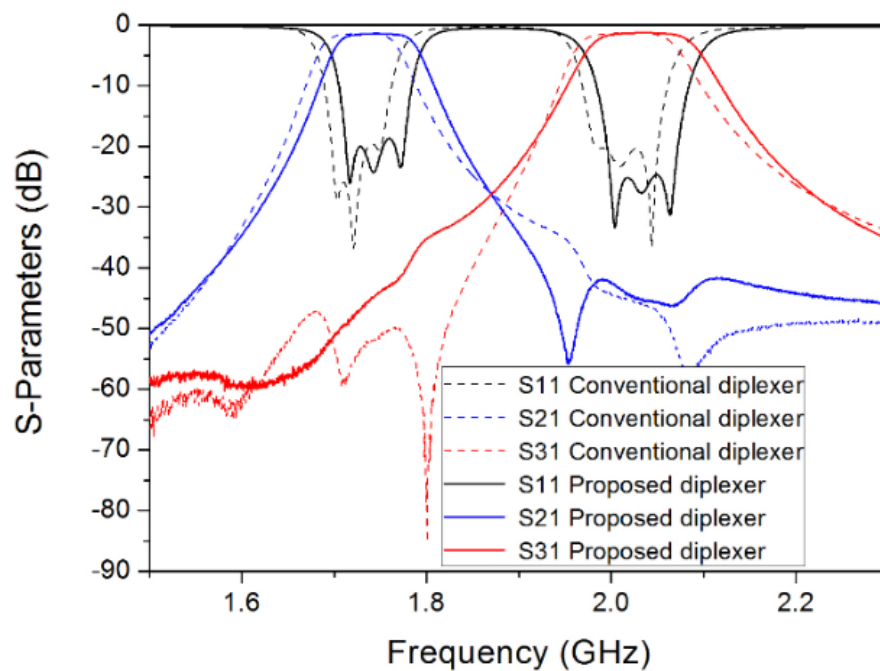


Figure 4.10 Measured frequency responses of the two diplexers

### 4.3.3 Current Density Distribution and Implication on Power Handling

The current distributions of both diplexers are simulated and presented in Fig. 4.11. By comparing the current density, the power handling capability of the diplexers was investigated.

To carry out this investigation, the 1.8 GHz channel of both diplexers were excited and the current density distribution across the microstrip line collected from the middle of the channels at the circled area in Fig. 4.11. The current density distribution at 2.1 GHz was also collected from the circled areas in the high channels. A plot of the distribution at 1.8 GHz of the diplexer with ACJ is presented in Fig. 4.12(a) in comparison with that of the conventional T-junction diplexer. It shows that the T-junction diplexer has slightly higher current density. The same observation can be made at 2.1 GHz as shown in Fig. 4.12(b). This seems to indicate the ACJ diplexer may have slightly higher power handling capability. It is worth mentioning that the limitation imposed by the simulation software used for this investigation could not allow for accurate values of the current density as it is highly dependent on the size of the subsections. In this investigation, the smallest subsection used is 0.01 mm and the comparison was made when the same subsection is used for both diplexers. Although it is difficult to draw a definitive conclusion about the current density and the implied power handling, the comparison does show, at least, there is a slight difference in the current distribution when the resonant junction is used to replace the transmission line junction.

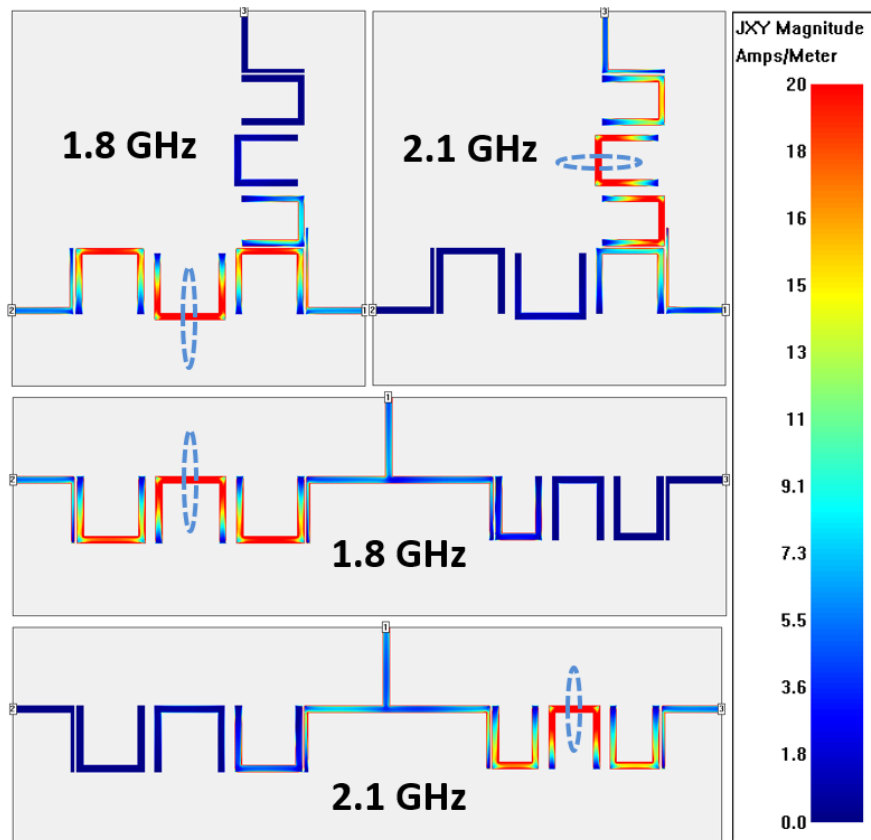
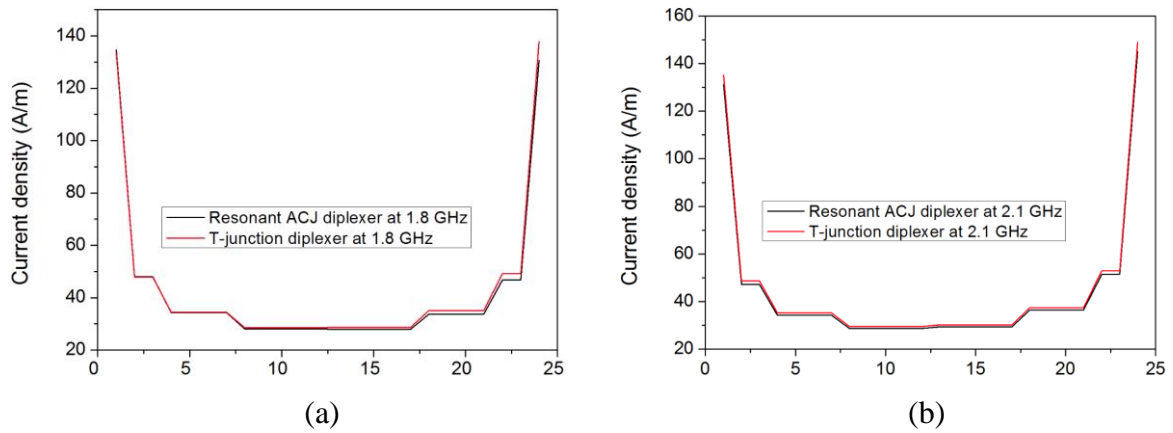


Figure 4.11 Simulated current distribution of the two diplexers, plotted using the same current density scale.



**Figure 4.12 Simulated current density distribution across the microstrip lines at the circled areas of Fig. 4.11: (a) 1.8 GHz; (b) 2.1 GHz. The range of the X-axis is proportional to the width of the microstrip line.**

## 4.4 Summary

In this chapter, the conventional diplexer based on a transmission-line T junction and the resonant junction diplexer based on the MPFN concept has been compared in terms of their physical dimensions, current distribution and the frequency responses. It is evident the ACJ based diplexer has a more compact structure by the elimination of the transmission line junction. However, in this case study, this is at a cost of rejection and isolation at the low band as shown in Fig. 4.7 and Fig. 4.8. An improved rejection and isolation may be achievable by further optimisation of the coupling and the structure around the junction. Although the finding of this comparison does not dictate a limitation of the junction resonator in the diplexer, it is plausible to highlight the potential challenge about the rejection and isolation in the design of diplexers and multiplexers based on the MPFN concept with junction resonators.

# Chapter 5: Diplexers and Filters using Patch Resonators

This chapter presents an investigation of patch resonators into three designs - a bandpass filter, a dual-band bandpass filter and a diplexer. It also looks into the behaviours, and the role the dual-mode patch resonator plays in the implementation of these designs. The microstrip technology is used due to its low cost, ease of manufacture and low profile. As discussed in Chapter 2, a square patch resonator has a dual-mode property, which means that it resonates at two orthogonal frequencies. The two degenerate frequencies of the patch resonator are explored in the works carried out in this chapter.

In the BPF implementation, a three-pole 2.6 GHz Chebyshev filter is designed using a mixture of hairpin and patch resonators. One mode of the patch resonator is used to couple with two hairpin resonators while the other mode provides the transmission zero to have improved the frequency selectivity of the filter.

The dual-band bandpass filter utilised the square patch resonator as a signal combiner and splitter. The orthogonal mode of the patch when fed through a common port, allows the patch to function as a signal splitter or combiner. With these properties of the patch resonator, the dual-band bandpass filter is designed to have dual coupling paths.

In the diplexer implementation, the patch resonator is also used for signal splitting and combining. The channel filters share the patch resonator which in return contributed to the resonant poles of the filter. This technique used in this work resulted in a reduced circuit size from a supposedly six resonators to five resonators.

First, the properties of a patch resonator will be discussed.

## 5.1 Properties of a Patch Resonator

The square patch resonator is a dual-mode resonant structure. It has two degenerate modes of a geometrically symmetrical resonator. The dual-mode square patch resonators have been

widely used in the realisation of many RF/microwave filtering devices [131, 132]. This is mainly based on its feature as to be used as a doubly tuned resonant circuit, and moreover the halving of the required number of resonators in a circuit leading to a compact circuit arrangement.

The characteristic of a square patch resonator is already presented in Chapter 2. A detailed guide on how to realise the coupling between the orthogonal modes as well as the  $Q_{\text{ext}}$  of the resonator is presented in this section using a square patch resonating at 3.99 GHz and 4.39 GHz.

- **Square resonator with one mode excited**

The concerned centre frequency ( $f_0$ ) of the square patch is defined by (5.1). (2.1) is then used to calculate the electrical dimension (D) of the square resonator.

$$f_0 = \frac{f_1 + f_2}{2} = 4.185 \text{ GHz} \quad (5.1)$$

Using the Sonnet EM simulator, the electrical dimension was simulated and optimised to the specification of  $f_0$  as presented in Fig. 5.1. The current distribution is presented in Fig. 5.2.

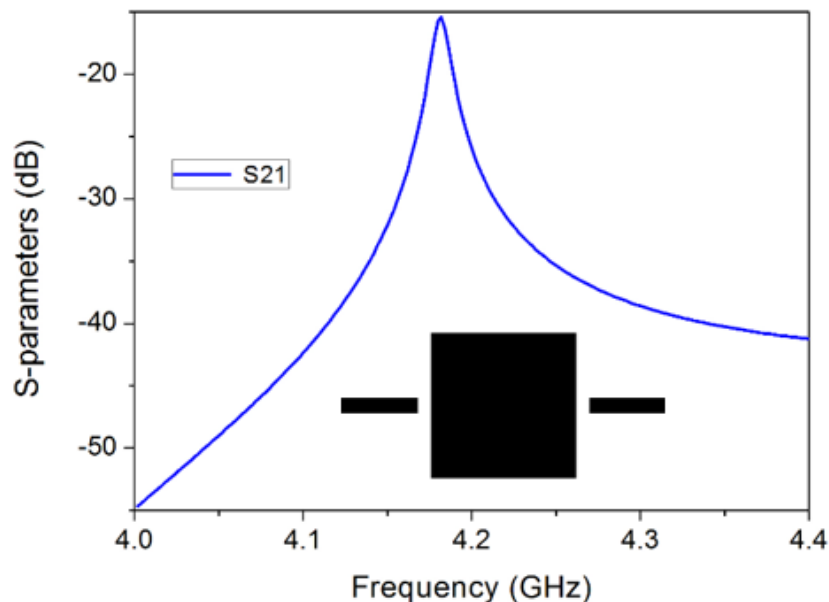


Figure 5.1 Simulation response with an inset of the layout used



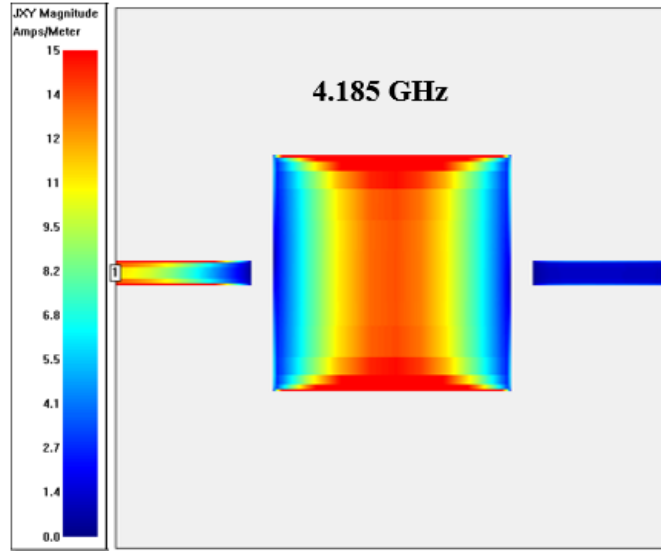


Figure 5.2 Simulated current distribution

- **Excitation of dual-mode and the coupling between them**

The square resonator is then perturbed/chamfered into a dual-mode patch resonator to resonate at 3.99 GHz and 4.39 GHz as shown in Fig. 5.3. This is characterised using a coupling coefficient ( $K$ ) as presented in (5.2).  $K$  is used in extracting the length of perturbation ( $X$  in Fig. 5.3) in the dual-mode patch. This is simulated and optimised to specification (3.99 GHz and 4.39 GHz).

$$K = \frac{FBW_0}{\sqrt{g_1 g_2}} = 0.865 \quad (5.2 a)$$

$$FBW_0 = FBW_1 + FBW_2 \left( \frac{\omega_2 + \omega_1}{\omega_2 - \omega_1} \right) = 0.838 \quad (5.2 b)$$

where  $FBW_0$  is the overall fractional bandwidth of both frequency channels [133], required to accommodate the  $FBW_1$  (4%) and  $FBW_2$  (4%) which is for the upper and lower band.  $g_0 = g_4 = 1.0$ ,  $g_1 = g_3 = 0.8516$  and  $g_2 = 1.1032$  as obtained for a three-pole Chebyshev response with a ripple factor of 0.043 dB.

Fig. 5.3 presents the coupling topology used and the achieved resonant peaks. The current distribution at both resonant peaks is presented in Fig. 5.4. Fig. 5.5 presents the parameter studies where the coupling coefficient is plotted against the perturbation length,  $X$ .

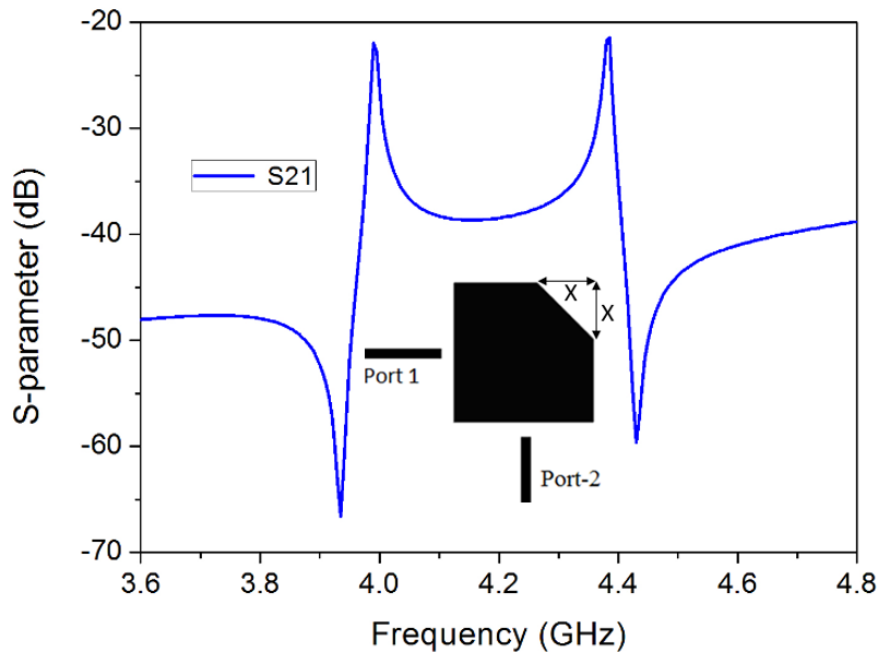


Figure 5.3 Simulation response of the dual-mode patch resonator

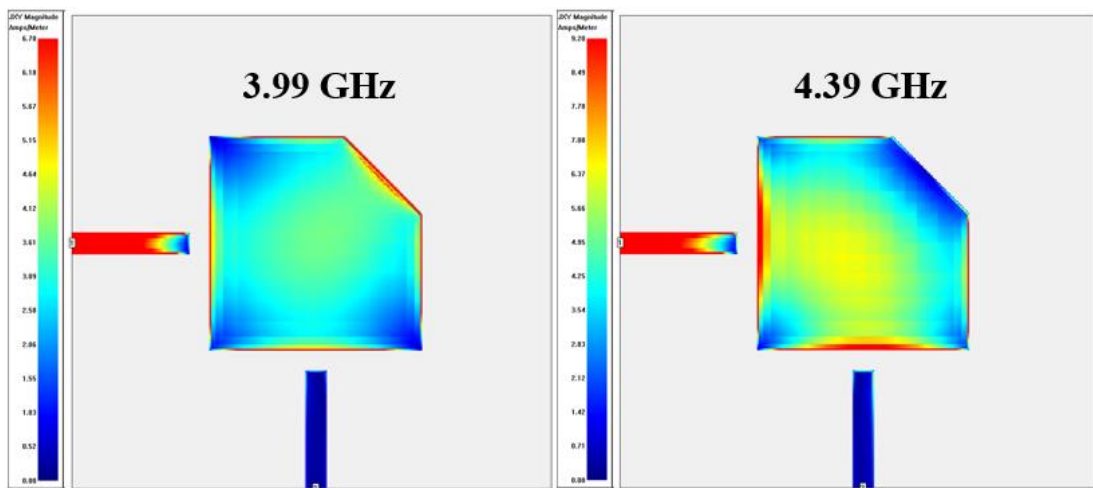


Figure 5.4 Simulated current distribution at both modes

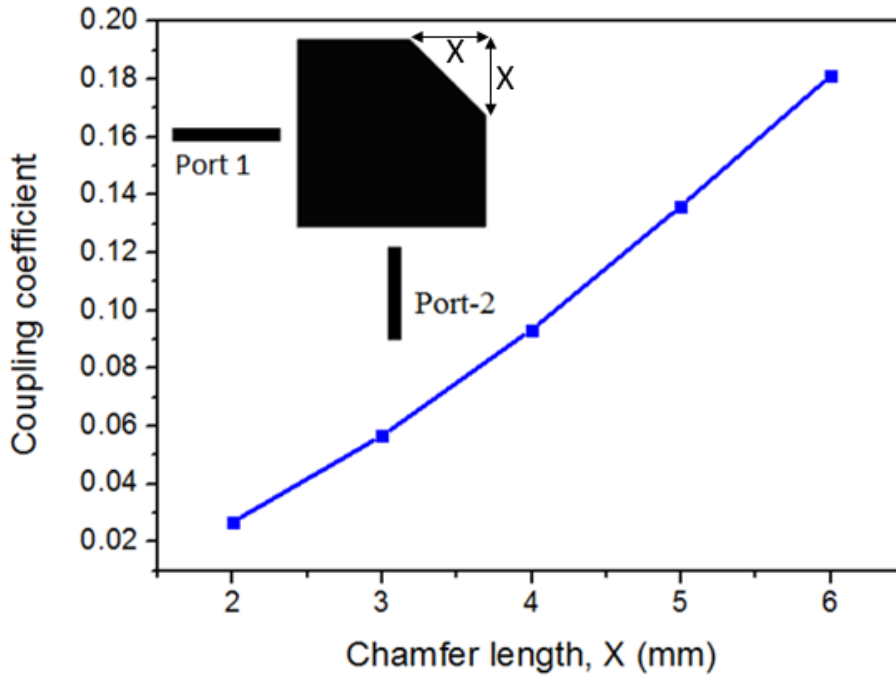


Figure 5.5 Coupling coefficient between the two modes of a perturbed patch as a function of X

- **Finding the  $Q_{ex}$  of the patch resonator**

The external quality factor  $Q_{ex}$  of the patch is obtained in this stage. (5.3) is used for the calculation. As the patch resonant poles are seen as individual poles, it should be attached to their individual channel filters with similar frequencies. They will need to have the same  $Q_{ex}$  for their input and output feeds. (5.4) is used for extracting the  $Q_{ex}$  for physical dimensioning.

$$Q_{ex} = \frac{g_1 g_0}{FBW_1} = 21.29 \quad (5.3)$$

$$Q_{ex,1(2)} = \frac{f_{1(2)}}{\Delta f_{1(2)}} \quad (5.4)$$

where  $f_{1(2)}$  is the low and high band centre frequency respectively,  $\Delta f_{1(2)}$  is the 3dB bandwidth of the resonance curves. Fig. 5.6 shows the layout used while Fig. 5.7 shows the  $Q_{ex}$  simulated responses at both frequencies.  $S_{21}$  and  $S_{31}$  is used for extracting the  $Q_{ex}$  for the low band and the high band respectively.

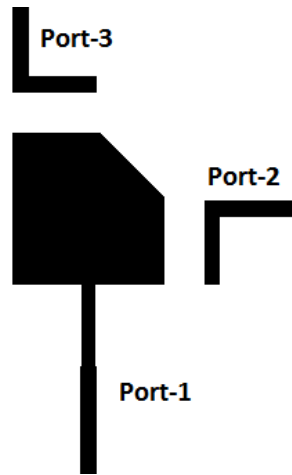


Figure 5.6 Simulation layout used for  $Q_{ex}$  extraction

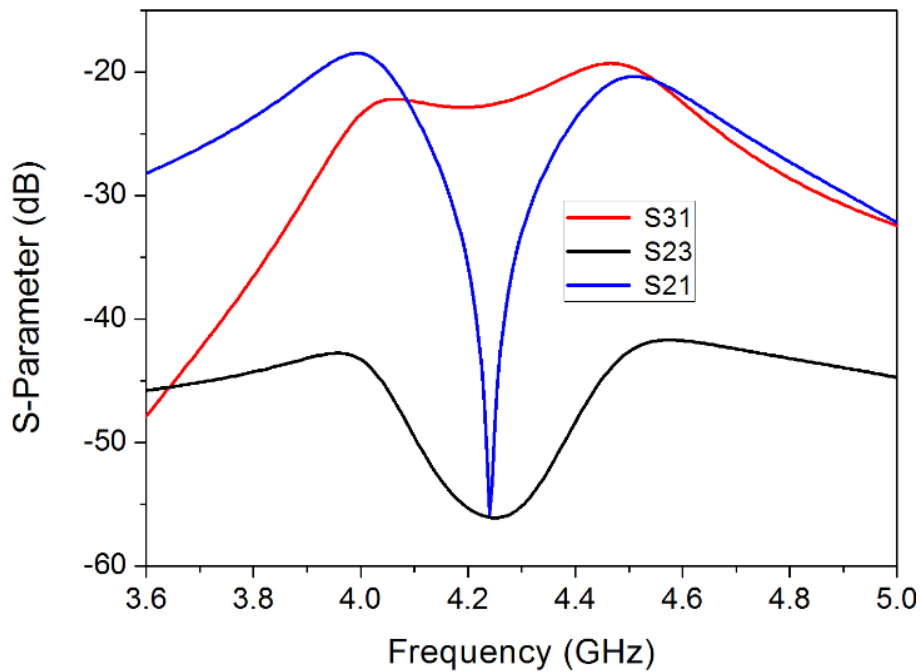


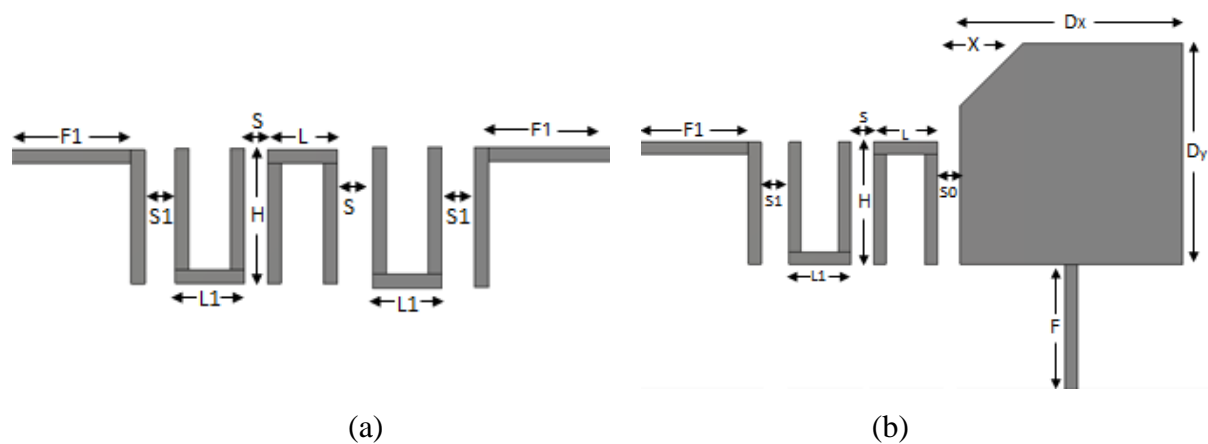
Figure 5.7 Typical simulated responses of the layout shown in Fig. 5.6.

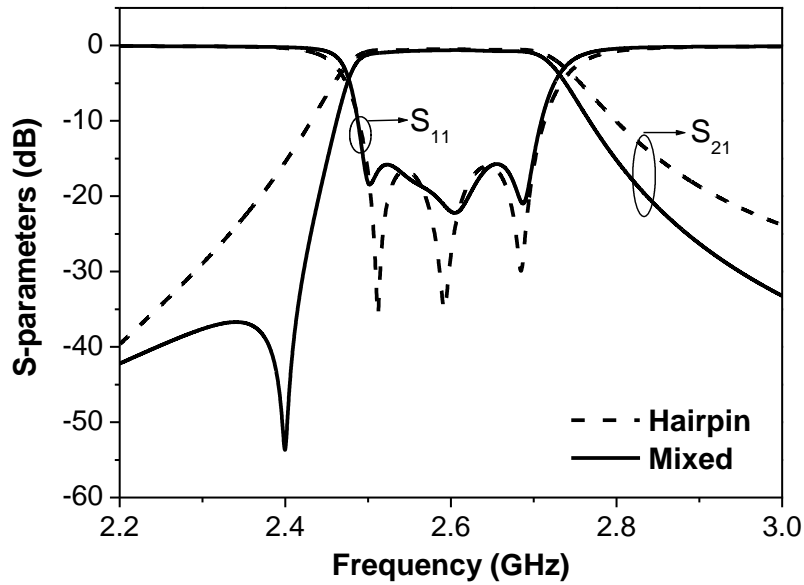
## 5.2 Bandpass Filter with Transmission Zero (Design-1)

A design of a BPF with a mixed hairpin and patch resonator is presented in this section. The aim is to present a new implementation technique of transmission zeros in an in-line coupled filter, by exploring the combined use of single-mode and dual-mode resonators. This is to be achieved without resorting to cross coupling between nonadjacent resonators, separate side-line resonators or extracted poles [134 - 139]. A mixture of two single-mode hairpin resonators

and one dual-mode patch resonators have been adopted in this design with one asymmetric transmission zero. These three resonators are coupled in-line. The patch is used for its dual-mode properties. One mode is coupled to the hairpins forming the transmission path, whereas the other orthogonal mode generates the transmission zero. By the introduction of the patch, an improved frequency selectivity through an independently controllable transmission zero is achieved. This approach has been verified by a three-pole filter at 2.6 GHz with 8% bandwidth, 16 dB return loss and a transmission zero at 2.4 GHz.

As a reference design for comparison, a conventional all-pole hairpin bandpass filter, as shown in Fig. 5.8(a), was first designed following the general filter implementation procedure. Using a passband ripple factor of 0.043 dB for a three-pole Chebyshev lowpass prototype, the  $g$  values were derived from [140] with  $g_0 = g_4 = 1.0$ ,  $g_1 = g_3 = 0.8516$  and  $g_2 = 1.1032$ . These were converted to the coupling parameters used for the physical dimensioning of the microstrip resonators. After designing the conventional all-pole BPF of 2.6 GHz to specification, the last hairpin resonator was replaced with a patch resonator, as shown in Fig. 5.8(b). The dual-mode patch resonator resonates at 2.4 GHz and 2.6 GHz. For coupling purposes, the 2.6 GHz mode is coupled to the hairpin forming the transmission path while the 2.4 GHz mode determines the transmission zero. Fig. 5.8(a) and (b) shows the circuit layout of the conventional three-pole hairpin filter and the mixed hairpin and patch filter with dimensions. Fig. 5.8(c) shows the simulated  $S$ -parameters of both the conventional hairpin filter and the hairpin-patch filter, which clearly exhibits a transmission zero at 2.4 GHz. Fig. 5.9 illustrates the simulated current distribution on the mixed resonator filter at 2.6 GHz. The patterns of the current distribution on the patch broadly agree with the one in Fig. 2.1.





(c)

Figure 5.8. Circuit layouts of (a) the hairpin filter and (b) the hairpin-patch filter;  $F = 10$ ,  $F1 = 8.73$ ,  $L = 5.07$ ,  $L1 = 4.96$ ,  $S = 1.24$ ,  $S1 = 0.26$ ,  $S0 = 0.68$ ,  $X = 5$ ,  $H = 9.73$ ,  $D_x = D_y = 17.59$ ; unit: mm. (c) The simulated responses of the mixed hairpin-patch filter in comparison with a conventional hairpin filter of the same order.

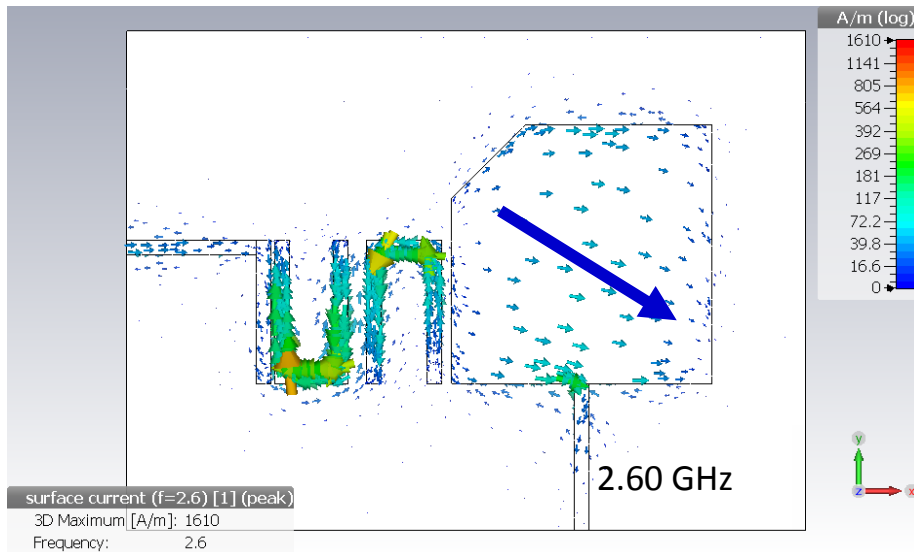
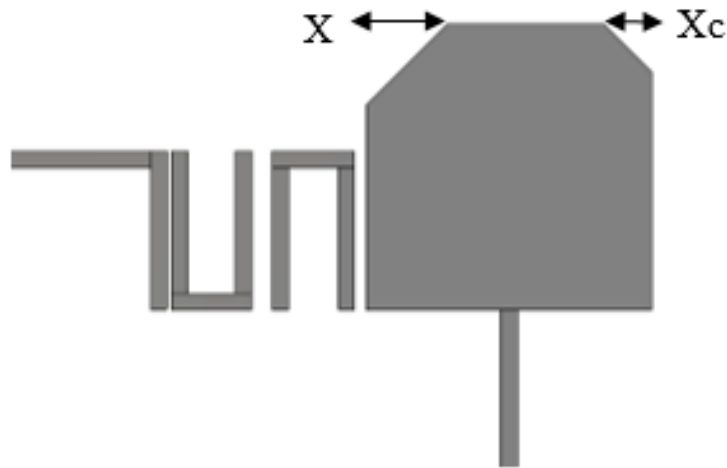


Figure 5.9 Simulated current distribution of the hairpin-patch filter at 2.6 GHz.

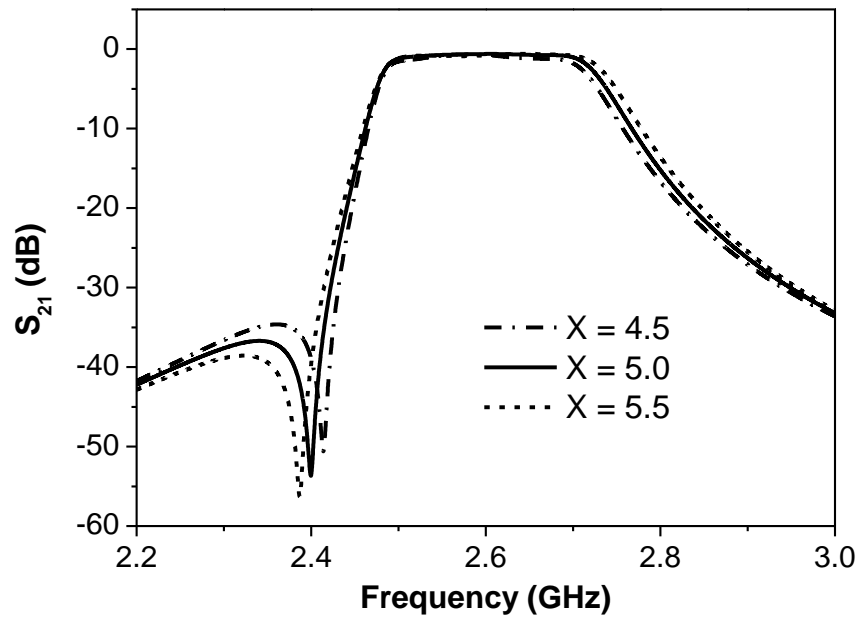
It is noted that in this design the coupling matrix was not extracted to represent the required frequency response with the prescribed transmission zero. The physical dimensions of the hairpin-patch filter was guided by the conventional hairpin filter and its responses. After replacing the last resonator of the conventional hairpin filter with the patch, parameter studies and optimisations have been used to achieve the required passband return loss and the

transmission zero. The feedline to the first hairpin resonator as well as the first two hairpins is kept unchanged. The dimensions that have been optimised are the size of the patch, the chamfers, and the tapping point of the feed line at the patch.

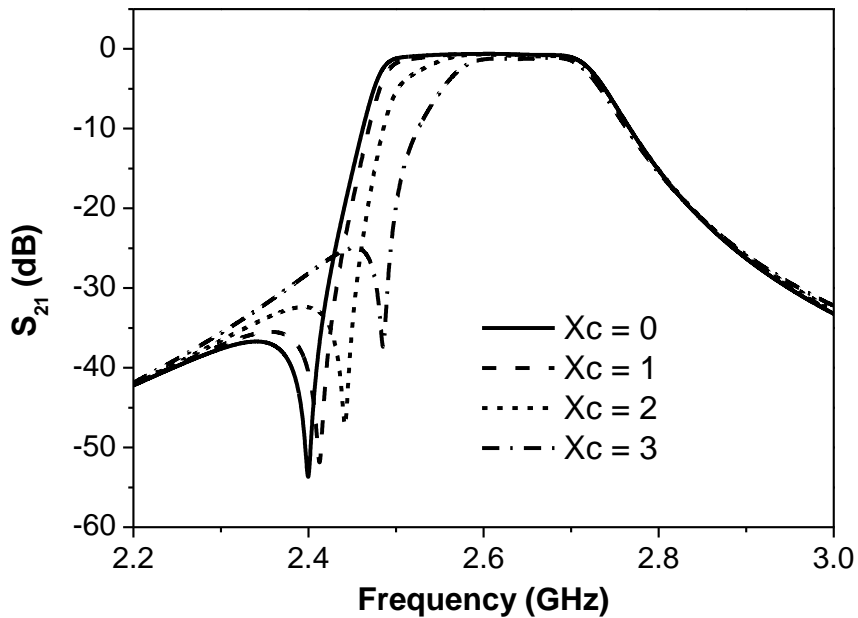
The more effective way to change the transmission zero is to alter the longer diagonal path in the patch. This can be achieved by introducing the chamfer  $X_c$  as shown in Fig. 5.10(a), or an extension stub if the transmission zero frequency were to be lowered. The parameter study considered the effect of the chamfers in the patch. Two chamfers ( $X$  and  $X_c$ ) are shown in Fig. 5.10(a). The chamfer  $X$  determines the higher mode at around 2.6 GHz. Fig. 5.10(b) illustrates the change of response as a function of the chamfer  $X$ . As the chamfer also controls the coupling between the two orthogonal modes of the patch, the overall bandwidth has been affected. The transmission zero is also shifted slightly as a result. From Fig. 5.10(c), it can be seen that the increase of  $X_c$  pushes the transmission zero to higher frequency but hardly affects the upper edge of the passband. In the case of this design with the transmission zero at 2.4 GHz, this chamfer  $X_c$  is not required. The size of the patch, the tapping point of the feedline to the patch and the coupling between the patch and the hairpin are other parameters that can be adjusted in optimisation. If more degrees of freedom are required, stubs or slots can be added to the patch.



(a)



(b)



(c)

Figure 5.10 Parameter studies. (a) Layout; (b) The change of  $S_{21}$  with  $X$ ; (c) The change of  $S_{21}$  with  $X_c$ .

All simulations were done using CST Microwave Studio. The Roger RO3010 substrate with a nominal dielectric constant of 11.2, loss tangent of 0.0023 and substrate thickness of 1.27 mm was used for the design. Fabrication was done using the milling method with LPKF ProtoMat S63 circuit board plotter. In order to prevent radiation losses and preserve the high Q-factor of the patch, the circuit is housed in a metallised box. Fig. 5.11 shows the fabricated device. Agilent Network Analyser N5230A was used to measure the fabricated device. A comparison



between the simulated and measured results is presented in Fig. 5.12. It can be seen from the simulated and measured responses that a reasonably good agreement has been achieved. The transmission zero can be identified at 2.446 GHz. There is a significant shift of the measured responses to higher frequency by nearly 50 MHz. This is partly due to the over-milling of the circuit when the parameters of the milling machine are not optimised to process the ceramic-filled Roger RO3010 substrate. The variation of the dielectric constant of the substrate is another important factor. The dielectric constant used in the simulation was 11.2. This was found to be higher than the actual values by subsequent designs using the same substrate. As discussed in more details in Section 5.4. The minimum measured insertion loss ( $S_{21}$ ) in the passband is 1.3 dB, and the return loss ( $S_{11}$ ) is better than 13 dB.

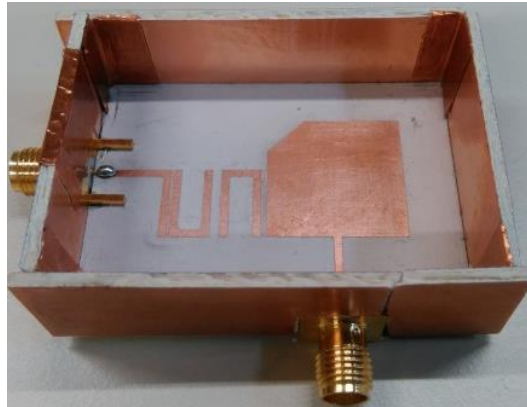


Figure 5.11 Photo of the fabricated filter with its box lid removed.

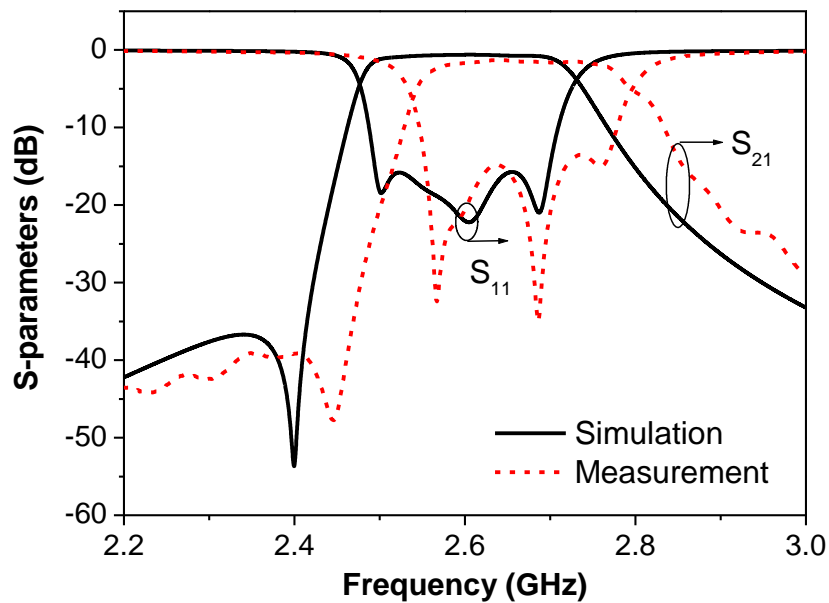


Figure 5.12 Simulated and measured responses of the hairpin-patch filter.

## 5.3 Diplexer with a Patch Resonator as its Junction (Design-2)

This section of work presents a novel diplexer using hairpin resonator filters which are joined using a dual-mode patch resonator. The patch is made to resonate at the centre frequencies of the two channel filters in corresponding modes. The patch functions as a signal splitter/combiner in the circuit. It also functions as a resonant pole for each of the channel filters. To implement this technique, a diplexer with channel centre frequencies of 3.99 GHz and 4.39 GHz and a 4% fractional bandwidth on each channel is presented. To illustrate the proposed design, Fig. 5.13 (a) and (b) presents a comparison of the circuit topology for a conventional diplexer and that of the proposed diplexer technique. Fig. 5.13(b) is essentially the same as the topology in Fig. 4.3. Instead of using two asynchronously coupled resonators, here one dual-mode patch is used.

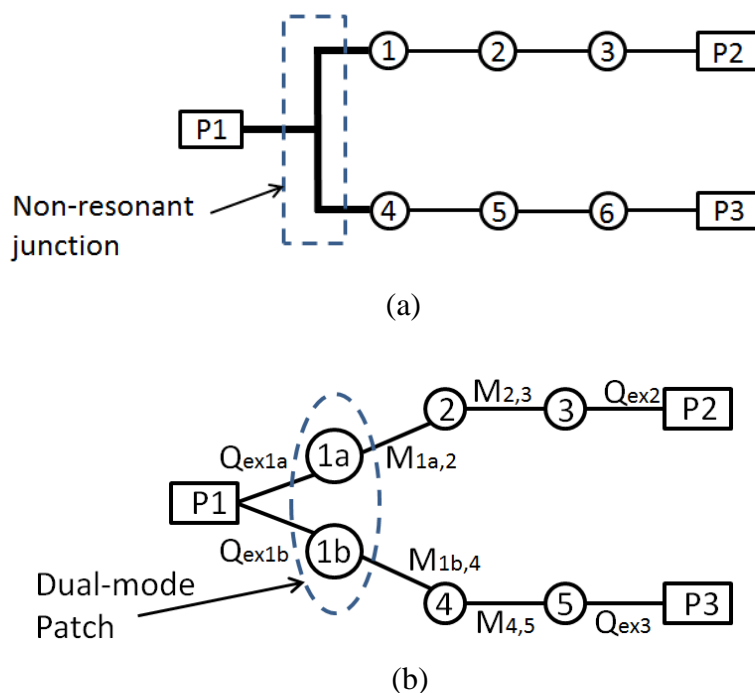
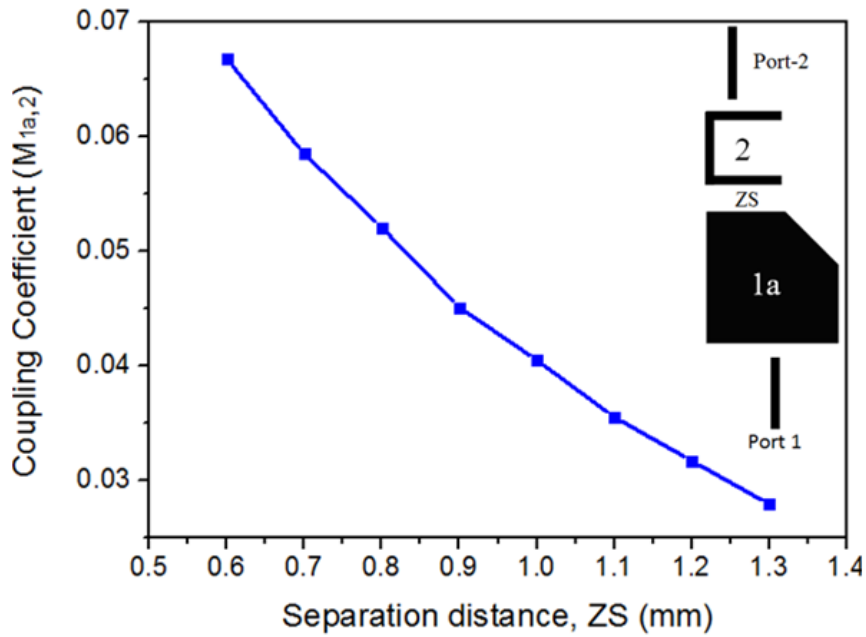


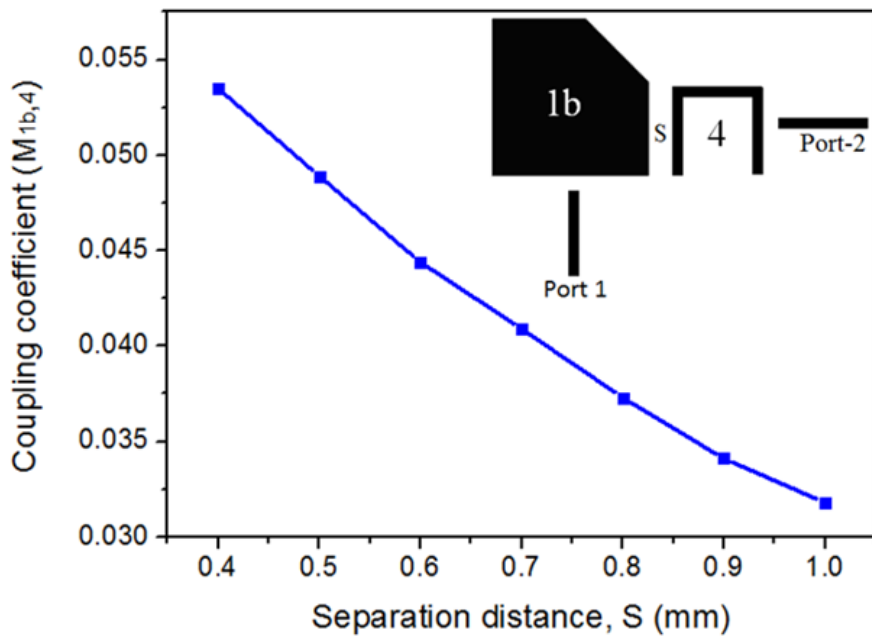
Figure 5.13 Coupling topology of diplexers: (a) Conventional technique; (b) Proposed technique

To meet the design specification, two three-pole Chebyshev hairpin BPFs operating at 3.99 GHz and 4.39 GHz were separately designed to the specification of 20 dB and 4% fractional bandwidth (FBW) each. In joining the two filters, a patch resonator was used, thereby avoiding

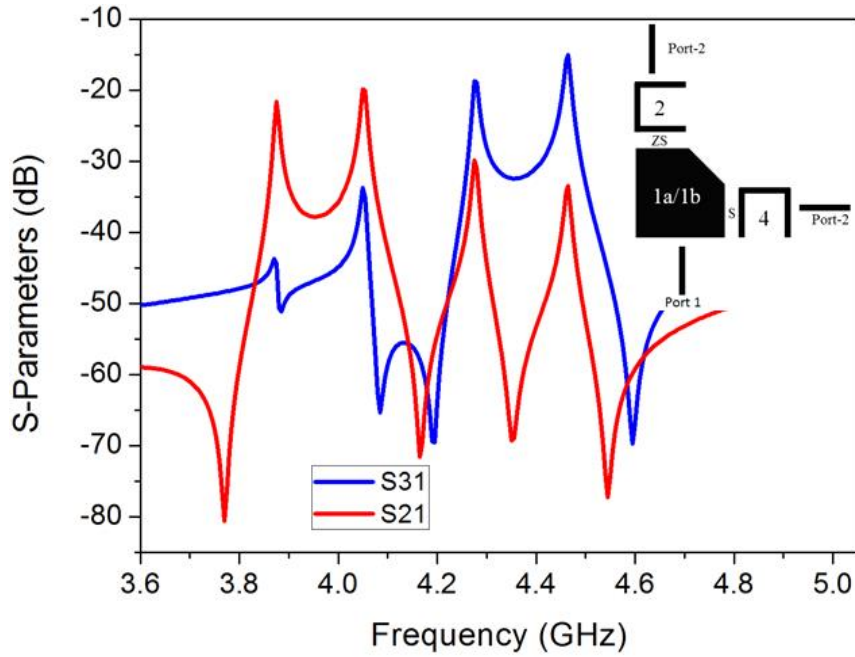
the conventional technique which uses a non-resonant transmission line based T-junction circuit. The patch resonator, been a dual-mode, is then used to replace the first hairpin resonator of both channel filters. The coupling configuration used in joining the channel filters is shown in Fig. 5.14(a) and (b) while (c) shows the eigen-mode response of the coupled structure. The peaks can be used for the determination of the coupling gaps according to the required coupling coefficient.



(a)



(b)



(c)

**Figure 5.14(a) Coupling coefficient  $M_{1a,2}$  against  $Z_S$ ; (b) Coupling coefficient  $M_{1b,4}$  against  $S$ ; (c) Simulated resonance curves from the assembled resonator 1, 2 and 4. The inset shows the layout used in the simulation.**

For the patch resonator to function effectively as the common resonator for both channel filters, its quality external factor ( $Q_{ext}$ ) will have to match with that of the channel filters. The design curve used in determining the  $Q_{ext}$  is an inset in the curve responses presented in Fig. 5.15. After the assembling of the resonators, an optimisation process was undertaken. Fig. 5.16(a) presents the layout of the design with dimensions while Fig. 5.16(b) presents the simulated response in comparison with the measured response [86]. The thick lines represent the measured response while the dashed lines represent the simulated response. It can be seen from the responses that a reasonably good agreement is achieved at both passbands with the return loss measured at about 15 dB. Due to the machining tolerance, the measured results can be seen shifted to the higher frequency by approximately 5 MHz. The minimum measured insertion loss in the passband is less than 2 dB. The high passband has a reduced bandwidth. In Fig. 5.17, the current distribution at both channels of the diplexer is presented, and it can be seen that the patch performs well as a signal splitter in the circuit.

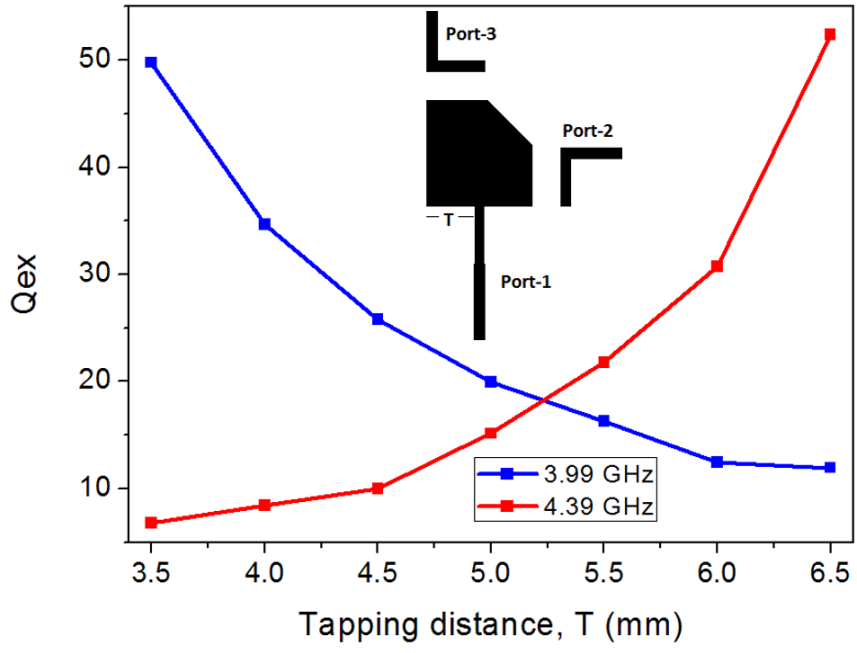
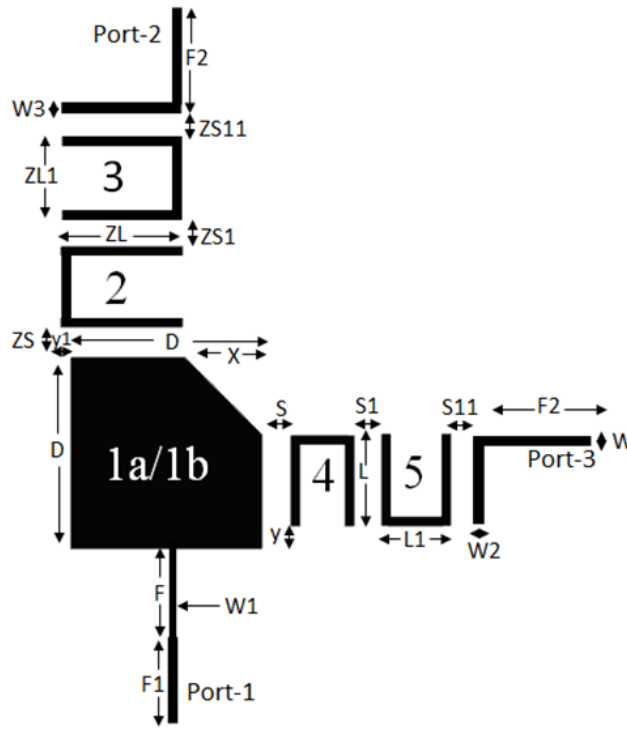
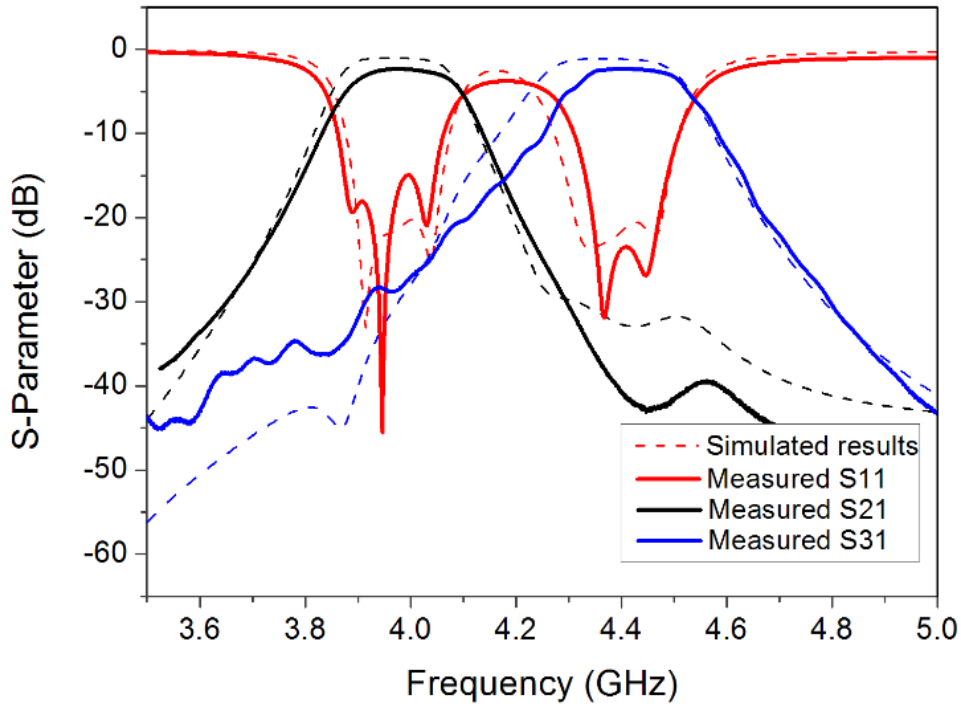


Figure 5.15 Design curve used to extract  $Q_{ex1a}$  and  $Q_{ex1b}$



(a)



(b)

Figure 5.16 (a) Design layout (unit: mm);  $ZL = 5.4$ ,  $ZL1 = 3.9$ ,  $ZS = 1$ ,  $ZS1 = 1.4$ ,  $ZS11 = 0.2$ ,  $L = 5$ ,  $L1 = 3.4$ ,  $S = 0.84$ ,  $S1 = 1.26$ ,  $S11 = 0.2$ ,  $D = 10.9$ ,  $X = 4.6$ ,  $F = 6$ ,  $F1 = 5$ ,  $F2 = 10$ ,  $W = 1.1$ ,  $W1 = 0.9$ ,  $W2 = 0.6$ ,  $W3 = 0.9$ ,  $y = 0.5$ ,  $y1 = 1.6$ ; (b) Measured responses in comparison with full-wave simulations.

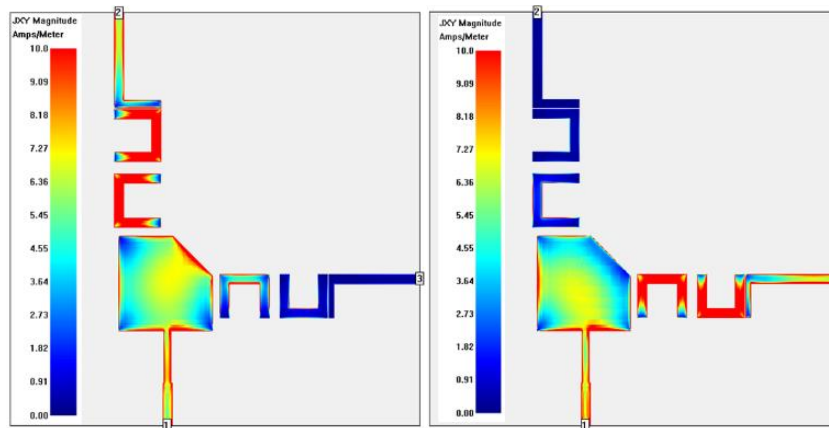


Figure 5.17 (a) Current distribution at 3.99 GHz (b) current distribution at 4.39 GHz

The prototype of this design is shown in Fig. 5.18 using Rogers 3010 substrate with a thickness of 1.27 mm, a relative permittivity of 10.8 and a loss tangent of 0.0022. Fabrication was performed using LPKF ProtoMat S63 micro-milling process, and Agilent Network Analyser N5230A was used for measurement. Simulations were performed using the EM simulator Sonnet Suites.

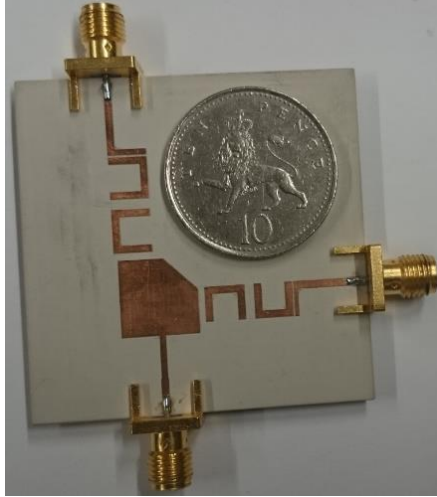


Figure 5.18 Photograph of the fabricated diplexer with the dual-mode patch junction.

## 5.4 Dual-band BPF (Design-3)

After the patch-hairpin filter in Section 5.2 and the patch-resonator enabled diplexer in Section 5.3, a dual-band bandpass filter with dual coupling paths is presented in this section, again using dual-mode patch resonators. The filter is formed of two dual-mode patch resonators, one half-wavelength or one full-wavelength straight-line resonator and a hairpin resonator. The patch resonators acted as a signal splitter, combiner and resonant pole in the dual-band bandpass filter. The patch resonators are coupled to each other via the hairpin and the straight-line resonators. The design implementation using a full wavelength straight-line resonator resulted in a dual-band response with two transmission zeros located in the outer bands. As a design variation, the full-wavelength straight-line resonator is replaced with a half wavelength straight-line resonator. From the achieved response, it was shown that the position of the transmission zeros shifted from the outer bands to the inner bands, but with one transmission zero present. The former presented an improved out of band rejection while the latter presented an improved in-band separation and selectivity.

The design uses the coupling topology presented in Fig. 5.19. The first dual-mode patch resonator provides the orthogonal modes for the resonant nodes 1a and 1b. The second patch resonator provides the modes for the node 3a and 3b. The high passband path is coupled through the single-mode resonator 2', whereas the low passband is coupled through resonator 2. This topology became possible as the orthogonal modes of the patch acted as a signal splitter

and combiner for the high and low-passbands, allowing both channels to share the same input and output ports.

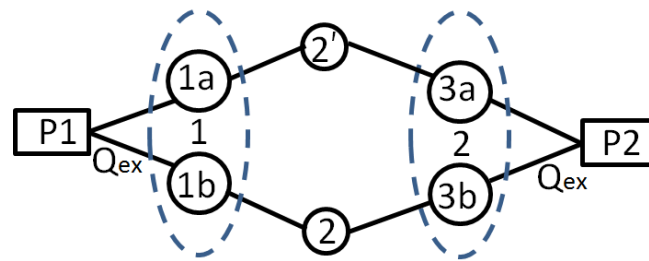


Figure 5.19 Dual-band bandpass filter coupling topology

For demonstration, a dual-band bandpass filter operating at 1.8 GHz and 2.1 GHz with 4% FBW is prototyped. To meet the design requirement, the  $Q_{ext}$  of the filter is first obtained on a patch resonator, resonating at 1.8 GHz and 2.1 GHz as presented in Fig. 5.20.

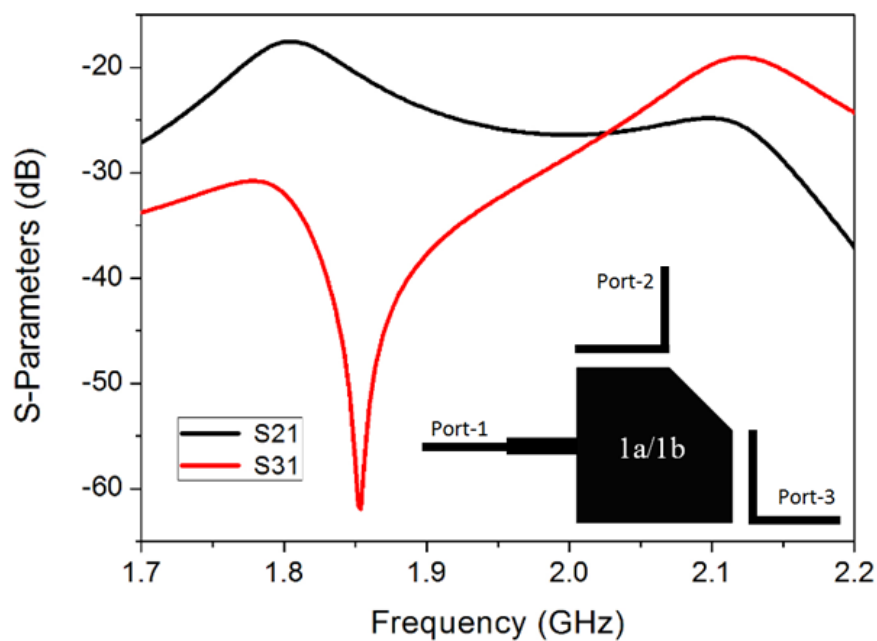
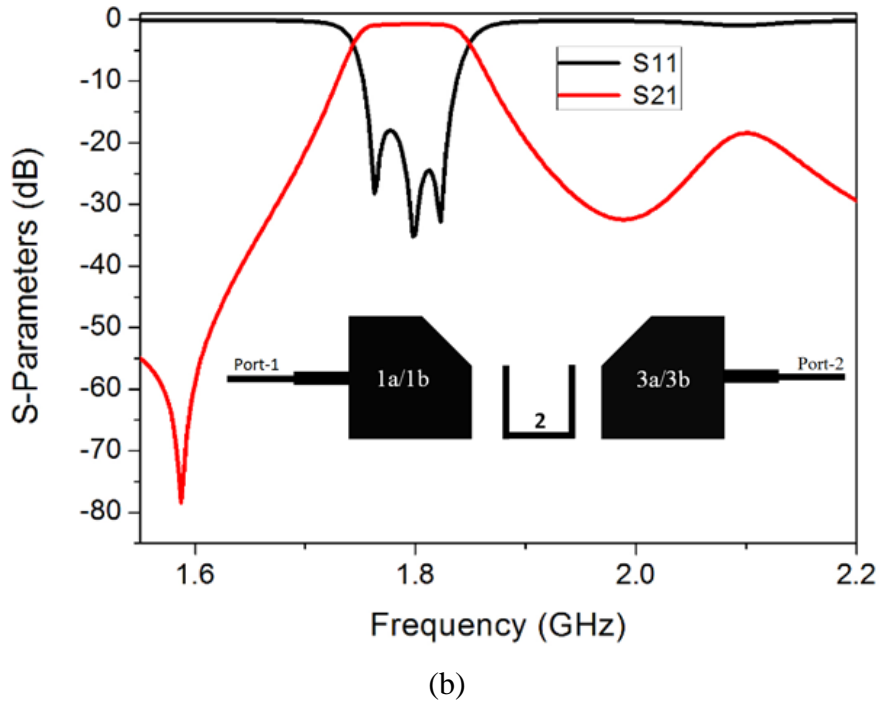
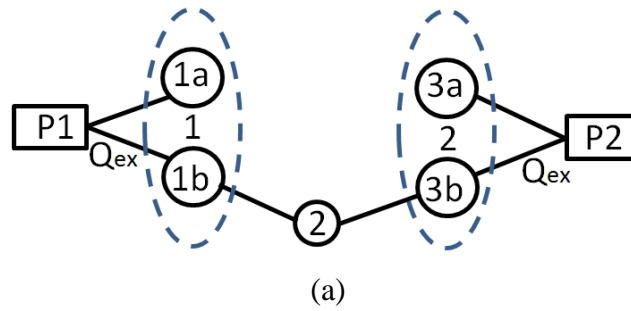


Figure 5.20 Arrangement for external Q-factor extraction and the typical responses

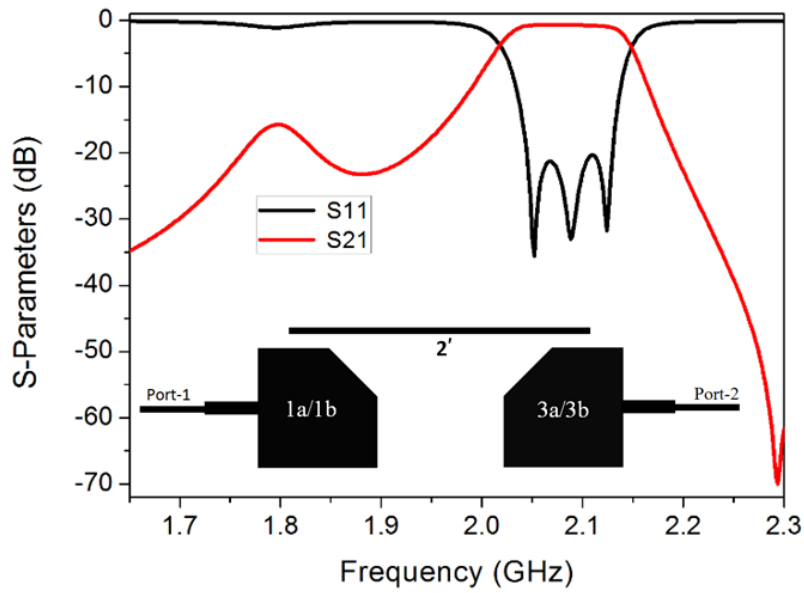
After obtaining the physical dimensions of the patch resonator, two patch resonators were then coupled together via a 1.8 GHz hairpin resonator to form the path for the low band at 1.8 GHz. Fig. 5.21(a) illustrates the coupling topology with the intended lower path only while Fig. 5.21(b) shows the simulated response.



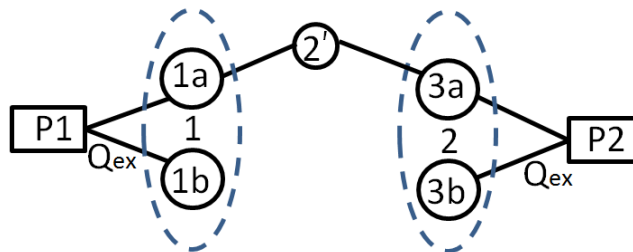


**Figure 5.21 (a) Coupling topology; (b) Simulated response of the low passband**

As for the path of the high band, a 2.1 GHz line resonator is used to couple the patches. First, a full wavelength straight-line resonator is adopted as shown in the inset of Fig. 5.22(a). Without the hairpin resonator for the low band, the three-pole high band filter is achieved as shown in Fig. 5.22(a). It is important to point out that during optimisation, only the length of the straight line and its coupling gap with the two patch resonators were adjusted. This is to avoid distorting the already achieved low-passband. Fig. 5.22(b) presents the coupling topology.



(a)



(b)

**Figure 5.22 (a) Simulated response of the high passband; (b) Coupling topology with a  $\lambda$  line resonator**

It can be seen from the simulated responses that the signal path is barely affected by the removal of the single-mode resonator in the opposite path, which makes the two passbands controllable independently.

To further analyse this design, the full wavelength straight-line resonator is replaced with a half wavelength straight-line resonator. Due to size constraints, the half wavelength straight line resonator was pushed downward in between the two patch resonators. This is to strengthen the coupling between the two patches and the half wavelength straight line resonator. On the other hand, it also increased the adjacent couplings between the low modes of the two patches and the half wavelength straight-line resonator. The resultant effect is an introduction of a transmission zero between the two passbands and the cancellation of the transmission zeros earlier introduced by the full wavelength straight-line. Fig. 5.23 illustrates the simulated response achieved with an inset of the design topology.

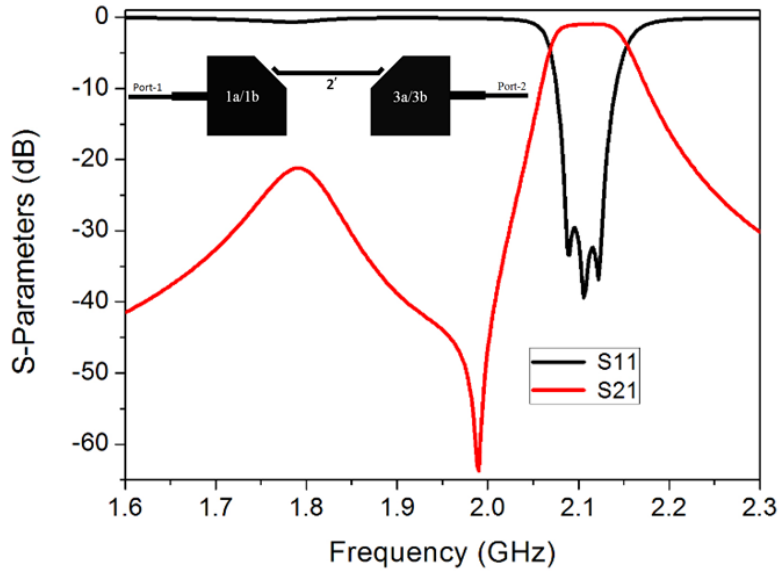


**Figure 5.23 High passband topology and response with a  $\lambda/2$  line resonator**

To form the dual-band BPF circuit, the mixed full-wavelength straight-line and patch resonator filter and the mixed half-wavelength straight-line and patch resonator filter had the hairpin resonator inserted back into its place of low-channel. Although interference effects are noticed after the insertion of the hairpin resonator, it can be compensated by optimising the coupling between the hairpin and the two patch resonators. This was done by reducing the coupling strength through moving the hairpin resonator lower along the y-axis. Fig. 5.24 and Fig. 5.25(b) shows the simulated responses of the two designs in comparison to the measured response with an inset of the fabricated design. It can be noticed that there are two transmission zeros achieved in the outer band region of the filter with the full wave straight line resonator. This indicates improved selectivity within the passbands. It can also be noticed that within the guard band, the rejection is only 19 dB which is caused by the weak coupling created by the patch perturbation. By using the half-wavelength resonator, the rejection can be significantly increased due to the resultant adjacent coupling as shown in Fig. 5.25(a).

The high passband has narrower bandwidth. This is due to the fabrication restriction imposed on the design. The minimum coupling gap which the fabrication process can handle is 0.2 mm. The optimised circuit layout with dimensions of both designed dual-band BPF is shown in Fig. 5.26 (a) and (b), where Fig. 5.26(a) is for the dual-band BPF with the full-wavelength straight line resonator and (b) is with the half-wavelength straight line resonator.

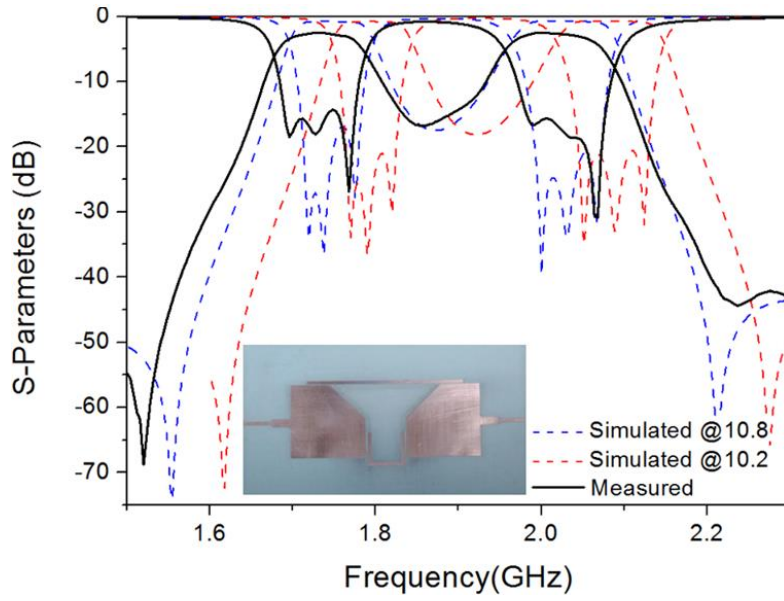


Figure 5.24 Simulated and measured responses of the filter in Fig. 5.19 with the inset showing the fabricated design

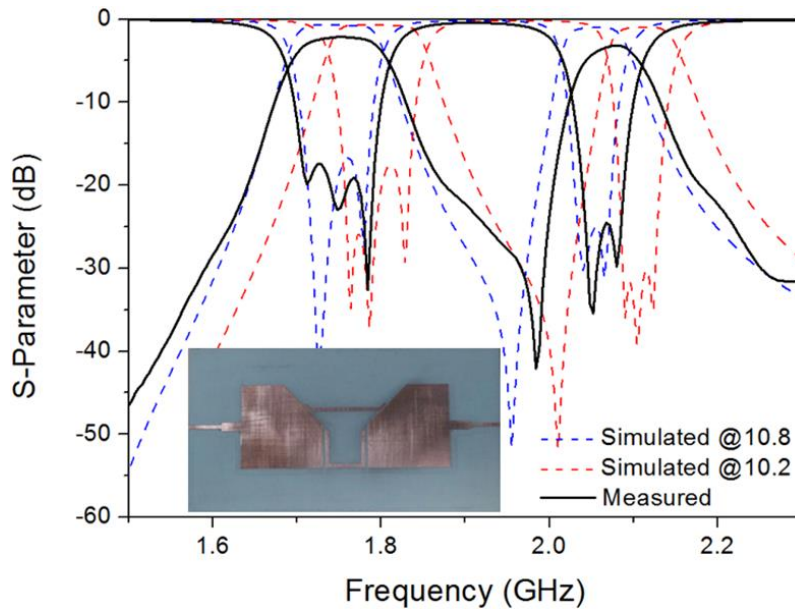
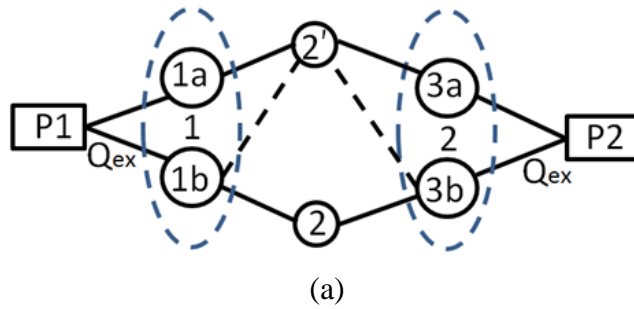
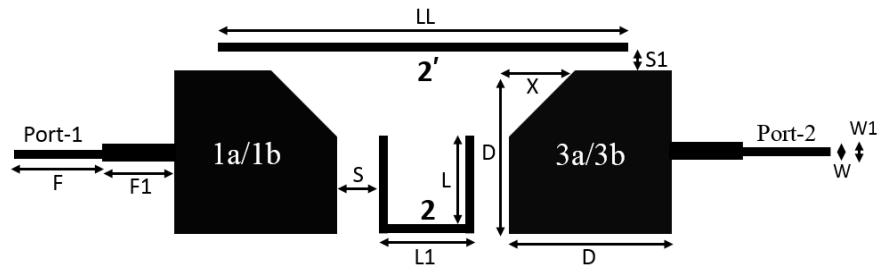
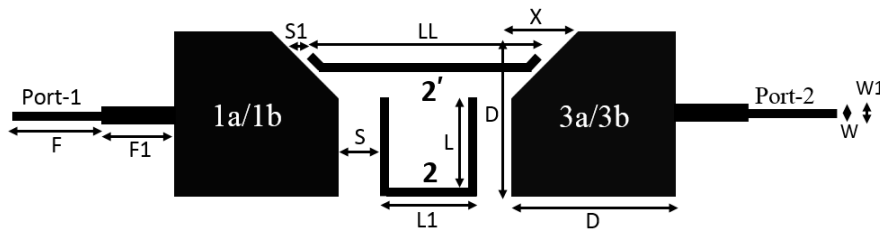


Figure 5.25 Simulated and measured responses of the filter in Fig. 5.25(a) with the inset showing the fabricated design.

It has been shown that this filter can perform well as a single BPF for the low passband or the high passband if the coupling path of the other is removed. Being a six-pole design, this topology led to a reduction in the total number of required resonators from six to four. This design was fabricated on Rogers 3010 substrate with a thickness of 1.27 mm, relative permittivity of 10.2 (used in simulation) and loss tangent of 0.002. Simulations were performed using the EM simulator Sonnet Suites.



**Figure 5.26 (a) Circuit layout dual-band BPF with  $\lambda$  resonator:**  $F = 10$  mm,  $F1 = 6$  mm,  $S = 0.7$  mm,  $S1 = 0.2$  mm,  $L = 11.3$  mm,  $L1 = 10.1$  mm,  $LL = 53.2$  mm,  $D = 25.2$  mm,  $X = 12.4$  mm,  $W = 1.2$  mm,  $W1 = 2.8$  mm



**Figure 5.27 (b) Circuit layout dual-band BPF with  $\lambda/2$  resonator:**  $F = 10$  mm,  $F1 = 6$  mm,  $S = 0.7$  mm,  $S1 = 0.2$  mm,  $L = 11.3$  mm,  $L1 = 10.1$  mm,  $LL = 26.2$  mm,  $D = 25.2$  mm,  $X = 12.4$  mm,  $W = 1.2$  mm,  $W1 = 2.8$  mm.

Measurements were done using the Agilent Network Analyser N5230A. From the simulated and measured responses compared in Fig. 5.24, it is noticed that both bands of the measured shifted to the left by approximately 20 MHz, while both return losses are at about 14 dB with insertion loss of about 2.5 dB. The simulated and measured responses in Fig. 5.25(b) also showed a frequency shift to the left by approximately 20 MHz with the insertion loss of about 3 dB. The return loss of the low passband is about 22 dB while the high passband is about 25 dB with a transmission zero at 1.99 GHz. After fabricating the circuits using different techniques as well as comparing the performance with several transmission-line type resonators based on the same RO3010 substrate, it has been found that the significant frequency shift is mainly caused by the variation of the dielectric constant from the one (10.2) used in the simulation. Although the value of 10.2 has been found more suitable for microstrip-line filters,

for the patch resonators with more E-fields in the Z-direction perpendicular to the patch, the so-called ‘design Dk’ of 11.2 seems to represent the material better. Simulations show that a value of 10.8 fits the measurement best as can be seen in Fig. 5.24 and 5.25. This is consistent with the anisotropic property of the RO3010 substrate.

## 5.5 Summary

In this chapter, the uses of patch as a dual-mode resonator are explored for single band filters, diplexers and dual-band filters.

Section 5.2 utilised the orthogonal mode of a patch resonator to create an improved filtering function in an in-line coupled filter. One mode of the patch resonator was coupled in-line with the rest of the filter resonators while the other mode generates a transmission zero to improve the out-of-band rejection.

In Section 5.3, a patch resonator was used in the design of a novel and compact type of microwave diplexer composed exclusively of coupled resonators. From the design, it can be observed that the signal combination is obtained through distributed couplings between the resonators of each channel. The patch resonator functioned as a signal splitter, combiner and at the same time contributing to the resonant poles of both channel filters.

Finally, Section 5.4 employed two patch resonators in the implementation of a dual-band BPF. Using dual coupling paths in the design, the patch resonators acted as a signal splitter and combiner allowing the divergence and convergence of signals in the circuit.

# Chapter 6: Diplexers with a Split-Ring Resonant Junction

After the design of the diplexer with a patch resonant junction presented in chapter 5, a diplexer based on all-resonant structures and using split-ring resonator (SRR) is presented in this chapter. The aim here is to develop more compact and improved selective channel responses in the diplexer than that of the diplexer with patch resonant junction. The dual-mode patch resonator and the split-ring resonator (SRR) has two distinctive features in their responses as explained in chapter 2. The SRR has an inter-band transmission zero as shown in Fig. 2.2, making it very useful in the design of an improved selective frequency response. The dual-mode patch resonator has two transmission zeros in the outer resonances as shown in Fig. 5.3. In comparing the sizes of both resonators at the same resonant frequencies, the SRR occupies less space than the dual-mode patch resonator. This design utilises the inter-band transmission zero in the SRR to achieve an improved selective response in the guard band of a widely separated channels of a diplexer.

In the implementation, the SRR is utilised because of its dual-mode properties. The characteristics of an SRR have been discussed in Section 2.4.2. As stated, an SRR can be designed using two half-wavelength open-loop resonators with one nested inside the other. The resultant coupling configuration resulted in a response with an inscribed bandstop in-between the resonant modes. Also, the coupling between the two open-loops gives an opportunity to control the separation between the two modes, paving the way for this type of resonator to be used in diplexers of either adjacent or widely separated frequency channels.

Before the diplexer, the channel filter implementation will be first investigated aiming for an improved frequency-selective BPF. A three-pole BPF will be designed and optimised to specification. An SRR is then used to replace the first resonator of the BPF. The insertion of the SRR will result in an introduction of transmission zero which is created by a cross coupling between the parallel coupled open-loop resonators and the adjacent mode of the SRR. This technique was carried out on two different filters in correspondence to the dual-modes of the SRR.

For the diplexer implementation, an asynchronously tuned SRR was used in joining two separately designed channel filters. Without incurring any extra space for the junction, the SRR, being a dual-mode resonator, also functioned as a resonant pole for each channel filter. A diplexer operating at 2 GHz and 3 GHz with 4% fractional bandwidth and 20 dB return loss will be demonstrated. The interactions between the SRR and the channel filters were also investigated.

## **6.1 Split-Ring Resonator (SRR) as the Junction Resonator**

In the designs presented in this Chapter, an SRR, resonating at 2 GHz and 3 GHz, is used. It is formed of two open-loop resonators of 2 GHz and 3 GHz which are asynchronously coupled to each other. As shown in Fig. 2.2, the SRR produced an inter-band transmission zero [141], which is a very useful feature in increasing the isolation between the two modes. The difficulty working with this resonator is that only the outer loop can easily couple with adjacent resonators or the feed lines [142]. In Section 2.4.2, the design procedure for an edge coupled SRR has been demonstrated. It is used as a resonant junction in joining two BPFs in a diplexer implementation. This is achieved by using the SRR to replace the first resonator of each of the two BPFs.

The external quality factor of the SRR is calculated using (3.5) while (5.4) is used for extracting the  $Q_{ex}$  for the physical dimensioning. To determine the Q-factor for the common port, the coupling arrangement shown as the inset in Fig. 6.1 is used. The feed-line at port-1 was tapped to the SRR while the feed-lines at port-2 and port-3 were weakly coupled to the resonator. The common feedline was adjusted both in position and width to achieve the required external couplings at both 2 and 3 GHz.



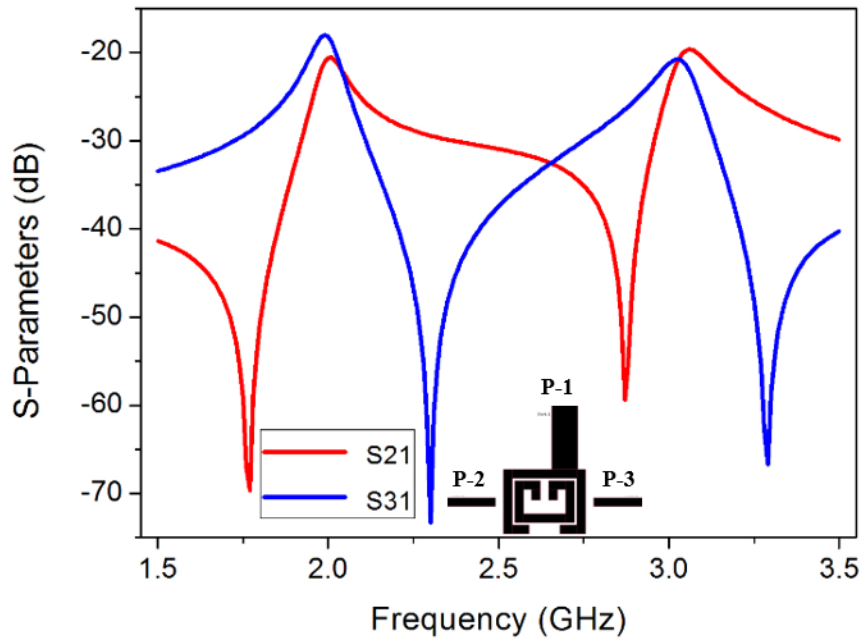


Figure 6.1 Topology and typical response used to extract external Q-factors

From the responses presented in Fig. 6.1, there is a transmission zero at about 2.8 GHz between port-1 and 2 while a transmission zero at about 2.3 GHz occurs between port-1 and 3. These transmission zeros create an improved frequency selective response. For instance, if a corresponding channel of 3 GHz is to be coupled to the SRR, a transmission zero at about 2.8 GHz is expected. If a corresponding channel of 2 GHz is to be coupled, a transmission zero at about 2.3 GHz is expected. To demonstrate this, two BPFs corresponding to the two channel filters have been designed first in the next section.

## 6.2 Bandpass Filters Using Open-Loop and SRR

The BPFs are designed using two open-loop resonators and one SRR. The two filters are at 2 GHz and 3 GHz of 4% fractional bandwidth at 20 dB return loss. Fig. 6.2 and Fig. 6.3 show the filter topology at 2 GHz and 3 GHz respectively.

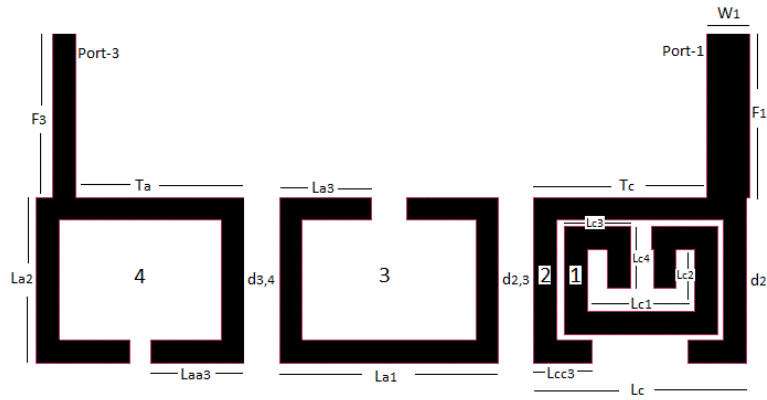


Figure 6.2 BPF at 2 GHz

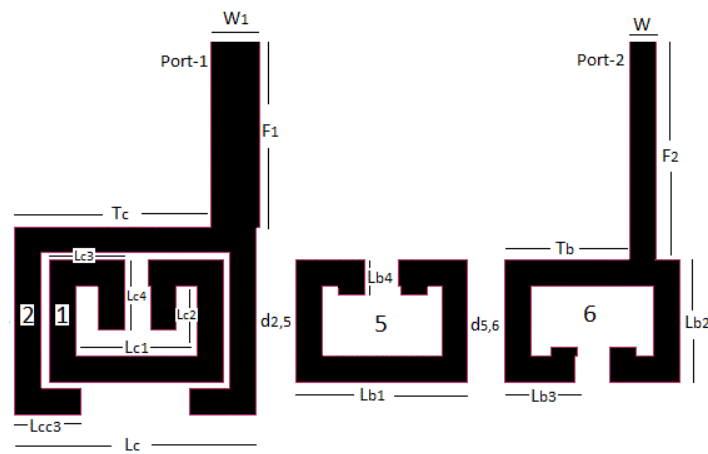


Figure 6.3 BPF at 3 GHz

Fig. 6.4 presents the simulated current distribution of the 2 GHz and 3 GHz filters. Fig. 6.5 and Fig. 6.6 presents the simulated and measured responses of the 2 GHz and the 3 GHz filters respectively.

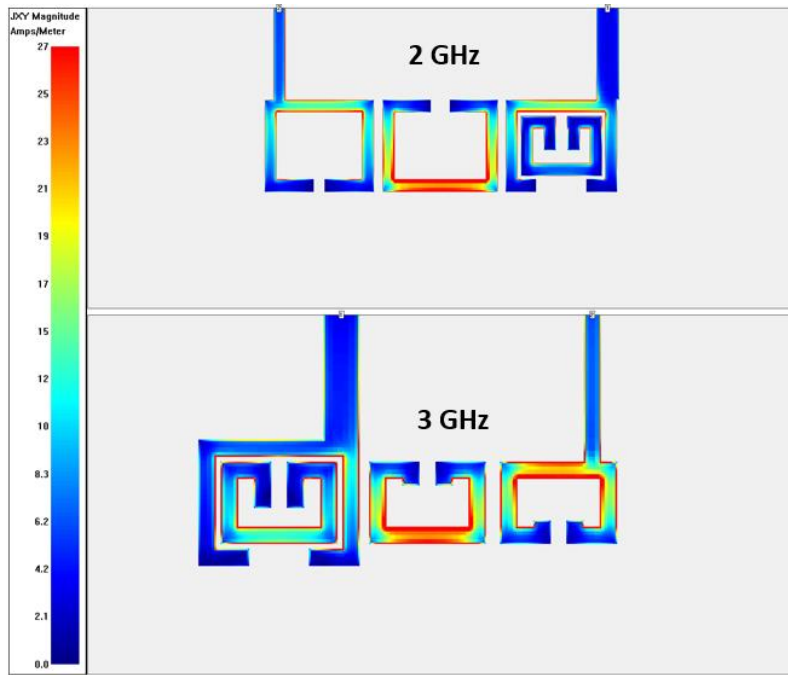


Figure 6.4 Simulated current distribution of the 2 GHz and 3 GHz filters

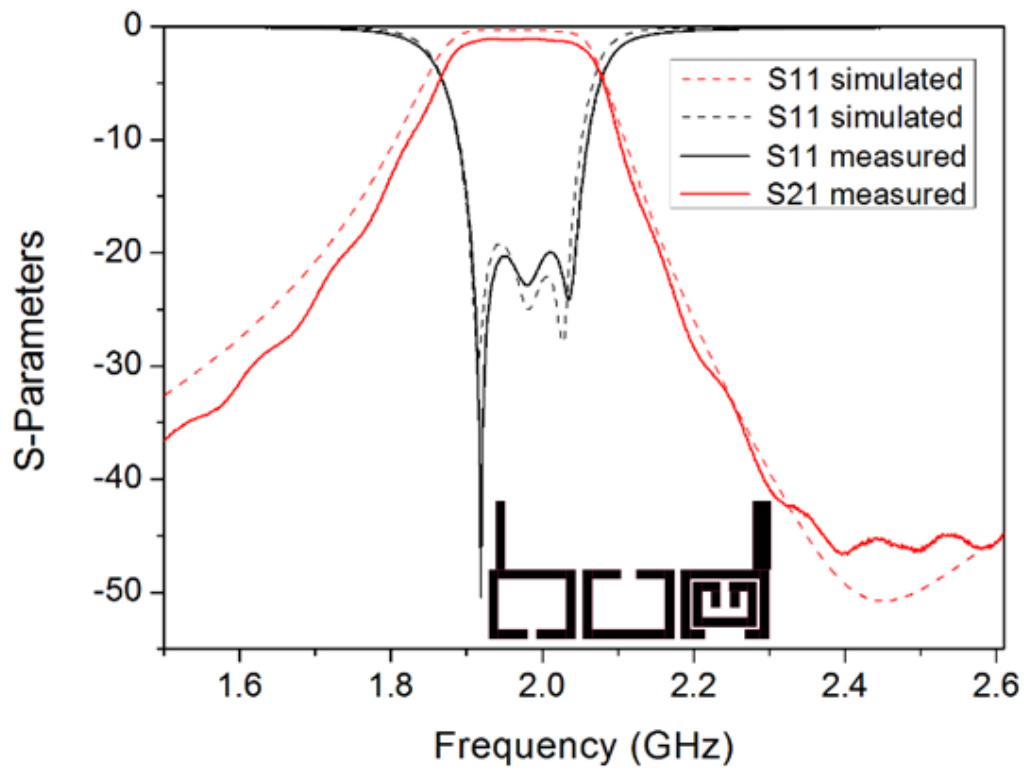


Figure 6.5 Simulated and measured response of the 2 GHz filter with the SRR

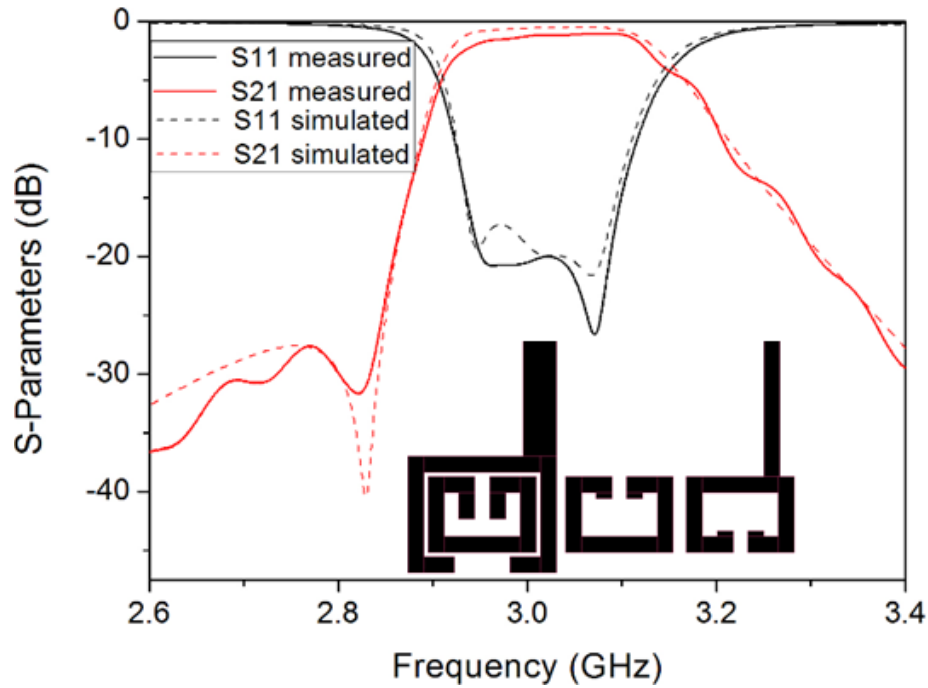


Figure 6.6 Simulated and measured response of the 3 GHz filter with the SRR

The individual channel filters were all fabricated using the Rogers 3010 substrate with a thickness of 1.27 mm, relative permittivity of 10.2 and loss tangent of 0.002. Fabrication and measurement were done using LPKF ProtoMat S63 micro-milling process and Agilent Network Analyser N5230A respectively. The measured responses are in good agreement with the simulated responses. It can be noticed that in Fig. 6.5, the measured insertion loss is about 2 dB while the return loss maintains the 20 dB. The position of the transmission zero can be seen at 2.43 GHz. Fig. 6.6 shows that the measured response maintains the same bandwidth with the simulated response, the insertion loss is about 2 dB while the return loss is about 20 dB and the transmission zero at 2.83 GHz.

### 6.3 Diplexer Implementation Using SRR as the Common Resonant Junction

This section presents a diplexer that uses an asynchronously tuned SRR as a common resonator to connect two channel filters. The SRR comprises two nested open-loop resonators resonating at two different frequencies corresponding to the two passbands of the diplexer respectively. This differs from [93] in that the nested resonators there are synchronously tuned, whereas

these are asynchronously tuned in this work resulting in more widely separated channels. The two channels at 2 GHz and 3 GHz each with a 4% fractional bandwidth were separately designed as discussed in Section 6.2 and joined together using the SRR. The SRR contains the first resonator of each channel filter, resulting in reduced circuit size. Very importantly, this also removes the need for any separate junction structures either based on transmission lines or resonators. Fig. 6.7 illustrates the proposed diplexer with SRR serving as a common resonant circuit completing the channel filter representing resonator 3 and 4. The SRR also forms part of the complete channel filter representing resonators 5 and 6.

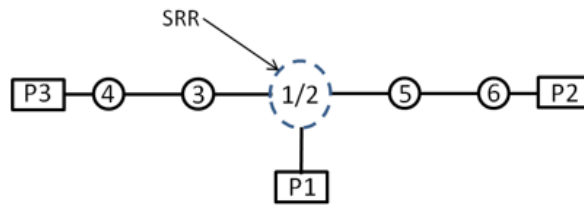


Figure 6.7 Topology of a diplexer using SRR as resonant junction

### 6.3.1 Design

The layout of the proposed diplexer with its dimensions is presented in Fig. 6.8. Using the three-pole Chebyshev low-pass prototype derived from [65, 118] with a ripple factor of 0.043, the coupling coefficient and Q-factors for physical dimensioning of the resonators can be obtained.

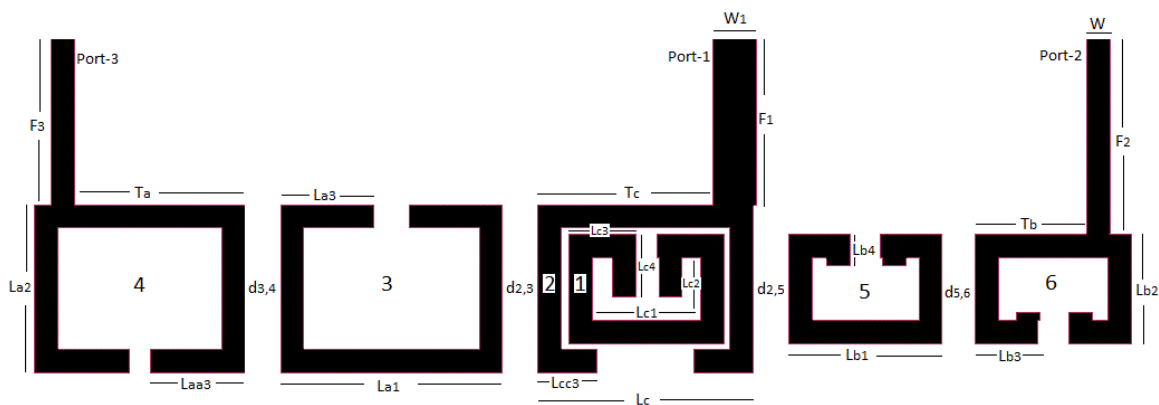
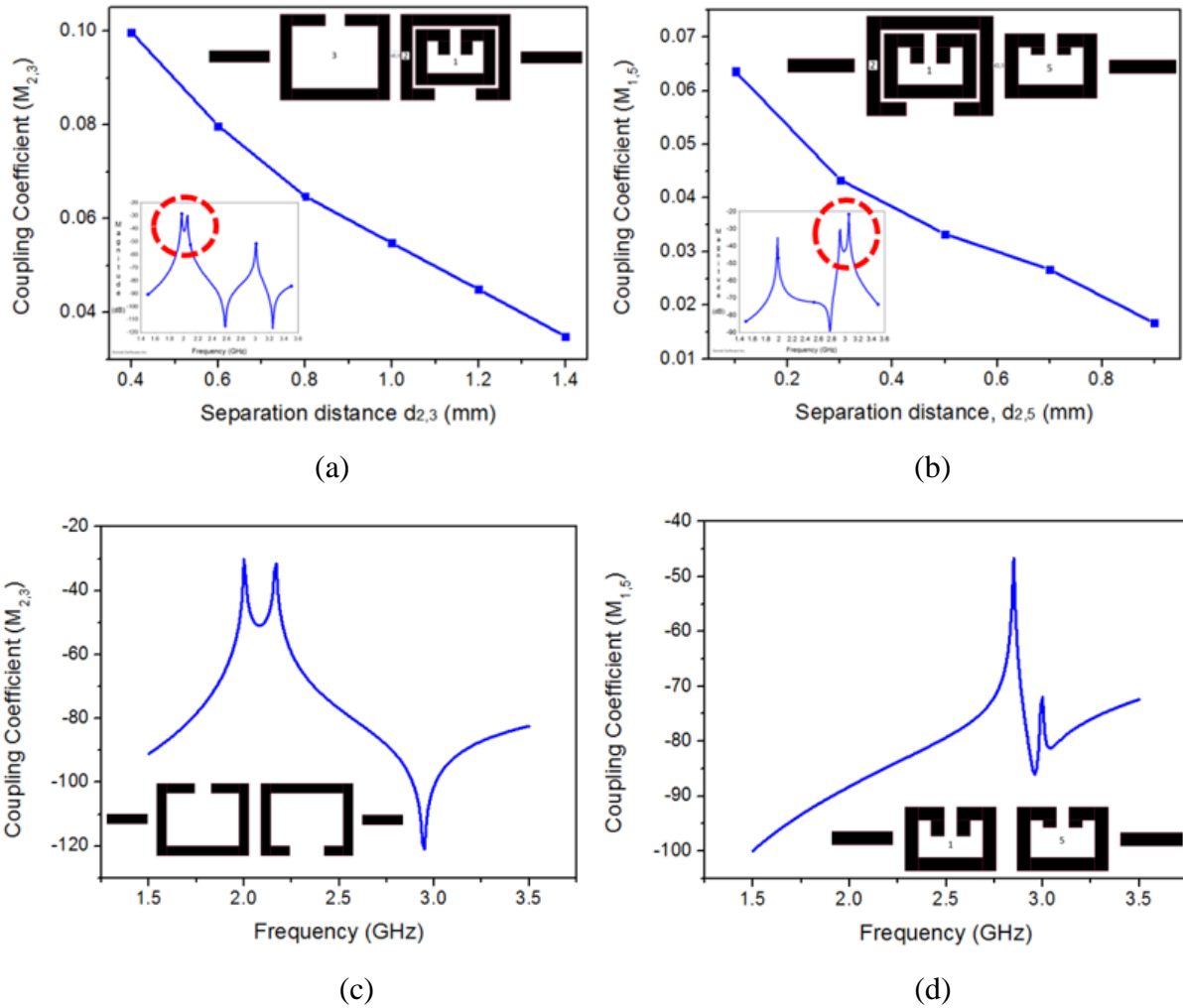


Figure 6.8 Diplexer layout.  $F1 = 7.9 \text{ mm}$ ,  $F2 = 9.3 \text{ mm}$ ,  $F3 = 7.9 \text{ mm}$ ,  $Ta = 8.1 \text{ mm}$ ,  $Tb = 5.3 \text{ mm}$ ,  $Tc = 8.3 \text{ mm}$ ,  $La1 = 10.2 \text{ mm}$ ,  $La2 = 8 \text{ mm}$ ,  $La3 = 4.5 \text{ mm}$ ,  $Laa3 = 4.6 \text{ mm}$ ,  $Lb1 = 7.5 \text{ mm}$ ,  $Lb2 = 5.2 \text{ mm}$ ,  $Lb3 = 3.3 \text{ mm}$ ,  $Lcc3 = 2.9 \text{ mm}$ ,  $Lc1 = 7.6 \text{ mm}$ ,  $Lc2 = 5.2 \text{ mm}$ ,  $Lc3 = 3.3 \text{ mm}$ ,  $Lc4 = 3.1 \text{ mm}$ ,  $d2,3 = 0.5 \text{ mm}$ ,  $d3,4 = 0.8 \text{ mm}$ ,  $d2,5 = 0.7 \text{ mm}$ ,  $d5,6 = 0.8 \text{ mm}$ ,  $W = 1.2 \text{ mm}$ ,  $W1 = 2.1 \text{ mm}$

In Fig. 6.8, the channel filter of the high passband is composed of resonators 1, 5 and 6 with resonator 1 being the inner ring of the SRR. Resonators 2, 3 and 4 represent the low passband channel filter with resonator 2 being the outer ring of the SRR. When analysed, it is noticed that a cross-coupling [93] is also established between resonator 1 of the SRR and resonator 3 and 5 of the two channel filters. This established cross-coupling resulted in the introduction of additional transmission zeros in the diplexer [93, 143]. The coupling coefficients and external Q-factors used for physical dimensioning of the channel filters as well as the diplexer were achieved using (3.4) and (5.3) respectively.

### 6.3.2 Coupling

The required coupling coefficient between the low passband channel filter and the SRR is achieved by adjusting the coupling distance  $d_{2,3}$ . Fig. 6.9 (a) illustrates the coupling coefficient  $M_{2,3}$  as a function of  $d_{2,3}$  with the inset showing a typical response. The red dashed line circles the resonant peaks used for calculating  $M_{2,3}$ . It should be noted that resonator 1 was present in the simulation to represent its potential loading effect. To couple the channel filter of high passband to the SRR, the change of coupling coefficient  $M_{1,5}$  as a function of  $d_{2,5}$  is investigated when resonator 2 is present, as shown in Fig. 6.9 (b) where the red dashed line circles the resonant peaks used for calculating  $M_{1,5}$ . It is worth noting that resonator 2 enhanced the coupling between resonator 1 and 5. Without it, the coupling would be weak. Fig. 6.9 (c) illustrates the coupling response of Fig. 6.9 (a) without the loading effect of resonator 1. Fig. 6.9 (d) illustrates that of Fig. 6.9 (b) without the loading effect of resonator 2. Fig. 6.9 (c) and (d) shows the importance of resonator 1 or 2 being present in obtaining the coupling coefficient of  $M_{2,3}$  or  $M_{1,5}$ .



**Figure 6.9 (a).  $M_{2,3}$  against  $d_{2,3}$  with the inset of topology and typical response; (b)  $M_{1,5}$  against  $d_{2,5}$  with the inset of topology and typical response; (c) Coupling response of Fig. 6.9 (a) without resonator 1; (d) Coupling of Fig. 6.9 (b) without resonator 2.**

Fig. 6.10 presents the resonant responses of the four resonators 1, 2, 3 and 5 when coupled together. These achieved peaks of the eigenmodes can also be used in finding the coupling coefficients of  $M_{2,3}$  and  $M_{1,5}$ . Again, it can be observed that the inter-band transmission zero as in Fig. 6.1 is still preserved but at a slightly higher frequency due to the adjacent open-loop resonators of the SRR.

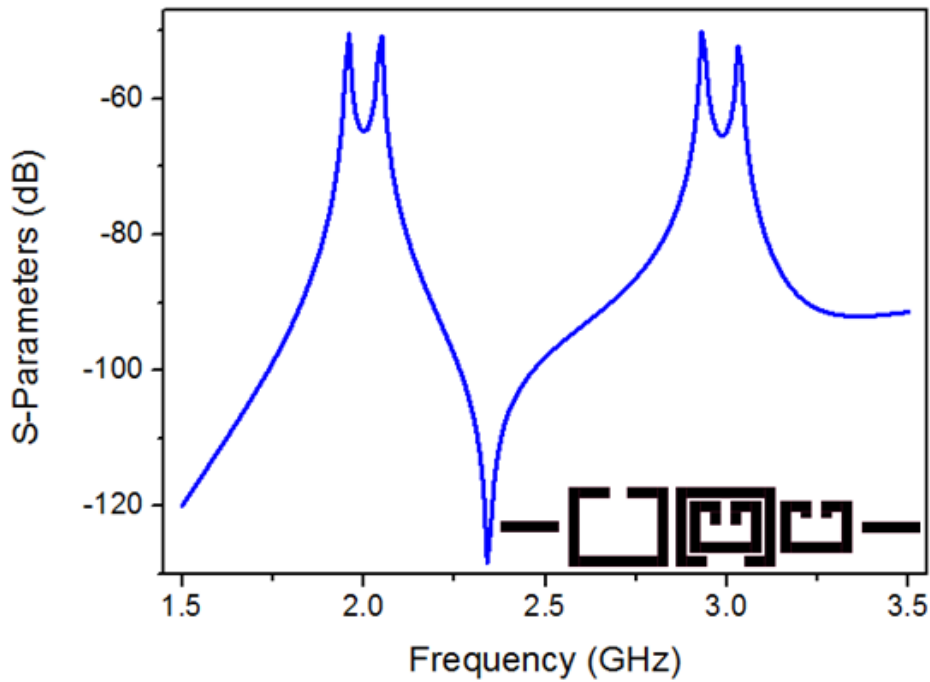


Figure 6.10. Eigen-mode response and topology

### 6.3.3 Simulation Results

Fig. 6.11 illustrates the simulated responses with dashed lines. It can be seen that the responses meet the design specifications of 20 dB and FBW of 4%, making the lower passband to operate from 1.96 GHz to 2.04 GHz and the higher passband to operate from 2.94 GHz to 3.06 GHz. It is also noted when compared with Section 6.2, that the two transmission zeros observed in the two separate channel filters are preserved within the guard band of the diplexer. Fig. 6.12 shows the simulated current distribution of the two channels during operation at 2 GHz and 3 GHz. According to the current distribution, it is evident that the SRR can operate as a signal splitter and combiner for the two channel filters.



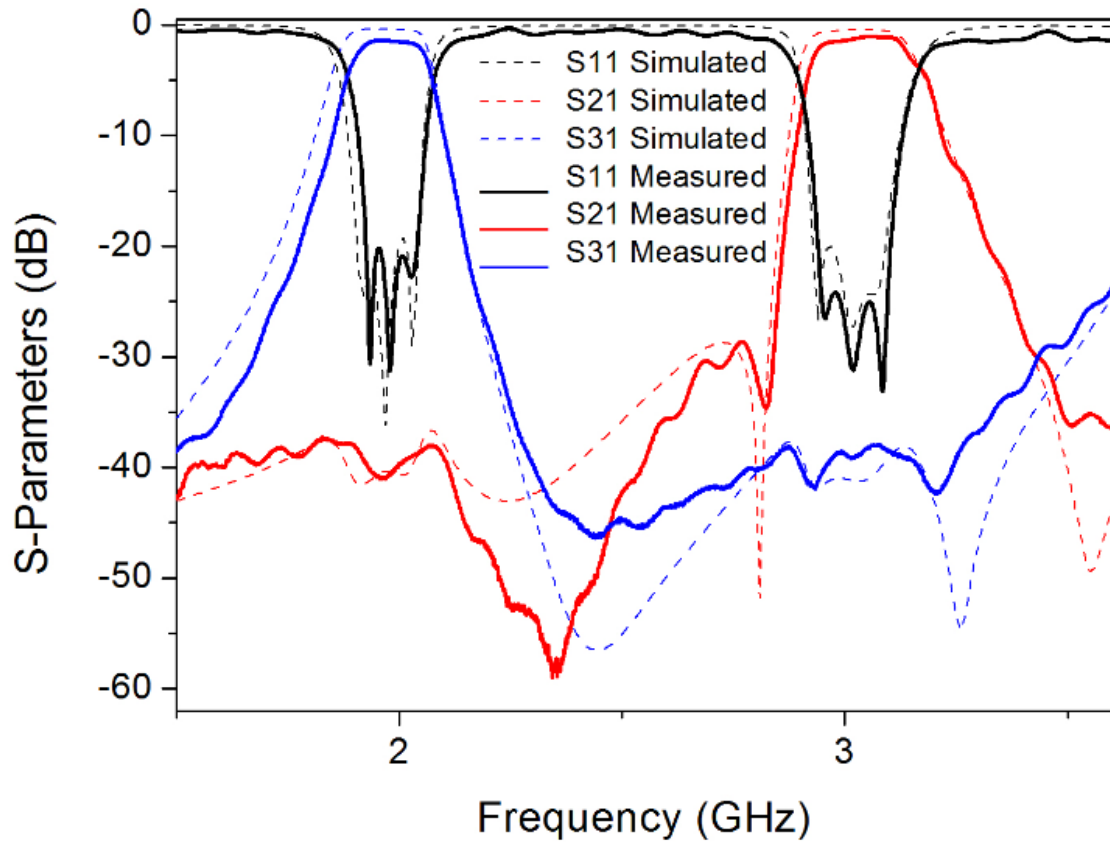


Figure 6.11 Simulated and measured responses of the diplexer

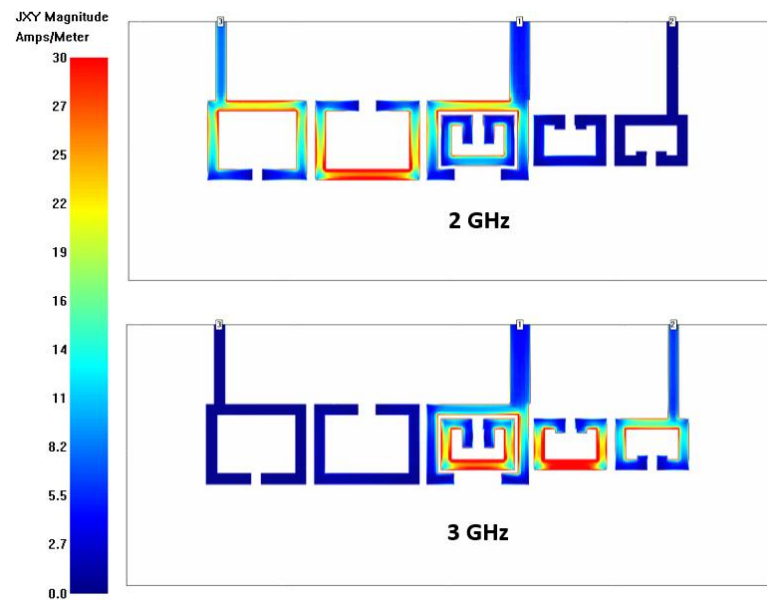


Figure 6.12 Simulated current distribution of the diplexer at 2 and 3 GHz

### 6.3.4 Fabrication and Measurements

The designed diplexer was fabricated on Rogers 3010 substrate with a thickness of 1.27 mm, relative permittivity of 10.2 and loss tangent of 0.002. Fig. 6.13 shows the fabricated diplexer circuit. The measured response is displayed in Fig. 6.11 using solid lines in comparison with the simulated responses. Measurements and simulations are in good agreement with each other. It can be seen that the measured response has its low passband frequency shifted to the higher by about 5 MHz, the high passband frequency shifted to the higher by about 2 MHz. The return loss is 22 dB and 25 dB for the low and high passband respectively. The insertion loss is about 2 dB for both passbands. These small discrepancies were mainly due to fabrication tolerance and the variation of the dielectric constant of the high permittivity dielectric material.

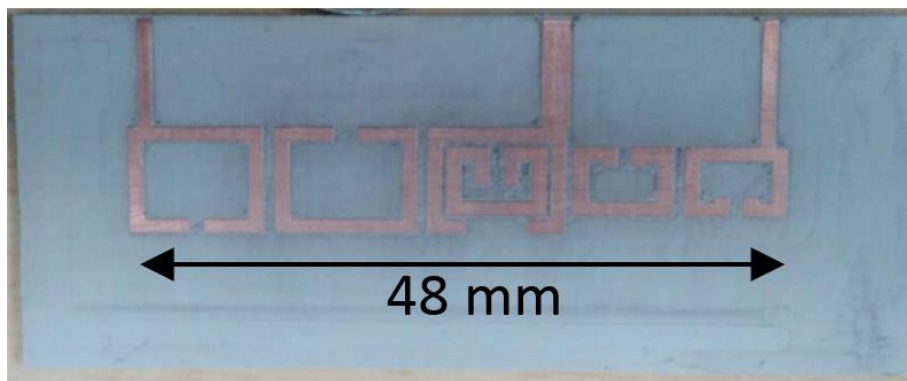


Figure 6.13 Photo of the fabricated diplexer

### 6.4 Compact Dual-Band Bandpass Filter Using SRR

Apart from the junction resonators of diplexers, the dual-mode property of the SRR can be applied to dual-band filters. In this section, the asynchronously coupled open-loop resonator in the SRR is explored to realise a dual-band filter with widely separated bands. A pair of such SRR are coupled together to form the dual-band BPF. As compared with [124], this structure is easier to extract coupling coefficients between resonators and to adjust the positions of the two bands. Besides these features, this design is more compact when compared with its counterparts in [124, 144, 145] as one open-loop resonator is nested into the other.

The compact dual-band BPF is proposed and designed to meet the following specifications:

- Centre frequency of the lower and upper passbands,  $f_{0,BPL}$  and  $f_{0,BPU}$ : 2 GHz and 3 GHz
- Passband return loss: 20 dB
- Fractional Bandwidth of lower and upper passband,  $FBW_L$  and  $FBW_U$ : 2 %

The dual-band BPF has two poles on each band with a Chebyshev response having a ripple factor of 0.043 dB. The corresponding g-values [118] are  $g_0 = g_3 = 1.2210$ ,  $g_1 = 0.6648$ ,  $g_2 = 0.5445$ . The coupling coefficient and the Q-factor used for the physical dimensioning of the dual-band BPF can be calculated using (3.4) and (5.3) respectively.

The physical dimensions of the dual-mode SRR are achieved using the method discussed in Section 2.4.2 while the external Q-factor is achieved as explained in Fig. 6.1. The resonators are then assembled to create the coupling topology as shown in Fig. 6.14 where the dashed line represents the coupling between the inner resonators of the two SRRs labelled as resonator 1 and 1' while the thick line represents the coupling between the outer resonators of the two SRRs labelled as resonator 2 and 2'. Fig. 6.15 presents the simulated response with widely separated band with two transmission zeros in the guard band. Fig. 6.16 displays the layout of the dual-band BPF. The design was not prototyped but to show a potential capability of the SRR in dual-band filter implementation.

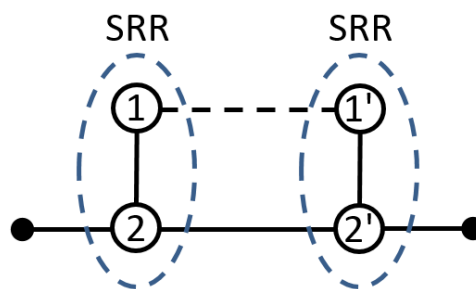


Figure 6.14 Dual-band BPF coupling topology

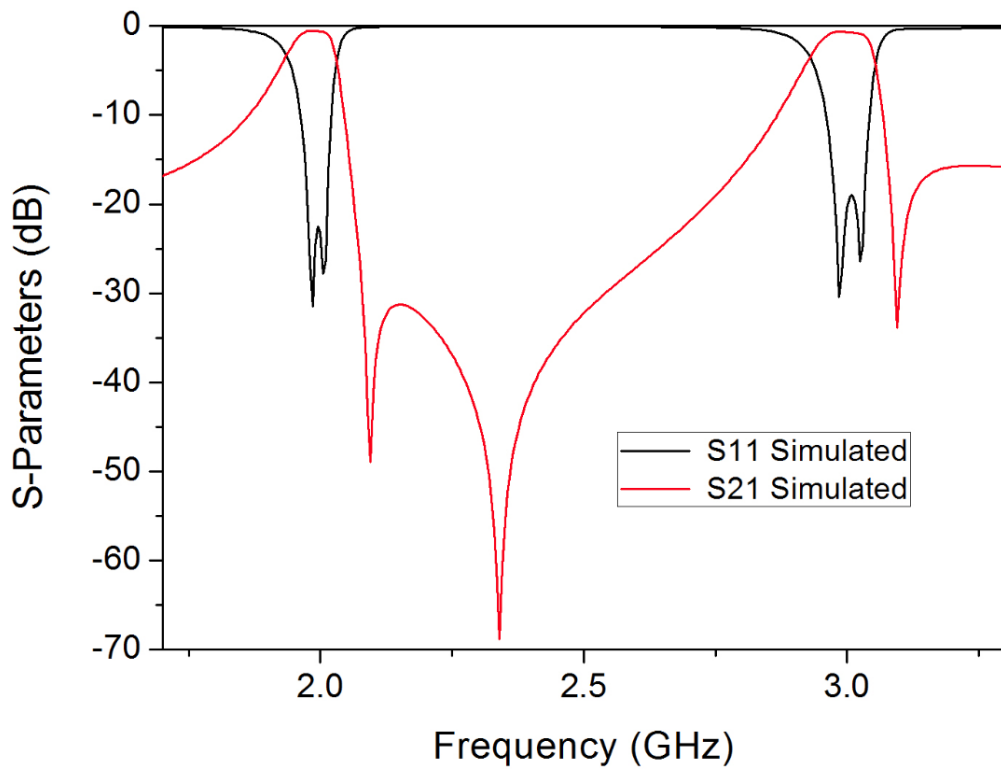


Figure 6.15 Dual-band BPF simulated response

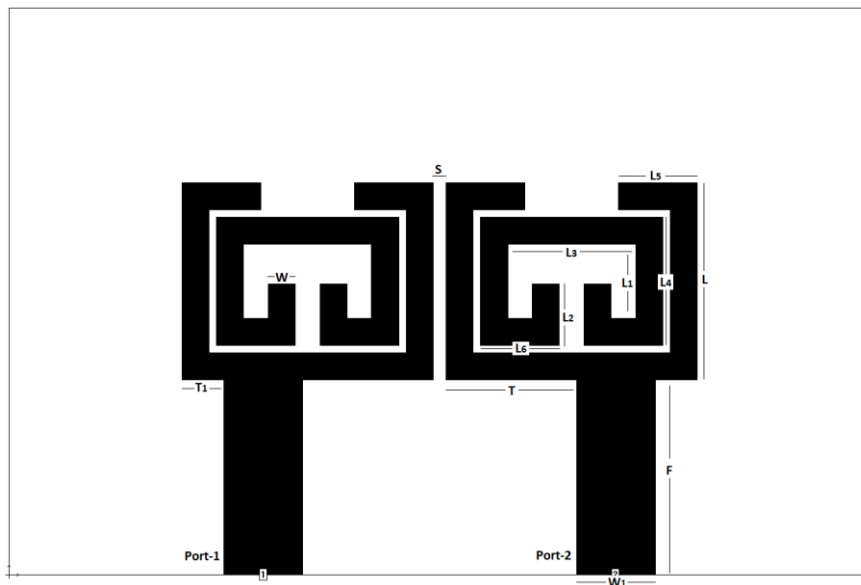


Figure 6.16 Layout of the dual-band BPF.  $F = 7.9$  mm,  $L = 8$  mm,  $L1 = 3$  mm,  $L2 = 2.5$  mm,  $L3 = 5.2$  mm,  $L4 = 5.2$  mm,  $L5 = 3.2$  mm,  $L6 = 3.2$  mm,  $W = 1.1$  mm,  $W1 = 3.2$  mm,  $T = 5.3$  mm,  $T1 = 1.7$  mm,  $S = 0.2$  mm

## 6.5 Summary

In this chapter, the asynchronously coupled SRR has been utilised in the design of BPFs, a diplexer and a dual-band BPF. The SRR was used to replace the first resonator in a three-pole hairpin BPF; this resulted in an improved frequency selective response when compared with three-pole conventional hairpin filters. This application is then extended to the design of a diplexer. The diplexer is designed to have a compact junction structure using the SRR. The SRR, being a dual-mode resonator, acted as a signal splitter and combiner for the two channels of the diplexer and at the same time as a resonant pole for each channel. The diplexer being an all-resonator based diplexer achieved three poles for each channel using four single-mode resonators and one SRR. This resulted in a compact circuit size as the need for the conventional transmission line based junction is eliminated. The filters and diplexer were successfully designed and tested to operate at 2 GHz and 3 GHz passbands, with the passbands operating at 4% fractional bandwidth each with 20 dB return loss. Besides, a dual-band BPF is also designed using two coupled SRRs. The SRRs were coupled in parallel to generate a dual-band BPF response. The dual-band BPF operates at 2 GHz and 3 GHz with a 2% fractional bandwidth and 20 dB return loss each. This shows the versatility of SRR in the design of microwave filters and diplexers.

# Chapter 7: Integrated Filtering Antenna

## 7.1 Introduction

The filters, diplexers and antennas are part of the major components in wireless systems such as satellites, and base stations. Conventionally, the designs of these devices, using their fundamental theorem are quite different, leading to the creation of specialist filters, diplexers or antennas. During the design process, the input ports and or output ports of these devices are assumed to have an interface of 50 Ohms. It is assumed that by maintaining the 50 Ohm interface, that the response will be maintained after connection and commissioning. In practice, this may not be the case, because a connection between devices introduces losses from mismatches, especially when the components are of different bandwidths. A deteriorated performance may well be noticed. To overcome the degradation and make the circuit more compact, the integration and co-design of the separate components is a solution. This process involves the elimination of the 50 Ohm interface between the antenna and the filter or diplexer.

The designs presented here are the filter and antenna integration, diplexer and antenna integration and finally, an integration of a dual-band bandpass filter and an antenna. The integration of these devices will reduce the complexity of the system. This is because of the elimination of some of the feeding/matching circuit [130, 146 - 149]. It is also worth mentioning that the feed networks of the antennas are effectively replaced with filters. The integration process made the antennas function as a resonating pole to the filter. Besides, the insertion losses introduced by the interconnection between the antenna and filter are removed.

An integration of a bandpass filter and an orthogonal mode patch antenna is first proposed and demonstrated using filter synthesis. Using the orthogonal mode of the patch antenna, two filter antennas were designed, one operating at 1.8 GHz and the other operating at 2.4 GHz. As shown in [150, 151], in the integrated designs, the absence of an interconnection-related insertion loss and higher order harmonics are evident in the responses achieved. Besides, the bandwidth can be controlled by adjusting the coupling distance between the resonating poles of the filter and the radiating element of the antenna [152].

From the applications perspective, in a communication base station, a duplexer is used to allow the transmitter and the receiver to share one antenna port. To avoid much interference between the two channels, a high isolation is required between the transmitting and the receiving ports of the duplexer. Fig. 7.1(a) presents the conventional cascade of a duplexer with an antenna in such a system. To avoid the possible problems mentioned above, the 50 Ohm interface matching network, as well as the cable between the duplexer and the antenna, can be eliminated. Fig. 7.1(b) provides an alternative method of using one antenna with the duplexer in an integrated system.

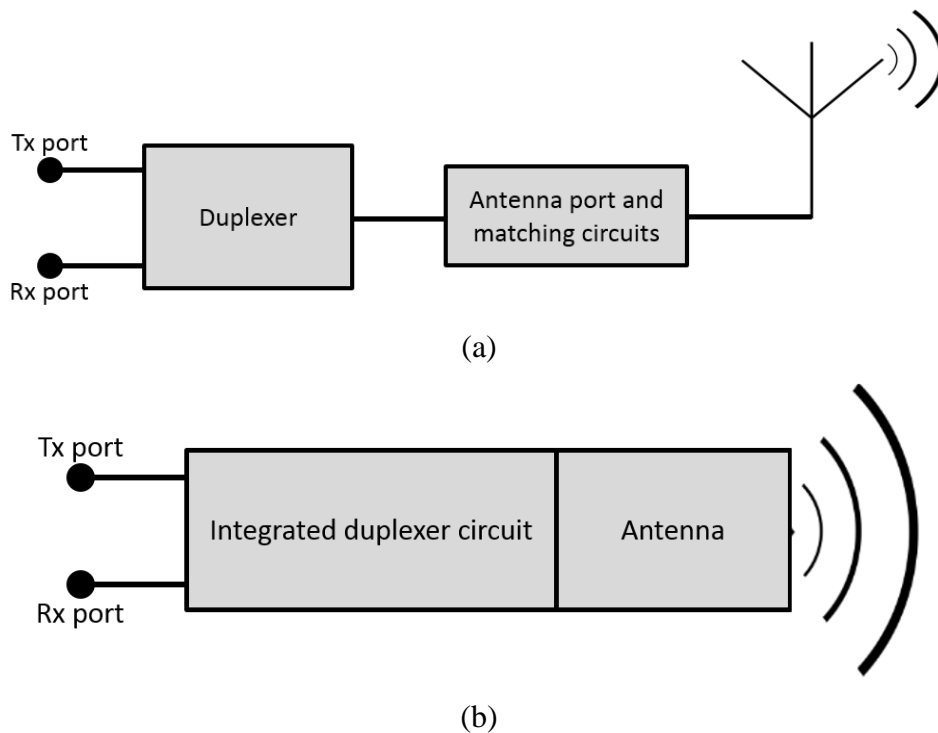


**Figure 7.1 Duplexer and antenna (a) Conventional cascaded subsystem (b) Integrated duplexer-antenna**

An integration of the duplexer and antenna is demonstrated in this chapter for achieving a multi-function RF front end component. This is achieved by utilising the orthogonal modes of a rectangular patch antenna to function as a resonant structure, radiating structure, signal splitter and combiner in a duplexer-antenna design. Using two sets of hairpin resonators on each channel and a radiating antenna as a resonant junction makes the circuit more compact with ease to implement. The compactness comes from the absence of the 50 Ohm interface and matching network which could have come between them in a conventional (cascaded network) counterpart as well as the use of the antenna as a resonant junction. This is different from [153],

where the duplexer is coupled to the antenna through a slot in a stacked form. Here, the antenna and the duplexer are designed on the same plane using the direct edge coupling technique.

The last design to be presented will use a patch antenna as a resonating and radiating structure in a dual-band bandpass filtering antenna. The design is based on a two-pole bandpass filter response on each channel, making it a total of four poles in the dual band response. Using a two-patch structure, this design was achieved. One dual-mode patch resonator, resonating at 1.8 GHz and 2.1 GHz was used to act as the first resonator of the design while the second resonator is a patch antenna. By using a through-hole coupling technology, the resonators were placed back to back with a common ground between the resonators. The resonators and the design topology used resulted in a miniaturised circuit.

## 7.2 Duplexer-Antenna

### 7.2.1 Design Specifications

The design utilised two channel filters and one resonating antenna. The filters were designed to meet the three-poles Chebyshev ripple factor of 0.043 dB with lowpass prototype obtained from [118] where the g-values of  $g_0 = g_4 = 1.0$ ,  $g_1 = g_3 = 0.8516$  and  $g_2 = 1.1032$ . The g-values were then used for obtaining the coupling coefficient and the input/output quality factors used for the design of the filters. Using the hairpin resonators, one filter was designed for 1.8 GHz and the other 2.4 GHz. These filters were designed to have 4% FBW with a return loss of 20 dB each. The width (W) and the length (L) of the patch antenna are calculated using (7.1) [154]. The antenna being a rectangular patch, possesses a dual-mode response depending on the feeding position used.

$$W = \frac{C_0}{2f_0 \sqrt{\frac{\epsilon_r + 1}{2}}} \quad (7.1 a)$$

$$L_{eff} = \frac{C_0}{2f_0 \sqrt{\epsilon_{eff}}} - 2\Delta l \quad (7.1 b)$$



where  $\epsilon_r$  is the dielectric constant,  $C_0$  is the speed of light in free space and  $L_{eff}$  is the effective length of the resonant element,  $\epsilon_{eff}$  is the effective dielectric constant as expressed in (3.1 c), and  $\Delta l$  is the line extension and expressed as

$$\Delta l = 0.412 \cdot h \left[ \frac{0.262 + \frac{W}{h}}{0.813 + \frac{W}{h}} \right] \left[ \frac{\epsilon_{eff} + 0.3}{\epsilon_{eff} - 0.258} \right] \quad (7.1 c)$$

As explained in the Introduction, the aim is to integrate antennas and filters while eliminating the 50 Ohm interface and matching network. This is possible when the antenna and the filters are designed together. Here, the filtering characteristics of the filters are preserved by making the radiation quality factor of the patch to be equal to the external quality factor at the filter input. This results in the patch's radiated power (gain response) to be similar to that of the insertion loss response of the filter with minimum insertion loss response in the passband (high gain) and high rejection in the off-band (low gain). In the designs, the antenna is used to replace the third resonator of the filters.

## 7.2.2 Filtering Antenna

First, the design of each channel filter with the integrated antenna will be investigated. This is based on utilising the orthogonal modes of a rectangular patch antenna. Each mode of the patch antenna will be integrated with its corresponding narrow band filter individually, creating two different filtering antenna responses using the same patch antenna.

To demonstrate this, a 1.8 GHz three-poles hairpin filter had its third resonator removed and replaced with the patch antenna as shown in Fig. 7.2. The coupling coefficient of the resonator 2 and the patch antenna shown in Fig. 7.2(b) is made to be the same as that of the coupling coefficient of the resonator 2 and resonator 3 of the filter shown in Fig. 7.2(a). This is extracted using the arrangement shown in Fig. 7.3(a) with its achieved simulated response presented in Fig. 7.3(b). The coupling between the resonator and the patch is controlled by adjusting the coupling distance,  $S$ . After extracting the coupling distance, the filtering antenna is then assembled and optimised to specification. The 1.8 GHz bandpass filter is now converted into a filtering antenna. The simulated response of the filtering antenna is presented in Fig. 7.4.

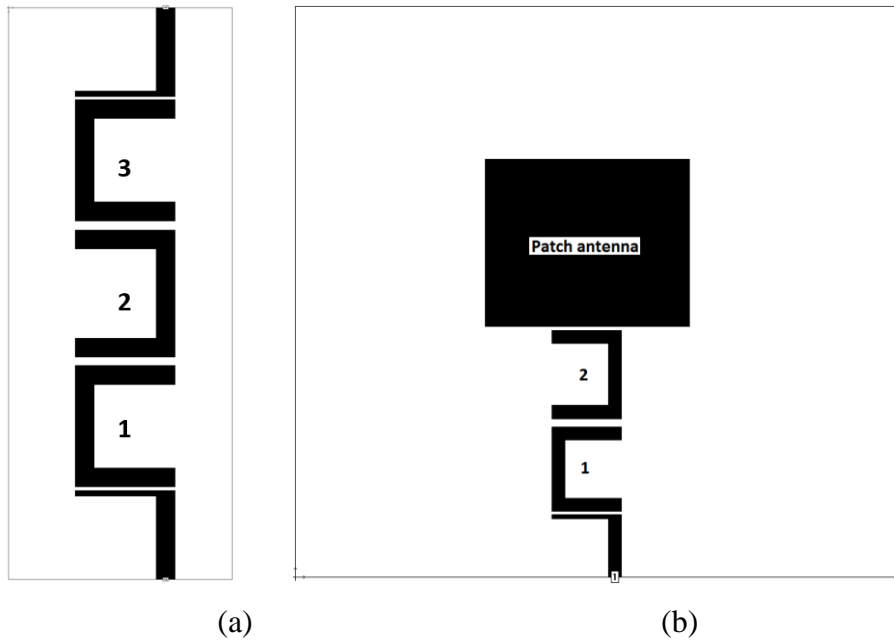


Figure 7.2 (a) 1.8 GHz hairpin filter layout; (b) 1.8 GHz hairpin and patch filtering antenna layout

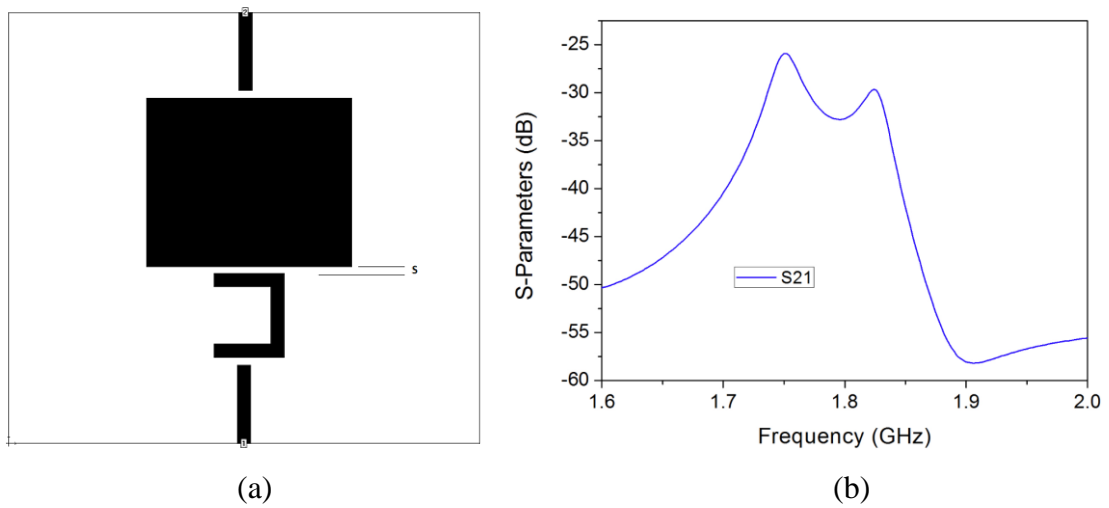


Figure 7.3 Extracting the coupling coefficient (a) layout; (b) response

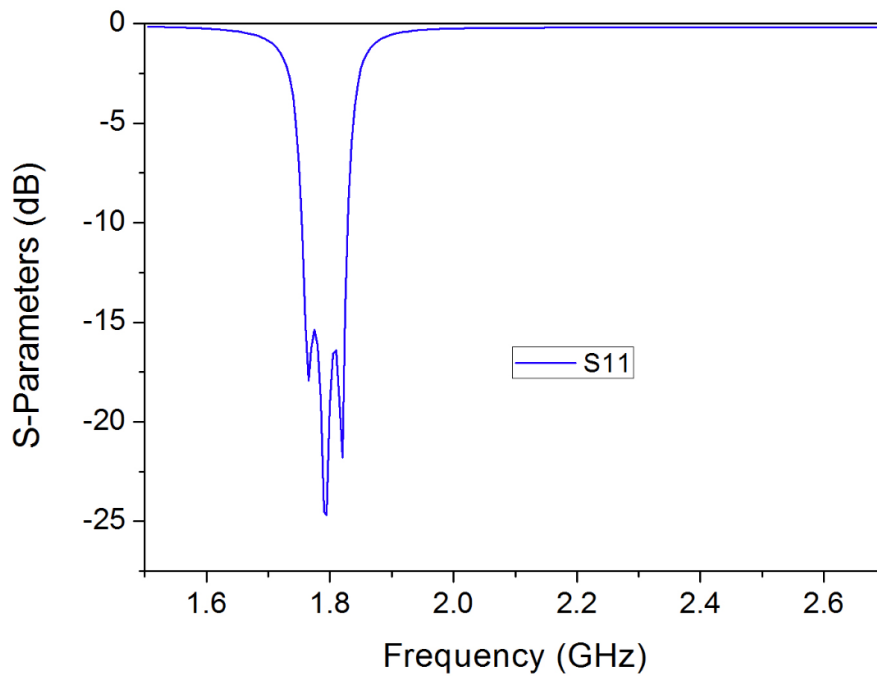


Figure 7.4 Simulated 1.8 GHz hairpin and patch filtering antenna response

The same procedures were used in the design of a 2.4 GHz filtering antenna. The second mode (2.4 GHz) of the patch antenna is in-line coupled to a 2.4 GHz filter. This is done by replacing the third resonator of the 2.4 GHz filter with the patch antenna, followed by optimisation. Fig. 7.5(a) presents the design topology of the 2.4 GHz filtering antenna while Fig. 7.5(b) presents its simulated response.

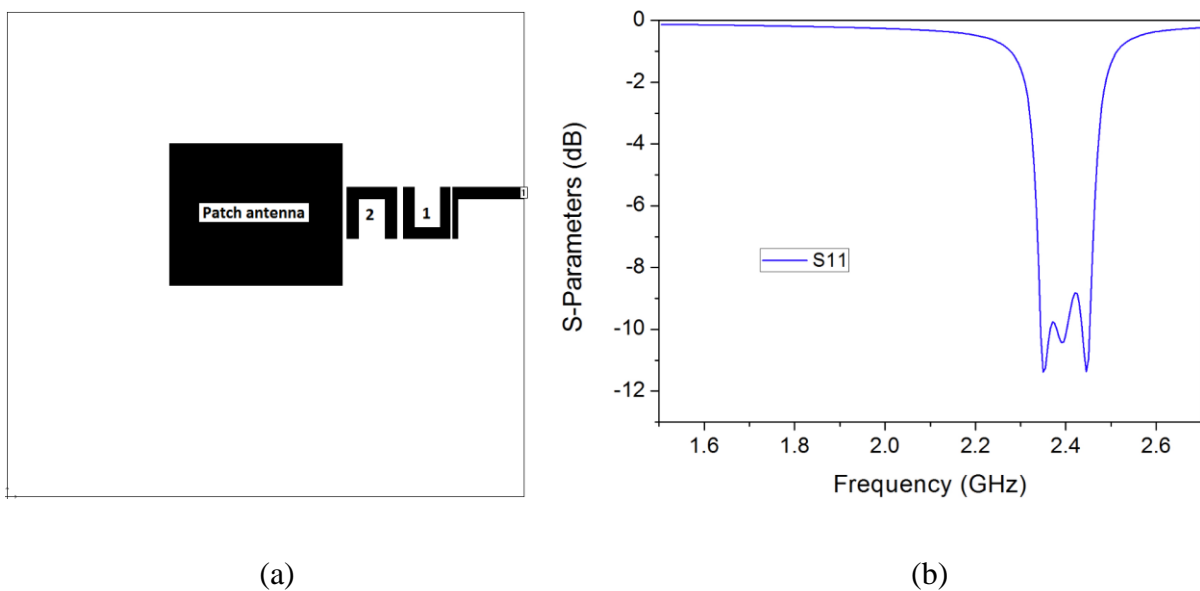


Figure 7.5 2.4 GHz filtering antenna (a) layout ;(b) response

These two filtering antennas have demonstrated the integration of a three-pole narrow band filter with a patch antenna on the same circuit plane using the general coupled filter synthesis. The next step is to utilise both modes of the patch antenna to combine the two filtering-antennas into a duplexer-antenna.

### 7.2.3 Duplexing Antenna Design

The two individually designed filters of 1.8 GHz and 2.4 GHz are integrated with an antenna to form a duplexing antenna. The 1.8 GHz filter will serve the receiving channel for the downlink while the 2.4 GHz channel will serve the transmitting channel for the uplink. The antenna used is an orthogonal mode patch antenna of 1.8 GHz and 2.4 GHz frequency, calculated using (7.1). Fig. 7.6(a) presents the coupling topology of the duplexer-antenna in a conventional cascaded design while Fig. 7.6(b) presents the proposed coupling topology.

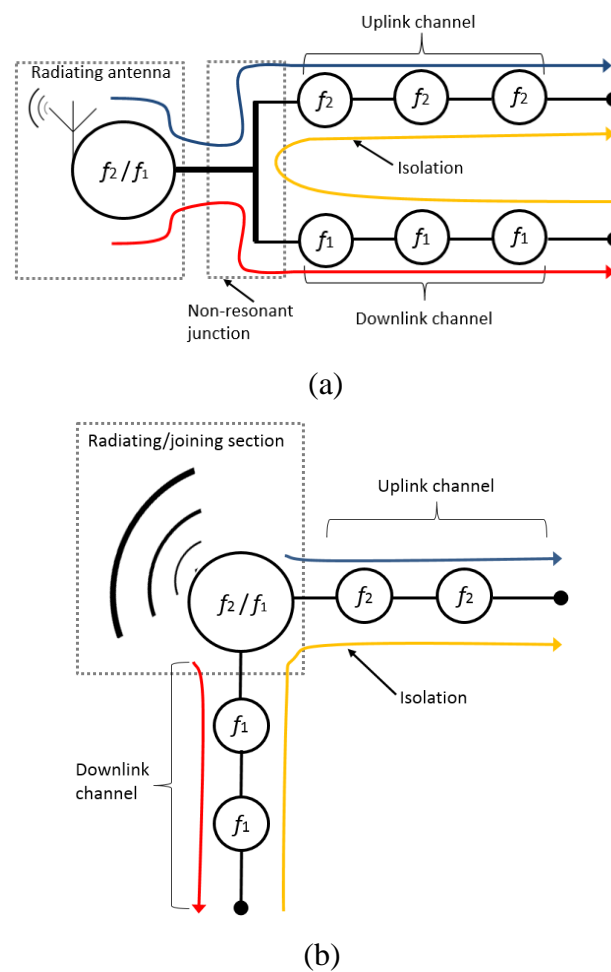
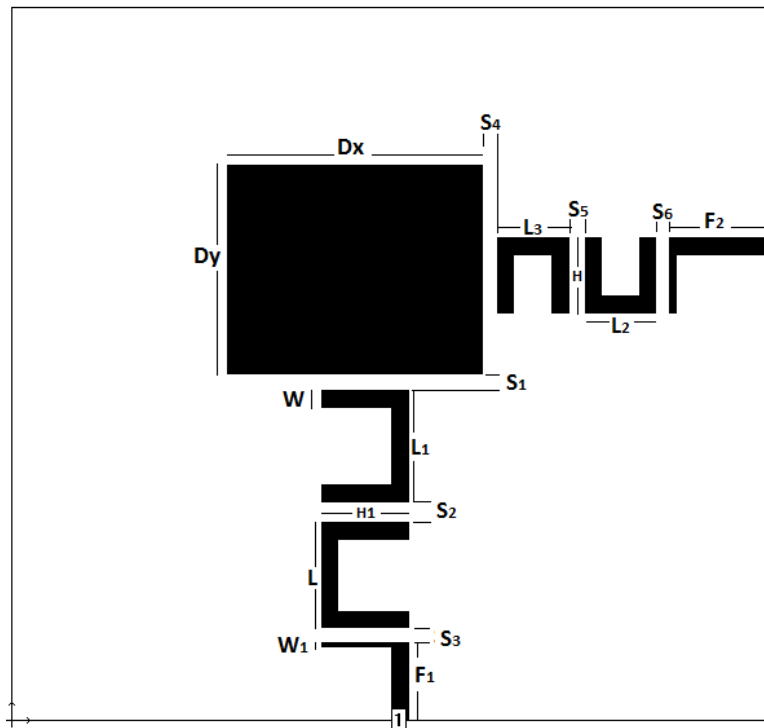


Figure 7.6 Coupling topology (a) conventional; (b) proposed

The design layout is presented in Fig. 7.7 with the achieved dimensional parameters after optimisation.



**Figure 7.7** Designed duplexer antenna layout with parameters.  $D_x = 52.5$  mm,  $D_y = 43$  mm,  $S_1 = 1.05$  mm,  $S_2 = 2.1$  mm,  $S_3 = 0.3$  mm,  $S_4 = 0.25$  mm,  $S_5 = 2$  mm,  $S_6 = 0.3$  mm,  $F_1 = 15$  mm,  $F_2 = 20$  mm,  $H = 15.5$  mm,  $H_1 = 17.9$  mm

The S-parameters of the optimised duplexing antenna is presented in Fig. 7.8. Fig. 7.8 illustrates the low channel from 1.764 GHz to 1.836 GHz and the upper channel from 2.352 GHz to 2.448 GHz. The responses show that the design meets the 4% FBW on each channel. Fig. 7.8 presents the isolation between the channels (ports  $S_{21}$ ) at about 43 dB in comparison with  $S_{11}$  and  $S_{22}$ . It can also be observed that the three poles for each channel are clearly identifiable in the Figure which indicates the contribution of the antenna as a resonant pole for each channel. This design has shown good filtering functions with a sharp skirt at the band edges with a good guard band. These responses with enhanced features are due to the integration of the duplexer and the antenna which eliminated the 50 Ohm interface between them. The design strategy ensured that all the resonators including the antenna contribute to the filtering functions.

It should be noted that the two bands operate orthogonal polarisations in this design. This is different from [153] where consistent polarisations were realised for the two duplexing channels.

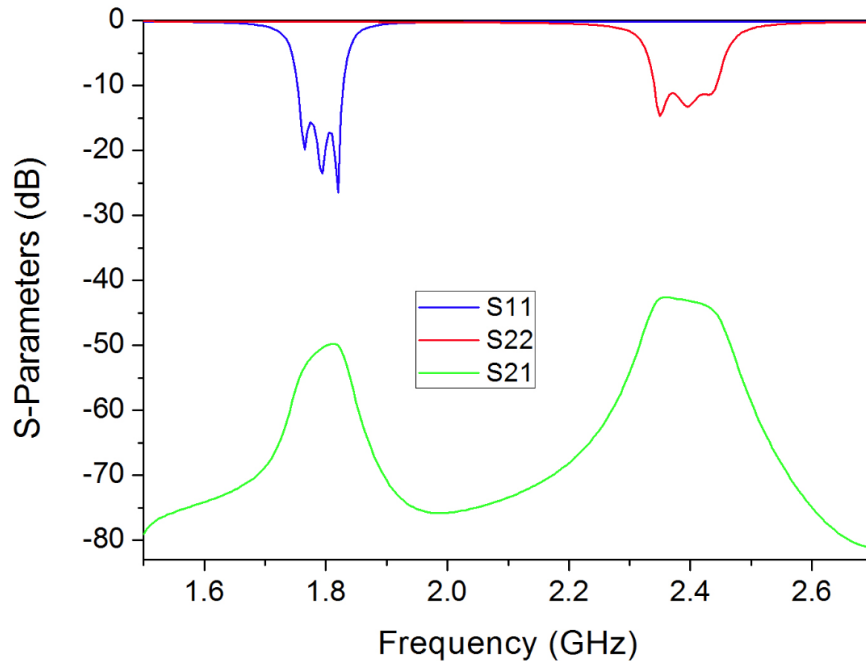


Figure 7.8 Simulated duplexer antenna isolation between two channels (ports) and the frequency responses

### 7.3 Dual-Band Bandpass Filtering Antenna

Now that a duplexer antenna with dual polarization has been demonstrated, similar design concept will be applied to a design of a dual-band dual-polarisation antenna using a dual-mode patch antenna and a dual-mode patch resonator. The dual-band bandpass filter is co-designed with four poles in the filtering response, two poles on each channel. The dual-mode resonator performs the signal splitting and combining function in the circuit, designed for 1.8 GHz and 2.1 GHz. The dual-mode antenna performs the radiating functions and also contributes to resonating poles of the dual band filter. The coupling between the resonator and the antenna is achieved using a coupling slot, while the resonator and the antenna are placed in a back-to-back position with a common ground. The coupling slot technique is to realise the required coupling but avoid radiation interference between the antenna and the resonator. Fig. 7.9 presents the design configuration of the dual-band bandpass filtering antenna. Fig. 7.9(a) shows the front view of the design with a dual-mode patch resonator and the feedline. Fig. 7.9(b)

shows the side view with a relative permittivity of 3.55 and a thickness of 3.048 mm. Fig 7.9(c) shows the back view with an orthogonal mode patch antenna. The dual-mode patch resonator of the front view operates similarly as the resonator in Chapter 5. The perturbed corner creates the two modes at 1.8 GHz and 2.1 GHz respectively. Two slots are used to couple to the two orthogonal modes of the patch antenna. Fig. 7.10 presents the coupling topology of the dual band filtering antenna.

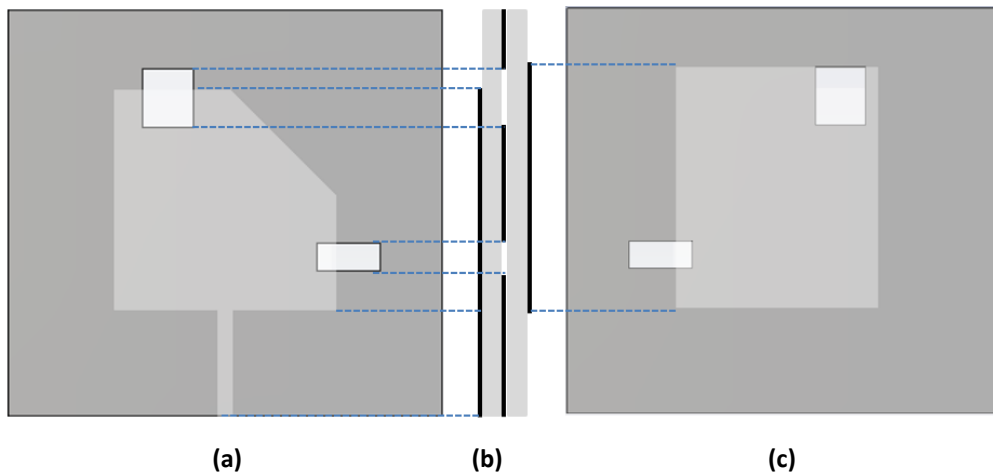


Figure 7.9 Dual-band bandpass filtering antenna (a) front view; (b) side view; (c) back view

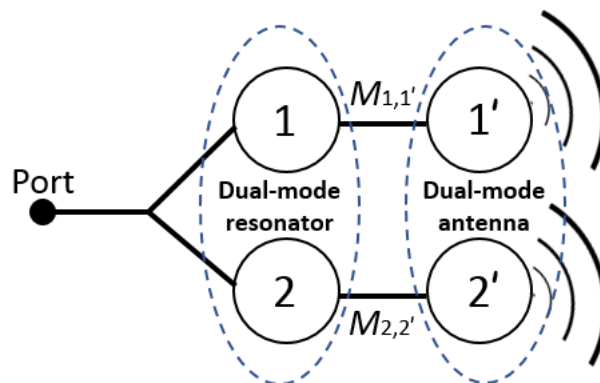


Figure 7.10 Dual band bandpass filtering antenna coupling topology

The simulated S-parameters after optimisation is presented in Fig. 7.11 in comparison with the measured response. It can be noticed that there is frequency shift to the right for the measured response of about 20 MHz on the low band and about 8 MHz on the high band. The simulated farfield radiation pattern at 1.8 GHz is presented in Fig. 7.12. Fig. 7.13 presents the measured farfield radiation pattern on the E-plane at 1.8 GHz for the cross polarisation in comparison with the 2.1 GHz for the co polarisation. Fig. 7.14 presents the simulated farfield radiation pattern at 2.1 GHz. The Fig. 7.15 presents the measured farfield radiation pattern on the H-

plane at 2.1 GHz for the cross polarisation in comparison with the 1.8 GHz for the co polarisation.

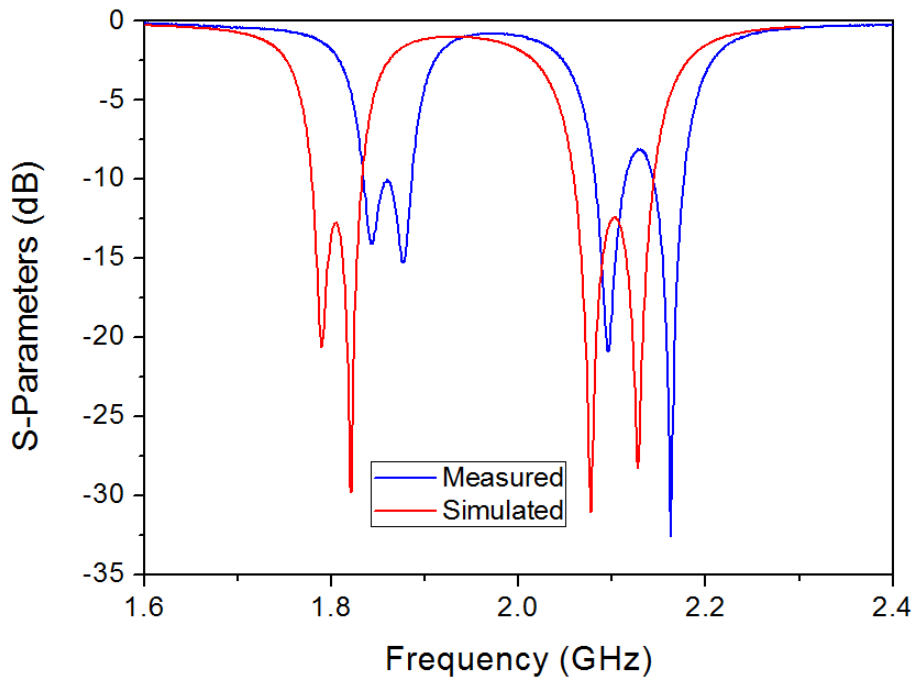
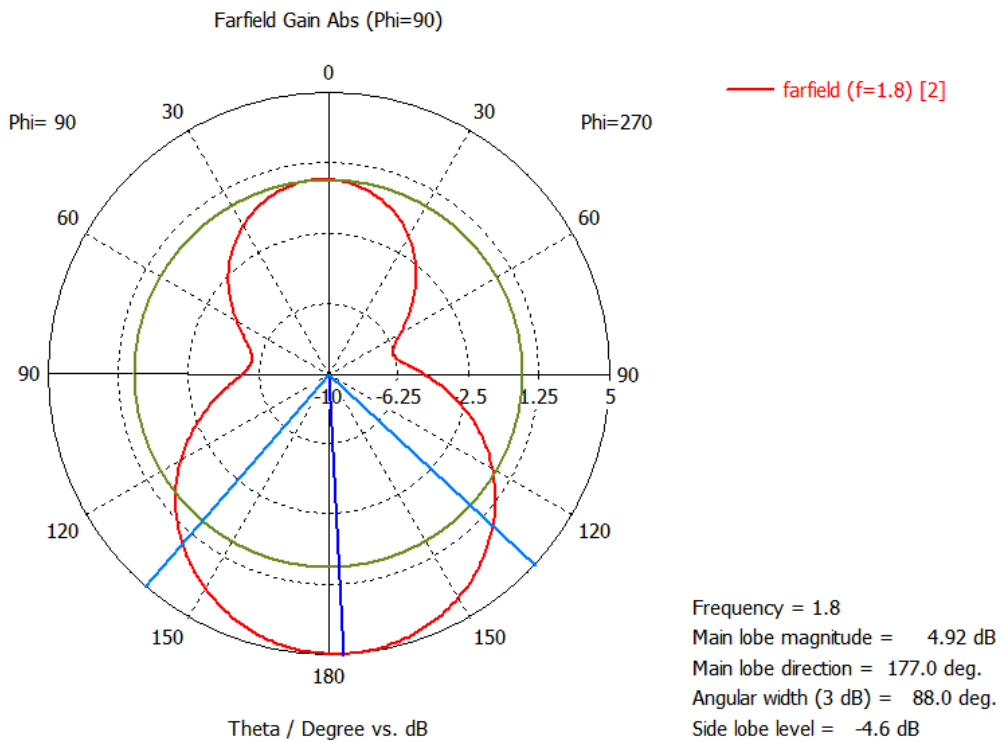
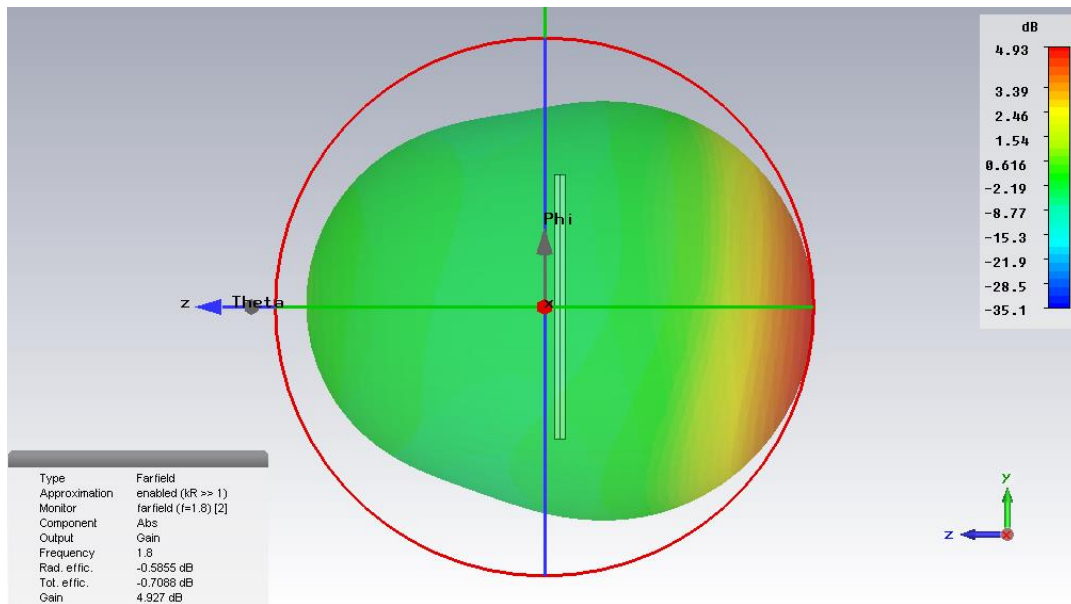


Figure 7.11 Simulated S-parameter response – impedance matching



(a)





(b)

Figure 7.12 Simulated farfield radiation pattern at 1.8 GHz

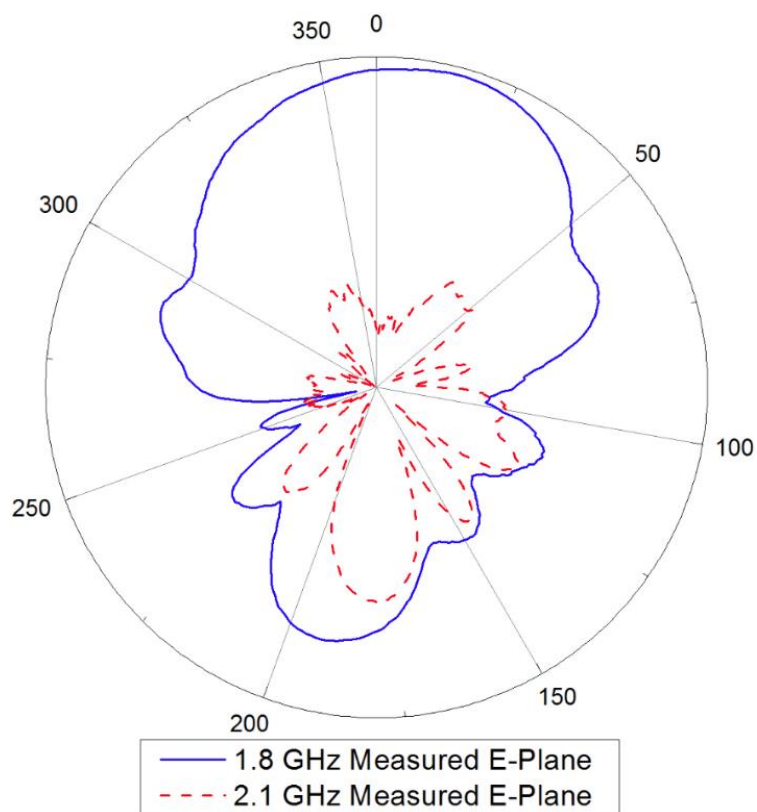
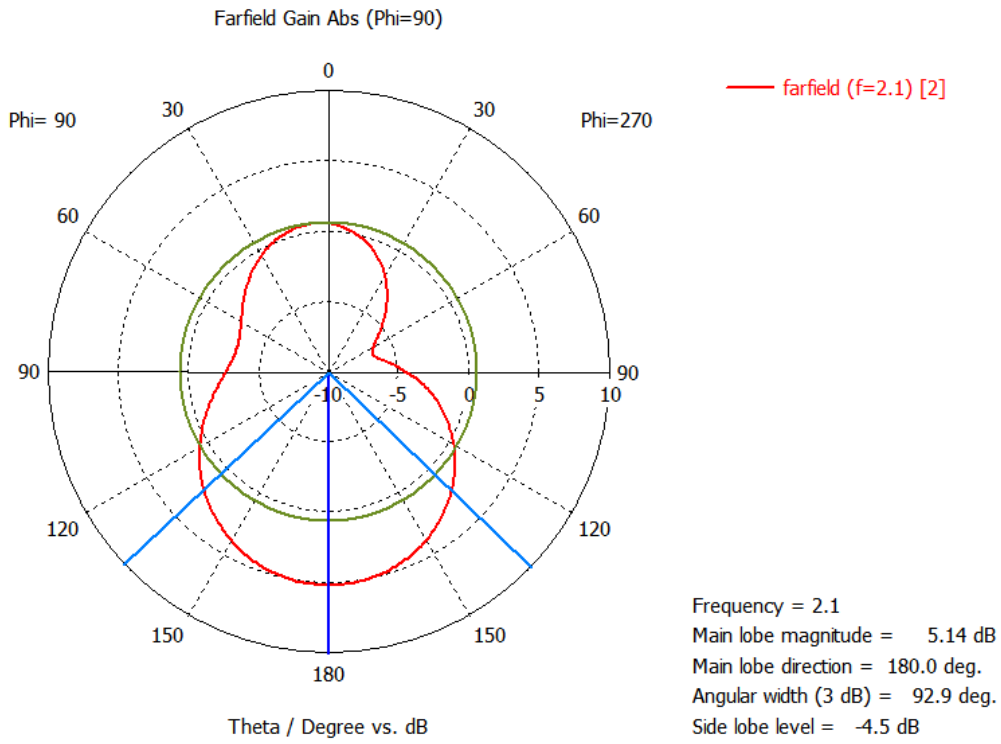
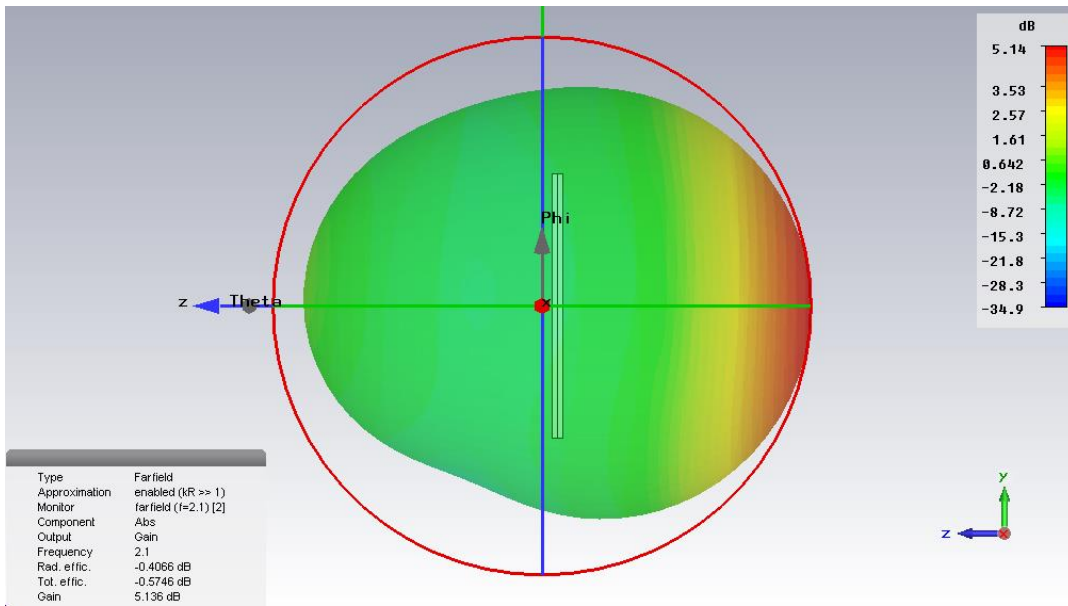


Figure 7.13 Measured Fairfield radiation patterns on the E-plane at 1.8 GHz (cross-polarisation) and 2.1 GHz (co-polarisation)



(a)



(b)

Figure 7.14 Simulated farfield radiation pattern at 2.1 GHz

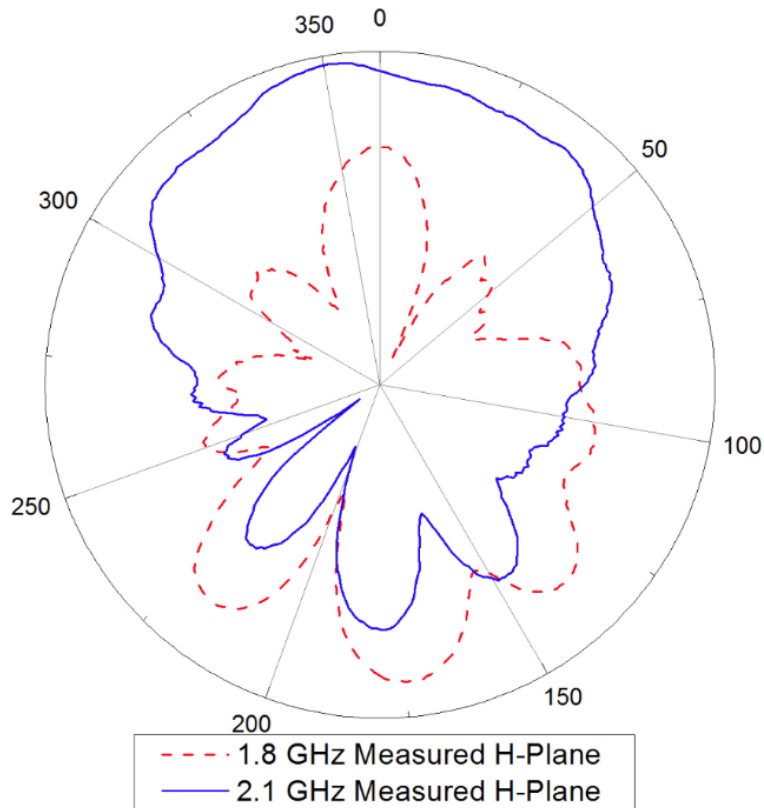


**Figure 7.15 Measured Fairfield radiation patterns on the H-plane at 1.8 GHz (co-polarisation) and 2.1 GHz (cross-polarisation)**

## 7.4 Summary

This chapter has demonstrated the possibility of integrating an antenna with filters, duplexers and dual-band filters. The integration process followed the general filter synthesis procedure; this made the design process simple to implement. Starting from the first design where a three-pole filtering antenna was presented, the antenna was treated as a resonator. This design technique is extended to the duplexing antenna and the dual-band bandpass filtering antenna which are more complicated circuitries. Compared with the conventional cascade designs, the presented designs are more compact in size with improved frequency selectivity. The bandwidths of the filtering antennas responses can be controlled by adjusting the coupling gap between the antenna and the resonators or the coupling slots in the case of the dual-band bandpass filtering antenna.

However, the designs presented here have some limitations. Both the duplexer-antenna and the dual-band filtering antenna operate different and orthogonal polarisations in the two bands. The practical applications would be restricted to the scenarios where polarisation diversity is desired.

# Chapter 8: Four-Port Filter Network

Almost all the filtering networks reported in this thesis as well as those in the literature have a single input and multiple outputs. In this chapter, the design concept of a multi-input multi-output filtering network will be demonstrated using two four-port networks. A multi-input multi-output (MIMO) filter and diplexer, and a mast head combiner (MHC) will be designed and presented. The design drives are concentrated on a miniaturised circuit size by applying an all-resonant-structure design technique in the implementations. The asynchronously coupled junction (ACJ) technique is utilised again in all the designs.

The design of the MIMO filter and diplexer was based on the idea of having a filtering network with the capability to function as a multi-purpose filter with different channel response. In this case, it functions as a diplexer with different channel responses, depending on the port(s) of excitation.

The MHC also utilised the ACJ technique in the implementation, allowing the embedding together of three filters of which two have the same channel response while the other have a different channel response.

## 8.1 Multi-Input Multi-Output (MIMO) Filter and Diplexer

As explained in the introduction, this design is proposed to have a multi-purpose function. It can be used as a filter and/or diplexer. Its operating frequencies are 1.8 GHz, 2.1 GHz and 2.6 GHz, all having a 20 dB return loss and 4% FBW. By using all resonant structures in the design, the general filter synthesis technique is applied using (3.4), (3.5), and (5.4) where necessary. The coupling topology used for the design is presented in Fig. 8.1. The resonators 1, 2 and 3 represents the 1.8 GHz filter. Resonators 4, 5 and 6 represents the 2.1 GHz filter while resonators 7, 8 and 9 represents the 2.6 GHz filter.

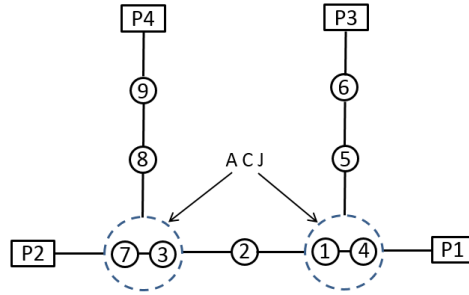


Figure 8.1 Multi-input multi-output filter and diplexer coupling topology

To achieve the proposed design, the first resonator of 1.8 GHz filter is asynchronously coupled to the first resonator of 2.1 GHz filter. That is resonator 1 coupled to resonator 4 and their Q-factor determined using the general filter synthesis. The technique used in coupling both resonators together is well explained in Section 4.2. The first resonator of the 2.6 GHz filter is then asynchronously coupled to the last resonator of 1.8 GHz channel. That is resonator 7 coupled to resonator 3 as shown in Fig. 8.1.

After designing the two required ACJs, the remaining resonators of the filters are then synchronously coupled to their respective path to the ACJ followed by optimisation to achieve the required response properties. The design layout is presented in Fig. 8.2(a) with optimised parameter values achieved while Fig. 8.2(b) shows the block diagram of the circuit. It can be seen that a coupled feedline is utilised in the design.

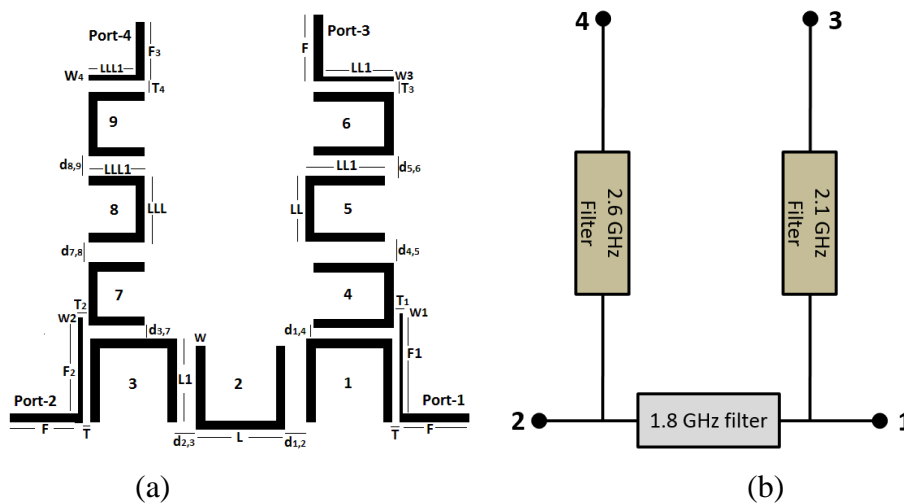


Figure 8.2 (a) Proposed design layout; (b) Circuit block diagram.  $F = 10\text{mm}$ ,  $F_1 = 15\text{mm}$ ,  $F_2 = 15\text{mm}$ ,  $T = 0.4\text{mm}$ ,  $T_1 = 0.2\text{mm}$ ,  $T_2 = 0.38\text{mm}$ ,  $T_3 = 1\text{mm}$ ,  $T_4 = 0.4\text{mm}$ ,  $W = 1.2\text{mm}$ ,  $W_1 = 0.4\text{mm}$ ,  $W_2 = 0.6\text{mm}$ ,  $W_3 = 0.6\text{mm}$ ,  $L = 9.6\text{mm}$ ,  $L_1 = 11.5\text{mm}$ ,  $LL = 6.6\text{mm}$ ,  $LL_1 = 11\text{mm}$ ,  $d_{1,2} = d_{2,3} = 1.46\text{mm}$ ,  $d_{1,4} = d_{3,7} = 0.22\text{mm}$ ,  $d_{4,5} = 1.65\text{mm}$ ,  $d_{5,6} = 1.7\text{mm}$ ,  $d_{7,8} = 1.84\text{mm}$ ,  $d_{8,9} = 1.82\text{mm}$

The simulated responses of the Multi-Input Multi-Output filter and diplexer are presented in Fig. 8.3 and Fig. 8.4, where Fig. 8.3 illustrates the response of a diplexer at 1.8 GHz and 2.1 GHz at the chosen port-1 as the common port. Fig. 8.4 illustrates that of 1.8 GHz and 2.6 GHz diplexer at the chosen port-2 as the common port. Fig. 8.3 and Fig. 8.4 are the two diplexers that can be selected from this circuit. It can be seen that these selections are through the choice of excitation port.

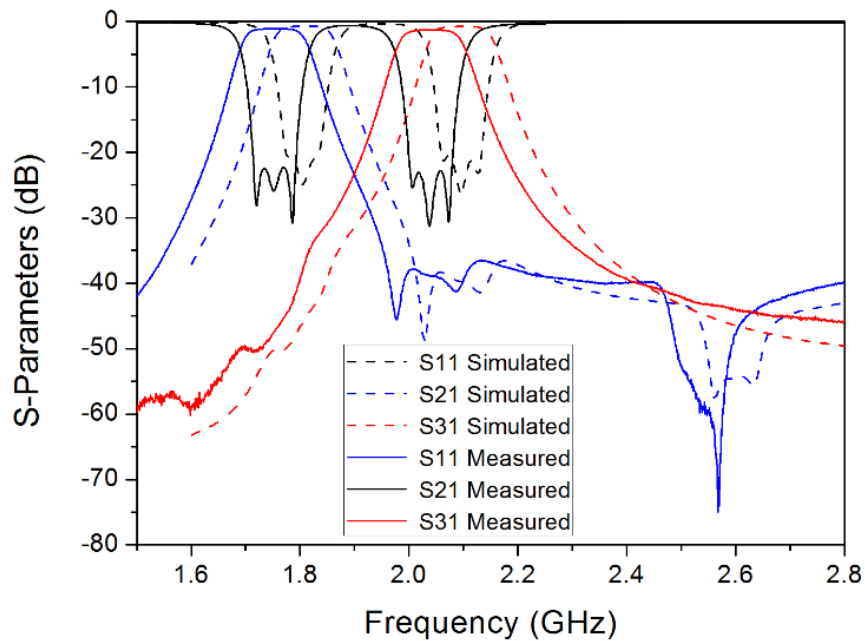


Figure 8.3 The duplexing responses when Port-1 is excited as the common port.

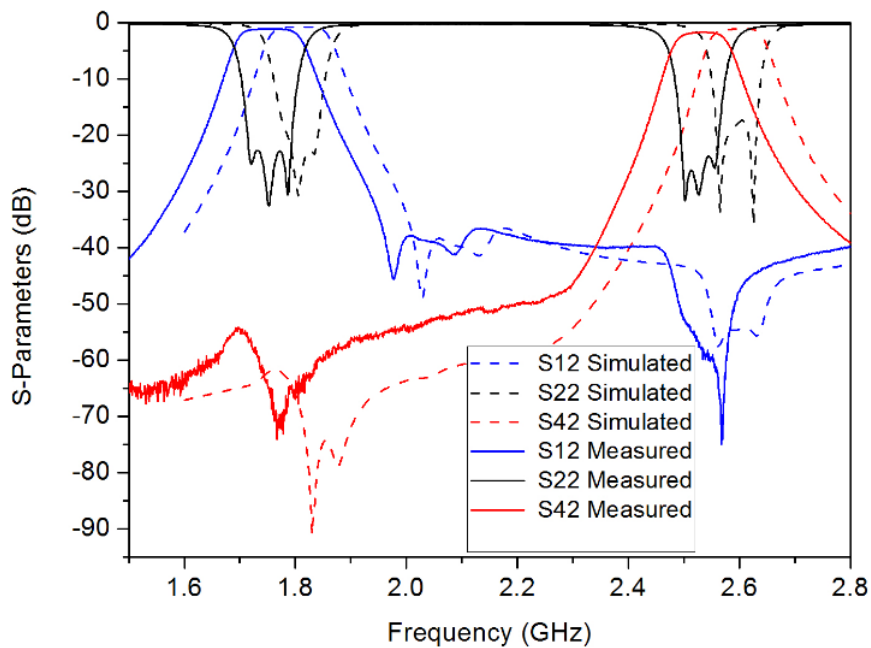
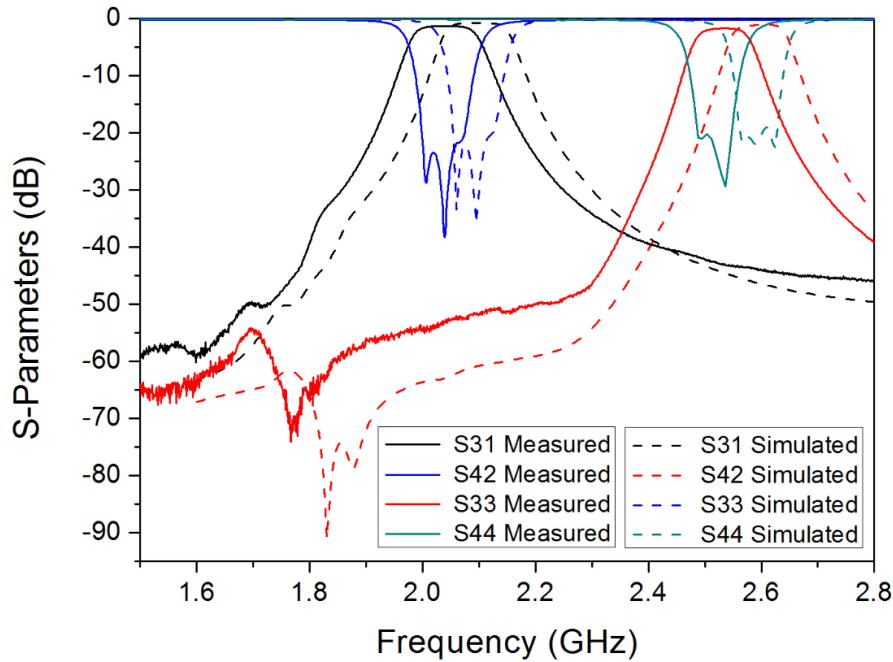


Figure 8.4 The duplexing responses when Port-2 is excited as the common port.

Fig. 8.5 presented a situation where the MIMO network is selected to function as two filters. This situation allowed the two possible channel filters to operate at the same time, that is 2.1 GHz filter and 2.6 GHz filter. In this case, port-1 and port-3, as well as the port-2 and port-4, are utilised for this purpose. In Fig. 8.3, 8.4 and 8.5, the measured responses are also presented for comparison with the simulations.



**Figure 8.5 Dual filter operation mode**

From the responses presented, all the return losses are over 20 dB. Measurements and simulations show reasonably good agreement except for the frequency shift of 10 MHz. This is believed to be due to the thinning of the substrate from milling as well as the tolerance of the dielectric constant of high permittivity anisotropic substrate material used for prototyping. Fig. 8.6 presents the isolation response between port-1 and port-4, port-2 and port-3 as well as port-3 and port-4. The solid lines represent the measured responses while the dashed lines represent the simulated responses.



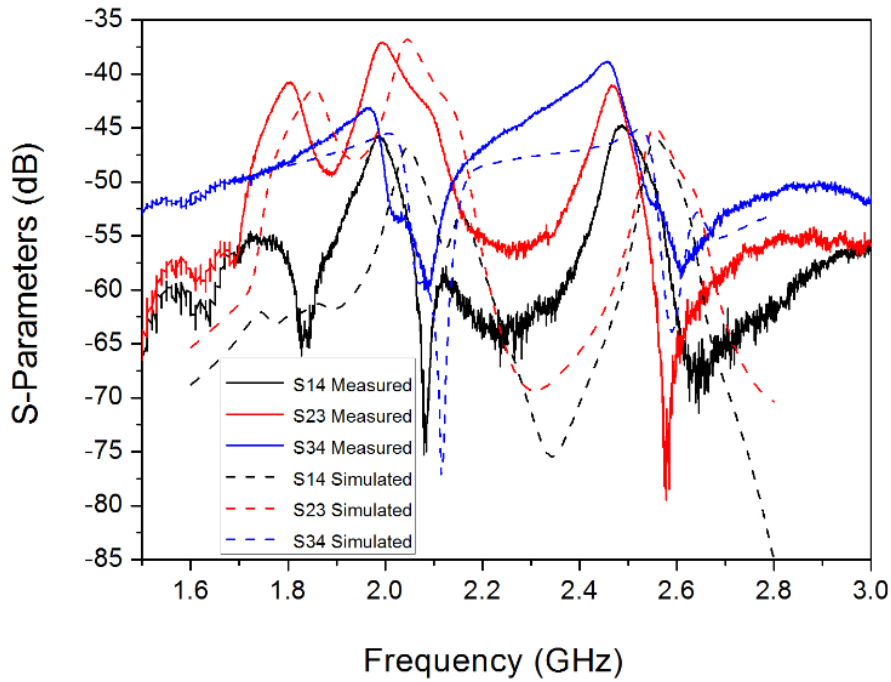


**Figure 8.6 Measured and simulated isolation responses**

The designed MIMO filter and diplexer were prototyped using the Rogers 3010 substrate with a thickness of 1.27mm, a relative permittivity of 10.8 and a loss tangent of 0.0022 and are shown in Fig. 8.7. Measurements were taken using the Agilent Network Analyser N5230A and compared with the simulated responses.

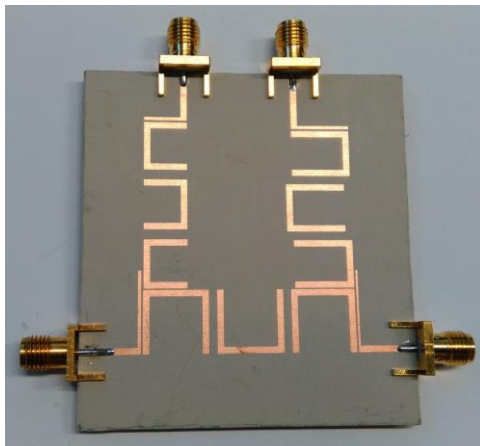


**Figure 8.7 Prototyped multi-input multi-output filter and diplexer**

The current distribution of the channels during operation is presented in Fig. 8.8 using the same current density scale. A good illustration can be seen when the 1.8 GHz frequency channel is in operation, the current density distribution at 1.8 GHz channel is at its peak. At 2.1 GHz and 2.6 GHz channels, the current density distribution is at its lowest level. If the current is then

considered at 2.1 GHz and 2.6 GHz frequencies, it will be noticed that at 1.8 GHz frequency, the current density distribution will be at its lowest level.

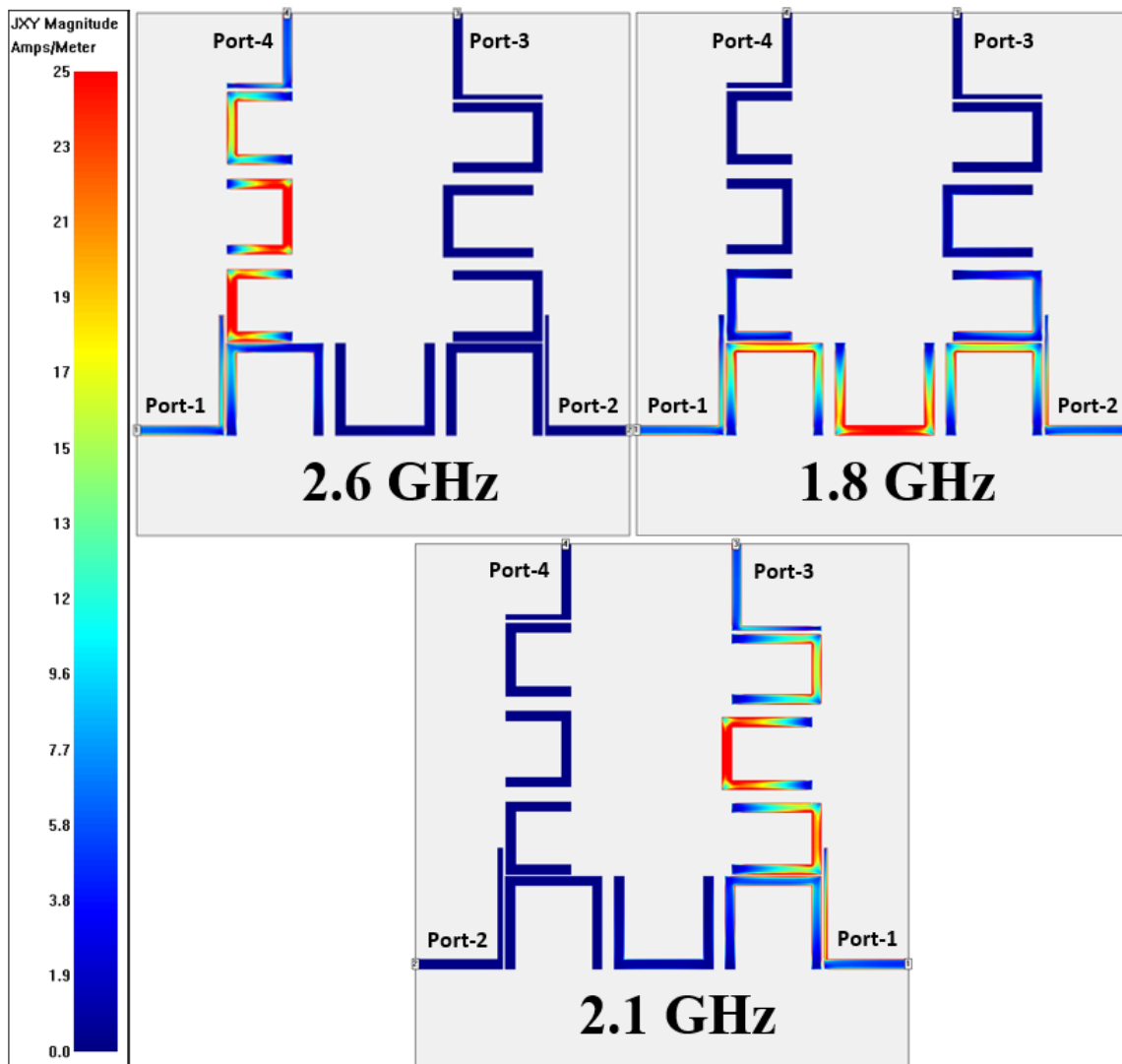


Figure 8.8 Current density distribution of the MIMO filtering network

## 8.2 MastHead Combiner (MHC)

In the communication system, the transceiver output is normally connected to an antenna using selective diplexer which permits the TX and RX to share a common antenna; this is common in most communications systems. This common antenna is mostly mounted on the top of a communication mast, so a transmission line with a considerable length will be required for the transceiver connection. The transmission line will in effect introduce additional losses which

worsen the overall noise figure of the receiving system. This scenario is illustrated in Fig. 8.9 where the TX and RX (transceiver) are connected to a diplexer close by.

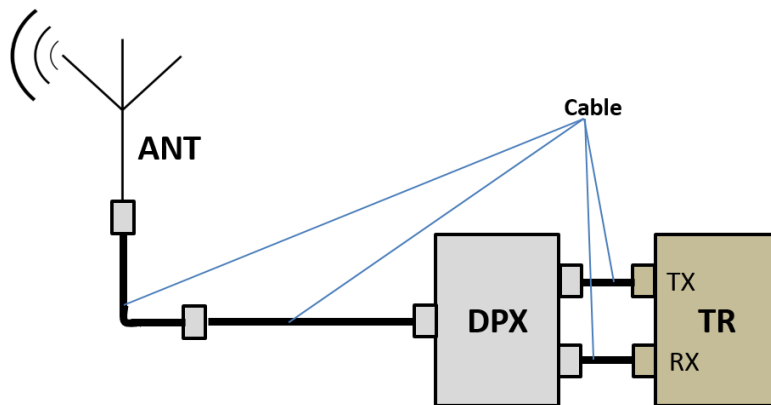


Figure 8.9 Classical connection in an antenna and transceiver module

In recent time, it was suggested that the noise figure degradation caused by the cable losses could be compensated by introducing a Low Noise Amplifier (LNA) at the receiver chain while preserving the connection of TX to the antenna [155, 156]. The MastHead Combiner (MHC) is the device which allows the addition of the LNA as shown in Fig. 8.10.

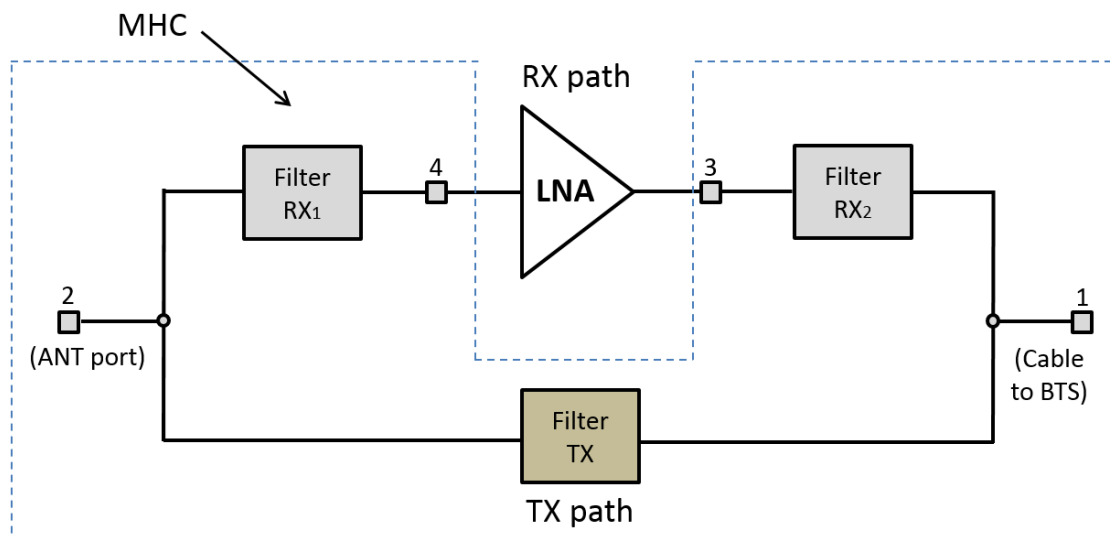


Figure 8.10 Masthead combiner allowing the introduction of an LNA at the antenna output

As can be seen from Fig. 8.10, the MHC is the passive device with four ports. It is made up of three filters. The  $RX_1$  and  $RX_2$  filters of the MHC provides the protection of LNA input and output against the TX signal. The losses of the  $RX_1$  filter should be at the lowest possible while the TX filter provides the TX signal path. It is worth mentioning that these filters ( $RX_1$ ,  $RX_2$

and TX) may possess multi-band response depending on the application requirement [156]. In the next section, a design approach for a microstrip MHC is presented.

The approach presented here uses the Asynchronously Coupled Junction (ACJ) as described in Section 4.2 to represent the two junctions of the MHC. The three channel filters required for this design were separately designed to have a three-pole Chebyshev ripple factor of 0.043 dB and to meet a 4% FBW each with a 20 dB return loss. The conventional hairpin resonators were used for the design of the filters for the MHC. They operate at 1.8 GHz for the TX channel, 2.1 GHz for the RX<sub>1</sub> and RX<sub>2</sub> channels. Fig. 8.11 presents the coupling topology of the design with a block diagram of an LNA (not included in the design). The circuit layout is presented in Fig. 8.12(a) with the optimised dimension parameters achieved and listed in the caption while Fig. 8.12(b) shows the block diagram of coupling topology used.

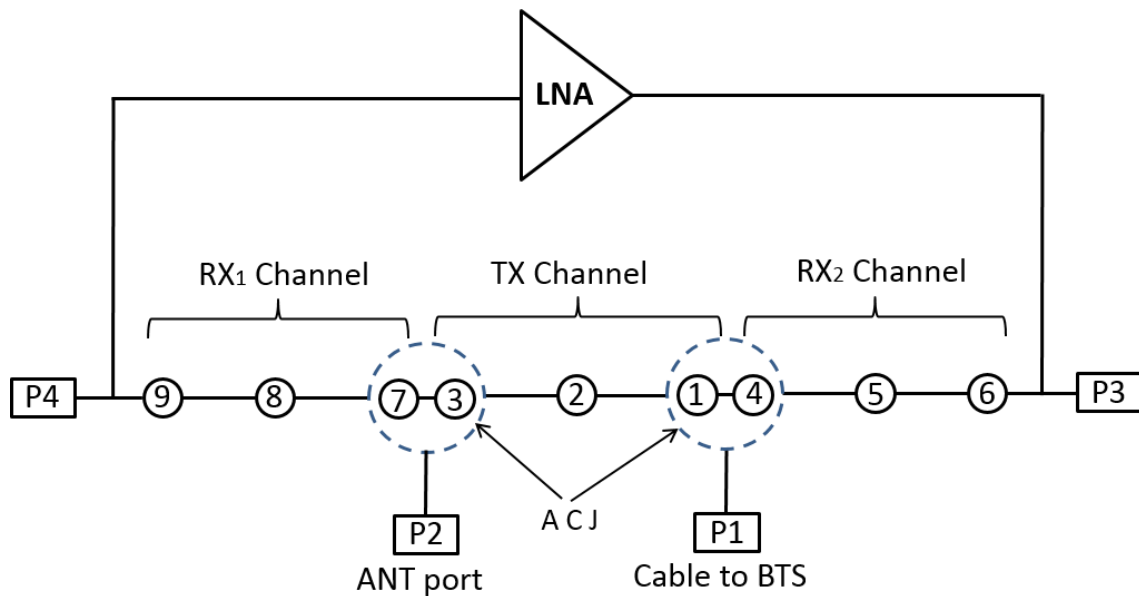
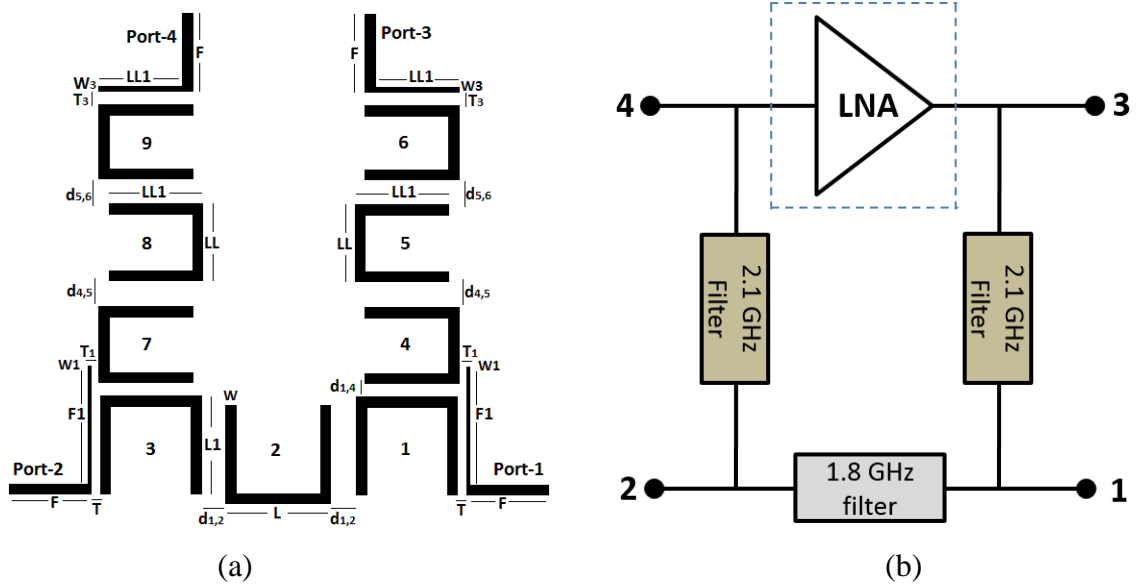


Figure 8.11 Masthead combiner coupling topology with an LNA connected



**Figure 8.12 Proposed microstrip MHC: (a) design layout (b) coupling topology.  $F = 10\text{mm}$ ,  $T = 0.4\text{mm}$ ,  $T_1 = 0.2\text{mm}$ ,  $T_3 = 0.4\text{mm}$ ,  $W = 1.2\text{mm}$ ,  $W_1 = 0.4\text{mm}$ ,  $W_3 = 0.6\text{mm}$ ,  $L = 9.85\text{mm}$ ,  $L_1 = 11.5\text{mm}$ ,  $LL = 6.6\text{mm}$ ,  $LL_1 = 11\text{mm}$ ,  $d_{1,2} = 1.7\text{mm}$ ,  $d_{1,4} = 0.2\text{mm}$ ,  $d_{4,5} = 1.6\text{mm}$ ,  $d_{5,6} = 1.6\text{mm}$**

From Fig. 8.11, the resonators 1, 2 and 3 represents the TX filter while the resonators 7, 8 and 9 represents the RX<sub>1</sub> filter and resonators 4, 5 and 6 represents the RX<sub>2</sub> filter. The two required ACJs are identified using dashed ring circles where resonators 3 and 7 forms the ACJ or a node linking the TX filter and RX<sub>1</sub> filter. The resonators 1 and 4 forms the second ACJ or the node linking the TX filter and the RX<sub>2</sub> filter. This makes the MHC look more like a double diplexer sharing one TX filter in a branch, just as that of Fig. 8.2 for the MIMO filter/diplexer. In fact, the MHC represents a special case where two branches (7-8-9 and 4-5-6) are of the same frequency.

The external Q-factors of the three filters and the two nodes used for the MHC are calculated using (3.5). (3.4) is used for obtaining the coupling coefficient between the coupled resonators of the three filters as well as the two coupled resonators that make up the ACJ. After obtaining the physical dimensions of the ACJ, the ACJ are then used in joining the three designed filters of 1.8 GHz and two 2.1 GHz. The individually designed two 2.1 GHz filters had their first resonator removed and replaced with the ACJ while the 1.8 GHz filter, had its first and third resonator removed and replaced with the ACJ. The removing of the resonators and replacing them with the ACJ makes the circuit more compact.

Fig. 8.13 presents the simulated responses of the MHC results using dashed lines for the RX<sub>1</sub> filter and the TX filter. Due to symmetry, the frequency response of the RX<sub>2</sub> filter and the TX filter will be identical to that of the RX<sub>1</sub> and TX filter. It can be seen that the responses achieved in the simulation met the specification of 4% FBW and 20 dB return loss at both passbands with an isolation around 30 dB on the RX<sub>1</sub> channel, while the TX channel has about 43 dB. The Fig. 8.13 also presents the measured results using thick lines in comparison with the simulated response. The comparison indicates that the measured responses of the TX channel have a frequency shift of about 10 MHz to the left with a bandwidth of 5 MHz more than the simulated response. The return loss is about 15 dB with an insertion loss of about 2.5 dB. The measured RX<sub>1</sub> channel have approximately the same bandwidth with the simulated response. A return loss of 18 dB and insertion loss of 2 dB is also recorded from the measured result. The measured isolation response is at about 28 dB for the RX<sub>1</sub> channel and about 48 dB on the TX channel. The prototyped design is presented in Fig. 8.15 measuring around 62 mm in length.

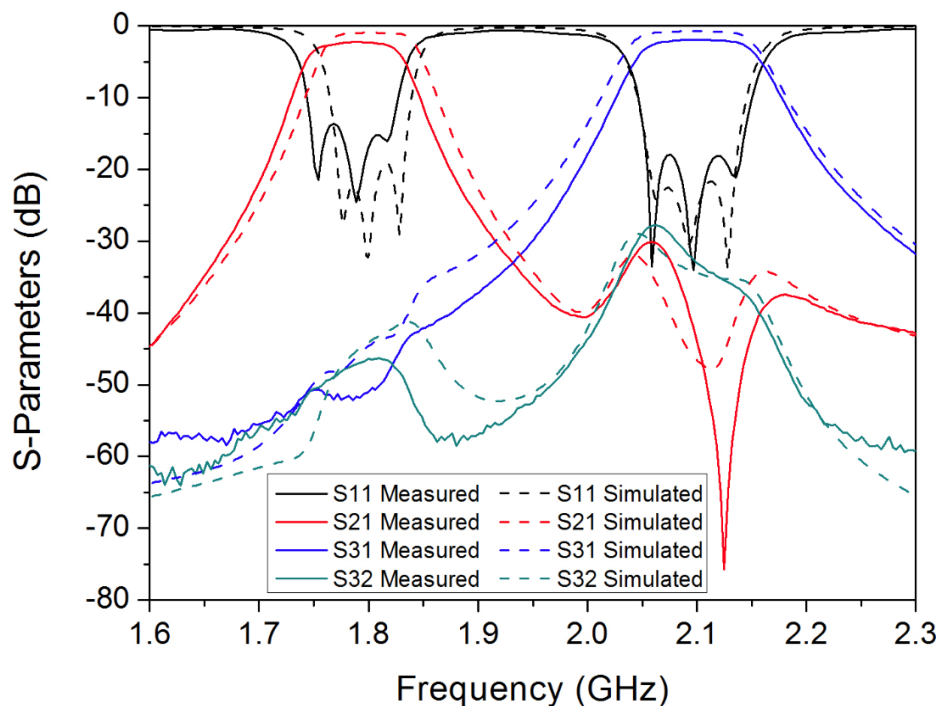


**Figure 8.13 Simulated response of MHC showing RX channel, TX channel and isolation response**

The current distribution of the MHC during operation at the TX and RX<sub>1</sub> channels are presented in Fig. 8.14. Due to symmetry, the pattern of current distribution on the RX<sub>1</sub> channel will be the same on the RX<sub>2</sub> channel.

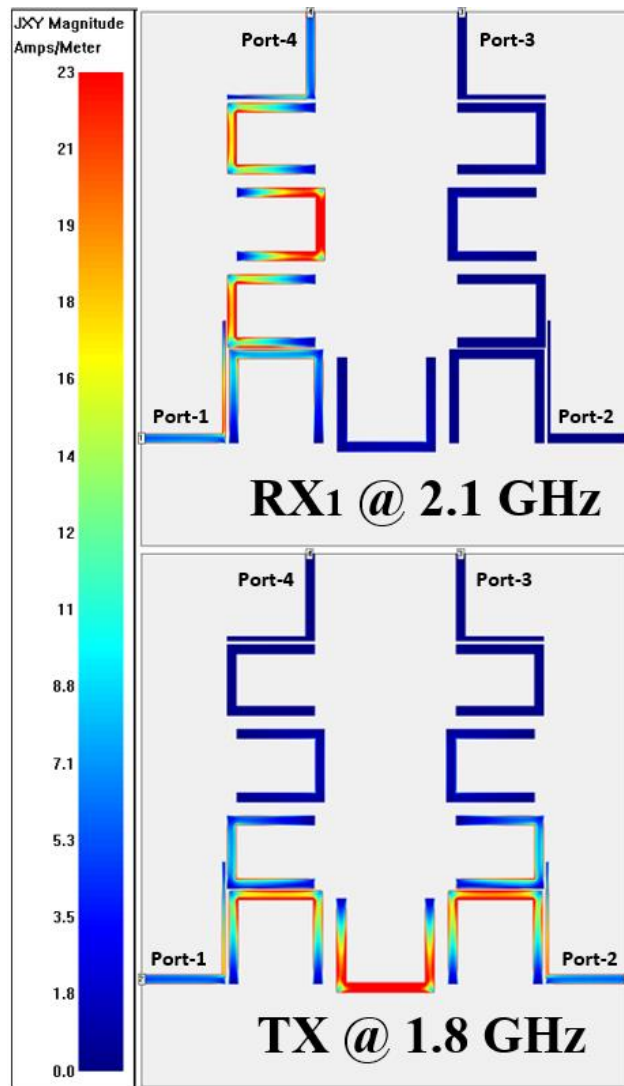


Figure 8.14 Current density distribution at TX, and RX1 channels

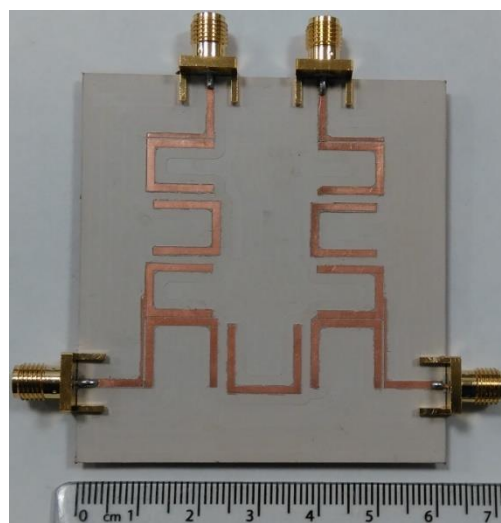


Figure 8.15 Prototyped MHC circuit

## 8.3 Summary

In this chapter, two four-port devices based on the MPFN concept is presented. All the designs are based on extending the capability of the Asynchronous Coupled Resonant Junction (ACJ) discussed in Chapter 4. The designs demonstrated the feasibility of realising multi-input multi-output (MIMO) filter/diplexer whose frequency selectivity relies on the choice of the excitation ports. At this stage, no specific application about the proposed multi-port devices is identified apart from the Masthead combiner. However, this represents a new design opportunity offered by the coupled-resonator filtering networks for future development. The designed MIMO filter/diplexer has the capability to function as a switchable diplexer and filters.



# Chapter 9: Conclusions and Future Work

In this chapter, the results and main findings of work reported in this thesis is summarised and conclusions are made, leading to recommendations for future work.

## 9.1 Conclusions

This thesis presented a number of devices ranging from single band filters, dual-band filters, diplexers, four-port networks to the integration of antennas with filters or duplexers. The research carried out is based on the MPFNs concept which utilises the general filtering network analyses, comprising of all resonant structures.

Chapter 2 presented the literature review of some relevant works in filters and diplexers as well as dual-mode resonators. It also demonstrated some theoretical and practical design of some resonant structures with emphasis on the dual-mode resonators. In Chapter 3, the theoretical background and design methods used for the realisation of filtering devices were presented. It covered from the basic concept, the realisation of the normalised LPF, the coupling matrix and the quality external factors. The theoretical implementation of bandpass filters and dual-band bandpass filters using the lumped element is also presented.

The rest of the chapters concentrated on the device miniaturisation based on MPFNs concepts. In Chapter 4, a comparison was drawn based on the conventional T-junction diplexer and a proposed compact diplexer using an Asynchronous Coupled Resonant Junction (ACJ). The comparison concentrated on their performance of signal responses, power handling capability and isolation as well as the physical sizes for a possible replacement for the conventional diplexers. The concept used in achieving the ACJ was also utilised in Chapter 8 on Four-port filtering network for the design of double diplexers used for Multi-input Multi-output (MIMO) diplexers and filters. The MIMO diplexers and filters demonstrated the capability of selecting discrete operation frequencies depending on the excitation ports, which makes it a great utility when multiple operation modes are to be used by the same receiver. An extension of the Four-port filtering network created a design on Masthead Combiner (MHC). The MHC utilised the Asynchronously Coupled Junction as a node to perform the signal splitting and combining and

to join the TX and RX channels. The MHC allows the addition of a Low Noise Amplifier (LNA) at the receiver chain while preserving the connection of TX to the antenna, this compensates for the noise figure degradation caused by the cable losses in communication systems.

The properties of an orthogonal mode patch resonator were presented in Chapter 5. Each mode of the patch resonator was fully utilised in the applicable designs. Firstly, an orthogonal mode patch resonator was used with two hairpin resonators to create a bandpass filter with the high selective property. In the design, one mode of the patch resonator corresponding to the centre frequency of the filter is coupled in a parallel combination with the two hairpin resonators to create a three-pole filtering response. The second mode of the patch resonator then created the much need transmission zero required for the high selectivity of the filtering response. A diplexer was also designed using a dual-mode patch resonator. In the implementation, the dual-modes of the patch resonator were coupled to the corresponding filters with the same resonant frequencies. Using two channel filters in the design, the patch resonator contributed a resonant pole to each channel filter and acted as the signal splitter and combiner in the circuit. By integrating the dual-mode patch resonator in the design, a reduction in the number of required resonators was evident as a miniaturised device for the front-end component in the base station communication system. The design and implementation of a dual-band bandpass filter using dual coupling paths are also presented. Two dual-mode patch resonators were used as a signal splitting and combining component in the circuit. The first patch resonator splits the incoming signals into its corresponding mode of the patch resonator before sending it into the coupling network of the circuit. On reaching the second patch resonator, the frequencies were then combined and sent to the output port. This concept permits the design to function as a double filter, allowing each filter to function independently.

In Chapter 6, the Split-Ring Resonator (SRR) was presented as a dual-mode resonator. The SRR was designed using two open-loop resonators of 2 GHz and 3 GHz. The 3GHz resonator was nested in the 2 GHz resonator during the implementation. The two resonators were asynchronously coupled to achieve widely separated channels as opposed by the conventional SRR that uses synchronous coupling technique and can only achieve narrow separated channels. The SRR was used to design two bandpass filters with improved selective responses. A diplexer was also presented to utilise the two modes of the SRR as a contributing mode to

the channel filters as well as a signal splitter and combiner. Also presented in Chapter 6 was a dual-band bandpass filter using two coupled SRR for a high selective filtering response.

In Chapter 7, an integration of antenna with a filter, duplexer and dual band filter is presented. In each of the presented designs, the antenna functions as a resonant pole for each channel and a radiating element for antenna function. The general filter synthesis is used during the implementation of the designs. This helped in the elimination of the 50 Ohm interface between the filter and the antenna in a conventional topology. With filter integration, a three-pole filtering antenna is proposed using two hairpin resonators and one antenna. In the implementation, the antenna was seen as a resonator with radiating element and was treated as so by allowing it to have a coupling coefficient with the next resonator as the same coupling coefficient with the other two resonators.

In the duplexing antenna, the antenna used was a rectangular patch with some dual-mode properties. The dual-modes of the patch antenna were coupled to the corresponding channel filters meant for the uplink and downlink channels. The isolation between the channels was at 43 dB which is very good compared with other published works. A dual-band bandpass filtering antenna was also presented. The design utilised one dual-mode patch resonator and one dual-mode patch antenna to achieve a four-pole dual-band filtering antenna response. Using a slot coupling, the resonator and the antenna were placed back to back with a common ground. One input feedline was attached to the dual-mode patch resonator with a known quality external factor equivalent to quality radiation factor of the dual-mode patch antenna. The design and coupling topology used for the design has made it very compact when compared with the cascaded topology used for the conventional counterpart.

The table 9.1 below presents the list of all the research presented in this thesis. It indicates the chapters where the designs are presented, including simulation software, fabrication and material used,. It also points to conclusion that the concept derived from the conventional two-port filters can be applied to the design of MPFN components such as diplexers, multiplexers and MastHead Combiners. In addition, it can also be extended to the development of integrated filtering-antenna, integrated duplexing-antenna and integrated dual band filtering-antenna.

**Table 9-1 List of completed work**

Chapter	Design	Simulation tools used	Fabrication	Material
3	Coupled resonator dual-band bandpass filter	Agilent	YES	RT/Duroid 6010LM 10.2, t = 1.27
4	Conventional diplexer	Sonnet	YES	Rogers 3010 10.8, t = 1.27
4	Resonant junction diplexer	Sonnet	YES	Rogers 3010 10.8, t = 1.27
5	Bandpass filter with transmission zero	CST	YES	Rogers 3010 11.2, t = 1.27
5	Diplexer with a patch resonator as its junction	Sonnet	YES	Rogers 3010 10.8, t = 1.27
5	Dual band BPF with dual coupling path	Sonnet	YES	Rogers 3010 10.2, t = 1.27
6	Diplexer Implementation Using SRR as the Common Resonant Junction	Sonnet	YES	Rogers 3010 10.2, t = 1.27
6	Compact Dual-Band Bandpass Filter Using SRR	Sonnet	NO	Rogers 3010 10.2, t = 1.27
7	Duplexing Antenna	Sonnet	NO	Rogers 4003C 3.55, t = 1.524
7	Dual-Band Bandpass Filtering Antenna	CST	YES	Rogers 4003C 3.55, t = 1.524
8	Multi-input Multi-output (MIMO) Filter and Diplexer	Sonnet	YES	Rogers 3010 10.8, t = 1.27
8	MastHead Combiner (MHC)	Sonnet	YES	Rogers 3010 10.8, t = 1.27

All the result comparisons presented indicate a reasonably good agreement between the simulated and measured results. It can be noticed that some frequency shifts were noticed in the measured responses. These shifts were due to the materials used for the prototyping of the designed circuits, post prototype tuning and measurement errors. The biggest frequency shifts can be noticed in the prototyped designs involving mixed resonators on the same substrate material. When compared with the simulated response, the shift can be attributed to the variation of the dielectric constant used in the simulation and the prototyped. Also, using the same substrate, the dielectric constant of the material suitable for microstrip-line filters will not be the same for the patch resonators with more E-fields in the Z-direction perpendicular to the patch. This seems to be consistent with the anisotropic property of most of the material substrate used.

Some of the examples relating to that is presented in Chapter 5 using Rogers 3010 substrate with the same thickness but with different relative permittivity. The bandpass filter with transmission zero has a significant shift of the measured responses to higher frequency by nearly 50 MHz when prototyped using relative permittivity of 11.2. The diplexer with a patch resonator as its junction has its measured frequency shifted at about 10 MHz when prototyped with a relative permittivity of 10.8 and finally, the dual band BPF with dual coupling path is noticed to have both bands of the measured shifted to the left by approximately 20 MHz when prototyped with a relative permittivity of 10.2.

To analyse the frequency shifts, the dual band BPF with dual coupling path is fabricated using different techniques as well as comparing the performance with several transmission-line type resonators based on the same RO3010 substrate. It has been found that the significant frequency shift is mainly caused by the variation of the dielectric constant from the one (10.2) used in the simulation. Although the value of 10.2 has been found more suitable for microstrip-line filters, for the patch resonators with more E-fields in the Z-direction perpendicular to the patch, the so-called 'design Dk' of 11.2 seems to represent the material better. Simulations show that a value of 10.8 fits the measurement best as can be seen in Fig. 5.24 and 5.25. This is consistent with the anisotropic property of the RO3010 substrate.

## 9.2 Future Work

Based on the findings on Compact diplexer presented in Chapter 4, a more compact diplexer with an improved response might be achievable if the diplexer topology is changed. It is recommended that a trisection topology on each branch of the channel filters are employed, this will result in a more compact circuit with an introduction of two transmission zeros, one from each channel. By controlling the introduced TZs, a high selective response is achievable either at the guard band or outside the diplexer bandwidth.

The diplexer with a dual-mode patch resonator presented in Chapter 5 can be extended to a four-channel multiplexer. The dual-mode patch resonator can be coupled to two other dual-mode patch resonators of different resonant frequencies. The three coupled dual-mode resonators can be arranged in a bifurcated topology where they function as the resonant junctions performing the signal splitting and combining functions. This work will result in a more complicated topology when the channel filters are attached.

The diplexer with a Split Ring Resonator (SRR) junction can be extended to a triplexer if another channel filter can be coupled to the harmonic response of the SRR which is at about 4 GHz. The SRR utilised two open-loop resonators of different frequencies. Three resonators of different frequencies may be used for the SRR and then used for a triplexer implementation. In that case, the controlling of the resonant frequencies during optimisation of the circuit becomes difficult as the interaction between the SRR and the channel filters becomes very sensitive to change.

The ACJ can be used as a resonant node in designing two diplexers of the same properties and then joined back to back using the same technique. The implementation of the ACJ technique in such topology will lead to an extension to the design of an Interference Rejection Diplexer (IRD). This can be achieved by creating an  $180^\circ$  phase shift between the channels at the load port [157, 158] resulting to a rejection of about 50 dB and above between ports.

## References

- [1] M. L. Chuang and M. T. Wu, "Microstrip Diplexer Design Using Common T-Shaped Resonator," *IEEE Microwave and Wireless Components Letters*, vol. 21, no. 11, pp. 583-585, Nov. 2011.
- [2] S. T. G. Bezerra and M. T. de Melo, "Microstrip diplexer for GSM and UMTS integration using ended stub resonators," *Microwave and Optoelectronics Conference, 2007. IMOC 2007. SBMO/IEEE MTT-S International, Brazil, 2007*, pp. 954-958.
- [3] M. L. Chuang and M. T. Wu, "Microstrip Multiplexer and Switchable Diplexer with Joint T-Shaped Resonators," *IEEE Microwave and Wireless Components Letters*, vol. 24, no. 5, pp. 309-311, May 2014.
- [4] T. Yang, P. L. Chi and T. Itoh, "Compact Quarter-Wave Resonator and Its Applications to Miniaturized Diplexer and Triplexer," *IEEE Transactions on Microwave Theory and Techniques*, vol. 59, no. 2, pp. 260-269, Feb. 2011.
- [5] Y. Wu, Y. Liu, Q. Xue, S. Li and C. Yu, "Analytical Design Method of Multiway Dual-Band Planar Power Dividers with Arbitrary Power Division," *IEEE Transactions on Microwave Theory and Techniques*, vol. 58, no. 12, pp. 3832-3841, Dec. 2010.
- [6] M. Kishihara, K. Yamane, I. Ohta and T. Kawai, "A design of multi-stage, multi-way microstrip power dividers with broadband properties," *Microwave Symposium Digest, 2004 IEEE MTT-S International, 2004*, pp. 69-72 Vol.1.
- [7] A. Alaqeel, H. Shaman, S. Almorqi, O. Haraz, S. Alshebeili and A. r. Sebak, "Butterfly-shaped slot coupled microstrip 90° hybrid couplers for K- and Ka-band millimeter-wave radar applications," *Microwave Symposium (MMS), 2014 14th Mediterranean, Marrakech, 2014*, pp. 1-3.
- [8] C. W. Tang and M. G. Chen, "Synthesizing Microstrip Branch-Line Couplers With Predetermined Compact Size and Bandwidth," in *IEEE Transactions on Microwave Theory and Techniques*, vol. 55, no. 9, pp. 1926-1934, Sept. 2007.
- [9] X. Shang, Y. Wang, W. Xia, M.J. Lancaster, "Novel Multiplexer Topologies Based on All-Resonator Structures," *IEEE Transactions on Microwave Theory and Techniques*, Vol 61, Issue 11, 2013, Pages 3838 – 3845.
- [10] R. Wang and J. Xu, "Synthesis and design of microwave diplexers with a common resonator junction," *Microwave and Millimeter Wave Technology (ICMMT), 2012 International Conference on, Shenzhen, 2012*, pp. 1-4.
- [11] T. Skaik and M. Lancaster, "Coupled Resonator Diplexer without External Junctions," *Journal of Electromagnetic Analysis and Applications*, pp. 238-241, March, 2011.

- [12] D. A. Tubail and T. F. Skaik, "Synthesis of coupled resonator-based multiplexers with generalised structures using coupling matrix optimisation," *Electronics Letters*, vol. 51, no. 23, pp. 1891-1893, 11 5 2015.
- [13] T. Yang, P. L. Chi and T. Itoh, "High Isolation and Compact Diplexer Using the Hybrid Resonators," *IEEE Microwave and Wireless Components Letters*, vol. 20, no. 10, pp. 551-553, Oct. 2010.
- [14] C. Chen, H. Wu and W. Wu, "High Isolation DBR Diplexer Using In-Line SCMRC", *Progress in Electromagnetics Research C*, Vol. 22, 97–108, 2011.
- [15] S. Bastioli, L. Marcaccioli and R. Sorrentino, "An original resonant Y-junction for compact waveguide diplexers," *Microwave Symposium Digest, 2009. MTT '09. IEEE MTT-S International*, Boston, MA, 2009, pp. 1233-1236.
- [16] H. Chung and J. Sharp, "Modelling partially magnetised Y-junction circulator," *Passive RF and Microwave Components*, IET Seminar on, Birmingham, 2010, pp. 5-20.
- [17] R. I. Cameron and M. Yu, "Design of manifold-coupled multiplexers," *IEEE Microwave Magazine*, vol. 8, no. 5, pp. 46-59, Oct. 2007.
- [18] T.F. Skaik, M.J. Lancaster, F. Huang, "Synthesis of multiple output coupled resonator circuits using coupling matrix optimisation," *Microwaves, Antennas & Propagation, IET*, vol.5, no.9, pp.1081-1088, June 27, 2011.
- [19] M. Guglielmi, "Optimum CAD procedure for manifold diplexers," *Microwave Symposium Digest, 1993., IEEE MTT-S International*, Atlanta, GA, USA, 1993, pp. 1081-1084 vol.2.
- [20] C.-F. Chen, T.-Y. Huang, C.-P. Chou and R.-B. Wu, "Microstrip diplexers design with common resonator sections for compact size, but high isolation," *IEEE Transactions on Microwave Theory and Techniques*, vol. 54, no. 5, pp. 1945-1952, May 2006.
- [21] T. Skaik, "Novel star-junction coupled-resonator multiplexer structures," *Progress In Electromagnetics Research Letters*, Vol. 31, 113-120, 2012.
- [22] Y. Wang and M. J. Lancaster, "An Investigation on the coupling characteristics of a novel multiplexer configuration," *Microwave Conference (EuMC), 2013 European*, Nuremberg, 2013, pp. 900-903.
- [23] T. F. Skaik and D. A. Tubail, "Novel multiplexer topologies based on coupled resonator structures," *Microwave Symposium (MMS), 2015 IEEE 15th Mediterranean*, Lecce, 2015, pp. 1-4.
- [24] T. Skaik, "Star-Junction X-band Coupled Resonator Multiplexer," *Proceedings of the 12th Mediterranean Microwave Symposium*, Istanbul, Turkey, Sept 2012.
- [25] J.-S. Hong and S. Li, "Theory and experiment of dual-mode microstrip triangular patch resonators and filters," *IEEE Transactions on Microwave Theory and Techniques*, vol. 52, no. 4, pp. 1237-1243, April 2004.



- [26] E. Ogbodo, Y. Wang, and P. B. Rapajic, "Bandpass filters with mixed hairpin and patch resonators," *Progress in Electromagnetics Research C*, Vol. 59, 101-106, 2015.
- [27] J.-S. Hong and M. J. Lancaster, "Design of highly selective microstrip bandpass filters with a single pair of attenuation poles at finite frequencies," *IEEE Transactions on Microwave Theory and Techniques*, vol. 48, no. 7, pp. 1098-1107, Jul 2000.
- [28] K. Rabbi and D. Budimir, "Miniaturised sharp rejection bandpass filter with reconfigurable bandwidth for UWB applications," *Microwave Conference (EuMC), 2013 European*, Nuremberg, 2013, pp. 1023-1026.
- [29] R.-Y. Yang, C.-M. Hsiung, C.-Y. Hung, and C.-C. Lin, "Design of a high band isolation diplexer for GPS and WLAN system using modified stepped-impedance resonators," *Progress In Electromagnetics Research*, Vol. 107, 101-114, 2010.
- [30] T. Nagao, "Diplexer and Broadbanding Operations of Stripline Y-Junction Circulators," 1977 *IEEE MTT-S International Microwave Symposium Digest*, San Diego, CA, USA, 1977, pp. 516-518.
- [31] A. Morini and T. Rozzi, "Constraints to the optimum performance and bandwidth limitations of diplexers employing symmetric three-port junctions," *IEEE Transactions on Microwave Theory and Techniques*, vol. 44, no. 2, pp. 242-248, Feb 1996.
- [32] Y. L. Cheng, H. W. Chen, P. D. Huang and C. Y. Chang, "A W-band quadrature hybrid coupled substrate integrated waveguide diplexer," *2015 Asia-Pacific Microwave Conference (APMC)*, Nanjing, 2015, pp. 1-3.
- [33] R. R. Mansour, F. Rammo and V. Dokas, "Design of hybrid-coupled multiplexers and diplexers using asymmetrical superconducting filters," *Microwave Symposium Digest, 1993.*, *IEEE MTT-S International*, Atlanta, GA, USA, 1993, pp. 1281-1284 vol.3.
- [34] C. Carceller, P. Soto, V. Boria, M. Guglielmi and J. Gil, "Design of Compact Wideband Manifold-Coupled Multiplexers," *IEEE Transactions on Microwave Theory and Techniques*, vol. 63, no. 10, pp. 3398-3407, Oct. 2015.
- [35] C. E. Saavedra, "Diplexer using a circulator and interchangeable filters," *2008 7th International Caribbean Conference on Devices, Circuits and Systems*, Cancun, 2008, pp. 1-5.
- [36] N. K. Andrzejewski and E. J. Pietraszewski, "Waveguide Multiplexer with Eight Contiguous Channels in X Band," *Microwave Conference, 1979. 9th European*, Brighton, UK, 1979, pp. 392-396.
- [37] C. Caloz and T. Itoh, "Electromagnetic Metamaterials: Transmission Line Theory and Microwave Applications: the engineering approach," *John Wiley & Sons* 2006.
- [38] C. H. Chen, H. Wu, and W. Wu, "High isolation dbr diplexer using in-line scmrc," *Progress In Electromagnetics Research C*, Vol. 22, 97-108, 2011.

- [39] A. Manchec, E. Rius, C. Quendo, C. Person, J. F. Favennec, P. Moroni, J. C. Cayrou and J. L. Cazaux, "Ku-Band Microstrip Diplexer Based on Dual Behavior Resonator Filter," 2005 IEEE MTT-S International Microwave Symposium Digest, pp. 525-528.
- [40] K. Singh and K. Ngachenchaiyah, "Notch Implemented Dual Behavior Resonator Filter and Diplexer at Ku-band," *Microwave Journal*, April 12, 2010.
- [41] K. Lu, G.-M. Wang, H.-Y. Xu and X. Yin, "Design of Compact Planar Diplexer Based on Novel Spiral-Based Resonators," *Radio Engineering*, Vol. 21, No. 1, April, 2012.
- [42] W. T. Hung, S. Y. Chang and S. Y. Chen, "High isolation, compact microstrip diplexers using quarter-wave stepped-impedance resonators," 2010 Asia-Pacific Microwave Conference, Yokohama, 2010, pp. 1747-1750.
- [43] A. R. Brown and G. M. Rebeiz, "A high-performance integrated K-band diplexer," *IEEE Transactions on Microwave Theory and Techniques*, vol. 47, no. 8, pp. 1477-1481, Aug 1999.
- [44] L. Maloratsky, *Integrated Microwave Front-ends with Avionics Applications*. Artech House, 2012.
- [45] K. L. Wu and W. Meng, "A Direct Synthesis Approach for Microwave Filters With a Complex Load and Its Application to Direct Diplexer Design," *IEEE Transactions on Microwave Theory and Techniques*, vol. 55, no. 5, pp. 1010-1017, May 2007.
- [46] F. M. Vanin, F. Frezza, and D. Schmitt, "Computer-aided design of y-junction waveguide diplexers," *Progress In Electromagnetics Research C*, Vol. 17, 203-218, 2010.
- [47] T. S. King, A. T. Y. Ying, and S. H. Tiong, "A microstrip diplexer using folded hairpins," *RF and Microwave Conference (RFM), 2011 IEEE International*, Seremban, Negeri Sembilan, 2011, pp. 226-229.
- [48] X. Wang, Q. Y. Wang, Y. H. Zhao and H. Li, "Design of a Compact Diplexer," *Art of Miniaturizing RF and Microwave Passive Components, 2008. IMWS 2008. IEEE MTT-S International Microwave Workshop Series on*, Chengdu, 2008, pp. 170-172.
- [49] M. H. Weng, C. Y. Hung and Y. K. Su, "A Hairpin Line Diplexer for Direct Sequence Ultra-Wideband Wireless Communications," *IEEE Microwave and Wireless Components Letters*, vol. 17, no. 7, pp. 519-521, July 2007.
- [50] D. Zayniyev and D. Budimir, "Microstrip three-port 4-channel multiplexers using dual-band bandpass filters for wireless applications," 2008 IEEE Antennas and Propagation Society International Symposium, San Diego, CA, 2008, pp. 1-4.
- [51] J. Chen, X. Zhang and Q. Xue, "Dual-band bandpass filter and diplexer based on double-sided parallel-strip line," *Microwave Symposium Digest, 2008 IEEE MTT-S International*, Atlanta, GA, 2008, pp. 675-678.
- [52] Q. Xue and J. X. Chen, "Compact diplexer based on double-sided parallel-strip line," *Electronics Letters*, vol. 44, no. 2, pp. 123-124, January 17 2008.

- [53] T. Yang and G. M. Rebeiz, "A Simple and Effective Method for 1.9–3.4-GHz Tunable Diplexer With Compact Size and Constant Fractional Bandwidth," *IEEE Transactions on Microwave Theory and Techniques*, vol. 64, no. 2, pp. 436-449, Feb. 2016.
- [54] X. Guan, F. Yang, H. Liu and L. Zhu, "Compact and High-Isolation Diplexer Using Dual-Mode Stub-Loaded Resonators," *IEEE Microwave and Wireless Components Letters*, vol. 24, no. 6, pp. 385-387, June 2014.
- [55] C. Chen, T. Huang, C. Chou and R. Wu, "Microstrip diplexers design with common resonator sections for compact size, but high isolation," *IEEE Transactions on Microwave Theory and Techniques*, vol. 54, no. 5, pp. 1945-1952, May 2006.
- [56] A. García-Lampérez, R. Gómez-García and M. Salazar-Palma, "Compact diplexer with edge-coupled and nonbianisotropic split-ring resonators," *Microwave Symposium Digest (MTT), 2012 IEEE MTT-S International*, Montreal, QC, Canada, 2012, pp. 1-3.
- [57] P. Zhao and K. L. Wu, "Circuit model extraction for computer-aided tuning of a coupled-resonator diplexer," *2015 IEEE MTT-S International Microwave Symposium*, Phoenix, AZ, 2015, pp. 1-3.
- [58] H. Ezzeddine, S. Bila, S. Verdeyme, F. Seyfert and D. Pacaud, "Coupling topologies for realizing compact microwave diplexers with dual-mode cavities," *Microwave Symposium Digest (MTT), 2010 IEEE MTT-S International*, Anaheim, CA, 2010, pp. 880-883.
- [59] X. Shang, Y. Wang, W. Xia and M. J. Lancaster, "Novel Multiplexer Topologies Based on All-Resonator Structures," *IEEE Transactions on Microwave Theory and Techniques*, vol. 61, no. 11, pp. 3838-3845, Nov. 2013.
- [60] A. Garcia-Lamperez, M. Salazar-Palma and T. K. Sarkar, "Compact multiplexer formed by coupled resonators with distributed coupling," *2005 IEEE Antennas and Propagation Society International Symposium*, Washington, DC, 2005, pp. 89-92 Vol. 1A.
- [61] W. Xia, X. Shang and M. J. Lancaster, "Responses comparisons for coupled-resonator based diplexers," *Passive RF and Microwave Components, 3rd Annual Seminar on*, London, 2012, pp. 67-75.
- [62] T. F. Skaik, M. J. Lancaster and F. Huang, "Synthesis of multiple output coupled resonator circuits using coupling matrix optimisation," *IET Microwaves, Antennas & Propagation*, vol. 5, no. 9, pp. 1081-1088, June 27 2011.
- [63] G. Macchiarella, "Synthesis of Star-Junction Multiplexers," *IEEE Microwave Magazine*, vol. 12, no. 6, pp. 101-109, Oct. 2011.
- [64] G. Macchiarella and S. Tamiazzo, "Synthesis of Star-Junction Multiplexers," *IEEE Transactions on Microwave Theory and Techniques*, vol. 58, no. 12, pp. 3732-3741, Dec. 2010.
- [65] J.-S. Hong "Microstrip Filters for RF/Microwave Applications," John Wiley & Sons, Inc. 2011.

- [66] R. R. Mansour, B. Jolley, Shen Ye, F. S. Thomson and V. Dokas, "On the power handling capability of high temperature superconductive filters," *IEEE Transactions on Microwave Theory and Techniques*, vol. 44, no. 7, pp. 1322-1338, Jul 1996.
- [67] J.-S. Hong and M. J. Lancaster, "Microstrip triangular patch resonator filters," *Microwave Symposium Digest. 2000 IEEE MTT-S International*, Boston, MA, USA, 2000, pp. 331-334 vol.1.
- [68] F. S. Thomson, R. R. Mansour, Shen Ye and W. Jolley, "Current density and power handling of high-temperature superconductive thin film resonators and filters," *IEEE Transactions on Applied Superconductivity*, vol. 8, no. 2, pp. 84-93, June 1998.
- [69] J. Xiao, Q. Chu and H. Huang, "Band tunable microstrip bandpass filter using defected single patch resonator," *Antennas, Propagation and EM Theory, 2008. ISAPE 2008. 8th International Symposium on*, Kunming, 2008, pp. 1029-1032.
- [70] J. K. Xiao, Xiao-Peng Zu, Hui-Fen Huang and Wei-Li Dai, "Multi-mode bandstop filter using defected equilateral triangular patch resonator," *Antennas Propagation and EM Theory (ISAPE), 2010 9th International Symposium on*, Guangzhou, 2010, pp. 1252-1255.
- [71] J. K. Xiao, Qing-Xin Chu and Yun Wang, "New patch resonator bandpass filter with wideband and tunable operation," *2008 Asia-Pacific Microwave Conference*, Macau, 2008, pp. 1-3.
- [72] J. Xiao, H. Huang and W. Ji, "Wideband microstrip bandpass filter using single patch resonator," *Microwave and Millimeter Wave Technology, 2008. ICMMT 2008. International Conference on*, Nanjing, 2008, pp. 1470-1473.
- [73] J. L. Li, J. P. Wang, X. S. Yang and B. Z. Wang, "A study of dual-mode patch resonator-based microwave filters," *Microwave and Millimeter Wave Technology (ICMMT), 2010 International Conference on*, Chengdu, 2010, pp. 48-51.
- [74] J. L. Li, S. W. Qu and Q. Xue, "Compact Dual-Mode Patch Resonator for Filter Applications," *Art of Miniaturizing RF and Microwave Passive Components, 2008. IMWS 2008. IEEE MTT-S International Microwave Workshop Series on*, Chengdu, 2008, pp. 83-86.
- [75] L. Zhu, B. C. Tan and S. J. Quek, "Miniaturized dual-mode bandpass filter using inductively loaded cross-slotted patch resonator," *IEEE Microwave and Wireless Components Letters*, vol. 15, no. 1, pp. 22-24, Jan. 2005.
- [76] L. Zhu, P. M. Wecowski and K. Wu, "New planar dual-mode filter using cross-slotted patch resonator for simultaneous size and loss reduction," *IEEE Transactions on Microwave Theory and Techniques*, vol. 47, no. 5, pp. 650-654, May 1999.
- [77] O. Akgun, B. S. Tezekici and A. Gorur, "Reduced-size dual-mode slotted patch resonator for low-loss and narrowband bandpass filter applications," *Electronics Letters*, vol. 40, no. 20, pp. 1275-1276, 30 Sept. 2004.

- [78] J. K. Xiao and H. F. Huang, "Square patch resonator bandstop filter," *Communication Technology (ICCT)*, 2010 12th IEEE International Conference on, Nanjing, 2010, pp. 104-107.
- [79] K. Phaebua and C. Phongcharoenpanich, "Characteristics of a microstrip semi-circular patch resonator filter," *Electrical Engineering/Electronics, Computer, Telecommunications and Information Technology*, 2008. ECTI-CON 2008. 5th International Conference on, Krabi, 2008, pp. 273-276.
- [80] R. Z., L. Zhu and S. Luo, "Characterization of a slotted circular patch resonator for adjustable dual-mode dual-band bandpass filters," *Microwave Symposium Digest (MTT)*, 2012 IEEE MTT-S International, Montreal, QC, Canada, 2012, pp. 1-3.
- [81] R. Zhang, L. Zhu and S. Luo, "Dual-Mode Dual-Band Bandpass Filter Using a Single Slotted Circular Patch Resonator," *IEEE Microwave and Wireless Components Letters*, vol. 22, no. 5, pp. 233-235, May 2012.
- [82] K. R. Jha and G. Singh, "Microstrip Low-Pass Filter Using Hexagonal Patch with Wide Stopband," *Communication Systems and Network Technologies (CSNT)*, 2011 International Conference on, Katra, Jammu, 2011, pp. 250-252.
- [83] R. J. Mao and X. H. Tang, "Novel Dual-Mode Bandpass Filters Using Hexagonal Loop Resonators," *IEEE Transactions on Microwave Theory and Techniques*, vol. 54, no. 9, pp. 3526-3533, Sept. 2006.
- [84] L. Murmu, G. Singh and S. Das, "Hexagonal bandpass filter using open end step impedance stub perturbation," *Microwave and Photonics (ICMAP)*, 2013 International Conference on, Dhanbad, 2013, pp. 1-4.
- [85] Y. K. Singh, P. Abdulla and A. Chakrabarty, "Miniaturized bandpass filter using a dual-mode octagonal patch resonator," *2009 Asia Pacific Microwave Conference*, Singapore, 2009, pp. 2511-2514.
- [86] E. A. Ogbodo, Y. Wu and Y. Wang, "Microstrip diplexers with dual-mode patch resonant junctions," *2016 46th European Microwave Conference (EuMC)*, London, United Kingdom, 2016, pp. 1155-1158.
- [87] X. Guan et al., "A novel microstrip diplexer with a common square ring resonator for WCDMA," *2016 IEEE International Workshop on Electromagnetics: Applications and Student Innovation Competition (iWEM)*, Nanjing, 2016, pp. 1-3.
- [88] G. Prigent and T. M. Vu, "Design of an input multiplexer using dual-band planar filters," *Microwave Symposium Digest (IMS)*, 2013 IEEE MTT-S International, Seattle, WA, 2013, pp. 1-3.
- [89] A. Pradeep, S. Mridula and P. Mohanan, "Design of an Edge-Coupled Dual-Ring Split-Ring Resonator," *IEEE Antennas and Propagation Magazine*, vol. 53, no. 4, pp. 45-54, Aug. 2011.

- [90] C. Saha, J. Y. Siddiqui, S. Mukherjee and R. Chaudhuri, "Estimation of the resonant frequency and magnetic polarizability of an edge coupled circular split ring resonator with rotated outer ring," 2010 Annual IEEE India Conference (INDICON), Kolkata, 2010, pp. 1-4.
- [91] M. R. Vidyalakshmi. and S. Raghavan, "A CAD model of triangular Split Ring Resonator based on equivalent circuit approach," Applied Electromagnetics Conference (AEMC), 2009, Kolkata, 2009, pp. 1-4.
- [92] A. Genc, R. Baktur and R. J. Jost, "Dual-Bandpass Filters with Individually Controllable Passbands," IEEE Transactions on Components, Packaging and Manufacturing Technology, vol. 3, no. 1, pp. 105-112, Jan. 2013.
- [93] G.-L. Alejandro, G.-G. Roberto, S.-P. Magdalena, "Compact diplexer with edge-coupled and nonbianisotropic split-ring resonators," Microwave Symposium Digest (MTT), 2012 IEEE MTT-S international, vol., no., pp.1-3, 17-22 June 2012.
- [94] A. G. Lamperez and M. S. Palma, "Dual band filter with split-ring resonators," Microwave Symposium Digest, 2006. IEEE MTT-S International, San Francisco, CA, 2006, pp. 519-522.
- [95] H. Zhu and J. Mao, "A bandstop filter based on non-bianisotropic complementary split ring resonators (NBCSRRs)," Electrical Design of Advanced Packaging and Systems Symposium (EDAPS), 2011 IEEE, Hanzhou, 2011, pp. 1-4.
- [96] P. de Paco, O. Menendez, and J. Marin, "Dual-band filter using non-bianisotropic splitting resonators," Progress In Electromagnetics Research Letters, Vol. 13, 51-58, 2010.
- [97] J. K. Xiao and Z. H. Wang, "Novel Compact Hairpin SIR Bandpass Filters with Defected Ground Structure," Microwave and Millimeter Wave Technology, 2007. ICMMT '07. International Conference on, Builin, 2007, pp. 1-3.
- [98] D. Chung and B. Han, "HTS microstrip filters using H-type resonators," IEEE Transactions on Applied Superconductivity, vol. 11, no. 1, pp. 388-391, Mar 2001.
- [99] C. H. Lee, C. I. G. Hsu, S. X. Wu and P. H. Wen, "Balanced quad-band diplexer with wide common-mode suppression and high differential-mode isolation," IET Microwaves, Antennas & Propagation, vol. 10, no. 6, pp. 599-603, 4 24 2016.
- [100] T. Sugchai, J. Rattapon and K. Sommart, "A Design of Wide-Stopband Microstrip Diplexers with Multiorder Spurious-Mode Suppression Using Stepped-Impedance Resonators," 2012 Spring Congress on Engineering and Technology, Xian, 2012, pp. 1-4.
- [101] Y. C. Chiang and H. S. Peng, "Design of microstrip diplexer constructed with step impedance resonance ring structures," 2014 International Symposium on Next-Generation Electronics (ISNE), Kwei-Shan, 2014, pp. 1-3.
- [102] Z. He, Y. Shi and X. Wei, "Compact dual-band BPF with improved stopband," Electronic Packaging Technology (ICEPT), 2014 15th International Conference on, Chengdu, 2014, pp. 1404-1406.

- [103] W. Chen, Y. j. Zhao and X. j. Zhou, "Compact and high selectivity dual-band dual-mode microstrip BPF with folded SIR," Microwave Workshop Series on Millimeter Wave Wireless Technology and Applications (IMWS), 2012 IEEE MTT-S International, Nanjing, 2012, pp. 1-3.
- [104] S. Sun, and L. Zhu, "Compact dual-band microstrip bandpass filter without external feeds," IEEE Microwave and Wireless Components Letters, vol. 15, no. 10, pp. 644-646, Oct. 2005.
- [105] F. Wei, P. Y. Qin, Y. J. Guo and X. W. Shi, "Design of multi-band bandpass filters based on stub loaded stepped-impedance resonator with defected microstrip structure," IET Microwaves, Antennas & Propagation, vol. 10, no. 2, pp. 230-236, 1 29 2016.
- [106] J. Xu, "Compact Microstrip Tri-Band Bandpass Filter Using New Stubs Loaded Stepped-Impedance Resonator," IEEE Microwave and Wireless Components Letters, vol. 26, no. 4, pp. 249-251, April 2016.
- [107] H. Liu, P. Wen, H. Jiang and Y. He, "Wideband and Low-Loss High-Temperature Superconducting Bandpass Filter Based on Metamaterial Stepped-Impedance Resonator," IEEE Transactions on Applied Superconductivity, vol. 26, no. 3, pp. 1-4, April 2016.
- [108] T. Yan, D. Lu, J. Wang and X. H. Tang, "High-Selectivity Balanced Bandpass Filter With Mixed Electric and Magnetic Coupling," IEEE Microwave and Wireless Components Letters, vol. 26, no. 6, pp. 398-400, June 2016.
- [109] Y. Zhan, J. Chen and H. Tang, "Miniaturized LTCC bandpass filter using transmission line dual-mode resonator," Electromagnetics (iWEM), 2014 IEEE International Workshop on, Sapporo, 2014, pp. 22-23.
- [110] J. K. Xiao, Q. X. Chu and H. F. Huang, "New wideband microwave bandpass filter using single triangular patch resonator with low permittivity substrate," Communication Systems, 2008. ICCS 2008. 11th IEEE Singapore International Conference on, Guangzhou, 2008, pp. 608-612.
- [111] A. L. C. Serrano and F. S. Correra, "A miniaturized bandpass filter with two transmission zeros using a novel square patch resonator," Microwave and Optoelectronics Conference, 2007. IMOC 2007. SBMO/IEEE MTT-S International, Brazil, 2007, pp. 941-945.
- [112] H. Chen, D. Jiang and Y. Wan, "A miniature low-loss wideband dual-mode BPF with harmonic suppression," 2015 IEEE International Conference on Communication Problem-Solving (ICCP), Guilin, 2015, pp. 530-532.
- [113] L. H. Zhou, J. Shi and J. X. Chen, "Differential dual-band bandpass filter using multi-mode stub-loaded dumbbell-shaped resonator," 2016 IEEE International Workshop on Electromagnetics: Applications and Student Innovation Competition (iWEM), Nanjing, 2016, pp. 1-3.

- [114] Z. C. Zhang, Q. X. Chu and F. C. Chen, "Compact Dual-Band Bandpass Filters Using Open-/Short-Circuited Stub-Loaded  $\lambda/4$  Resonators," *IEEE Microwave and Wireless Components Letters*, vol. 25, no. 10, pp. 657-659, Oct. 2015.
- [115] S. Lu, B. You and Y. Wang, "A novel dual-band bandpass filter using stub-loaded resonators," 2015 IEEE 16th International Conference on Communication Technology (ICCT), Hangzhou, 2015, pp. 393-395.
- [116] L. Lin, Y.-T. Zhao, B. Wu, and C.-H. Liang, "Design of compact quad-channel diplexer using quad-mode stub-loaded resonators," *Progress In Electromagnetics Research Letters*, Vol. 51, 87-93, 2015.
- [117] S. J. Fiedziuszko, D. Doust and S. Holme, "Satellite L-band output multiplexer utilizing single and dual mode dielectric resonators," *Microwave Symposium Digest, 1989.*, IEEE MTT-S International, Long Beach, CA, USA, 1989, pp. 683-686 vol. 2.
- [118] D. M. Pozar, *Microwave Engineering*. 3rd ed. New York: Wiley, 2005.
- [119] S. B. Cohn, "Direct-coupled-resonator filters," *Proceedings of the IRE*, Vol. 45, No.2, 187- 196, 1957.
- [120] G. Matthaei, L. Young, and E. M. T. Jones, *Microwave Filters, Impedance-matching Networks, and Coupling Structures*, Artech Houston, Boston, 1980.
- [121] A. Zaiki, *Microwave systems design*. 1st ed. New York: Springer Singapore, 2013.
- [122] X. Guan, Z. Ma, P. Cai, Y. Kobayashi, T. Anada and G. Hagiwara, "Synthesis of dual-band bandpass filters using successive frequency transformations and circuit conversions," *IEEE Microwave and Wireless Components Letters*, vol. 16, no. 3, pp. 110-112, March 2006.
- [123] H. Shaman and J. S. Hong, "Ultra-Wideband (UWB) Bandpass Filter With Embedded Band Notch Structures," *IEEE Microwave and Wireless Components Letters*, vol. 17, no. 3, pp. 193-195, March 2007.
- [124] E. A. Ogbodo, Y. Wang, and K. S. K. Yeo, "Microstrip dual-band bandpass filter using U-shaped resonators," *Progress In Electromagnetics Research Letters*, Vol. 59, 1-6, 2016.
- [125] Z. Kordiboroujeni and J. Bornemann, "Mode-matching analysis and design of substrate integrated waveguide T-junction diplexer and corner filter", *International Journal of Numerical Modelling: Electronic Networks, Devices and Fields*, vol. 28, no. 5, pp. 497-507, 2014.
- [126] H. Zhang and G. James, "A broadband T-junction diplexer with integrated iris filters", *Microwave and Optical Technology Letters*, vol. 17, no. 1, pp. 69-72, 1998.
- [127] P. Zhao and K. Wu, "An Iterative and Analytical Approach to Optimal Synthesis of a Multiplexer With a Star-Junction", *IEEE Transactions on Microwave Theory and Techniques*, vol. 62, no. 12, pp. 3362-3369, 2014.



- [128] Y. Wu, Y. Wang and E. A. Ogbodo, "Microstrip wideband diplexer with narrow guard band based on all-resonator structures," 46th European Microwave Conference (EuMC), London, United Kingdom, 2016, pp. 1163-1166.
- [129] H. Son and C. Pyo, "Design of RFID tag antennas using an inductively coupled feed", Electronics Letters, vol. 41, no. 18, p. 994, 2005.
- [130] G. Mansour, M. J. Lancaster, P. S. Hall, P. Gardner and E. Nugoolcharoenlap, "Design of Filtering Microstrip Antenna Using Filter Synthesis Approach," Progress in Electromagnetics Research (PIER), vol. 145, 2014, pp. 59-67.
- [131] K. Chang, and L. Hsieh, Microwave Ring Circuits and Related Structures, 2<sup>nd</sup> Edition, John Wiley and Sons Ltd., 2004.
- [132] J.S. Hong, and M.J. Lancaster, Microstrip Filters for RF/Microwave Application, New York, Wiley, 2001.
- [133] G. Matthaei, E. Jones and L. Young, Microwave filters, impedance-matching networks, and coupling structures. New York u.a: McGraw-Hill, 1964.
- [134] C.K Liao; C.Y Chang, "Design of microstrip quadruplet filters with source-load coupling," IEEE Transactions on Microwave Theory and Techniques, vol. 53, no. 7, pp. 2302-2308, July 2005.
- [135] Y. Yang, M. Yu and Q. Wu, "Advanced Synthesis Technique for Unified Extracted Pole Filters," IEEE Transactions on Microwave Theory and Techniques, vol. 64, no. 12, pp. 4463-4472, Dec. 2016.
- [136] P. Zhao and K. L. Wu, "A direct synthesis approach of bandpass filters with extracted-poles," 2013 Asia-Pacific Microwave Conference Proceedings (APMC), Seoul, 2013, pp. 25-27.
- [137] N. Yildirim, O. A. Sen, Y. Sen, M. Karaaslan and D. Pelz, "A revision of cascade synthesis theory covering cross-coupled filters," IEEE Transactions on Microwave Theory and Techniques, vol. 50, no. 6, pp. 1536-1543, Jun 2002.
- [138] J.D Rhodes, and J.R Cameron, "General Extracted Pole Synthesis Technique with Applications to Low-Loss TE<sub>011</sub> Mode Filters," Microwave Theory and Techniques, IEEE Transactions on, vol.28, no.9, pp.1018,1028, Sep 1980.
- [139] K.S.K. Yeo, M.J. Lancaster, and Hong, Jia-Sheng "The Design of Microstrip Six-Pole Quasi-Elliptic Filter with Linear Phase Response Using Extracted-Pole Technique", IEEE Trans. Microwave Theory and Technique, 40(2), pp. 321-327, 2001.
- [140] D. Pozar, Microwave and RF wireless systems. New York: John Wiley, 2001.

- [141] M. L. Chuang and M. T. Wu, "Microstrip diplexer design using common T-shaped resonator," *IEEE Microwave. Wireless Components. Letter.*, vol. 21, no. 11, pp. 583-585, Nov. 2011.
- [142] A. Garcia-Lamperez and M. Salazar-Palma, "Dual band filter with split-ring resonators," *2006 IEEE MTT-S International Microwave Symposium Digest*, San Francisco, CA, 2006, pp. 519-522.
- [143] S. Amari, M. Bekheit and F. Seyfert, "Notes on bandpass filters whose inter-resonator coupling coefficients are linear functions of frequency," *2008 IEEE MTT-S International Microwave Symposium Digest*, Atlanta, GA, USA, 2008, pp. 1207-1210.
- [144] H. Miyake, S. Kitazawa, T. Yamada, and Y. Nagatomi, "A miniaturised monolithic dual band filter using ceramic lamination technique for dual mode portable telephones," *IEEE MTT-S Int. Dig.*, 1997, pp. 789-792.
- [145] L. C. Tsai, and C. W. Hsue, "Dual-band bandpass filters using equal-length coupled serial-shunted lines and Z-transform technique," *IEEE Trans. Microw. Theory Tech.*, vol. 52, no. 4, pp. 1111-1117, Apr. 2004.
- [146] F. Queudet, I. Pele, B. Froppier, Y. Mahe, and S. Toutain, "Integration of Pass-Band Filters in Patch Antennas," *Proc. 32nd Eur. Microw. Conf.*, 2002, pp. 685–688.
- [147] A. Abbaspour-Tamijani, J. Rizk, and G. Rebeiz, "Integration of filters and microstrip antennas," *Proc. IEEE AP-S Int. Symp.*, Jun. 2002, pp. 874–877.
- [148] T. L. Nadan, J. P. Coupez, S. Toutain, and C. Person, "Optimization and miniaturization of a filter/antenna multi-function module using a composite ceramic-foam substrate," *IEEE MTT-S Int. Microw. Symp. Dig.*, Jun. 1999, pp. 219–222.
- [149] C. X. Mao, S. Gao, Z. P. Wang, Y. Wang, F. Qin, B. Sanz-Izquierdo, Q. X. Chu, "Integrated filtering-antenna with controllable frequency bandwidth," *2015 9th European Conference on Antennas and Propagation (EuCAP)*, Lisbon, 2015, pp. 1-4.
- [150] L. Yang, P. Cheong, L. Han, W. W. Choi, K. W. Tam and K. W., "Miniaturized Parallel Coupled-Line Filter-Antenna With Spurious Response Suppression," *Antenna Wireless Propag. Lett.*, vol. 10, 2011, pp. 726–729.
- [151] D. Zayniyev and D. Budimir, "An Integrated Antenna-Filter with Harmonic Rejection," *3rd European Conf. on Antennas and Propag.*, 2009, pp. 393-394.
- [152] C. Mao, S. Gao and Y. Wang, "Stub-loaded resonator-fed filtering patch antenna with improved bandwidth," *2016 46th European Microwave Conference (EuMC)*, London, 2016, pp. 317-320.
- [153] C. X. Mao, S. Gao, Y. Wang, F. Qin and Q. X. Chu, "Compact Highly Integrated Planar Duplex Antenna for Wireless Communications," *IEEE Transactions on Microwave Theory and Techniques*, vol. 64, no. 7, pp. 2006-2013, July 2016.

- [154] H. Werfelli, K. Tayari, M. Chaoui, M. Lahiani and H. Ghariani, "Design of rectangular microstrip patch antenna," 2016 2nd International Conference on Advanced Technologies for Signal and Image Processing (ATSIP), Monastir, 2016, pp. 798-803.
- [155] S. Tamiazzo, G. Macchiarella "Design and realization of filtering units in a triple-band masthead amplifier system for BTS of mobile communications", IEEE MTT-S Int. Microwave Symp. Dig., Seattle, Jun. 2013
- [156] G. Macchiarella and S. Tamiazzo, "Design of "masthead" combiners," 2015 European Microwave Conference (EuMC), Paris, 2015, pp. 686-689.
- [157] J. Konpang, M. Sandhu, N. Somjit and I. Hunter, "Four-port microstrip diplexer for RF interference rejection," 2016 13th International Conference on Electrical Engineering/Electronics, Computer, Telecommunications and Information Technology (ECTI-CON), Chiang Mai, 2016, pp. 1-4.
- [158] J. Konpang, M. Sandhu, N. Somjit and I. Hunter, "Novel RF interference rejection technique using a four-port diplexer," 2016 46th European Microwave Conference (EuMC), London, 2016, pp. 524-527.

## **Publications**

- [1] E. A. Ogbodo, Y. Wu and Y. Wang, "Microstrip diplexers with dual-mode patch resonant junctions," 2016 46th European Microwave Conference (EuMC), London, United Kingdom, 2016, pp. 1155-1158.
  
- [2] Y. Wu, Y. Wang and E. A. Ogbodo, "Microstrip wideband diplexer with narrow guard band based on all-resonator structures," 2016 46th European Microwave Conference (EuMC), London, United Kingdom, 2016, pp. 1163-1166.
  
- [3] E. A. Ogbodo, Y. Wang, and K. S. K. Yeo, "Microstrip dual-band bandpass filter using u-shaped resonators," Progress In Electromagnetics Research Letters, Vol. 59, 1-6, 2016.
  
- [4] E. A. Ogbodo, Y. Wang, and P. Rapajic, "Bandpass Filters with Mixed Hairpin and Patch Resonators", Progress In Electromagnetics Research C, Vol. 59, 101–106, 2015.
  
- [5] E. A. Ogbodo, Y. Wu and Y. Wang, "Dual-Path Dual-Band Filters Based On Patch Resonators," International Workshop on Electromagnetism (iWEM), London, United Kingdom, 2017.
  
- [6] E. A. Ogbodo, Y. Wu, P. Callaghan, and Y. Wang, "A Compact Diplexer with a Split-Ring Resonator Junction," Microwave and Optical Technology Letters, 2017.
  
- [7] E. A. Ogbodo, Y. Wu, P. Callaghan, and Y. Wang, "Asynchronous Coupling Resonant Junctions for Compact Diplexers and Multi-Port Filtering Networks," Microwave and Optical Technology Letters, (Accepted), 2017.

# Microstrip Diplexers with Dual-mode Patch Resonant Junctions

Eugene A. Ogbodo, Yun Wu, Yi Wang  
Engineering Science

University of Greenwich (Medway campus),  
Chatham Maritime, Kent, U.K.

e.a.ogbodo@gre.ac.uk; y.wu@gre.ac.uk; yi.wang@gre.ac.uk

**Abstract**— A conventional diplexer is made up of two channel filters which are connected to a transmission-line based signal distribution network. In this work, a novel diplexer has been proposed and designed using hairpin resonator filters that are joined together using a patch resonator. The patch being a dual-mode is made to resonate at the centre frequencies of the channel filters in corresponding modes. The patch functions as a signal splitter and at the same time as a resonant pole for each of the channel filters. A diplexer with the channel centre frequencies of 3.99 GHz and 4.39 GHz and 4% fractional bandwidth has been designed and tested. The simulated and measured results show very good agreements.

**Keywords**—Diplexer, Patch resonator; Dual-mode resonator

## I. INTRODUCTION

Dual mode microstrip resonators are playing an important role in the miniaturisation of microwave planar filters. Its popularity comes from its ability to take the place of two single mode resonators, thereby resulting in halving the number of required resonators for a given purpose. In the design of planar filters, microstrip resonators such as patch resonators are used extensively. In [1] a patch resonator was used to generate a transmission zero in a bandpass filter (BPF) response without resorting to any cross couplings, thereby resulting in improved frequency selectivity. Square patch resonators were applied in the design of BPFs in [2] and [3], whereas they were used to design dual-band BPFs in [4] and [5]. A particular area where the use of dual-mode or multi-mode resonators can be beneficial is in diplexer designs with resonant junctions [6]. Conventionally, channel filters in the diplexers are combined via transmission-line based junctions, as illustrated in Fig. 1(a), such as T-junctions, hybrid couplers, manifolds or circulators [7], [12] - [15]. However, the new diplexer configuration based on resonant junctions has attracted a lot of attention in the past few years. Different circuit techniques have been used. For instance, in [8] two novel multiplexer topologies based on all-resonator structures were reported at X-band using waveguide technology. In [9], a frequency division duplex (FDD) diplexer that integrates a T-shaped resonator and two sets of open-loop resonators was developed. The technique used in [9] was then extended into a multiplexer and a switchable diplexer in [10] using open-loop resonators. In [11], a compact diplexer was

proposed and designed using a stepped-impedance resonator (SIR) which acted as a common resonator.

In this paper, a novel diplexer structure has been proposed and designed using hairpin (HP) resonator filters with a 4% fractional bandwidth each at 3.99 GHz and 4.39 GHz respectively. These channel filters are linked together using a dual-mode patch resonator. Each of the channels was individually designed using a three-pole structure with proximity couplings. Using dual-mode patch resonator led to the reduction in the number of required resonators from a supposedly six resonators to five resonators. Fig. 1(b) illustrates the resonator topology and the coupling path of the proposed design as compared with the conventional topology shown in Fig. 1(a). The proposed diplexer layout is displayed in Fig. 2.

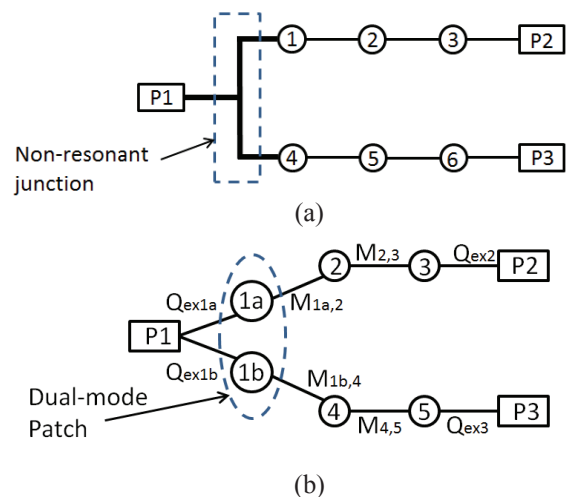


Fig. 1. (a) A conventional diplexer topology with a non-resonant junction; (b) The proposed diplexer topology with a resonant dual-mode junction.

## II. DESIGN

The proposed microstrip diplexer has been designed to meet the following specifications:

- Center frequency of the lower and upper passbands,  $f_{0,BPL}$  and  $f_{0,BPU}$ : 3.99 GHz and 4.39 GHz
- Passband return loss: 20 dB
- Fractional bandwidth (FBW) of the lower and upper passband, BWL and BWU: 4 %

All the simulations in this work were performed using EM simulator Sonnet Suites.

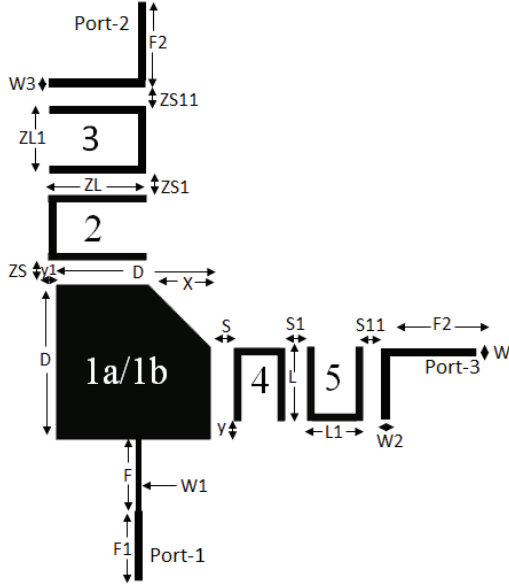


Fig. 2. Layout of the proposed diplexer (unit: mm);  $ZL = 5.4$ ,  $ZL1 = 3.9$ ,  $ZS = 1$ ,  $ZS1 = 1.4$ ,  $ZS11 = 0.2$ ,  $L = 5$ ,  $L1 = 3.4$ ,  $S = 0.84$ ,  $S1 = 1.26$ ,  $S11 = 0.2$ ,  $D = 10.9$ ,  $X = 4.6$ ,  $F = 6$ ,  $F1 = 5$ ,  $F2 = 10$ ,  $W = 1.1$ ,  $W1 = 0.9$ ,  $W2 = 0.6$ ,  $W3 = 0.9$ ,  $y = 0.5$ ,  $y1 = 1.6$ .

### A. Topology and coupling matrix

As shown in Fig. 1(b), the junction resonator has dual modes, denoted as 1a and 1b. The mode-1a is coupled to the resonator-2 and 3 to generate the lower channel, whereas the mode-1b is coupled to the resonator-4 and 5 to generate the upper channel. Each channel filter was designed separately to have a passband ripple factor of 0.043 dB using a three-pole Chebychev lowpass prototype derived from [16] with  $g$  values of  $g_0 = g_4 = 1.0$ ,  $g_1 = g_3 = 0.8516$  and  $g_2 = 1.1032$ . (1) and (2) are the required external quality factor  $Q_{ex}$  and coupling coefficients used for the physical dimensioning of the microstrip resonators and filters

$$M_{1a,2} = M_{2,3} = M_{1b,4} = M_{4,5} = \frac{FBW}{\sqrt{g_1 g_2}} = 0.041 \quad (1)$$

$$Q_{ex1a} = Q_{ex1b} = Q_{ex2} = Q_{ex3} = \frac{g_1 g_0}{FBW} = 21.29 \quad (2)$$

### B. Patch resonator

The patch resonator is used as the junction resonator in this design. The patch, of dual modes, acts as a resonant pole to each channel filter as well as a signal splitter in the diplexer. A half-wavelength square patch resonator is first made to resonate at the centre frequency of the diplexer. In other to generate the dual modes, a chamfer defined by the dimension

$X$  is introduced at one corner of the square resonator. By varying  $X$ , the dual-modes of the patch can be adjusted to the desired frequencies. Fig. 3 illustrates the resonant frequencies of the patch as a function of the chamfer length,  $X$ . When  $X$  is 4 mm, the resonance was split into 3.99 GHz and 4.39 GHz.

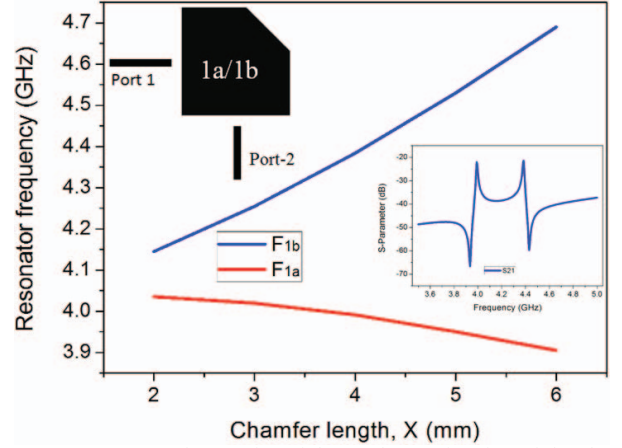


Fig. 3. Two resonance frequencies of the patch as a function of the chamfer length. The insets shows the layout used in th simulation and a typical simulated  $S_{21}$  response.

### C. Couplings

To obtain the external quality factor ( $Q_{ex1a}$  and  $Q_{ex1b}$ ) at the common port, a configuration as shown in Fig. 4 was used. At port-1, a feeder line was tapped to the patch resonator whereas port-2 and port-3 were weakly coupled to the patch. The feed line of port-1 was adjusted both in length and width. Using (3), the  $Q_{ex}$  towards both modes of the patch was obtained

$$Q_{ex} = \frac{f_0}{\Delta f} \quad (3)$$

where  $\Delta f$  is the 3-dB bandwidth measured from the peak of the resonance curve. Fig. 4 shows the typical resonance curves between port-1 and 2 and between port-1 and 3.

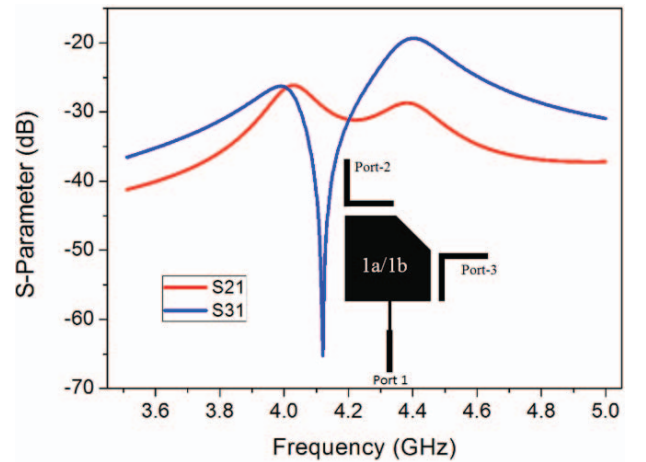
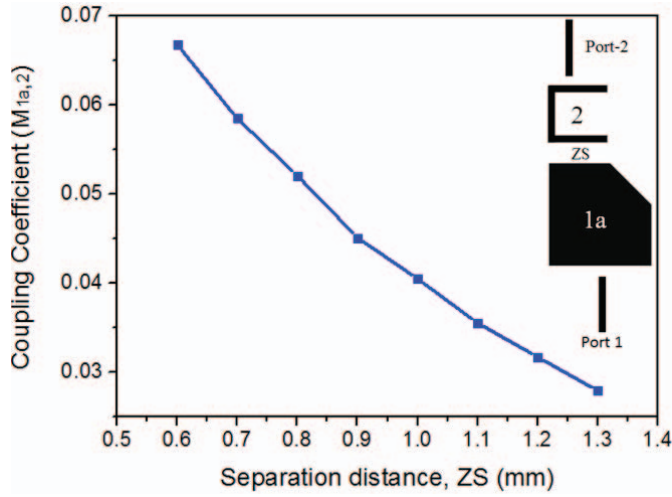


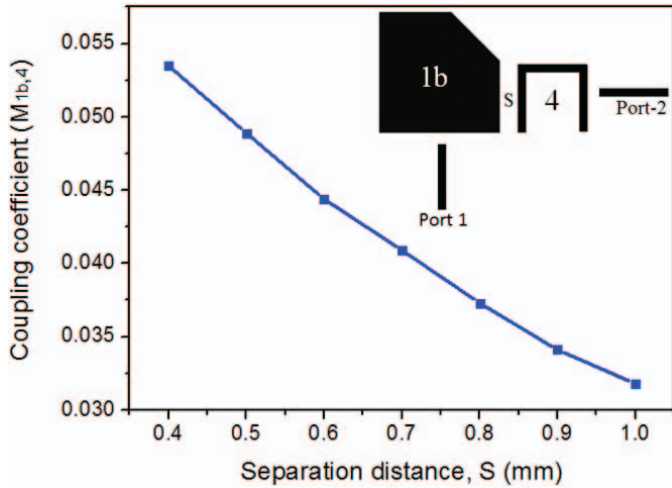
Fig. 4. Configuration used to extract  $Q_{ex1a}$  and  $Q_{ex1b}$  and the typical resonance curves.

The coupling coefficients,  $M_{1a,2}$  and  $M_{1b,4}$ , were extracted by varying the spacing,  $ZS$ , between the patch and resonator 2 and  $S$  between the patch and resonator 4 respectively. The layout configurations and the graphs of the coupling coefficient against  $ZS$  and  $S$  were plotted in Fig. 5(a) and (b). (4) was used to calculate the coupling coefficients. After obtaining the coupling coefficients around the patch separately, resonator 1, 2 and 4 were assembled together to evaluate the loading effect of the third port on the coupling. The two pairs of resonance peaks are shown in Fig. 6. It was observed that the interactive effect is not significant. These peaks can also be used in obtaining the coupling coefficients.

$$M_{1a,2} = M_{2,3} = M_{1b,4} = M_{4,5} = \frac{f_2^2 - f_1^2}{f_2^2 + f_1^2} \quad (4)$$



(a)



(b)

Fig. 5. (a) Coupling coefficient  $M_{1a,2}$  against  $ZS$  and (b) coupling coefficient  $M_{1b,4}$  against  $S$ .

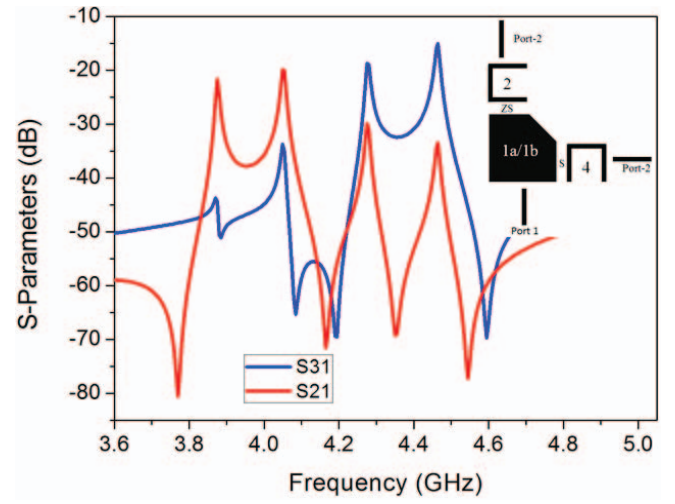


Fig. 6. Simulated resonance curves from the assembled resonator 1, 2 and 4. The inset shows the layout used in the simulation.

#### D. Diplexers

After extracting the coupling coefficients and the  $Q_{ex}$ , the diplexer was arranged as shown in Fig. 2 and optimized to specification. Fig. 7 shows the simulated response using dashed lines. Fig. 8(a) and (b) shows the current distributions when the diplexer operates at 3.99 GHz and 4.39 GHz. It can be seen that the currents are excited in orthogonal directions on the patch at different frequencies, which means the patch resonator splits the signal into two channels as proposed.

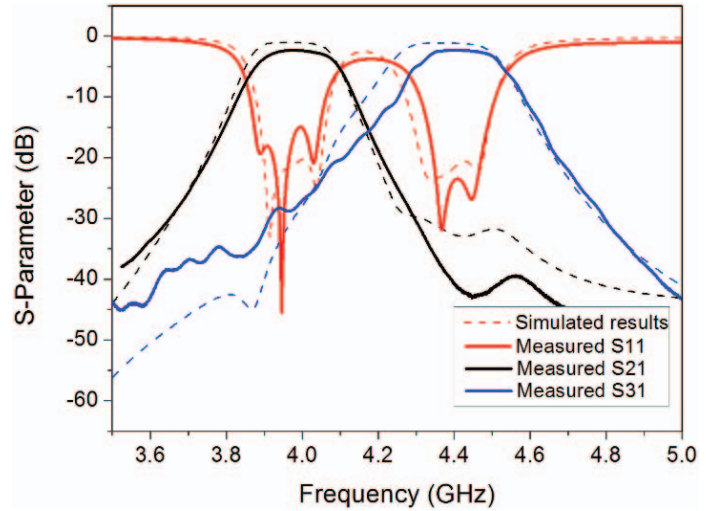


Fig. 7. Measured responses in comparison with full-wave simulations.

### III. FABRICATION AND MEASUREMENTS

The diplexer was made on a Rogers 3010 substrate with a thickness of 1.27 mm, a relative permittivity of 10.8 and a loss tangent of 0.0022. It was fabricated using LPKF ProtoMat S63



micro milling process and displayed in Fig. 9. Agilent Network Analyser N5230A was used for measurement. A comparison between the simulated (dash lines) and measured (thick lines) results are shown in Fig. 7. It can be seen that a reasonably good agreement is achieved at both passbands with the return loss measured at about 15 dB. Due to the machining tolerance, the measured results can be seen shifted to the higher frequency by approximately 5 MHz. The minimum measured insertion loss in the passband is less than 2 dB. The high passband has a reduced bandwidth.

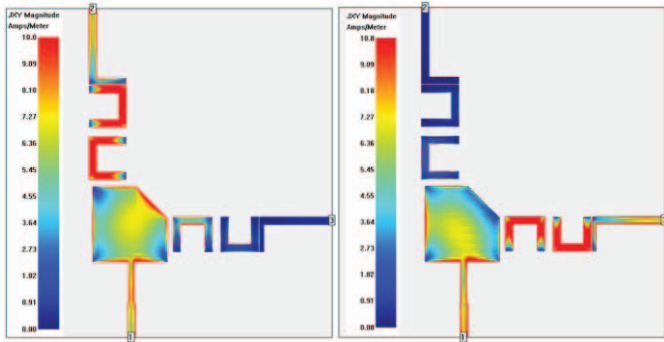


Fig. 8. (a) Current distribution at 3.99 GHz (b) current distribution at 4.39 GHz.

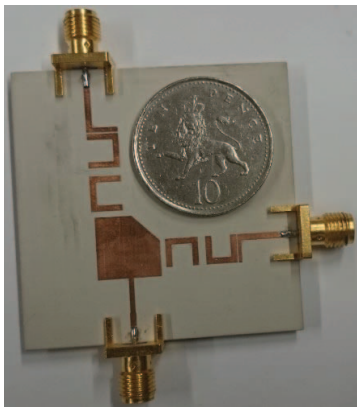


Fig. 9. Photograph of the fabricated diplexer with a dual-mode resonant junction.

#### IV. CONCLUSION

In this diplexer design, a patch resonator was used as a signal splitter as well as a resonant pole for each channel filter. The patch was used in joining two three-pole hairpin BPFs operating individually at the required passbands. The patch being a dual-mode replaced two resonators, one from each channel filter. This led to the circuit miniaturization by reducing the number of required resonators and removing the transmission line junction. The passband responses from the

measurements and simulations have shown a good agreement, verifying the feasibility of using a dual-mode resonant junction in the diplexer design. Another potential advantage of using the patch resonator is the exploration of other design variations with the patch and parasitic structures in improving the isolation and rejection performance of the diplexer.

#### REFERENCES

- [1] E. A. Ogbodo, Y. Wang, and P. Rapajic, "Bandpass Filters with Mixed Hairpin and Patch Resonators", *Progress In Electromagnetics Research C*, Vol. 59, 101–106, 2015.
- [2] R. Romero and O. Frazao, "Stopband-Improved Dual-Mode Bandpass filter Using Side-Slit Patch Resonator," *Microwave and Optical Technology Letters*, Vol. 49, No. 3, March 2007.
- [3] Y. M. Bo, X. D. Huang, and C. H. Cheng, "A Novel Bandpass Filter Using A resonator with Combined CPW and Microstrip Input/Output," *Microwave and Optical Technology Letters / Vol. 48*, No. 11, November 2006.
- [4] J.-X. Chen, Z. Xiu-Yin and Q. Xue, "Dual-Band Bandpass Filter and Diplexer Based on Double-sided Parallel-Strip Line", *IEEE MTT-S International Microwave Object Identifier*, 2008, pages 675-678.
- [5] S. Fu, B. Wu, J. Chen, S.-J. Sun and C-h Liang, "Novel Second-Order Dual-Mode Dual-Band Filters Using Capacitance Loaded Square loop Resonator," *IEEE Transactions on Microwave Theory and Techniques*, Vol. 60, No. 3, March 2012.
- [6] X. Shang, Y. Wang, W. Xia and M. J. Lancaster, "Novel Multiplexer Topologies Based on All-Resonator Structures," *IEEE Transactions on Microwave Theory and Techniques*, Vol. 61, No. 11, November 2013.
- [7] R. Cameron, M. Yu, "Design of manifold-coupled multiplexers," *IEEE Microwave Magazine*, vol.8, no.5, pp.46-59, 2007.
- [8] X. Shang, Y. Wang, X. Wenlin, M.J. Lancaster, "Novel Multiplexer Topologies Based on All-Resonator Structures," *IEEE Trans. Microwave Theory and Techniques*, vol 61, no. 11, 2013, pp. 3838 – 3845.
- [9] M. L. Chuang and M. T. Wu, "Microstrip Diplexer Design Using Common T-Shaped Resonator," *IEEE Microwave and Wireless Components. Letters*, Vol. 21, No. 11, Nov. 2011.
- [10] M. L. Chuang and M. T. Wu, "Microstrip Multiplexer and Switchable Diplexer with Joint T-Shaped Resonator," *IEEE Microwave and Wireless Components. Letters*, Vol. 24, No. 5, May 2014.
- [11] C. F. Chen, T. Y. Huang, C. P. Chou and R. B. Wu, "Microstrip Diplexers With Common Resonator Sections for Compact Size, But High Isolation," *IEEE Transactions on Microwave Theory and Techniques*, Vol. 54, No. 5, May 2006.
- [12] T. Yang, P.-L. Chi and T. Itoh, "High Isolation and Compact Diplexer Using the Hybrid Resonators," *IEEE Microwave and Wireless Components. Letters*, Vol. 20, No. 10, Oct. 2010.
- [13] C. Chen, H. Wu and W. Wu, "High Isolation DBR Diplexer Using In-Line SCMRC", *Progress In Electromagnetics Research C*, Vol. 22, 97–108, 2011.
- [14] T.F. Skaik, M.J. Lancaster, F. Huang, "Synthesis of multiple output coupled resonator circuits using coupling matrix optimisation," *Microwaves, Antennas & Propagation, IET*, vol.5, no.9, pp.1081-1088, June 27 2011.
- [15] S. Bastioli, L. Marcaccioli and R. Sorrentino, "An Original Resonant Y-junction for compact Waveguide Diplexers," *Proceeding of IEEE MTT-S International Microwave Symposium Digest*, Boston, 7-12 June 2009, pp. 1233-1236.
- [16] J.-S. Hong "Microstrip Filters for RF/Microwave Applications," John Wiley & Sons, Inc. 2011.



# Microstrip Wideband Diplexer with Narrow Guard Band Based on All-Resonator Structures

Yun Wu, Yi Wang, Eugene A. Ogbodo

Engineering Science

University of Greenwich (Medway campus),  
Chatham Maritime, Kent, U.K.

y.wu@gre.ac.uk; yi.wang@gre.ac.uk; e.a.ogbodo@greenwich.ac.uk

**Abstract**—This paper presents a wideband microstrip diplexer with adjacent channels based on an all-resonator structure. The diplexer demonstrates an overall bandwidth of 23.7% between 1.71 GHz and 2.17 GHz and a narrow guard band of only 40 MHz. Two trisection resonator structures are introduced to generate asymmetric transmission zeros to increase isolation between the two channels. The coupling matrix for the all-resonator diplexer is acquired. The diplexer is designed and fabricated on a Rogers RO4003C substrate. The measured results show insertion losses of 1.31 dB and 1.2 dB in the two channels, and an isolation of over 28 dB. These results are in good agreement with the simulation.

**Keywords**—diplexer; adjacent channels; cascaded trisection; all resonator structures

## I. INTRODUCTION

Diplexers and multiplexers are widely used for sharing a single antenna between a transmitter and a receiver or between multiple channels. They are key passive components in many modern wireless communication systems such as mobile communication systems employing frequency division duplex (FDD) [1]. Huge efforts have been made on diplexers and multiplexers with different structures [2]-[7]. Among these, planar structures are particularly popular because of its ease of fabrication, compact size and low-cost integration. The conventional approach of designing a diplexer is to optimize a transmission-line based T-junction or Y-Junction to connect two separately designed channel filters. In recent years, a new approach based on resonant junctions has been developed to replace the transmission-line junctions in search of a more compact multi-port topology. Lots of work has been focused on this type of structures and several synthesis and optimization methods have been developed [8]-[15]. Using this new approach, channel filters are connected via resonator junctions. The diplexer can be characterized by a single coupling matrix and the interaction between channel filters can be taken into account during the coupling matrix synthesis. However, due to the resonant nature of the junction and bandwidth limitation of physical resonators, the capability of such a diplexer topology to achieve a wide overall bandwidth has been a concern [15]. It is particularly challenging when the guard band is narrow because interaction between the two channel filters increases as

the guard band decreases. This problem could be further exacerbated in microstrip diplexers because of the limited range of the achievable electromagnetic coupling from the microstrip structures.

This work aims to tackle these challenges and demonstrate a wideband diplexer with a narrow guard band using the microstrip technology. The diplexer is designed based on an all-resonator structure and one common resonator is shared by both channel filters [14]. To achieve the required isolation between the two channels, a trisection-filter structure [16] is introduced in each channel so that a transmission zero can be generated in the adjacent channel.

## II. DIPLEXER DESIGN

### A. Topology and coupling matrix

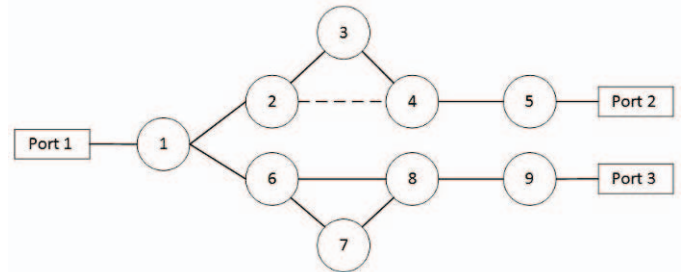


Fig. 1. Topology of the proposed diplexer.

The frequency ranges for the two channels of the microstrip diplexer are 1.71–1.88 GHz (channel A) and 1.92–2.17 GHz (channel B), respectively. The guard band between the two channels is 40 MHz, only 8.7 % of the overall bandwidth. The topology of the proposed diplexer is shown in Fig. 1. Each circle denotes a resonator. The lines between them denote the electromagnetic coupling, where the dashed line denotes the opposite sign of the coupling. Signal paths 1-2-3-4-5 and 1-6-7-8-9 correspond to the channel A and the channel B, respectively. Resonator 1 is the common resonator shared by the two channels. To increase isolation between the two channels, two trisection structures 2-3-4 and 6-7-8 are introduced in the two channels respectively. The opposite sign

of the cross couplings between 2 and 4 and between 6 and 8 generates two transmission zeros at the high side (1.92 GHz) of channel A and low side (1.88 GHz) of channel B.

Based on the topology in Fig. 1, a coupling matrix is acquired. Generally, a normalized matrix  $[A]$  can be written as [17]

$$[A] = [q] + p[U] - j[m] \quad (1)$$

where  $[U]$  is the  $N \times N$  identity matrix,  $[m]$  is the normalized coupling matrix.  $[q]$  is a diagonal matrix with only  $[q]_{ii} = 1/q_{e,i} \neq 0$ ,  $q_{e,i}$  is the normalized external quality factor from the port attached to the  $i$ -th resonator and

$$p = j \cdot (f/f_0 - f_0/f) / FBW \quad (2)$$

where  $FBW$  is the fractional bandwidth and  $f_0$  is the central frequency of the overall bandwidth of the diplexer. In this design,

$$FBW = (f_{B,2} - f_{A,1}) / f_0, f_0 = \sqrt{f_{A,1} \cdot f_{B,2}} \quad (3)$$

where  $f_{A,1} = 1.71$  GHz,  $f_{A,2} = 1.88$  GHz,  $f_{B,1} = 1.92$  GHz and  $f_{B,2} = 2.17$  GHz. The S-parameter of a multi-port network can be described as

$$S_{nn} = \pm \left( 1 - \frac{2}{q_{e,n}} [A]_{nn}^{-1} \right) \quad (4)$$

$$S_{mn} |_{m \neq n} = \frac{2}{\sqrt{q_{e,n} \cdot q_{e,m}}} [A]_{mn}^{-1} \quad (5)$$

where  $S_{nn}$  is the reflection coefficient from the port  $P_n$  which is attached to the  $n$ -th resonator, and  $S_{mn}$  is the transmission coefficient from port  $P_n$  to  $P_m$ . In the real frequency domain, the external quality factors and the coupling matrix can be found by

$$Q_{e,i} = q_{e,i} / FBW, M_{ij} = m_{ij} \cdot FBW \quad (6)$$

To generate the coupling matrix, a synthesis method based on optimization [18] is applied. For the optimization to converge fast, a carefully chosen initial matrix is highly desired. In this case, two 5<sup>th</sup>-order filters, each with one transmission zero, have been first looked into and their coupling matrices are obtained to provide the performance corresponding to each channel with the prescribed channel bandwidth, return loss (20 dB) and transmission zero. Then the initial matrix of the diplexer is formed by combining the two matrices from the individual filters. After optimization, the coupling coefficients and the external quality factors can be obtained as follows.

Mutual couplings:  $m_{1,2} = 0.1345$ ,  $m_{2,3} = 0.0537$ ,  $m_{3,4} = 0.0495$ ,  $m_{4,5} = 0.0837$ ;  $m_{1,6} = 0.1499$ ,  $m_{6,7} = 0.0667$ ,  $m_{7,8} = 0.0653$ ,  $m_{8,9} = 0.0109$ ;  $m_{2,4} = -0.0398$ ,  $m_{6,8} = 0.048$ ;

Self-couplings:  $m_{1,1} = 0$ ,  $m_{2,2} = -0.1385$ ,  $m_{3,3} = -0.0778$ ,  $m_{4,4} = -0.1479$ ,  $m_{5,5} = -0.1457$ ,  $m_{6,6} = 0.1156$ ,  $m_{7,7} = 0.0377$ ,  $m_{8,8} = 0.1218$ ,  $m_{9,9} = 0.119$ ;

External quality factors:  $q_{e,1} = 4.0797$ ,  $q_{e,5} = 10.1085$ ,  $q_{e,9} = 7.5955$ .

It can be seen from the coupling matrix that only the common resonator is tuned to  $f_0$  ( $m_{1,1} = 0$ ) whereas the others are asynchronously tuned ( $m_{i,i} \neq 0$  when  $i \neq 1$ ). On the other hand,  $m_{2,4}$  and  $m_{6,8}$  are non-zero and opposite in signs because of the requirement of asymmetric transmission zeros. The responses calculated using (4), (5) and the acquired coupling matrix are shown in Fig. 2. It can be seen that 30 dB isolation between the two channels is achieved due to the introduction of the asymmetric transmission zeros.

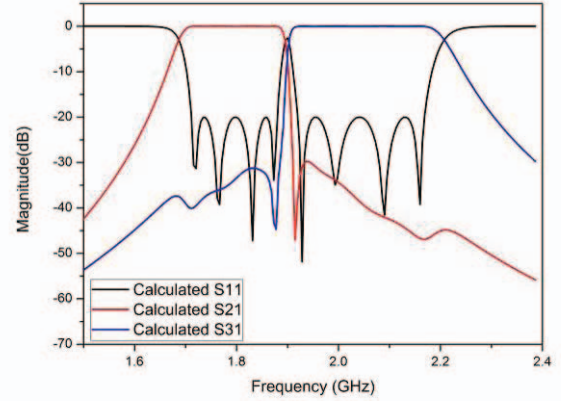


Fig. 2. Calculated responses of the diplexer from the acquired coupling matrix.

## B. Simulation

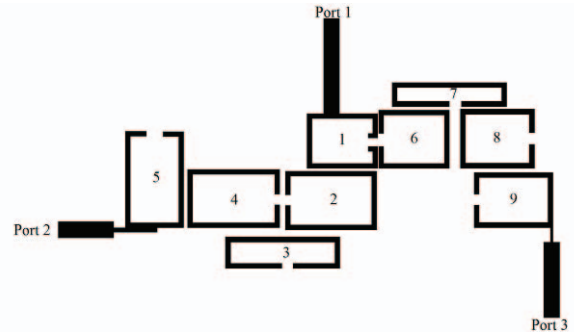


Fig. 3. Layout of the diplexer. The width of the feed lines is set to be 3.1 mm. The gaps  $d_{ik}$  between the resonators are  $d_{12} = 0.56$  mm,  $d_{23} = 1.46$  mm,  $d_{34} = 1.84$  mm,  $d_{45} = 0.74$  mm,  $d_{24} = 1.16$  mm;  $d_{16} = 0.22$  mm,  $d_{67} = 0.74$  mm,  $d_{78} = 0.56$  mm,  $d_{89} = 0.88$  mm,  $d_{68} = 2.14$  mm.

A Rogers RO4003C substrate with a dielectric constant of 3.55, a loss tangent of 0.0029 (nominal value at 10 GHz) and a thickness of 1.524 mm is selected for the design. Open loop resonators with a line width of 1 mm are chosen for the construction of the diplexer because they not only accommodate a compact layout, but also allow both positive and negative cross-couplings to be realized [16, 19]. To extract the coupling values from the simulated S-parameters, firstly the resonance frequency of each asynchronously tuned resonator is found by using the expression [20]

$$f_i = \frac{f_0}{\sqrt{1 - m_{ii}}} \quad (7)$$

where  $i$  denotes the index of the resonator and  $f_0$  is 1.94 GHz. The layout and of the microstrip circuit is shown in Fig. 3.

Resonator 2-3-4 and resonator 6-7-8 are designed as two trisection structures. The coupling between 2 and 4 is dominantly electric whereas the coupling between 6 and 8 is magnetic. The simulated weakly-coupled transmission responses of these trisection structures are shown in Fig. 4. It can be seen that transmission zeros are generated at the different sides due to the opposite sign of the couplings [16].

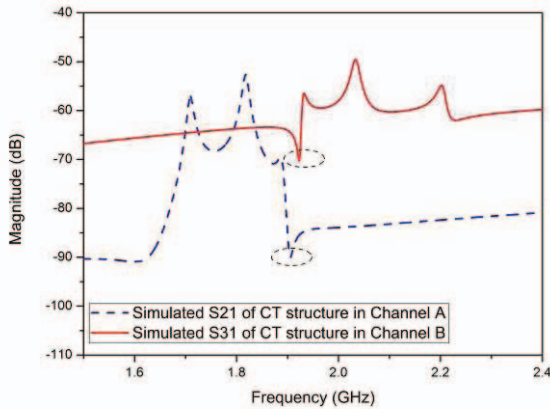


Fig. 4. Simulated transmission response of the trisection structures.

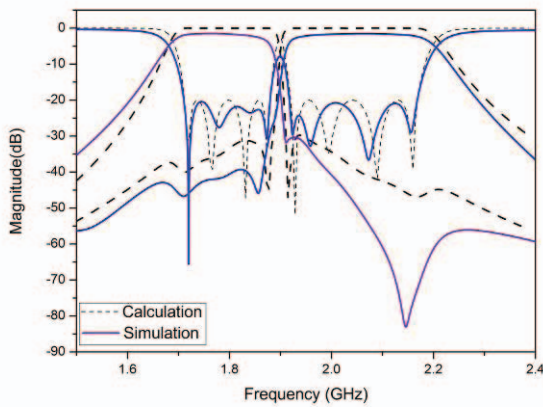


Fig. 5. Simulated results of the diplexer in comparison with the calculated.

The wide bandwidth demands strong external couplings. So the feed lines of the diplexer are tapped to the input and output resonators. External quality factors are extracted from the group delay and the phase of  $S_{11}$  [17]. The simulated transmission responses as compared with the calculated ones are shown in Fig. 5. The simulated insertion loss in each channel is 1.54 dB and 1.56 dB respectively, and the return losses are better than 20 dB in both channels. Isolations between the two channels are 28 dB. It can be seen that the simulated responses of channel B agree well with the calculations whereas there is a small difference in channel A.

The simulated lower side slope is flatter than the calculated. This is believed to be a result of the unexpected transmission zero at 2.15 GHz. This transmission zero can be attributed to the spurious cross coupling between resonator 1 and 4 which is not accounted for in the coupling matrix [21].

### III. FABRICATION AND MEASUREMENTS

Fabrication was made by LPKF ProtoMat S63 micro milling process and the prototype is shown in Fig. 6. The whole dimension of the circuit is 110 mm  $\times$  60 mm and the minimum gap used is 0.2 mm.

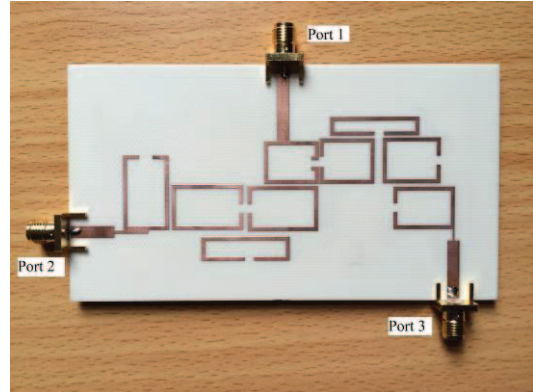


Fig. 6. Photograph of the fabricated diplexer.

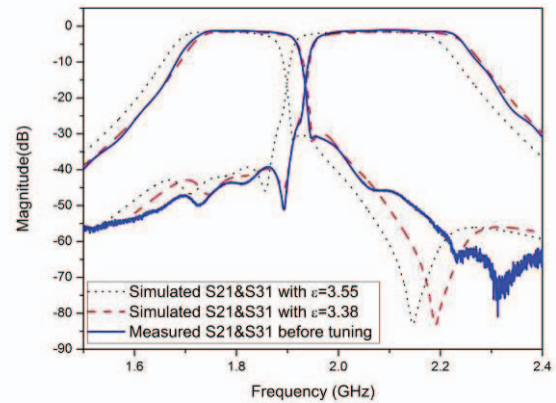


Fig. 7. Measured transmission responses of the diplexer in comparison with simulations.

The measurement was taken by Agilent N5230A network analyzer. Shown in Fig. 7 are the measured results as compared with two sets of simulations – one using a dielectric constants of 3.55 (the so-called design DK) and the other using 3.38 (the process DK from the supplier's date sheets). It can be seen that the measured frequency responses are higher than the simulated results with the dielectric constant 3.55, but almost in perfect agreement with the results from the dielectric constant 3.38. The apparent discrepancy from the use of the design DK may be caused by the tight edge couplings in the circuit as required by the broad overall bandwidth of the diplexer. Finally, the measured insertion losses are 1.31 dB and 1.2 dB in channel A and B.



The measured reflection responses of the diplexer, after tuning, are shown in Fig. 8. The simulation result with the dielectric constant of 3.38 is also displayed for comparison. A return loss of 20 dB and 18 dB is achieved in channel A and channel B respectively. It can also be found there are four reflection zeros in each channel as expected from the simulation. However, the post-fabrication tuning increases the bandwidth of channel A. The overall response shifts to lower frequencies because of the loading effect of the tuning materials.

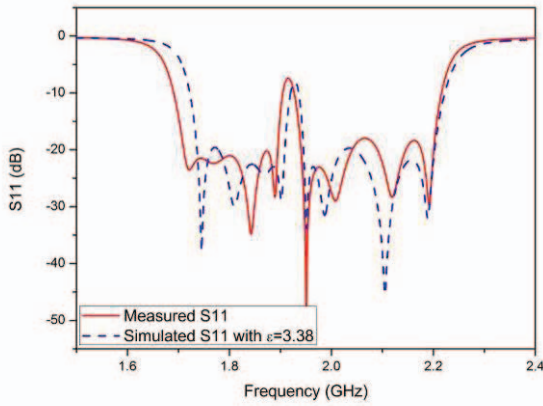


Fig. 8. Measured reflection responses of the diplexer after tuning.

#### IV. CONCLUSION

This paper presents a wideband microstrip diplexer with adjacent channels. The design is based on an all-resonator structure, and the overall bandwidth is 23.7%. Two trisection structures are used in order to make asymmetric transmission zeros to increase the isolation between the two channels. The diplexer is designed by using open loop resonators. The measured transmission response results show an insertion loss of 1.31 dB and 1.2 dB in channel A and channel B respectively, and an isolation of 28 dB between the two channels. Reasonably good agreement has been achieved between simulations and measurements.

#### REFERENCES

[1] R. V. Snyder, A. Mortazawi, I. Hunter, S. Bastioli, G. Macchiarella, and K. Wu, "Present and Future Trends in Filters and Multiplexers," *IEEE Trans. Microw. Theory Tech.*, vol. 63, pp. 3324-3360, 2015.

[2] F. Boone and W. Ke, "Nonradiative dielectric (NRD) waveguide diplexer for millimeter-wave applications," in *IEEE MTT-S Int. Microw. Symp. Digest*, 2003, pp. 1471-1474 vol.3.

[3] J. An, G. M. Wang, C. X. Zhang, and P. Zhang, "Diplexer using composite right-/left-handed transmission line," *Electron. Lett.*, vol. 44, pp. 685-687, 2008.

[4] T. Yang, P. L. Chi, and T. Itoh, "High Isolation and Compact Diplexer Using the Hybrid Resonators," *IEEE Microw. Wireless Compon. Lett.*, vol. 20, pp. 551-553, 2010.

[5] M. L. Chuang and M.-T. Wu, "Microstrip Diplexer Design Using Common T-Shaped Resonator," *IEEE Microw. Wireless Compon. Lett.*, vol. 21, pp. 583-585, 2011.

[6] P. Han-Sam and C. Yi-Chyun, "Microstrip Diplexer Constructed With New Types of Dual-Mode Ring Filters," *IEEE Microw. Wireless Compon. Lett.*, vol. 25, pp. 7-9, 2015.

[7] W.-H. Tu, W.-C. Hung, and T.-H. Du, "Design of Microwave Microstrip Multiband Diplexers for System in Package," *IEEE Trans. Compon. Packag. Technol.*, vol. 5, pp. 502-507, 2015.

[8] C. F. Chen, T. Y. Huang, C. P. Chou, and R. B. Wu, "Microstrip diplexers design with common resonator sections for compact size, but high isolation," *IEEE Trans. Microw. Theory Tech.*, vol. 54, pp. 1945-1952, 2006.

[9] R. J. Cameron, "General coupling matrix synthesis methods for Chebyshev filtering functions," *IEEE Trans. Microw. Theory Tech.*, vol. 47, pp. 433-442, 1999.

[10] F. Loras-Gonzalez, S. Sobrino-Arias, I. Hidalgo-Carpintero, D. Segovia-Vargas, and M. Salazar-Palma, "A novel Ku-band dielectric resonator triplexer based on generalized multiplexer theory," in *IEEE MTT-S Int. Microw. Symp. Digest*, 2010, pp. 884-887.

[11] G. Macchiarella and S. Tamiazzo, "Synthesis of Star-Junction Multiplexers," *IEEE Trans. Microw. Theory Tech.*, vol. 58, pp. 3732-3741, 2010.

[12] M. Sagawa, M. Makimoto, and Y. Sadahiko, "A Design Method of Bandpass Filters Using Dielectric-Filled Coaxial Resonators (Short Papers)," *IEEE Trans. Microw. Theory Tech.*, vol. 33, pp. 152-157, 1985.

[13] D. Swanson and G. Macchiarella, "Microwave filter design by synthesis and optimization," *IEEE Microw. Mag.*, vol. 8, pp. 55-69, 2007.

[14] X. B. Shang, Y. Wang, W. Xia, and M. J. Lancaster, "Novel Multiplexer Topologies Based on All-Resonator Structures," *IEEE Trans. Microw. Theory Tech.*, vol. 61, pp. 3838-3845, 2013.

[15] Y. Wang and M. J. Lancaster, "An Investigation on the coupling characteristics of a novel multiplexer configuration," in *Eur. Microw. Conf. (EuMC), 2013 European*, 2013, pp. 900-903.

[16] J. S. Hong and M. J. Lancaster, "Microstrip cross-coupled trisection bandpass filters with asymmetric frequency characteristics," *Microwaves, Antennas and Propagation, IEE Proceedings*, vol. 146, pp. 84-90, 1999.

[17] J. S. Hong and M. J. Lancaster, "Microstrip filters for RF/microwave applications," *Wiley*, 2001.

[18] X. Shang, Y. Wang, G. L. Nicholson, and M. J. Lancaster, "Design of multiple-passband filters using coupling matrix optimisation," *IET Microwaves Antennas Propag.* 6(1), 24-30.

[19] J. S. Hong and M. J. Lancaster, "Couplings of microstrip square open-loop resonators for cross-coupled planar microwave filters," *IEEE Trans. Microw. Theory Tech.*, vol. 44, pp. 2099-2109, 1996.

[20] C. H. Lin, C. H. Wang, and C. H. Chen, "A Simple Design Procedure for the Asynchronous Box-Section Filter," in *Micro. Conf., 2007. APMC 2007. Asia-Pacific*, 2007, pp. 1-4.

[21] J. B. Thomas, "Cross-coupling in coaxial cavity filters - a tutorial overview," *IEEE Trans. Microw. Theory Tech.*, vol. 51, pp. 1368-1376, 2003.

# Microstrip Dual-Band Bandpass Filter Using U-Shaped Resonators

Eugene A. Ogbodo<sup>1, \*</sup>, Yi Wang<sup>1</sup>, and Kenneth S. K. Yeo<sup>2</sup>

**Abstract**—Coupled resonators are widely used in the design of filters with dual-passband responses. In this paper, we present a dual-band bandpass filter using only couplings between adjacent resonators without cross-couplings. The dual-band bandpass filter with centre frequencies of 1747 MHz and 1879 MHz respectively is designed and fabricated using microstrip U-shaped resonators. Using the coupled resonator pair as a dual-band cluster, a miniaturised structure is achieved as compared to the conventional topology. The measured responses agree closely with the simulations.

## 1. INTRODUCTION

As the modern microwave communication equipment develops, there is a need for lighter and more efficient devices, which has led to the design of dual-band and multiband components, such as antennas, amplifiers, and filters. With the growing interest in the design of dual-band bandpass filter (BPF), many authors [1–5] have used different circuit models and microstrip geometries to achieve the dual-band BPFs. Two parallel filters were connected to actualise a dual-band BPF [5]. By inserting a stop-band into a wide-band, a dual-band filter was achieved [6]. Although [5] and [6] provided the desired responses, they lacked the flexibility to reduce the sizes of the structures. [7] employed stepped impedance resonators (SIRs) in the design of dual-band BPF. [8] used a dual-mode square patch resonator.

In this paper, a coupled U-shaped resonator pair is used to generate the two required pass band frequencies. Three such resonator pairs are then coupled together to form the dual-band BPF. Compared with [7] and [8], it is easier to adjust the positions of the two bands using the proposed structure. A synthesis method similar to [1] has been used to extract the coupling coefficients. However, in contrast to the design in [1] this filter has no DC path and has better out-of-band rejection performance below the lower passband down to DC.

## 2. FILTER DESIGN

A microstrip dual-band BPF has been proposed and designed to have the following specifications:

- Center frequency of the lower and upper passbands,  $f_{0,BPL}$  and  $f_{0,BPU}$ : 1747 MHz and 1879 MHz.
- Passband return loss: 20 dB.
- Fractional bandwidth of lower and upper passband,  $BW_L$  and  $BW_U$ : 4.3%.

A sixth-order Chebyshev dual-band BPF was designed to have a ripple factor of 0.043 dB. The design started with a normalised third-order low-pass prototype filter (LPF) [9] as shown in Fig. 1. The normalised LPF was then made to consist of only shunt reactive components by introducing admittance

---

*Received 23 July 2015, Accepted 3 February 2016, Scheduled 16 February 2016*

\* Corresponding author: Eugene A. Ogbodo (e.a.ogbodo@gre.ac.uk).

<sup>1</sup> Electrical, Electronic and Computer Engineering, University of Greenwich, Medway Campus, Kent, U.K. <sup>2</sup> School of Architecture, Computing and Engineering, University of East London, London, U.K..

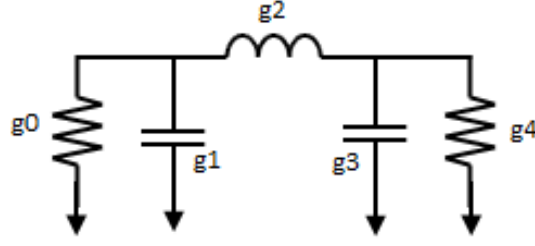


**Figure 1.** Normalised low pass prototype filter;  $g_0 = g_4 = 1$ ,  $g_1 = g_3 = 0.8515$  and  $g_2 = 1.1031$ .

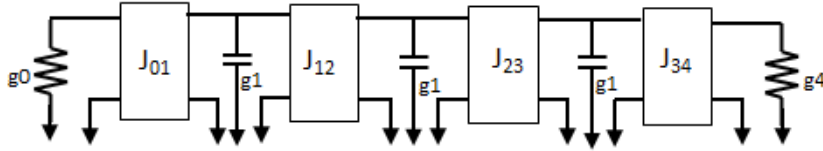


**Figure 2.** Normalised low pass filter with only shunt reactive components;  $J_{01} = J_{34} = 1$  and  $J_{12} = J_{23} = 0.879$ .

inverters ( $J$ -inverter) into the circuit [10]. At this stage, all the low-pass filter parameters are equal to  $g_1$  as shown in Fig. 2. The values of the  $J$ -inverters can be achieved using Eq. (1).

$$J_{01} = J_{n,n+1} = 1 \quad (1a)$$

where  $n$  is the order of the low pass filter. In this work,  $n = 3$ . For  $1 \leq m < n$ ,

$$J_{m,m+1} = \sqrt{\frac{g_1^2}{g_m g_{m+1}}} \quad (1b)$$

A further frequency transformation was carried out on the circuit by transforming the shunt reactive component (capacitor) into a dual-band BPF component. Each capacitor in the circuit was transformed into two shunt  $LC$  resonators, one of a series type and the other of a parallel type [1] as displayed in Fig. 3. The new parameter values can be obtained using Eq. (2).

$$L_a = \frac{\text{FBW}_0 Z_0}{g_1 \omega_c (\omega_2 - \omega_1)} \quad (2a)$$

$$C_a = \frac{1}{L_a \omega_0^2} \quad (2b)$$

$$L'_1 = \frac{\text{FBW}_0 (\omega_2 - \omega_1) Z_0}{g_1 \omega_c \omega_0^2} \quad (2c)$$

$$C'_1 = \frac{1}{L'_1 \omega_0^2} \quad (2d)$$

where  $\omega_c = 1$  rad/s (the cut-off angular frequency of the prototype low-pass filter),  $\omega_0$  is the centre angular frequency  $\omega_0 = \sqrt{\omega_1 \omega_2}$ ,  $\omega_1$  the centre angular frequency of the first passband,  $\omega_2$  the centre angular frequency of the second passband,  $\text{FBW}_1$  the fractional bandwidth for each of the pass bands, and  $\text{FBW}_0$  is defined as

$$\text{FBW}_0 = \text{FBW}_1 \frac{\omega_2 + \omega_1}{\omega_2 - \omega_1} = 1.174 \quad (2e)$$

To achieve the impedance scaling [8], the  $J$ -inverters were scaled using Eq. (3) where  $Z_0$  is the system impedance of  $50 \Omega$ . Fig. 4 shows the dual-band BPF circuit with the scaled impedance.

$$J'_{m,m+1} = \frac{J_{m,m+1}}{Z_0} \quad (3)$$

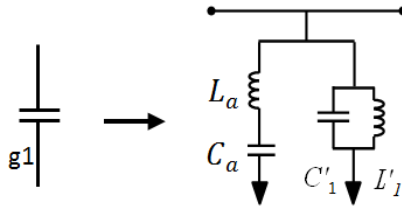


Figure 3. Low-pass to dual-band bandpass transformation.

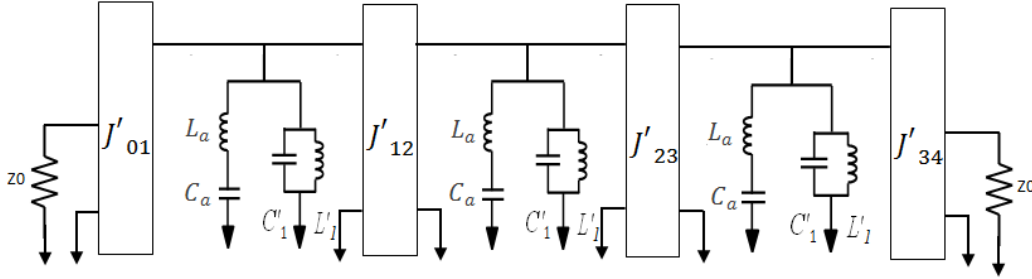


Figure 4. Dual-band BPF with shunt  $LC$  resonators;  $J'_{01} = J'_{34} = 0.02 \text{ S}$ ,  $J'_{12} = J'_{23} = 0.018 \text{ S}$ ,  $L_a = 82.659 \text{ nH}$ ,  $C_a = 0.093 \text{ pF}$ ,  $L'_1 = 0.441 \text{ nH}$  and  $C'_1 = 17.393 \text{ pF}$ .

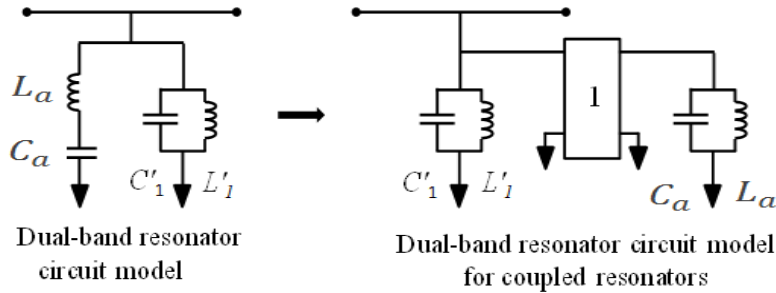


Figure 5. Dual-band resonator circuit model.

In order to achieve a dual-band bandpass filter circuit model with coupled resonators, the mixed series-parallel dual-resonator circuit is transformed into two resonators of the same type (parallel type) coupled through a unity  $J$ -inverter ( $J = 1 \text{ S}$ ) [1]. The transformation pattern used is shown in Fig. 5 whereas the final circuit model is shown in Fig. 6(a). Fig. 6(b) illustrates the coupling path of the dual-band BPF. It is clearly shown that there is no cross-coupling path in this topology. Without cross-coupling, the filter can be easily achieved using simple folded half-wavelength resonators. The calculated response from the circuit model of the dual-band BPF is presented with solid lines in Fig. 6(c). From the circuit model, the coupling coefficients of the dual-band filter can be determined using Eqs. (4) and (5) and the external quality factor  $Q_{ex}$  using Eq. (6) [3].

$$M_{1,1'} = M_{2,2'} = M_{3,3'} = J \sqrt{\frac{L'_1 L_a}{C'_1 C_a}} = 0.073 \quad (4)$$

$$M_{1,2} = M_{2,3} = J'_{12} \sqrt{\frac{L'_1}{C'_1}} = 0.089 \quad (5)$$

$$Q_{ex} = \frac{\omega_0 C'_1}{J'_{01}} = 9.9 \quad (6)$$

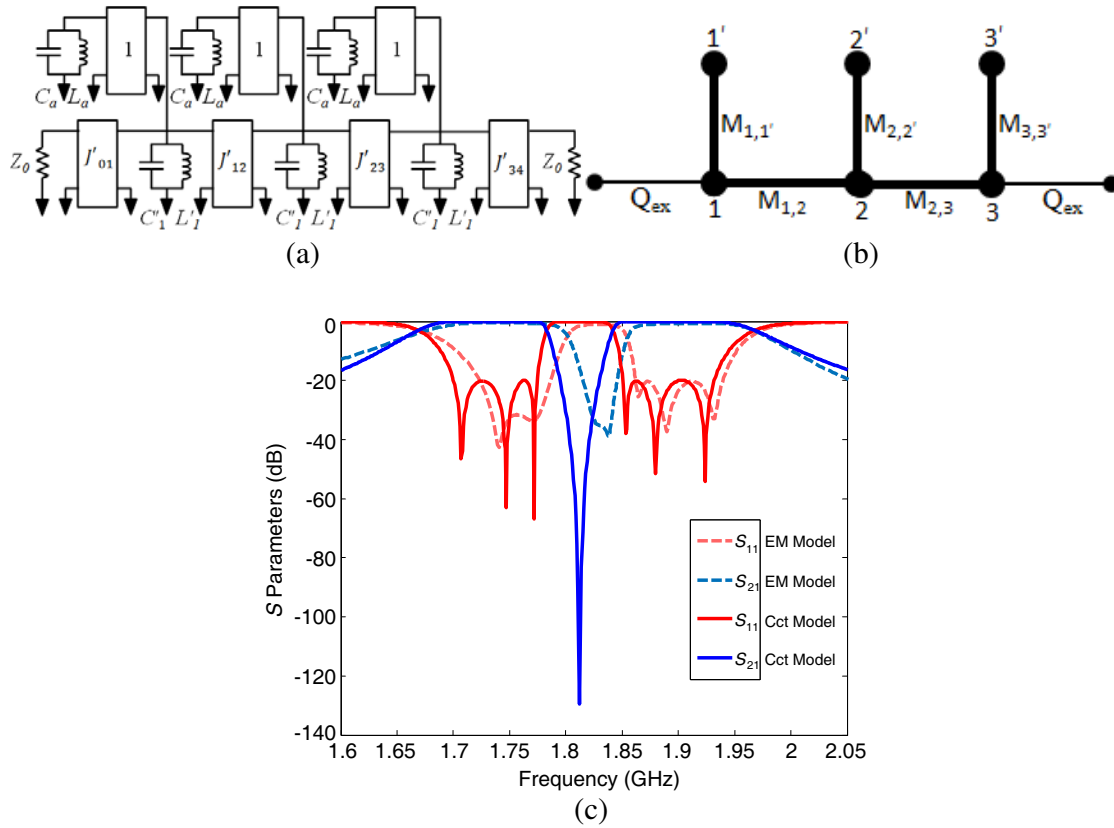


**Figure 6.** (a) Equivalent circuit model;  $L'_1 = 0.441$  nH,  $C'_1 = 17.393$  pF,  $C_a = 82.659$  nF,  $L_a = 0.093$  pH, (b) dual-band coupling path, and (c) the calculated responses from the circuit model and the simulated responses from the EM model.

### 3. MICROSTRIP IMPLEMENTATION

Here the U-shaped microstrip resonators [11, 12] were used in a parallel configuration. Using Agilent ADS EM simulator, full-wave electromagnetic (EM) simulations were performed to extract the coupling coefficients, as well as the external quality factor. With the arrangements of two U-shaped resonators

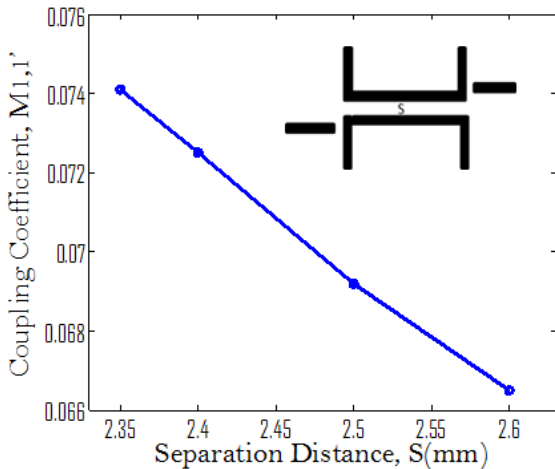


**Figure 7.** Coupling of  $M_{1,1'}$  against spacing ( $S$ ).

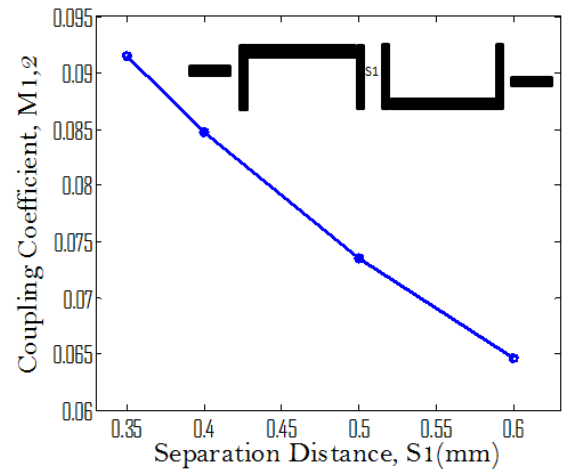


**Figure 8.** Coupling of  $M_{1,2}$  against spacing ( $S_1$ ).



as shown in Fig. 7, the coupled resonators resemble one dual-mode ‘cluster’ resonator which can be considered as a dual-band resonator. The coupling coefficients of  $M_{1,1'}$ ,  $M_{2,2'}$  and  $M_{3,3'}$  were extracted by varying the spacing ( $S$ ) between the two U-shaped resonators. A graph of the coupling coefficient against  $S$  was plotted. To determine the coupling coefficients of  $M_{1,2}$  and  $M_{2,3}$ , the configuration in Fig. 8 was simulated. The coupling coefficient against the spacing  $S_1$  is also illustrated.

In order to obtain the external quality factor at the input and output (I/O), an arrangement was set up as shown in Fig. 9. At Port-1, a 50 Ohm feeder line is tapped to the first resonator whereas Port-2 is weakly coupled to the resonator to remove the external coupling at Port-2. The tapping point of the feeder line as defined by  $Y$  on the resonator was adjusted. The length  $X$  of the resonator was reduced; this is to compensate the loading effect from the tapped feeder.

After extracting and satisfying the parameters needed for the design of the dual-band bandpass filter, the entire layout was put together as shown in Fig. 10. After optimisation, the simulated responses of the EM model were presented using dashed lines as shown in Fig. 6(c).

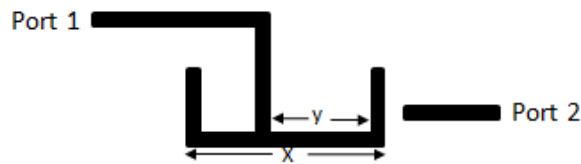


Figure 9. Resonator arrangement for extracting  $Q_{ex}$ .

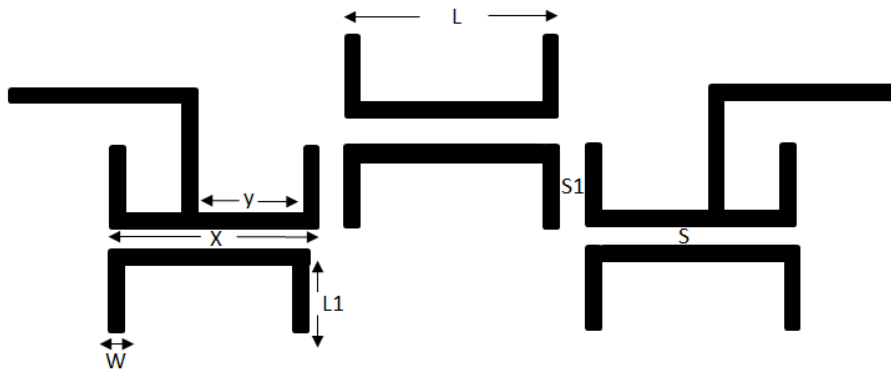


Figure 10. Dual-band microstrip filter layout.  $L = 17.2$  mm,  $L_1 = 6.8$  mm,  $W = 1.126$  mm,  $X = 17$  mm,  $S = 2.4$  mm,  $S_1 = 0.35$  mm,  $Y = 12$  mm.

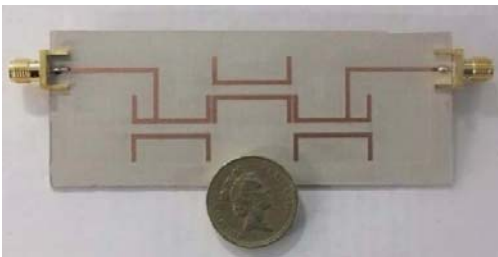


Figure 11. Fabricated microstrip dual-band filter.

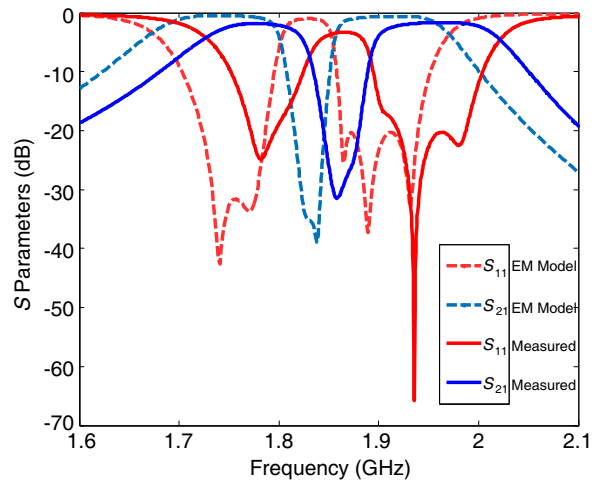


Figure 12. Simulated and measured responses.

#### 4. FABRICATION AND MEASUREMENTS

RT/Duroid 6010LM substrate from Rogers® was used for the fabrication. The dielectric constant of the material is 10.2 with a loss tangent of 0.0035 and a thickness of 1.27 mm. Fig. 11 shows the fabricated prototype. The microstrip dual-band filter was fabricated using Protomat C60 micro-milling process. Agilent E5062A Network Analyser was used to measure the filter. A comparison of the simulated and measured response is shown in Fig. 12. It can be seen that a reasonably good agreement is achieved at both passbands with a return loss close to 20 dB. Due to the machining tolerance, the measured responses can be seen shifted to the higher frequency by 40 MHz. The minimum measured insertion loss in the passband is less than 2 dB.

#### 5. CONCLUSION

In this paper, a dual-band BPF were proposed to have 1747 MHz and 1879 MHz for its low and high passband respectively. A pair of coupled U-shaped resonators behaving as a dual-band resonator cluster was arranged to resonate at the centre frequencies of the two passbands. Three pairs of the clusters were then coupled to each other in a parallel configuration. With this type of configuration, the realization of the dual bands can be achieved without resorting to any cross couplings. This design also has the flexibility to control the position of the two bands.

#### REFERENCES

1. Guan, X., Z. Ma, P. Cai, Y. Kobayashi, T. Anada, and G. Hagiwara, "Synthesis of dual-band filters using successive frequency transformations and circuit conversions," *IEEE Microwave and Wireless Component Letters*, Vol. 16, No. 3, 110–112, 2006.
2. Yeo, K. S. K. and M. J. Lancaster, "8 pole high temperature superconductor microstrip dual band bandpass filter design," *IEEE MTT-SIMS Digest*, 1–4, 2011.
3. Yeo, K. S. K., M. J. Lancaster, and J.-S. Hong, "The design of microstrip six-pole quasi-elliptic filter with linear phase response using extracted-pole technique," *IEEE Trans. Microw. Theory Tech.*, Vol. 49, No. 2, 321–327, 2002.
4. Zhao, L.-P., D. Li, Z.-X. Chen, and C.-H. Liang, "Novel design of dual-mode dual-band bandpass filter with triangular resonators," *Progress In Electronics Research*, Vol. 77, 417–424, 2007.
5. Miyake, H., S. Kitazawa, T. Yamada, and Y. Nagatomi, "A miniaturised monolithic dual band filter using ceramic lamination technique for dual mode portable telephones," *IEEE MTT-S Int. Dig.*, 789–792, 1997.
6. Tsai, L. C. and C. W. Hsue, "Dual-band bandpass filters using equal-length coupled serial-shunted lines and Z-transform technique," *IEEE Trans. Microw. Theory Tech.*, Vol. 52, No. 4, 1111–1117, Apr. 2004.
7. Chang, S. F., Y. H. Jeng, and J. L. Chen, "Dual-band step-impedance bandpass filter for multimode wireless LANs," *Electron. Lett.*, Vol. 40, 38–39, Jan. 2004.
8. Yeo, K. S. K. and A. O. Nwajana, "A novel microstrip dual-band bandpass filter using dual-mode square patch resonators," *Progress In Electromagnetics Research C*, Vol. 36, 233–247, 2013.
9. Matthaei, G., L. Young, and E. M. T. Jones, *Microwave Filters, Impedance-matching Networks, and Coupling Structures*, Artech Houston, Boston, 1980.
10. Cohn, S. B., "Direct-coupled-resonator filters," *Proceedings of the IRE*, Vol. 45, No. 2, 187–196, 1957.
11. Pozar, D. M., *Microwave Engineering*, 3rd Edition, Wiley, New York, 2005.
12. Hong, J. S., *Microstrip Filters for RF/Microwave Applications*, John Wiley & Sons, Inc., New Jersey, 2011.

## Bandpass Filters with Mixed Hairpin and Patch Resonators

Eugene A. Ogbodo\*, Yi Wang, and Predrag Rapajic

**Abstract**—This paper presents a new implementation technique of transmission zeros in an in-line coupled filter. Neither cross couplings between non-adjacent resonators nor separate side-line resonators have been used. Instead a mixture of single-mode hairpin resonators and dual-mode patch resonators have been adopted in a bandpass filter with one asymmetric transmission zero. The introduction of the patch led to an improved frequency selectivity through an independently controllable transmission zero. This approach has been verified by a three-pole filter at 2.6 GHz with 8% bandwidth and a transmission zero at 2.4 GHz. Good agreement has been shown between the measurements and the simulation.

### 1. INTRODUCTION

Conventional planar bandpass filters (BPF) are usually formed of coupled-resonators of the same type for the ease of modelling and implementation. Increasingly more sophisticated filters composed of a mixture of different types of resonators have been proposed for various purposes. Some were intended to use non-uniform  $Q$ -factors across the resonators to better control the passband flatness in lossy filters [1]. Others used specific resonators for dual purpose such as in the case of integrated filter antennas, where the resonant antenna element serves as the radiator as well as one resonant pole in a filter [2, 3]. The resonant antenna element is usually of a completely different structure and characteristic from the other resonators.

This work explores the combined use of single-mode and dual-mode resonators in order to introduce transmission zeros in an in-line coupled filter without resorting to cross coupling between nonadjacent resonators or separate side-line resonators. The most widely used approach to generate transmission zeros is to implement multiple transmission paths within the filter by using coupling between non-adjacent resonators [4] and/or between the source and load [5]. This usually requires complicated topology of resonators for cross couplings. Extracted pole is another technique that has been used to realise transmission zeros but without cross coupling [6]. This usually involves resonators from the side-line coupled to the main in-line coupled resonators with the help of non-resonant and phase shifting structures [7–9]. In terms of physical implementation, for waveguide filters, side-line cavities could tap into the in-line cavities [7, 8]. For planar filters, microstrip resonators could be connected to the feedline with added phase shifting elements [9]. This paper presented a new implementation technique of transmission zeros in an in-line coupled filter.

A mixture of two hairpins and one patch resonator are used to produce a three-pole filter with one transmission zero. The three resonators are in-line coupled without any quadruplet or triplet structures for cross coupling, nor side-line resonators for extracted poles. The patch is used for its dual modes. One mode is coupled to the hairpins forming the transmission path, whereas the other orthogonal mode generates the transmission zero. Such a configuration is simple but significantly increases the selectivity of the filter. The patch also provides sufficient degrees of freedom to make the transmission zero controllable.

---

*Received 29 July 2015, Accepted 18 September 2015, Scheduled 24 September 2015*

\* Corresponding author: Eugene Ogbodo (E.A.Ogbodo@greenwich.ac.uk).

The authors are with the Electrical, Electronic and Computer Engineering, University of Greenwich (Medway Campus), Kent, ME4 4TB, U.K..

## 2. DESIGN

### 2.1. Hairpin Three-Pole Bandpass Filter

The microstrip bandpass filter with mixed hairpin and patch resonators has been proposed to have the following specifications:

- Centre frequency of  $f_0$ , 2.6 GHz.
- Passband return loss: 16 dB.
- Fractional Bandwidth ( $FBW$ ): 8%.
- Transmission zero positioned at 2.4 GHz.

As a reference design for comparison, a conventional all-pole hairpin bandpass filter was first designed following the general filter implementation procedure. Using a passband ripple factor of 0.043 dB for a three-pole Chebyshev lowpass prototype, the  $g$  values were derived from [4] with  $g_0 = g_4 = 1.0$ ,  $g_1 = g_3 = 0.8516$  and  $g_2 = 1.1032$ . These were converted to the coupling parameters used for the physical dimensioning of the microstrip resonators as follows,

$$Q_{ex} = \frac{g_0 g_1}{FBW} \quad (1)$$

$$M_{12} = M_{23} = \frac{FBW}{\sqrt{g_1 g_2}} \quad (2)$$

where (1) gives the input and output external quality factor whereas (2) is the coupling coefficient between adjacent resonators.  $Q_{ex} = 10.645$ ,  $M_{12} = M_{23} = 0.083$ .

Full-wave simulations using CST Microwave Studio has been performed to find all the physical dimensions that provide the required coupling values. These values are extracted from the simulated  $S_{21}$  curves using the following equations [4].

$$Q_{ex} = \frac{f_0}{\Delta f} \quad (3)$$

$$M_{12} = M_{23} = \frac{f_2^2 - f_1^2}{f_2^2 + f_1^2} \quad (4)$$

These individual design steps resulted in the initial circuit layout, which was subject to further full-wave optimisation. Fig. 1(a) displays the conventional hairpin filter and Table 1 lists the dimensions. The Roger RO3010 substrate is used for the design. The nominal dielectric constant is 11.2 and the loss tangent is 0.0023. The substrate is 1.27 mm thick.

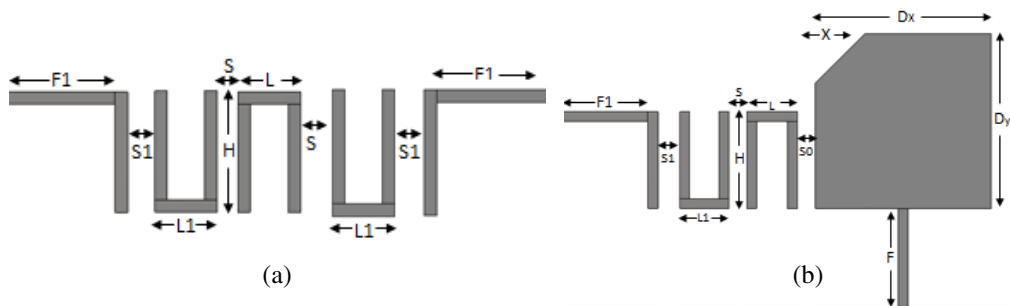


**Figure 1.** Circuit layouts of (a) the hairpin filter and (b) the hairpin-patch filter.

**Table 1.** Microstrip circuit dimensions in millimetre.

$F$	$F_1$	$L$	$L_1$	$S$	$S_1$	$S_0$	$X$	$H$	$D_x = D_y$
10	8.73	5.07	4.96	1.24	0.26	0.68	5	9.73	17.59

### 2.2. Square Patch Resonator and Mixed Hairpin-Patch Filter

To introduce a transmission zero in the three-pole filter without the complication of cross coupling or a separate side-line resonator for extracted poles, a dual-mode patch resonator is used in place of one of the hairpin resonator as shown in Fig. 1(b). The patch provides the orthogonal modes for the BPF, with one mode yielding the transmission path and the other yielding the transmission zero. The dimension of the required square resonator is estimated using  $D = Dx = Dy = \lambda_{0g}/2$  and  $\lambda_{0g} = c_0/f_0\sqrt{\epsilon_r}$ , where  $\lambda_{0g}$  is the guided-wavelength,  $c_0$  is the speed of light,  $\epsilon_r$  is the relative permittivity of 11.2,  $f_0$  is the centre frequency of the filter, and  $D$  is the dimension of the square patch.

The square is simulated to resonate at 2.5 GHz. A chamfer  $X$  is then introduced to the square resonator; this allows the patch to split into two resonant frequencies. When  $X = 5$  mm, the two frequencies generated were 2.45 GHz and 2.60 GHz. The eigen-mode solver in CST Microwave Studio has been used to study the resonant characteristics of the patch. Fig. 2 illustrates the simulated current distribution (phase = 90 deg for the plot) of the patch resonator with the arrows indicating the general direction of the currents. It is evident that the 2.45 GHz mode is orthogonal to the 2.6 GHz mode. From an equivalent circuit point of view, it is in parallel to the 2.6 GHz mode. The 2.60 GHz mode is coupled to the hairpin forming the transmission path. When the 2.45 GHz mode resonates, a stop band occurs creating the transmission zero.

In order to obtain the external quality factor ( $Q_{ex}$ ) at the output of the patch, an arrangement was set up as shown in Fig. 3(a). At port-1, a 50 Ohm feeder line was tapped to the square patch line resonator whereas the port 2 is weakly coupled to the square patch resonator. Using (3), the  $Q_{ex}$  of the square patch was obtained and calculated respectively. Fig. 3(b) illustrates the coupling arrangement used to calculate the coupling coefficient between the square patch and the adjacent resonator from (4). Fig. 1(b) and Table 1 show the circuit layout and dimensions after optimization, with the microstrip line width of 1.0 mm. Fig. 4 shows the simulated  $S$ -parameters of both the conventional hairpin filter

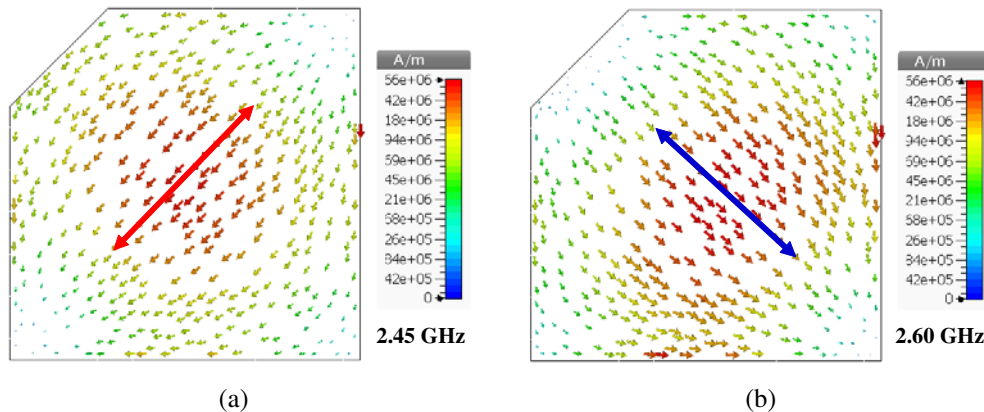


**Figure 2.** Current distribution for the orthogonal modes of the patch resonator.  $D_x = D_y = 18$  mm,  $X = 5$  mm.

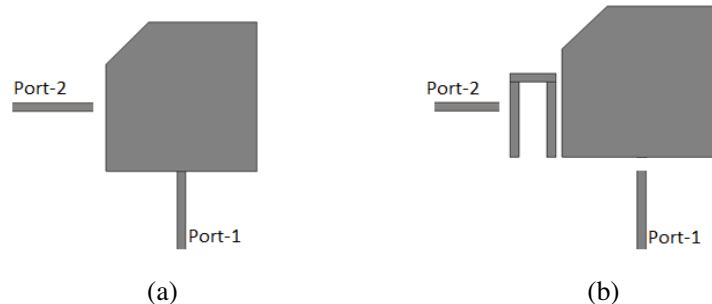


**Figure 3.** (a) Arrangement for extracting  $Q_{ex}$ ; (b) Arrangement for extracting coupling coefficients.

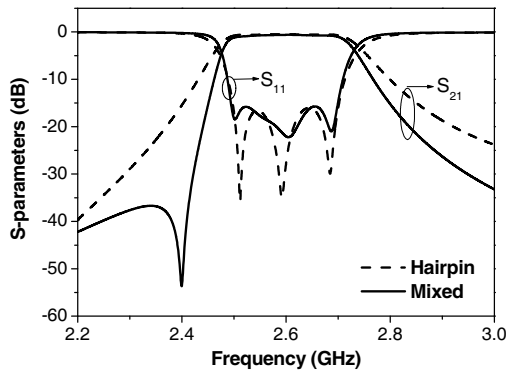


**Figure 4.** The simulated responses of the mixed hairpin-patch filter in comparison with a conventional hairpin filter of the same order.

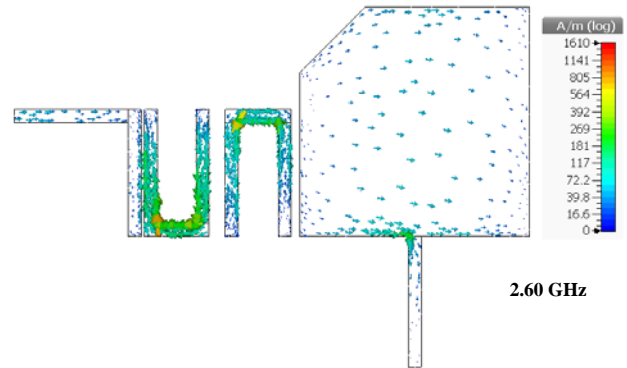


**Figure 5.** Simulated surface current distribution of the hairpin-patch filter at 2.60 GHz.

and the hairpin-patch filter, which clearly exhibits a transmission zero at 2.4 GHz. Fig. 5 illustrates the simulated current distribution (phase =  $90^\circ$  for the plot) on the mixed resonator filter at 2.6 GHz.

It has to be said that, in the design of the hairpin-patch filter, the coupling matrix was not extracted to represent the required frequency response with the prescribed transmission zero. The physical dimensioning of the hairpin-patch filter was guided by the conventional hairpin filter and its responses. After replacing the last resonator in Fig. 1(a) by the patch, parameter studies and optimizations have been used to achieve the required passband return loss and the transmission zero. The feedline to the first hairpin resonator as well as the first two hairpins are kept unchanged. The main dimensions that have been optimized include the size of the patch, the chamfers, and the tapping point of the feed line at the patch.

### 3. PARAMETER STUDY

The parameter study mainly looked into the effect of the chamfers in the patch. Two chamfers ( $X$  and  $X_c$ ) are shown in Fig. 6(a). The chamfer  $X$  determines the lower mode at around 2.6 GHz. Fig. 6(b) illustrates the change of response as a function of the chamfer  $X$ . As the chamfer also controls the coupling between the two orthogonal modes of the patch, the overall bandwidth has been affected. The transmission zero is also shifted slightly as a result. The more effective way to change the transmission zero is to alter the longer diagonal path, as indicated in Fig. 2(a), in the patch. This can be achieved by introducing the chamfer  $X_c$  as shown in Fig. 6(a), or an extension stub if the transmission zero frequency were to be lowered. From Fig. 6(c), it can be seen that the increase of  $X_c$  pushes the transmission zero to higher frequency but hardly affects the upper edge of the passband. In the case of the filter for Figs. 1 and 4 with the transmission zero at 2.4 GHz, this chamfer  $X_c$  is not required. The size of the patch ( $D_x$  and  $D_y$ ), the tapping point of the feedline to the patch and the coupling between the patch and the hairpin are other parameters that can be adjusted in optimization. If more degrees of freedom are required, stubs or slots can be added onto the patch.

It should also be noted that  $X_c$  not only shifts the transmission zero but also degrades it and affects the passband. This is because the chamfer  $X_c$  also impacts on the coupling between the two patch modes. After shifting the transmission zero, further optimisation of other parameters such as the size of the patch and the coupling between the patch and the hairpin is required to restore the passband.

### 4. FABRICATION AND MEASUREMENTS

The circuit is fabricated with the milling method using the LPKF ProtoMat S63 circuit board plotter. To prevent radiation loss and preserve the high  $Q$ -factor of the patch, the circuit is housed in a metalised box. Fig. 7 shows the fabricated device and Table 1 provides the microstrip circuit dimensions in

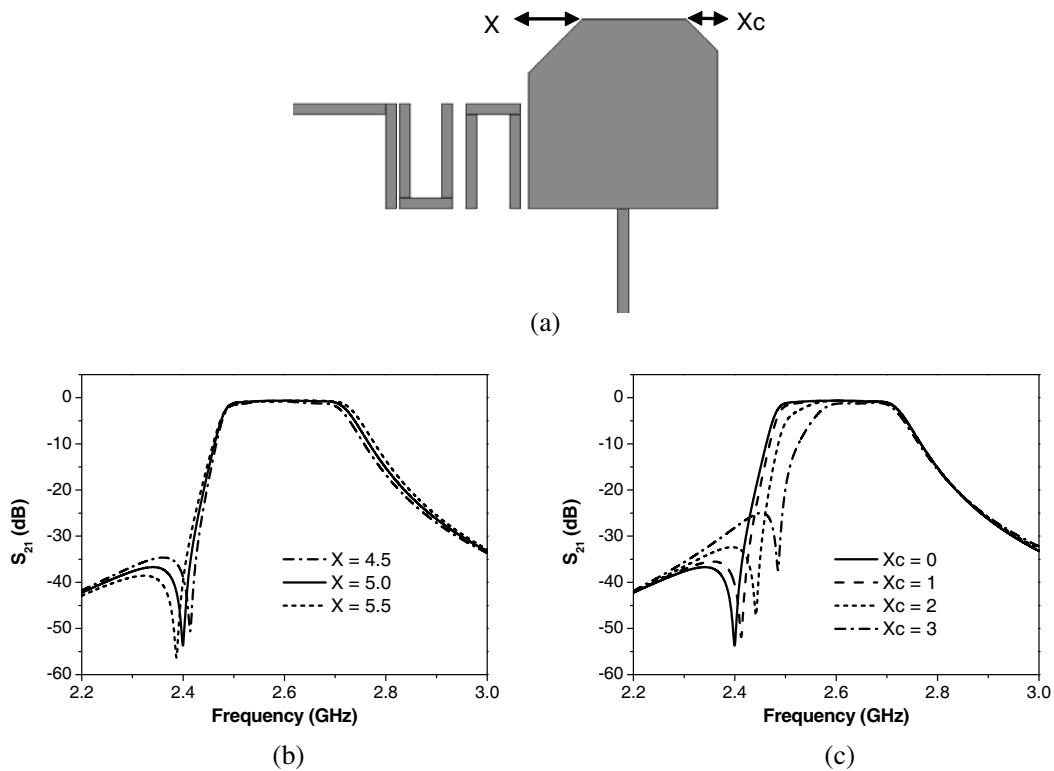


**Figure 6.** Parameter studies. (a) The chamfers  $X$  and  $X_c$ ; (b) The change of  $S_{21}$  with  $X$ ; (c) The change of  $S_{21}$  with  $X_c$ .

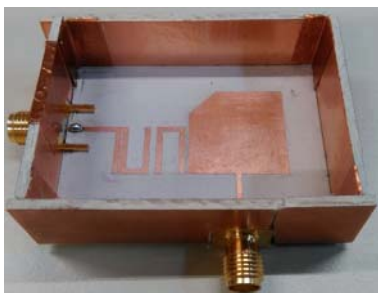


**Figure 7.** Photo of the fabricated filter with its box lid removed.

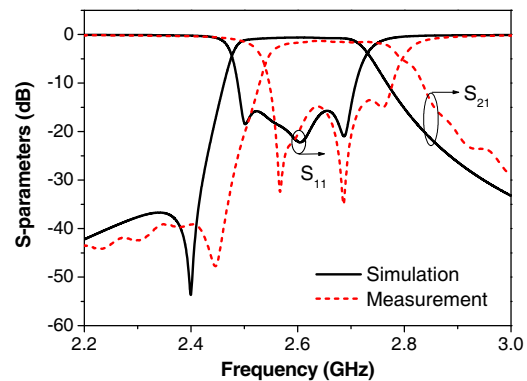


**Figure 8.** Simulated and measured responses of the hairpin-patch filter.

millimetre. Agilent Network Analyser N5230A was used to measure the fabricated device. A comparison between the simulated and measured results is shown in Fig. 8. It can be seen that a reasonably good agreement has been achieved. The transmission zero can be identified at 2.446 GHz. There is a significant shift of the measured responses to higher frequency by nearly 50 MHz. This is mainly due to the over-milling of the circuit when the parameters of the milling machine are not optimised to process the ceramic-filled Roger RO3010 substrate. The minimum measured insertion loss in the passband is 1.3 dB and the return loss is better than 13 dB.

## 5. CONCLUSION

A dual-mode patch resonator was used to replace one hairpin resonator in a three-pole hairpin bandpass filter. One of the dual modes is coupled to the filter to generate the third pole required for the filter while the other mode is used in generating the transmission zero. This combination resulted in improved frequency selectivity in the bandpass filter as compared with the conventional hairpin filter. The parameter studies have demonstrated the controllability of the transmission zero as well as the bandwidth of the mixed hairpin-patch filter. The circuit layout taken in actualizing this proposed design is relatively straight forward. It eliminates the need of cross coupling between non-adjacent resonators and presents a new way to implement the extracted pole. This leads to the possibility of integrating the dual-mode patch into other filtering networks such as diplexers and multiplexers, where reduced complexity in the resonator topology is highly desired. One challenge in the design and optimisation is the interdependence of the filter responses on multiple parameters in relationship to the patch resonator. Although a shielded patch resonator is desired for its higher  $Q$  than a microstrip resonator, the requirement for metal shielding is a limitation when the device form factor is the main design drive. Similar design concept can be employed using microstrip resonators that do not pose problems with radiation losses.

## REFERENCES

1. Meng, M. and I. Hunter, "The design of parallel connected filter networks with non-uniform  $Q$  resonators," *IEEE MTT-S Int. Microw. Symp. Dig.*, Vol. 61, No. 1, 372–381, June 17–22, 2012.
2. Yusuf, Y. and X. Gong, "Compact low-loss integration of high-3-D filters with highly efficient antennas," *IEEE Trans. Microw. Theo. Techn.*, Vol. 59, No. 4, 857–865, April 2011.
3. Mao, C. X., S. Gao, Z. P. Wang, Y. Wang, F. Qin, B. Sanz-Izquierdo, and Q. X. Chu, "Integrated filtering-antenna with controllable frequency bandwidth," *9th Europ. Conf. on Antennas and Propagation (EuCAP)*, April 12–17, 2015.
4. Hong, J.-S., *Microstrip Filters for RF/Microwave Applications*, John Wiley & Sons, Inc., 2011.
5. Liao, C. and C. Chang, "Design of microstrip quadruplet filters with source-load coupling," *IEEE Trans. Microwave Theory and Techniques*, Vol. 53, No. 7, 2302, 2308, July 2005.
6. Rhodes, J. and R. Cameron, "General extracted pole synthesis technique with applications to low-loss  $TE_{011}$  mode filters," *IEEE Trans. Microwave Theory and Techniques*, Vol. 28, No. 9, 1018–1028, September 1980.
7. Macchiarella, G. and M. Politi, "Use of generalized coupling coefficients in the design of extracted-poles waveguide filters with non-resonating nodes," *IEEE MTT-S Int. Microw. Symp. Dig.*, 1341–1344, June 2009.
8. Jedrzejewski, A., N. Leszczynska, L. Szydlowski, and M. Mrozowski, "Zero-pole approach to computer aided design of in-line SIW filters with transmission zeros," *Progress In Electromagnetics Research*, Vol. 131, 517–533, 2012.
9. Yeo, K., M. Lancaster, and J. Hong, "The design of microstrip six-pole quasi-elliptic filter with linear phase response using extracted-pole technique," *IEEE Trans. Microwave Theory and Technique*, Vol. 40, No. 2, 321–327, 2001.



# Dual-Path Dual-Band Filters Based On Patch Resonators

Eugene A. Ogbodo, Yun Wu, Yi Wang  
 Department of Engineering Science  
 University of Greenwich (Medway campus)  
 Chatham Maritime, Kent, U.K.

e.a.ogbodo@gre.ac.uk; y.wu@gre.ac.uk; yi.wang@gre.ac.uk

**Abstract**—A dual-band bandpass filter with dual coupling paths is presented in this work. The filter is formed of two dual-mode patch resonators, one half-wavelength or full-wavelength straight-line resonator and a hair-pin resonator. The patch resonators act as a signal splitter, combiner and resonant pole in the dual-band bandpass filter. The patch resonators are coupled with the hair-pin and the straight-line resonators. Two dual-band filters with different transmission zeros have been designed, simulated and tested. The effect of the variation of the dielectric constant has been studied.

**Keywords**— Dual-band bandpass filter, Patch resonator, dual mode resonator, coupling path

## I. INTRODUCTION

Dual-band bandpass filter (BPF) is a microwave device used in communication systems for selecting two wanted frequency bands while rejecting the unwanted frequencies. A dual-band BPF provides the opportunity to have two BPFs built together. It reduces cost and can occupy less space when compared with two BPFs with the same properties. In [1], three pairs of U-shaped resonators were coupled in a parallel configuration to achieve a dual-band BPF. In [2], a dual-band BPF was achieved by inserting a stop-band into a wideband BPF using a cascade connection. Similar stop bands have also been implemented using transmission zeros generated by manipulating the coupling matrix [3]. The above-mentioned are by no means an exhaustive list of the vast literature about dual-band filters but represent the typical implementation techniques.

In this work, a dual-band BPF is designed with two distinct coupling paths, one for the high-passband and one for the low-passband. A mixture of different resonators with dual-mode, single-mode, half wavelength or full wavelength resonators in a parallel configuration are used. Also, the signal path is barely affected by the removal of the single-mode resonator in the opposite path, which makes the two passbands potentially controllable independently.

## II. DESIGN

Fig. 1 illustrates the proposed coupling topology and the filter layout. It has three-poles on each passband making it a total of six poles for the dual-band BPF. It is designed to have a centre frequency  $f_0$  of 1.95 GHz with the low passband  $f_1$  at 1.8 GHz and high passband  $f_2$  at 2.1 GHz. It will meet the specification of 20 dB return loss and 4% fractional bandwidth

(FBW) for each passband. As can be seen from the coupling topology in Fig. 1(a), the first dual-mode patch resonator provides the orthogonal modes for the resonant node 1a and 1b. The second patch resonator provides the modes for the node 3a and 3b. The high-passband path will be coupled through the single-mode resonator 2', whereas the low-passband is coupled through resonator 2.

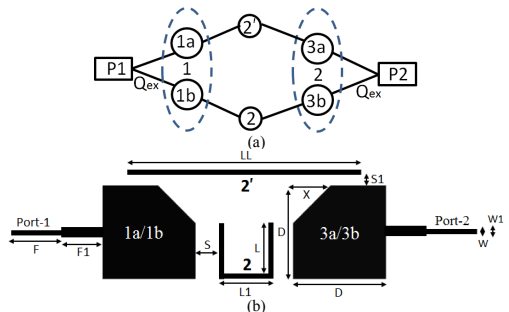


Fig. 1. (a) Coupling topology and (b) layout of the first dual-band BPF (not to scale):  $F = 10$  mm,  $F1 = 6$  mm,  $S = 0.7$  mm,  $S1 = 0.2$  mm,  $L = 11.3$  mm,  $L1 = 10.1$  mm,  $LL = 53.2$  mm,  $D = 25.2$  mm,  $X = 12.4$  mm,  $W = 1.2$  mm,  $W1 = 2.8$  mm

A general filter implementation procedure is followed. A three-pole Chebyshev lowpass prototype as obtained from [4] is used. The  $g$ -values are used to obtain the coupling parameters for the physical dimensioning of the microstrip resonators for the dual-band BPF. (1) and (2) were used to obtain the coupling coefficient between the resonators and the input/output quality factor respectively.

$$M_{1a,2'} = M_{2',3a} = M_{1b,2} = M_{2,3a} = \frac{FBW}{\sqrt{g_1 g_2}} = 0.041 \quad (1)$$

$$Q_{ex} = \frac{g_0 g_1}{FBW} = 21.29 \quad (2)$$

A half-wavelength square patch resonator resonating at  $f_0$  is perturbed into the dual resonances at  $f_1$  and  $f_2$  by cutting one corner as shown in Fig. 1(b). Two distinct coupling paths were devised to couple to the two resonance. This also enabled the design of the two bands separately without significant interactions between them. For the low band, the two patch resonators were coupled with a hairpin resonator to form the path at 1.8 GHz. Optimisation was performed to meet the design specification. As for the high

band, its coupling path were completed by using a full wavelength line resonator as shown in Fig 1(b). It is worth pointing out that during the optimisation only the length of the straight line and its coupling gap with the two patch resonators were adjusted. This has avoided distorting the already achieved low-passband. The simulated responses are shown in Fig. 2.

To further enhance the design, the full wavelength straight-line resonator is replaced with a half wavelength straight-line resonator as shown in Fig. 3. Due to size reasons, the half wavelength straight line resonator was pushed downward in between the two patch resonators. This strengthened the coupling. On the other hand, it also increased the cross couplings with the low modes of the two patch resonators as illustrated in Fig. 3(a). The resultant effect is an introduction of a transmission zero between the two passbands. The simulated responses are shown in Fig. 4.

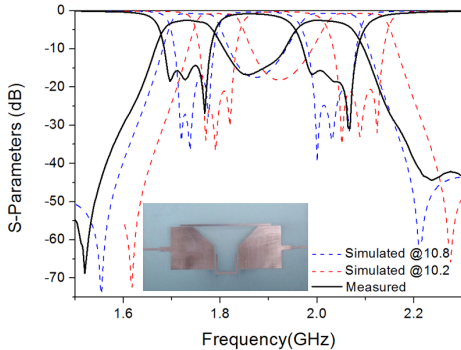


Fig. 2. Simulated and measured responses of the filter in Fig. 1 with the inset showing the fabricated design.

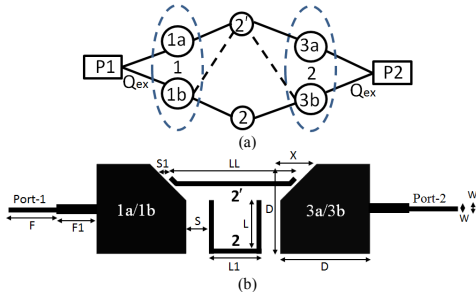


Fig. 3. (a) Coupling topology and (b) layout of the second dual-band BPF:  $F = 10$  mm,  $F1 = 6$  mm,  $S = 0.7$  mm,  $S1 = 0.2$  mm,  $L = 11.3$  mm,  $L1 = 10.1$  mm,  $LL = 26.2$  mm,  $D = 25.2$  mm,  $X = 12.4$  mm,  $W = 1.2$  mm,  $W1 = 2.8$  mm.

### III. FABRICATION AND MEASUREMENTS

The designs were fabricated on Rogers RO3010 substrate with a thickness of 1.27 mm, relative permittivity of 10.2 (used in simulations) and loss tangent of 0.002. Measurements were done using the Agilent Network Analyser N5230A. From the simulated and measured responses compared in Fig. 2, it is noticed that both bands of the measured shifted to the left by

approximately 20 MHz, while both return losses are at about 14 dB with insertion loss of about 2.5 dB. The simulated and measured responses in Fig. 4 also showed a frequency shift to the left by approximately 20 MHz with the insertion loss of about 3 dB. The return loss of the low passband is about 22 dB while the high passband is about 25 dB with a transmission zero at 1.99 GHz. After fabricating the circuits using different techniques as well as comparing the performance with several transmission-line type resonators based on the same RO3010 substrate, it has been found that the significant frequency shift is mainly caused by the variation of the dielectric constant from the one (10.2) used in the simulation. Although the value of 10.2 has been found more suitable for microstrip-line filters, for the patch resonators with more E-fields in the Z-direction perpendicular to the patch, the so-called ‘design  $Dk$ ’ of 11.2 seems to represent the material better. Simulations show that a value of 10.8 fits the measurement best as can be seen in Fig. 2 and 4. This is consistent with the anisotropic property of the RO3010 substrate.

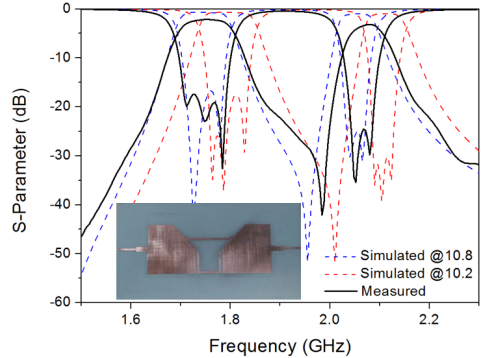


Fig. 4. Simulated and measured responses of the filter in Fig. 3 with the inset showing the fabricated design.

### IV. CONCLUSION

Two dual-band BPFs have been designed to have two coupling paths using the general filter synthesis method. The patch resonators performed the signal splitting and combining for the coupling paths and at the same time added to the resonant poles of each channel. The choice of the dielectric constant in the simulation has been found to have a significant impact on the performance of the filters which contain two different types of resonators – patch and microstrip line.

### REFERENCES

- [1] E. A. Ogbodo, Y. Wang, and K. S. K. Yeo, “Microstrip dual-band bandpass filter using U-shaped resonators,” *Progress In Electromagnetics Research Letters*, Vol. 59, 1-6, 2016.
- [2] L. C. Tsai, and C. W. Hsue, “Dual-band bandpass filters using equal-length coupled serial-shunted lines and Z-transform technique,” *IEEE Trans. Microw. Theory Tech.*, vol. 52, no. 4, pp. 1111-1117, Apr. 2004.
- [3] X. Shang, Y. Wang, G. L. Nicholson and M. J. Lancaster, “Design of multiple-passband filters using coupling matrix optimisation,” *IET Microw. Antennas Propag.*, vol. 6, no. 1, pp. 24-30, January 2012.
- [4] J.-S. Hong, “Microstrip Filters for RF/Microwave Applications,” John Wiley & Sons, Inc., 2011.

Received: 4 February 2017

DOI: 10.1002/mop.30740

# A compact diplexer with a split-ring resonator junction

Eugene A. Ogbodo  | Yun Wu |  
Peter Callaghan | Yi Wang

Department of Engineering Science, University of Greenwich (Medway Campus), Kent ME4 4TB, United Kingdom

## Correspondence

Yi Wang, Department of Engineering Science, University of Greenwich (Medway Campus), Kent ME4 4TB, United Kingdom.  
Email: yi.wang@gre.ac.uk

## Abstract

Diplexers are three-port filtering devices with a junction connecting two channel filters; the common port connects to an antenna which serves the two channel filters bearing the second and the third port. In the design of diplexers, the technique used in connecting the two channel filters is of great importance to the designers. This is because it determines the size, the effectiveness of signal splitting and combining as well as the ease in implementation. In this article, an asynchronously tuned double split-ring resonator (SRR) was used in joining the two channel filters. Without incurring any extra space for the junction, the SRR, being a dual-mode resonator, also functioned as a resonant pole for each channel filter. A diplexer operating at 2 GHz and 3 GHz with 4% fractional bandwidths and 20 dB return loss has been demonstrated. The interactions between the SRR and the channel filters were investigated. Good agreement between the simulated and the measured responses was achieved.

## KEYWORDS

asynchronous coupling, split ring resonator, synchronous coupling

## 1 | INTRODUCTION

Due to increasing demand in the communication system, there is need for robust and efficient devices to meet the traffic needs. A diplexer is one such device. It is conventionally designed by joining two channel filters using transmission line based junctions, hybrid couplers, manifolds, or circulators.<sup>1–5</sup> Recently, resonant junction based techniques were introduced.<sup>6</sup> This resulted in new diplexer topologies<sup>7–9</sup>

and reduction in circuit size.<sup>10,11</sup> A diplexer with a resonant junction tends to be more compact in size because the resonant junction stands as a resonating pole for each channel filter as well as a signal splitter and combiner. The transmission-line based signal-distribution network is no longer required. Such techniques have been reported by Shang et al.<sup>11</sup> where two novel multiplexer topologies based on all-resonator structures were implemented at X-band using waveguide technology. In the work by Zhao and Wu,<sup>12</sup> a diplexer with a resonant star-junction and a triplexer with a non-resonant node star-junction were presented using a synthesis approach. Alejandro et al.<sup>13</sup> presented a diplexer with a split-ring resonator (SRR) as a common resonator and signal splitter. In the work by Chuang and Wu,<sup>14</sup> a diplexer with a T-shaped junction resonator was presented. By extending the technique in the work by Chuang and Wu<sup>14</sup> using open-loop resonators, a multiplexer and switchable diplexer were designed.<sup>15</sup>

This work presents a diplexer that uses an asynchronously tuned SRR as a common resonator to connect two channel filters. The SRR comprises two nested open-loop resonators resonating at two different frequencies corresponding to the two passbands of the diplexer. This differs with the work by Alejandro et al.<sup>13</sup> in that the nested resonators these are synchronously tuned, whereas these are asynchronously tuned in this work resulting in more widely separated channels. The two channels at 2 GHz and 3 GHz each with a 4% fractional bandwidth were separately designed and joined together using the SRR. The SRR contains the first resonator of each channel filter, resulting in reduced circuit size. Very importantly this also removes the need of any separate junction structures either based on transmission lines or resonators. It allowed the SRR to be effectively merged into the channel filters. Figure 1 shows the difference between a conventional diplexer and the proposed diplexer topology.

## 2 | DESIGN

### 2.1 | Split ring resonator

Figure 2 illustrates the proposed diplexer layout and its dimensions. The diplexer consists of one SRR and two sets of open-loop resonators. Each passband was designed to meet the specifications of a fractional bandwidth (FBW) of 4%, and passband return loss of 20 dB. Using the three-pole Chebyshev low-pass prototype derived from the work by Hong and POZAR<sup>16,17</sup> with  $g$  values of  $g_0 = g_4 = 1.0$ ,  $g_1 = g_3 = 0.8516$ , and  $g_2 = 1.1032$ , the coupling coefficient and  $Q$ -factors for the physical dimensioning of the resonators can be obtained using Equations 1 and 2.

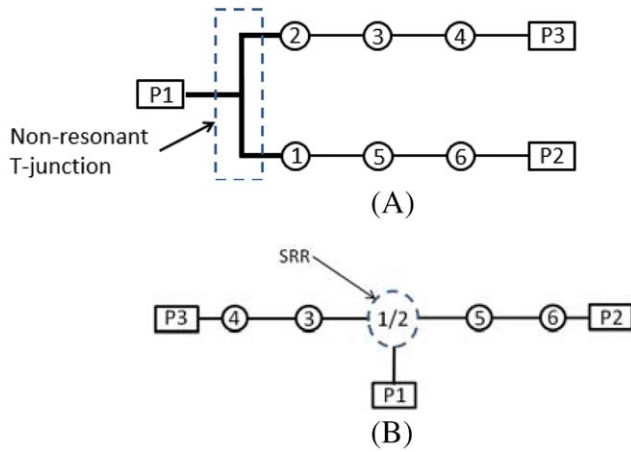


**FIGURE 1** A diplexer with six resonant poles: A, Conventional topology; B, Proposed topology. [Color figure can be viewed at [wileyonlinelibrary.com](http://wileyonlinelibrary.com)]

$$M_{2,3} = M_{3,4} = M_{1,5} = M_{5,6} = \frac{\text{FBW}}{\sqrt{g_{182}}} = 0.041 \quad (1)$$

$$Q_{\text{ex1}} = Q_{\text{ex2}} = Q_{\text{ex3}} = \frac{g_{180}}{\text{FBW}} = 21.29 \quad (2)$$

The two separately designed channel filters were then joined together using the SRR. In order to maintain the three-poles of the channel filters, the SRR acts as the first resonators of the two channel filters. This led to a reduction in the size of the diplexer. According to the diplexer topology of Figure 1B, the channel filters of the high passband are composed of resonators 1, 5, and 6 with resonator 1 being the inner ring of the SRR. Resonators 2, 3, and 4 represent the low passband channel filter with resonator 2 being the outer ring of the SRR. A cross-coupling is also established between resonator 1 of the SRR and resonator 3 and 5 of the two channel filters. This cross-coupling resulted in the introduction of additional transmission zeros in the

diplexer.<sup>13,18</sup> The SRR is made up of two nested open-loop resonators of 2 GHz and 3 GHz which are coupled to each other. As shown in Figure 3A, the SRR produced an inter-band transmission zero, which is a very useful feature in increasing the isolation between the two bands of the diplexer. The difficulty working with this resonator is that only the outer loop can be easily coupled with adjacent resonators or the feed lines.<sup>19</sup> Figure 3B shows the current distributions at the two resonant frequencies.

## 2.2 | Couplings

The required coupling coefficient between the low passband channel filter and the SRR is achieved by adjusting the coupling distance  $d_{2,3}$ . Figure 4A illustrates the coupling coefficient  $M_{2,3}$  as a function of  $d_{2,3}$  with the inset showing a typical response. It should be noted that resonator 1 was present in the simulation to represent its potential loading effect. To couple the channel filter of high passband to the SRR, the change of coupling coefficient  $M_{1,5}$  as a function of  $d_{2,5}$  is investigated when resonator 2 is present, as shown in Figure 4B. It is worth noting that resonator 2 enhanced the coupling between resonators 1 and 5. Without it, the coupling would be very weak.

Figure 5 shows the resonant responses of the four resonators—1, 2, 3, and 5 when coupled together. These achieved peaks of the eigen-modes can also be used in finding the coupling coefficients of  $M_{2,3}$  and  $M_{1,5}$ . Again, it can be observed that the inter-band transmission zero as in Figure 3 is still preserved but at a lower frequency due to the adjacent open loop resonators by the SRR. To determine the  $Q$ -factor for the common port, the coupling arrangement shown in Figure 6 was used. The feed-line at port 1 was tapped to the SRR while the feed-lines at port 2 and port 3 were weakly coupled to the adjacent resonator. The common feed-line

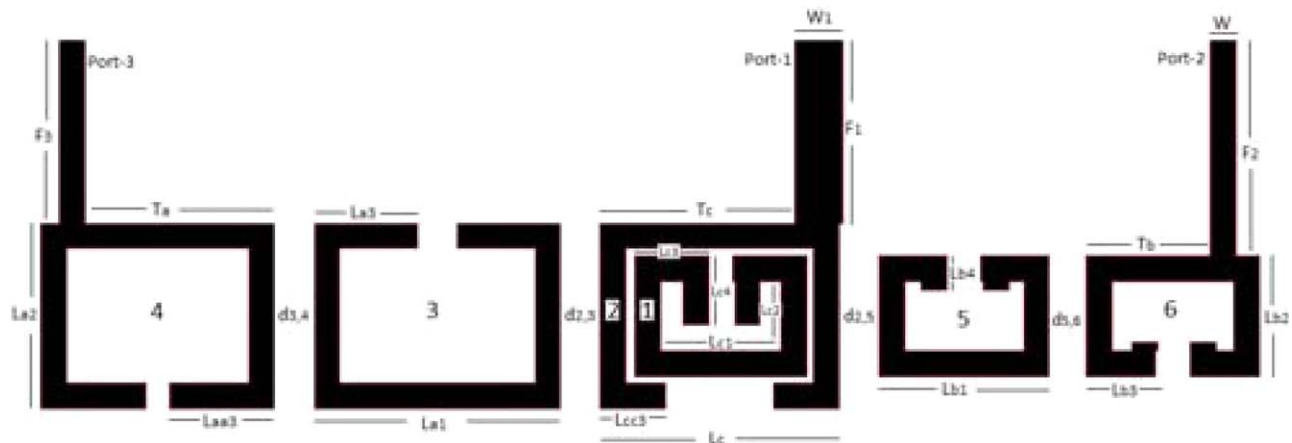


**FIGURE 2** Diplexer layout.  $F_1 = 7.9$  mm,  $F_2 = 9.3$  mm,  $F_3 = 7.9$  mm,  $T_a = 8.1$  mm,  $T_b = 5.3$  mm,  $T_c = 8.3$  mm,  $L_{a1} = 10.2$  mm,  $L_{a2} = 8$  mm,  $L_{a3} = 4.5$  mm,  $L_{aa3} = 4.6$  mm,  $L_{b1} = 7.5$  mm,  $L_{b2} = 5.2$  mm,  $L_{b3} = 3.3$  mm,  $L_{cc3} = 2.9$  mm,  $L_{c1} = 7.6$  mm,  $L_{c2} = 5.2$  mm,  $L_{c3} = 3.3$  mm,  $L_{c4} = 3.1$  mm,  $d_{2,3} = 0.5$  mm,  $d_{3,4} = 0.8$  mm,  $d_{2,5} = 0.7$  mm,  $d_{5,6} = 0.8$  mm,  $W = 1.2$  mm,  $W_1 = 2.1$  mm,  $S = 0.2$  mm. [Color figure can be viewed at [wileyonlinelibrary.com](http://wileyonlinelibrary.com)]

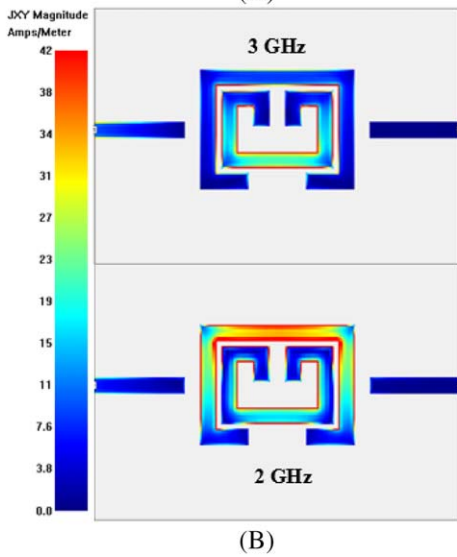
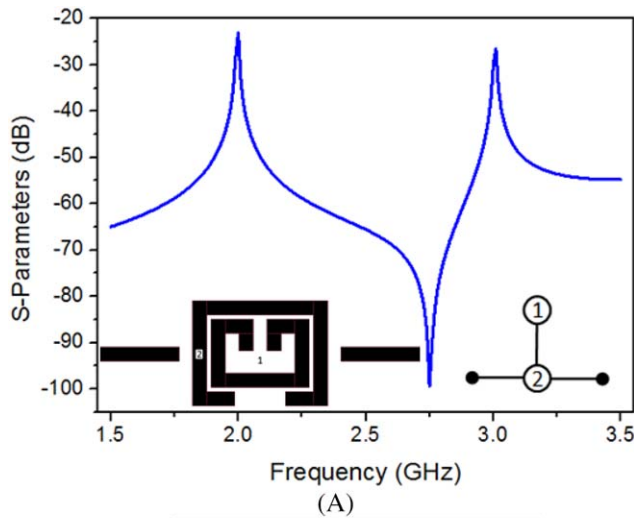


**FIGURE 3** SRR coupling topology: A, Response; B, current distribution. [Color figure can be viewed at wileyonlinelibrary.com]

was adjusted both in position and width to achieve the required external couplings at both 2 and 3 GHz. Equation (3) was used for the calculation of the  $Q$ -factor.

$$Q_{ex} = \frac{f_0}{\Delta f} \quad (3)$$

where  $\Delta f$  is the 3-dB bandwidth from the peak of the resonance curves and  $f_0$  represents the centre frequency of the resonance curves.

### 2.3 | Diplexer design

The diplexer design started by first investigating the behaviors of each channel filter with the SRR. The first resonator of each channel filter was replaced with the SRR and the simulated response observed. Using dashed lines, Figures 7 and 8 present the simulated responses achieved for the 2 GHz and 3 GHz band, respectively. It can be observed that a transmission zero

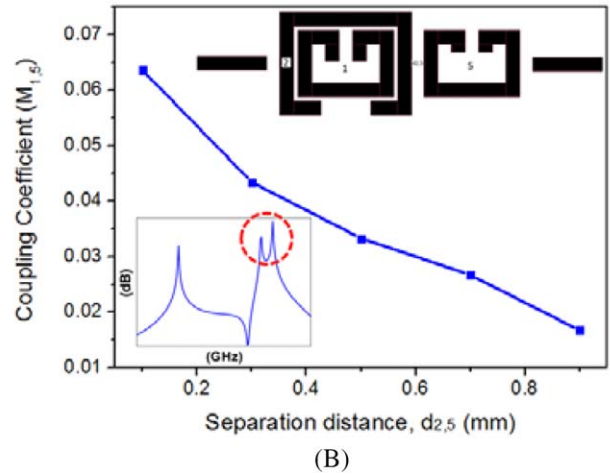
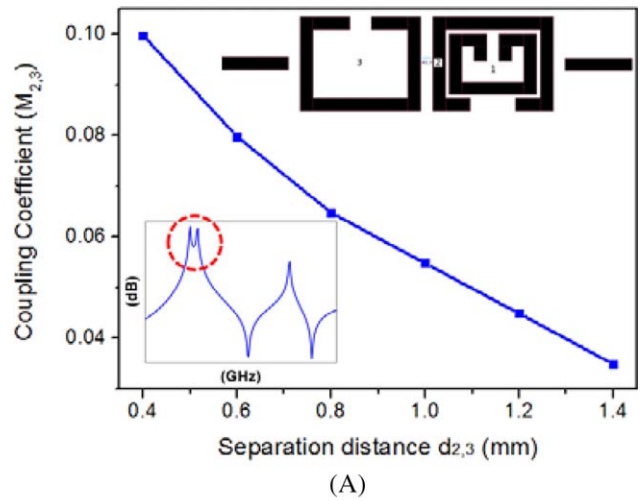


**FIGURE 4** A,  $M_{2,3}$  against  $d_{2,3}$  with the inset of topology and typical response; B,  $M_{1,5}$  against  $d_{2,5}$  with the inset of topology and typical response. [Color figure can be viewed at wileyonlinelibrary.com]

at 2.45 GHz occurs above the lower passband of the filter in Figure 7 whereas a transmission zero at 2.83 GHz occurs below the upper band of the filter in Figure 8.

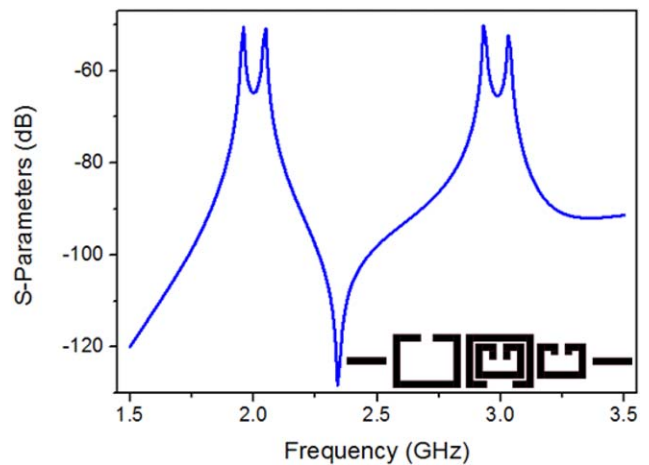


**FIGURE 5** Eigen-mode response and topology. [Color figure can be viewed at wileyonlinelibrary.com]



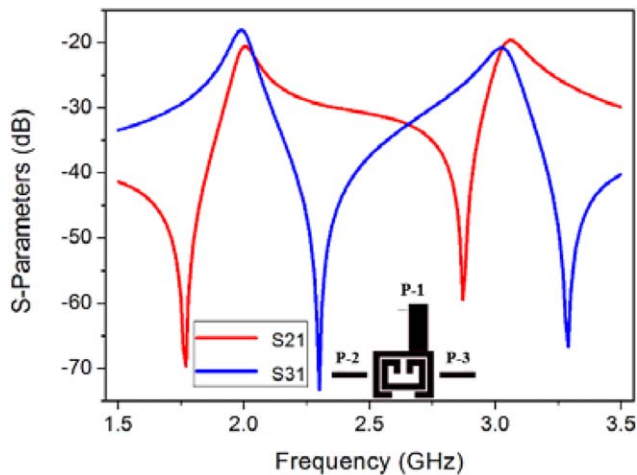


**FIGURE 6** Topology and typical response used to extract external  $Q$ -factors. [Color figure can be viewed at [wileyonlinelibrary.com](http://wileyonlinelibrary.com)]

The two separately designed channel filters were then joined together using the SRR as a common resonator, followed by optimization to meet the design specifications. Figure 9 illustrates the simulated responses in dashed lines. The responses meet the design specifications of 20 dB return loss and FBW of 4%, making the lower passband operate from 1.96 GHz to 2.04 GHz and the higher passband operate from 2.94 GHz to 3.06 GHz. It is also noted that the two transmission zeros observed in the two separate channel filters are preserved within the guard band of the diplexer. Figure 10 shows the simulated current distribution of the two channels during operation at 2 GHz and 3 GHz. It is evident that the SRR operates as a signal splitter and combiner for the two channel filters.

### 3 | FABRICATION AND MEASUREMENT

The individual channel filters and the diplexer were all fabricated on Rogers 3010 substrate with a thickness of 1.27 mm,

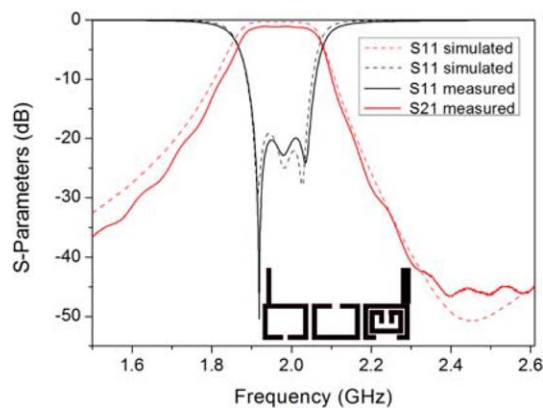


**FIGURE 7** Simulated and measured response of the 2 GHz filter with the SRR. [Color figure can be viewed at [wileyonlinelibrary.com](http://wileyonlinelibrary.com)]

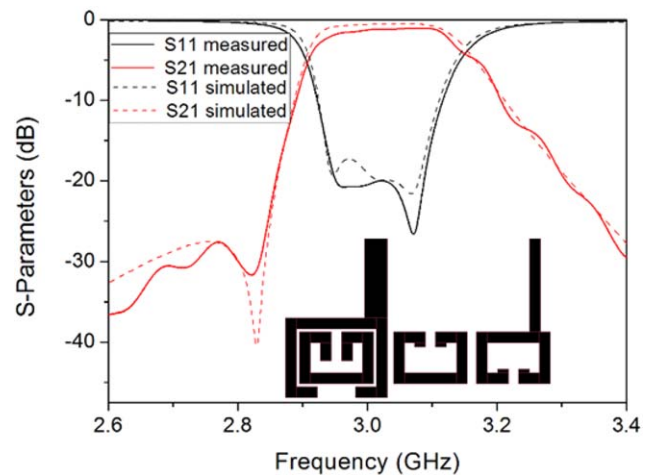


**FIGURE 8** Simulated and measured response of the 3 GHz filter with the SRR. [Color figure can be viewed at [wileyonlinelibrary.com](http://wileyonlinelibrary.com)]

a relative permittivity of 10.2, and loss tangent of 0.002. Prototypes were fabricated using a LPKF ProtoMat S63 micro milling process and then measured using an Agilent Vector Network Analyser model N5230A. Figure 11 shows the fabricated diplexer circuit. The measured responses are displayed in Figures 7–9 (solid lines) for comparison against the simulated responses. It can be seen that measurements and simulations are in good agreement with each other. Figure 7 shows that the measured response slightly shifted up by about 5 MHz, the insertion loss was about 2 dB and the return loss was at 20 dB. Figure 8 shows that the measured response maintained the same bandwidth with the simulated response. The insertion loss is about 2 dB while the return loss is about 20 dB. For the diplexer response shown in Figure 9, the measured response has its low passband frequency shifted to the higher by about 5 MHz, the high passband frequency shifted by about 2 MHz. The return loss is 22 dB and 25 dB for the low and high passband, respectively. The insertion loss is about 2 dB for both passbands. The small

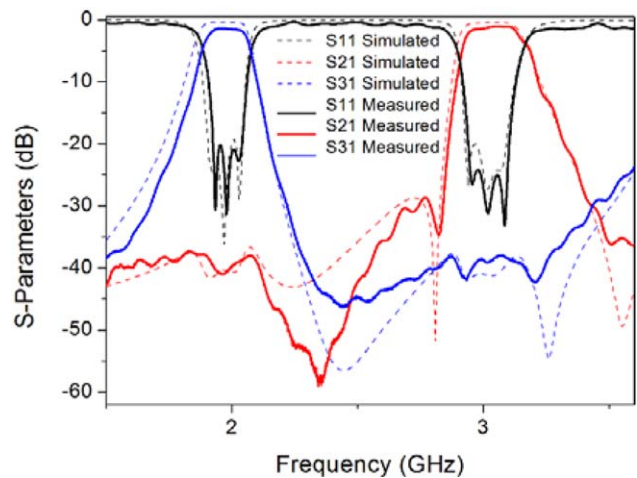


**FIGURE 9** Simulated and measured responses of the diplexer. [Color figure can be viewed at [wileyonlinelibrary.com](http://wileyonlinelibrary.com)]

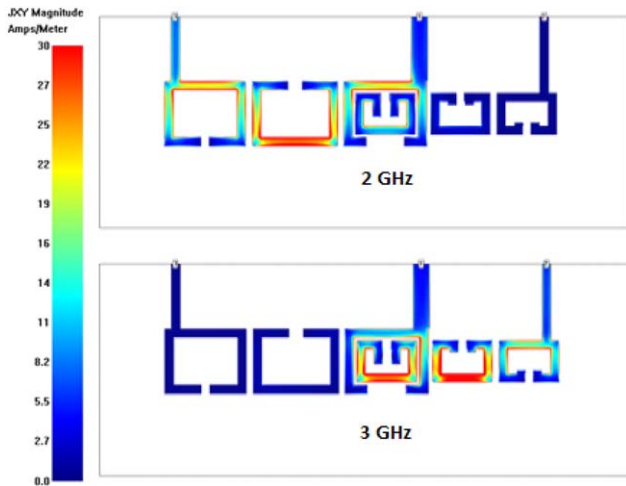


**FIGURE 10** Simulated current distribution of the diplexer at 2 and 3 GHz. [Color figure can be viewed at wileyonlinelibrary.com]

discrepancies were mainly due to fabrication tolerance and the variation of the dielectric constant for the high permittivity dielectric material.

#### 4 | CONCLUSION

In this article, a diplexer with a compact junction structure using a SRR was designed to operate at 2 GHz and 3 GHz passbands. It made use of an asynchronously tuned SRR as its common resonator joining two separately designed channel filters. By using the asynchronously tuned SRR, a diplexer having widely-separated channels was realized. The SRR, being a dual-mode resonator, acted as a signal splitter and combiner for the two channels and at the same time as a resonant pole for each channel. The proposed all-resonator based diplexer achieved three poles for each channel using four single-mode resonators and one dual mode SRR. This resulted in a reduced circuit size as the need for the conventional transmission-line based junction is eliminated.

#### REFERENCES

[1] Cameron R, Yu M. Design of manifold-coupled multiplexers. *IEEE Microwave Mag.* 2007;8(5):46–59.

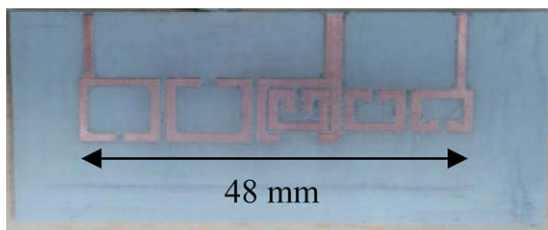


**FIGURE 11** Photo of the fabricated diplexer. [Color figure can be viewed at wileyonlinelibrary.com]

[2] Yang T, Chi P-L, Itoh T. High isolation and compact diplexer using the hybrid resonators. *IEEE Microwave Wireless Compon Lett.* 2010;20(10).

[3] Chen C, Wu H, Wu W. High isolation DBR diplexer using in-line SCMRC. *Prog Electromagn Res C.* 2011;22:97–108.

[4] Skaik TF, Lancaster MJ, Huang F. Synthesis of multiple output coupled resonator circuits using coupling matrix optimisation. *IET Microwaves Antennas Propag.* 2011;5(9):1081–1088.

[5] Bastioli S, Marcaccioli L, Sorrentino R. An original resonant Y-junction for compact waveguide diplexers. In *Proceeding of IEEE MTT-S International Microwave Symposium Digest*; 7–12 June 2009:1233–1236; Boston.

[6] Xia W, Shang X, Lancaster MJ. All-resonator-based waveguide diplexer with cross-couplings. *Electron Lett.* 2014;50(25):1948–1950.

[7] Wang R, Xu J. Synthesis and design of microwave diplexers with a common resonator junction. In: *2012 International Conference on Microwave and Millimeter Wave Technology (ICMMT)*; 2012:1–4; Shenzhen.

[8] Tubail DA, Skaik TF. Synthesis of coupled resonator-based multiplexers with generalised structures using coupling matrix optimisation. *Electron Lett.* 2015;51(23):1891–1893.

[9] Wang Y, Lancaster MJ. An Investigation on the coupling characteristics of a novel multiplexer configuration. In: *2013 European Microwave Conference (EuMC)*; 2013:900–903; Nuremberg.

[10] Ezzeddine H, Bila S, Verdeyme S, Seyfert F, Pacaud D. Coupling topologies for realizing compact microwave diplexers with dual-mode cavities. In: *2010 IEEE MTT-S International Microwave Symposium Digest (MTT)*; 2010:880–883; Anaheim, CA.

[11] Shang X, Wang Y, Wenlin X, Lancaster MJ. Novel multiplexer topologies based on all-resonator structures. *IEEE Trans Microwave Theory Tech.* 2013;61(11):3838–3845.

[12] Zhao P, Wu KL. An iterative and analytical approach to optimal synthesis of a multiplexer with a star-junction. *IEEE Trans Microwave Theory Tech.* 2014;62(12):3362–3369.

[13] Alejandro G-L, Roberto G-G, Magdalena S-P. Compact diplexer with edge-coupled and nonbianisotropic split-ring resonators. In: *2012 IEEE MTT-S International Microwave Symposium Digest (MTT)*; Montreal, Canada, 17–22 June 2012:1–3.

[14] Chuang ML, Wu MT. Microstrip diplexer design using common T-shaped resonator. *IEEE Microwave Wireless Compon Lett.* 2011;21(11):583–585.

[15] Chuang ML, Wu MT. Microstrip Multiplexer and Switchable Diplexer with Joint T-Shaped Resonator. *IEEE Microwave Wireless Compon Lett.* 2014;24(5).

[16] Hong J-S. *Microstrip Filters for RF/Microwave Applications*. Wiley; Hoboken, NJ, 2011.

[17] Pozar DM. *Microwave Engineering*. 3rd ed. New York: Wiley; 2005.

[18] Amari S, Bekheit M, Seyfert F. Notes on bandpass filters whose inter-resonator coupling coefficients are linear functions of frequency. In: *2008 IEEE MTT-S International Microwave Symposium Digest*; 2008:1207–1210; Atlanta, GA, USA.

[19] Lamperez AG, Palma MS. Dual band filter with split-ring resonators. In: *IEEE MTT-S International Microwave Symposium Digest 2006*; 2006:519–522; San Francisco, CA.

**How to cite this article:** Ogbodo EA, Wu Y, Callaghan P, Wang Y. A compact diplexer with a split-ring resonator junction. *Microw Opt Technol Lett.* 2017;59:2385–2390. <https://doi.org/10.1002/mop.30740>

Received: 17 February 2017

DOI: 10.1002/mop.30746

# A simple wideband electromagnetically fed circular polarized antenna for energy harvesting

Ismahayati Adam<sup>1</sup>  |

M. Najib M. Yasin<sup>2</sup> | Ping J. Soh<sup>1</sup> |

K. Kamardin<sup>3</sup> | Mohd Faizal Jamlos<sup>1</sup> |

Herwansyah Lago<sup>1</sup> | Muhamad. S. Razalli<sup>1</sup>

<sup>1</sup>School of Computer and Communication Engineering, Universiti Malaysia Perlis, Perlis 02600, Malaysia

<sup>2</sup>School of Microelectronic Engineering, Universiti Malaysia Perlis, Perlis 02600, Malaysia

<sup>3</sup>Computer Systems Engineering Group, Advanced Informatics School, Universiti Teknologi Malaysia, Kuala Lumpur 54100, Malaysia

## Correspondence

Ismahayati Adam, School of Computer and Communication Engineering, Universiti Malaysia Perlis, 02600 Perlis, Malaysia.

Email: ismahayati@unimap.edu.my

## Abstract

A novel of wideband circular polarization (CP) antenna with high gain that is suitable to harvest energy is proposed. In this article, our objective is to design an antenna that is capable of fully harvesting ambient RF energy. A survey on the feasibility of scavenging for RF energy was conducted through power density measurement in an urban area. Using the results, a CP antenna was designed to cover the frequency band from the largest RF contributors, ranging from 1.73 to 2.61 GHz in GSM1800, UMTS, WiMAX and the unlicensed industrial, scientific, and medical (ISM) bands. Hence, a simple single feed electromagnetic (EM) coupled circularly polarized antenna with high gain is presented. The wideband CP is achieved by implementing EM coupled feed with a defected ground plane structure. Experimental results showed the antenna achieved an axial ratio bandwidth of 25% with respect to

2.08 GHz center frequency. Furthermore, the antenna exhibits broad impedance bandwidth of 32.77% with the measured peak gain is 8.7 dBic at 2.05 GHz. The proposed antenna structure is simple and low cost with a size of  $0.462 \lambda_0$  and wide 22.1% axial ratio bandwidth.

## KEYWORDS

circular polarized antenna, microstrip antenna, RF energy harvesting, wideband

## 1 | INTRODUCTION

One of the important characteristic of antenna to be used in rectifying antenna (rectenna) is the capability to receive high electromagnetic energy. In ambient energy harvesting scenario, the incoming signal may come from multiple frequencies with an unknown angle of incidence. Thus, a rectenna with circular polarized antenna is advantageous as it can supply a nearly constant output direct current (DC) voltage irrespective to the orientation of the antenna.<sup>1–4</sup>

Theoretically, circular polarization (CP) is achieved by simultaneously feeding the radiating and nonradiating edges of patch antenna. However, such technique leads to larger and more complex antennas, as well as feeding losses. On the other hand, CP for a single feed antenna is introduced via perturbations in radiating elements by integrating slots, slits, notches, and loading stubs while adjusting the feed to obtain the appropriate matching.<sup>5–7</sup>

A typical antenna with simple single feed configurations is limited because of narrow AR bandwidth, within the range of 1%.<sup>10,11</sup> Several methods are proposed to alleviate this problem, including utilization of coplanar waveguide (CPW) feed,<sup>8,12–14</sup> additional slots,<sup>14</sup> coupling strip,<sup>15,16</sup> thickening of the substrate,<sup>9</sup> and fractal patches.<sup>17–19</sup>

A CPW-fed square slot antenna is introduced in Ref. [12], where a 17.21% AR bandwidth was successfully obtained at resonance of 2.44 GHz. The combined improvements from a CPW feed with slots, slits, and ground plane as demonstrated in Refs. [8] and [13] managed to enhance the AR bandwidth up to 44.9%. Additionally, the performance of a single probe-feed with U-slot and L-slot microstrip antennas with corner truncations and different substrate thicknesses is investigated in Ref. [9]. A maximum of AR bandwidth of 14% is obtained. Similarly, the deployment of coupled feed with slots as reported in Refs. [16] and [14] achieved an AR bandwidth of about 4.7% and 17.7%, respectively. Fractal structures are able to achieve AR bandwidths of up to 2%, 22.5%, and 0.78%.<sup>17–19</sup>

As wideband antennas in Refs. [8,13,14], and [21] typically require more complex designs, this work aims to



TABLE 4 Figure 7 results

Antenna characteristic	Resonance frequency (GHz)	Frequency range (GHz)	Reflection coefficient (dB)	Fractional bandwidth (%)	Bandwidth (MHz)
Simulated	2.58	2.35–3.1	−34.09	27.52	75
Measured	2.49	2.3–3.03	−19	27.39	74

range starts from 2.35 GHz 3.1 GHz with −34 dB at 2.58 GHz. The second resonance mode also appears but will be suppressed due the interest in 2.45 GHz project frequency. All differences between the values can be assign to SMA weld point and possible imperfections due corrosion process.

The measured bandwidth was not much affected by the problems above. A 74 MHz (27.39%) bandwidth could be achieved, while the simulated result presented a 75 MHz (27.52%) result, which means about 1% error. All results can be seen summarized in Table 4.

## 4 | CONCLUSIONS

The measured results presented a good agreement with the performed simulations and is easy to observe the device applicability and results agreement. The proposed device can be applied at any communication system which operates from 2.3 GHz to 3.03 GHz, including Wi-Fi devices inside ISM band like mobile, radiolocation, amateur services, communication between embedded systems based on Wi-Fi and other.

## ACKNOWLEDGMENT

The authors would like to acknowledge the financial support of Coordination of Improvement of Higher Education Personnel—CAPES and National Counsel of Technological and Scientific Development—CNPq.

## ORCID

Isaac Barros Tavares da Silva  <http://orcid.org/0000-0002-2351-291X>

## REFERENCES

- [1] John JD, Kraus WF, Linden DS, Colombano SP. Evolutionary Optimization of Yagi-Uda Antennas. Proc. of the Fourth International Conference on Evolvable Systems, p. 236–243, 2001.
- [2] Sun Y, Zhang H, Wen G, Wang P. Research Progress in Yagi Antennas. 2012 International Workshop on Information and Electronics Engineering (IWIEE), p. 2116–2121, 2012.
- [3] Yagi H, Uda S. Projector of the sharpest beam of electric waves. *Proc Imperial Acad.* 1926;2:49–52.
- [4] Deschamps GA. Microstrip Microwave Antennas. Third USAF Symposium on Antennas; 1953.

- [5] Qian Y, Deal WR, Kaneda N, Itoh T. Microstrip-fed quasi-Yagi antenna with broadband characteristics. *Electron Lett.* 1998;34(23):2194–2196.
- [6] Qian Y, Deal WR, Kaneda N, Itoh T. A uniplanar Quasi-Yagi antenna with bandwidth and low mutual coupling characteristics. *Antennas Propag Soc Int Symp.* 1999;924–927.
- [7] Peng X, Guangming W, Haipeng L. A Novel Design of Broadband Quasi-Yagi Antenna Loaded with Split-Ring Resonators. 2016 IEEE International Conference on Ubiquitous Wireless Broadband (ICUWB), 2016.
- [8] Liang Z, Liu J, Zhang Y, Long Y. A novel microstrip quasi yagi array antenna with annular sector directors. *IEEE Trans Antennas Propag.* 2015;63(10):4524–4529.
- [9] Pozar DM. *Microwave Engineering.* John Wiley & Sons, Hoboken, NJ; 2012.

**How to cite this article:** da Silva IBT, da Silva SG, da Silva MF, de Andrade HD. Quasi-Yagi microstrip antenna device design for directive wideband ISM application. *Microw Opt Technol Lett.* 2017;59:3042–3046. <https://doi.org/10.1002/mop.30871>

Received: 18 May 2017

DOI: 10.1002/mop.30877

# Asynchronously coupled resonant junctions for diplexers and multiport filtering networks

Eugene A. Ogbodo  |

Yun Wu | Peter Callaghan |

Yi Wang

Department of Engineering Science, University of Greenwich Kent, ME4 4TB, United Kingdom

## Correspondence

Yi Wang, Department of Engineering Science, University of Greenwich Kent, ME4 4TB, United Kingdom.  
Email: Yi.Wang@gre.ac.uk

**Abstract**

This article proposes the use of asynchronously coupled resonator junctions in the design of diplexers. This is to ease the control and implementation of the external couplings at the common port of an all-resonator-based diplexer. A comparison study has been performed between a conventional diplexer and the proposed diplexer. To further explore the possibilities of the proposed junction technique, a four-port multiport filtering networks was proposed and designed to function as a double diplexer. Good agreements have been achieved between the measurements of the prototype devices and the simulations.

**KEYWORDS**

asynchronous coupling, diplexers, multiport filter, resonant junction

**1 | INTRODUCTION**

Diplexers are three-port devices used in the communication systems for transmitting and receiving signals through a shared antenna. A diplexer is made up of two channel filters connected by a junction. In the case of conventional diplexers, the junction is usually formed of transmission lines in the form of T-junction<sup>1</sup> or Y-junction.<sup>2</sup> In addition to these, hybrid couplers,<sup>3</sup> manifolds,<sup>4</sup> or circulators<sup>5</sup> were also used. Recently, a new design approach which utilises resonant junctions was introduced into diplexer designs.<sup>6–8</sup> Circuit miniaturization is achieved when the resonating junction not only serves to split/combine signals but also as a resonant pole contributing to the frequency selectivity. Such techniques were reported in Refs. [8] and [9] using single-mode junction resonators and in Refs. [10–12] using dual-mode junction resonators such as T-shaped resonators,<sup>13</sup> stepped-impedance resonators (SIRs)<sup>14</sup> and patches.<sup>6</sup> The need for the junction resonator to couple in three ways to the

common port as well as to the two channels complicates the implementation. Single-mode junction resonators restrict the overall bandwidth of the signal that is allowed in a diplexer. For dual-mode junctions, the main challenge is the control of the external couplings to the two respective modes from a common port.

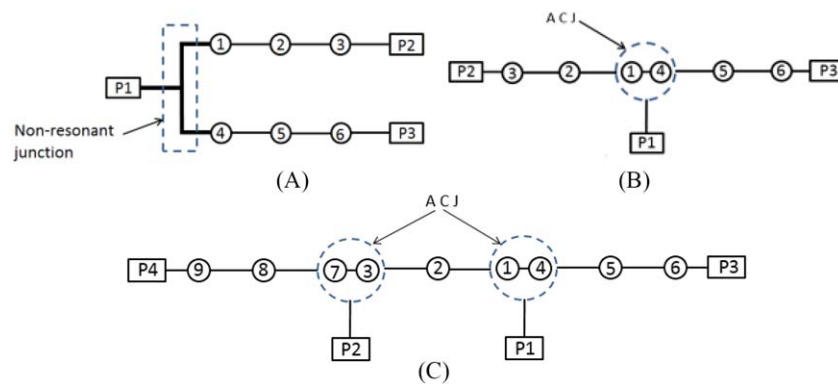
This work is built on from the design concept of resonant junctions but proposes the use of asynchronously coupled resonator junctions to ease the control and implementation of the external couplings at the common port. Two diplexers based on a conventional T-junction and the proposed resonant junction, as illustrated in Figure 1A,B, were first designed and compared. The proposed junction structure was then applied to demonstrate the realization of a four-port filtering network as illustrated in Figure 1C.

**2 | DIPLEXER DESIGN AND COMPARISON**

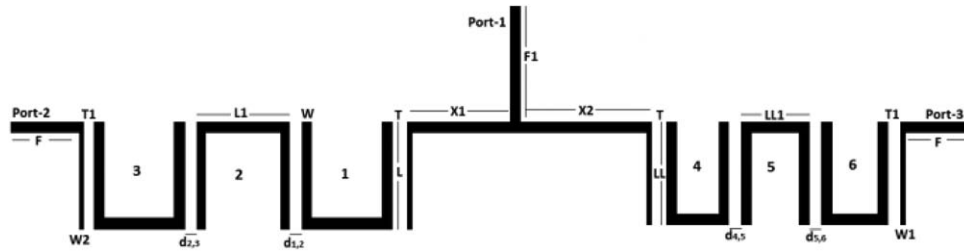
**2.1 | Layouts of diplexers**

Figure 1A demonstrates the topology of a conventional T-junction diplexer. The nonresonant T-junction is designed using  $\lambda/4$  transmission lines. Figure 1B demonstrates the proposed diplexer coupling topology where the dashed circle indicates the asynchronously coupled resonant junction (ACJ). The junction is essentially a pair of asynchronously tuned resonators of different resonating frequencies coupled together. The coupling topologies of Figure 1A,B are translated into their circuit layouts using microstrip technology as presented in Figures 2 and 3, respectively.

The conventional T-junction diplexer in Figure 2 and the proposed asynchronously coupled resonant junction diplexer in Figure 3 are both designed to operate at 1.8 GHz and 2.1 GHz with a 4% fractional bandwidth (FBW), and 20 dB return loss on each channel. Two channel filters operating at 1.8 GHz and 2.1 GHz were first separately designed to specifications using hairpin resonators. To join the channel filters,



**FIGURE 1** Coupling topologies of (A) a conventional diplexer, (B) the proposed diplexer, and (C) a four-port filtering network, where ACJ stands for asynchronously coupled resonator junction. [Color figure can be viewed at wileyonlinelibrary.com]



**FIGURE 2** Layout of the conventional diplexer.  $F = 10$ ,  $F1 = 13.7$ ,  $X1 = 13.8$ ,  $X2 = 17.6$ ,  $T = 0.3$ ,  $T1 = 0.4$ ,  $W = 1.2$ ,  $W1 = 0.6$ ,  $W2 = 0.6$ ,  $L = 11.5$ ,  $L1 = 9.95$ ,  $LL = 11$ ,  $LL1 = 6.59$ ,  $d_{1,2} = 1.77$ ,  $d_{2,3} = 1.77$ ,  $d_{4,5} = 1.75$ ,  $d_{5,6} = 1.75$ . Unit: mm

the T-junction transmission line was used for the conventional diplexer as shown in Figure 2. In the case of the proposed coupled resonant junction diplexer, the first resonators of both channel filters were asynchronously coupled together. A single feed-line from the common port was sequentially coupled to these two resonators through edge coupling. The technique resulted in a compact circuit. More importantly the external couplings from the common port to the two resonators serving the two respective channels can be readily controlled.

## 2.2 | Asynchronous coupling and $Q_{\text{ext}}$

The diplexers in Figure 3 are made up of two filters of  $f_1 = 1.8$  GHz and  $f_2 = 2.1$  GHz with 4% FBW each. These filters are designed to meet the three-pole Chebyshev ripple factor of 0.043 dB with a lowpass prototype derived from Refs [15] and [16] with  $g$ -values of  $g_0 = g_4 = 1.0$ ,  $g_1 = g_3 = 0.8516$ , and  $g_2 = 1.1032$ . The  $g$ -values are used in obtaining the coupling coefficients and external  $Q$ -factors used for the physical dimensioning of the resonators. Using

the general filter synthesis method, the coupling coefficients and external quality factors were derived from (1) and (2).

$$M_{1,2} = M_{2,3} = M_{4,5} = M_{5,6} = \frac{\text{FBW}}{\sqrt{g_1 g_2}} = 0.041 \quad (1)$$

$$Q_{\text{ex1}(L)} = Q_{\text{ex1}(H)} = Q_{\text{ex2}} = Q_{\text{ex3}} = \frac{g_1 g_0}{\text{FBW}} = 21.29 \quad (2)$$

where  $Q_{\text{ex1}(L)}$  and  $Q_{\text{ex1}(H)}$  are the external  $Q$ -factors from the common port to the low and high channel respectively. After individually designing the channel filters to specification, the first resonators of the 1.8 GHz and 2.1 GHz filters were coupled together to define the two channel frequencies as shown in Figure 4.

To achieve the external quality factors ( $Q_{\text{ext}}$ ) from the common port to the asynchronous coupled resonator junction, a coupled feed line was used as shown in Figure 5. Port-2 and port-3 in Figure 5 were weakly coupled to the resonators whereas the coupling gap, width and length of the feed line were adjusted to achieve the required  $Q_{\text{ext}}$  using (3).

$$Q_{\text{ex1}(L)/(H)} = \frac{f_{1(L)/(H)}}{\Delta f_{1(L)/(H)}} \quad (3)$$

where  $f_{1(L)/(H)}$  and  $\Delta f_{1(L)/(H)}$  are the centre frequencies and the 3 dB bandwidths of the resonance curves corresponding to the low and high channel. Figure 5A presents a graph of the

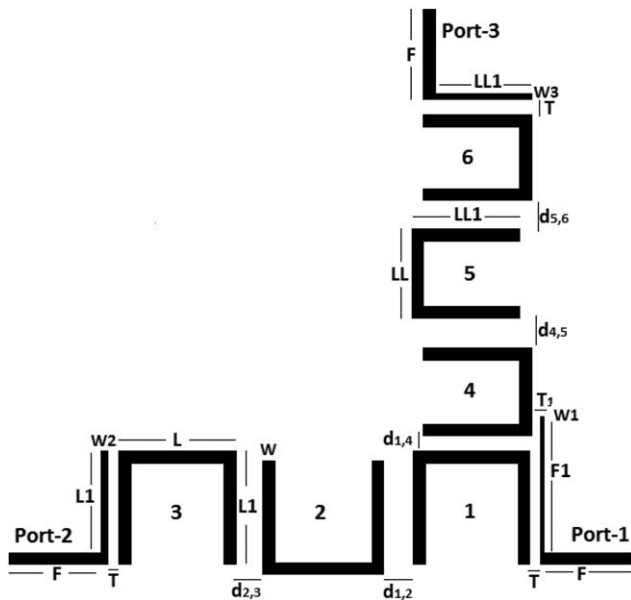


**FIGURE 3** Proposed diplexer.  $F = 10$ ,  $T = 0.4$ ,  $T1 = 0.2$ ,  $W = 1.2$ ,  $W1 = 0.4$ ,  $W2 = 0.6$ ,  $W3 = 0.6$ ,  $L = 9.6$ ,  $L1 = 11.5$ ,  $LL = 6.6$ ,  $LL1 = 11$ ,  $d_{1,2} = 1.7$ ,  $d_{1,4} = 0.2$ ,  $d_{2,3} = 1.7$ ,  $d_{4,5} = 1.65$ ,  $d_{5,6} = 1.7$ . Unit: mm

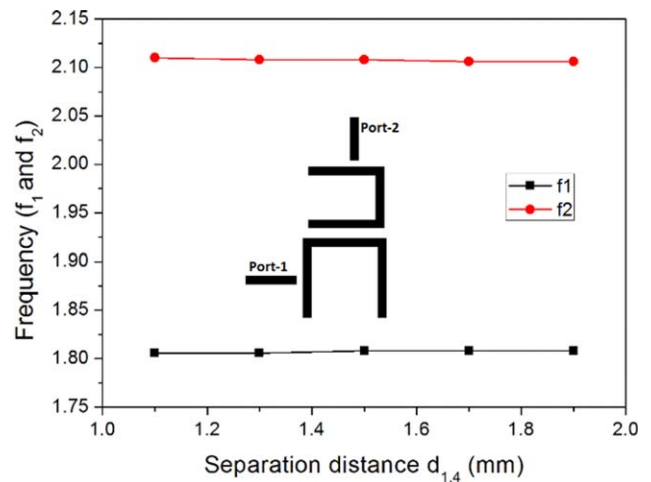


**FIGURE 4** Asynchronous coupling between resonator 1 and 4. [Color figure can be viewed at [wileyonlinelibrary.com](http://wileyonlinelibrary.com)]

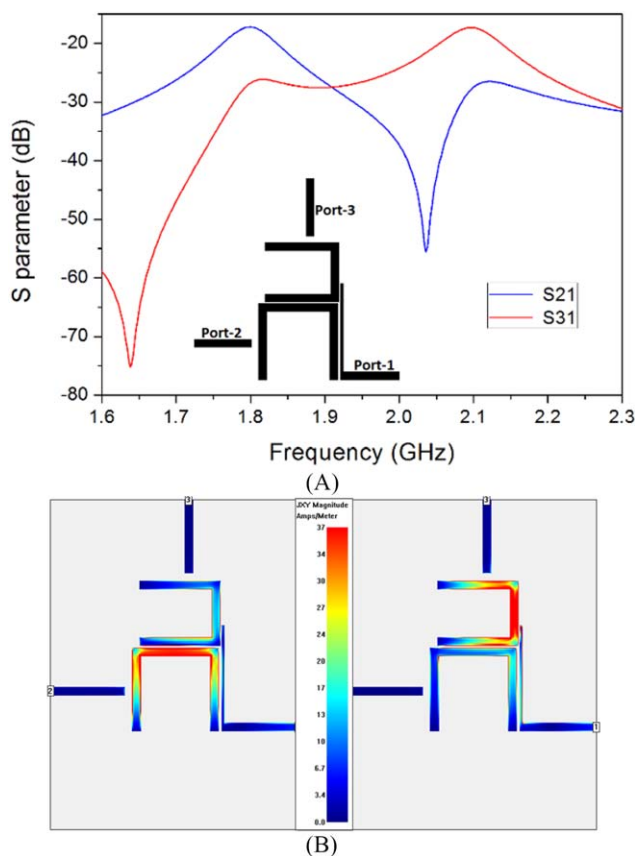


**FIGURE 5** (A) Simulated responses of the configuration used to extract  $Q_{ext}$ ; (B) Simulated current distribution at 1.8 GHz (left) and 2.1 GHz (right). [Color figure can be viewed at wileyonlinelibrary.com]

typical responses. Figure 5B shows the simulated current distribution at the resonator junction at 1.8 GHz and 2.1 GHz. It is evident that the ACJ acts as a signal splitter.

### 2.3 | Performance comparison

The EM software Sonnet is used for the simulation. Figures 2 and 3 present the achieved physical dimensions after

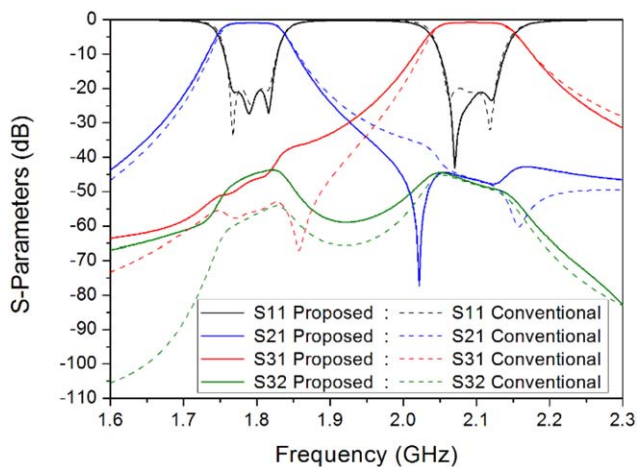


**FIGURE 6** Simulated responses of the proposed and the conventional diplexers. [Color figure can be viewed at wileyonlinelibrary.com]

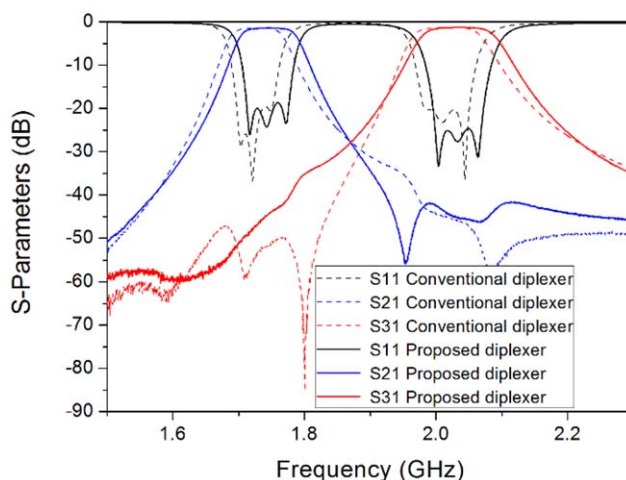


**FIGURE 7** Measured responses of the proposed and the conventional diplexer. [Color figure can be viewed at wileyonlinelibrary.com]

optimization. Figure 6 compares the achieved simulated responses of the proposed diplexer (solid lines) with the conventional T-junction diplexer (dash lines). While the two diplexers achieved similar rejection in the high band, the resonator junction provided less rejection in the low band. This is expected due to the lack of isolation between the two coupled resonators which is one shortcoming of resonant junctions. Rogers 3010 substrates with a thickness of 1.27 mm, a relative permittivity of 10.8 and a loss tangent of 0.0022 were used. Measurements were taken using Agilent Network Analyser N5230A. The measured responses of the two diplexers are presented in Figure 7. Good agreement between the simulations and measurements has been achieved.

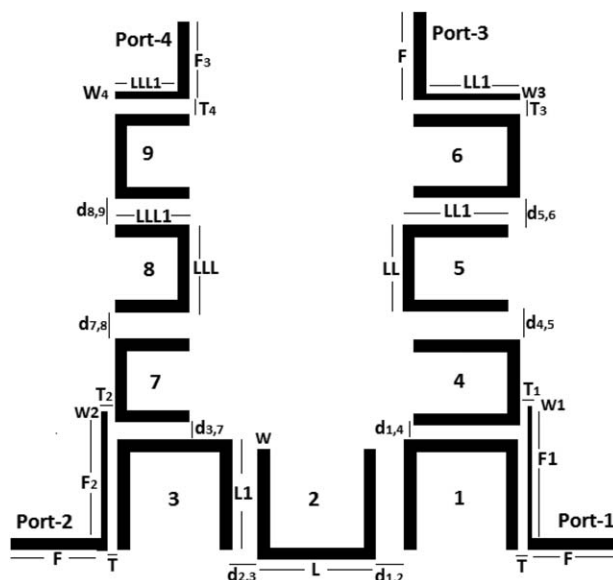


**FIGURE 8** Layout of the proposed double diplexer.  $F = 10$ ,  $F_1 = 15$ ,  $F_2 = 15$ ,  $T = 0.4$ ,  $T_1 = 0.2$ ,  $T_2 = 0.38$ ,  $W = 1.2$ ,  $W_1 = 0.4$ ,  $W_2 = 0.6$ ,  $W_3 = 0.6$ ,  $L = 9.6$ ,  $L_1 = 11.5$ ,  $LL = 6.6$ ,  $LL_1 = 11$ ,  $d_{1,2} = 1.46$ ,  $d_{1,4} = 0.2$ ,  $d_{2,3} = 1.48$ ,  $d_{3,7} = 0.22$ ,  $d_{4,5} = 1.65$ ,  $d_{5,6} = 1.7$ ,  $d_{7,8} = 1.84$ ,  $d_{8,9} = 1.82$ . Unit: mm



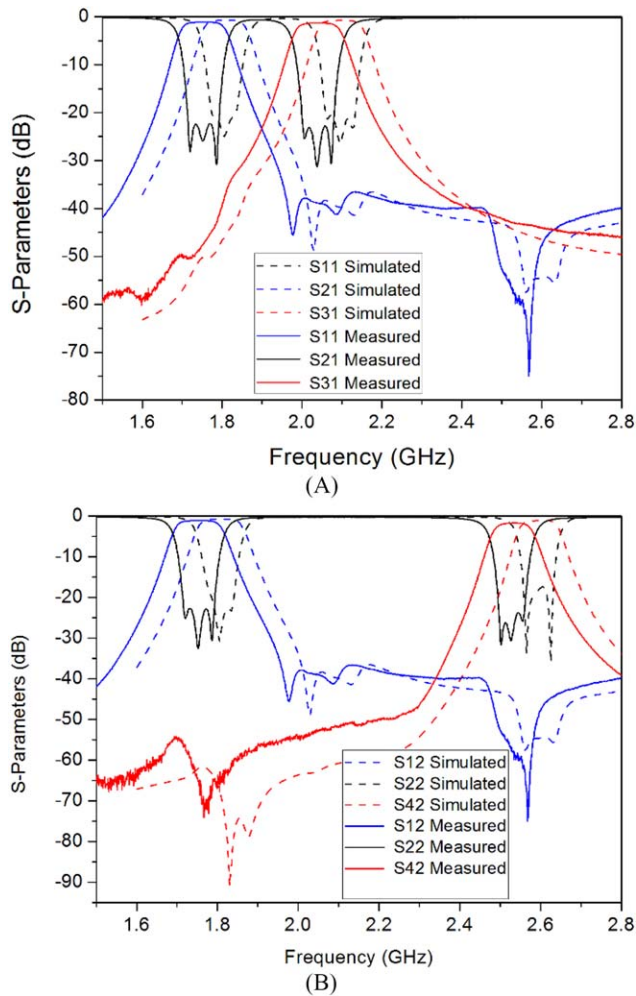


**FIGURE 9** Simulated and measured duplexing responses of the design in Figure 8 when (A) port-1 is the common port and (B) port-2 is the common port. [Color figure can be viewed at [wileyonlinelibrary.com](http://wileyonlinelibrary.com)]

### 3 | FOUR-PORT FILTERING NETWORK

To further explore the potentials of the coupled resonator junctions, a four-port filtering network in the form of two back-to-back diplexers is designed as illustrated in Figure 1C. It is not targeting any specific application at this stage but to demonstrate the capability of realizing multipoint coupled-resonator networks. From the coupling topology, the network contains two asynchronous coupled resonator junctions, three filters (three bands) and four ports. Figure 8 presents the design layout where resonators 1 and 4 as well as resonators 3 and 7 represent the asynchronous coupled resonator junctions. The resonators 1–3 forms the channel of 1.8 GHz, resonators 4–6 and resonators 7–9 forms the channels of 2.1 GHz and 2.6 GHz, respectively.

The design in Figure 8 is built on from the diplexer in Figure 3 by adding on a 2.6 GHz filter using another asynchronous coupled resonator junction. That is resonator 7

coupled to resonator 3. The coupling topology of this circuit offers this design an opportunity to function as switchable diplexers or even multi-input and multi-output filtering networks. Figure 9 presents two possible choices of selected diplexer channels. Figure 9A shows the frequency duplexing at 1.8 GHz and 2.1 GHz when the common port is port-1. Figure 9B shows the duplexing of 1.8 GHz and 2.6 GHz when the common port is port-2. All the return losses are below 20 dB. Measurements and simulations show reasonably good agreement except for the frequency shift of 10 MHz. This is believed to be due to the thinning of the substrate from milling as well as the tolerance of the dielectric constant of this high permittivity anisotropic substrate material. Figure 10 presents the isolation response between port-1 and port-4, port-2 and port-3 as well as port-3 and port-4. The solid lines represent the measured responses while the dashed lines represent the simulated responses.

### 4 | CONCLUSIONS

In this work, asynchronously coupled resonant junctions are proposed and investigated for applications in resonator-based diplexers and multipoint filtering networks. The proposed resonant junction structure succeeded in easing the implementation of external couplings at the common ports as compared with previous reported single-mode or dual-mode junctions. The comparison between a conventional T-junction diplexer and the proposed resonant junction diplexer has concluded a more compact structure of the proposed diplexer but at the cost of channel rejection. Better isolation between the asynchronously coupled resonators is desired at the junction. It is also worth mentioning that the asynchronous coupled resonator junction technique can be used in designing diplexers or multiplexers with both narrowly or widely separated

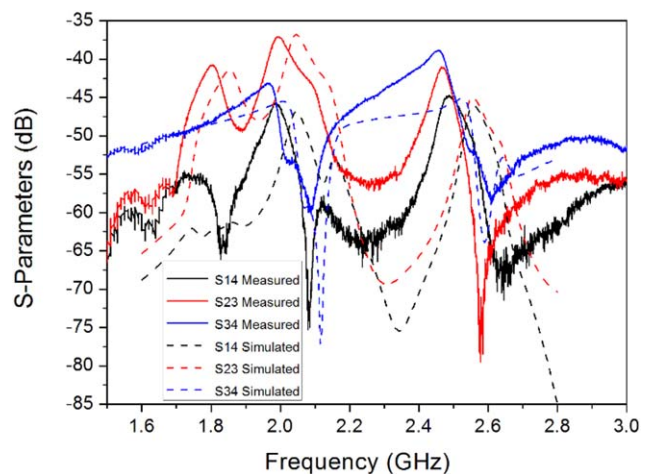


**FIGURE 10** Simulated and measured isolation responses of  $S_{14}$ ,  $S_{23}$ , and  $S_{34}$  of the design in Figure 8. [Color figure can be viewed at [wileyonlinelibrary.com](http://wileyonlinelibrary.com)]

channels. To further demonstrate the capability of the coupled junction, a four-port filtering network in the form of a double diplexer was presented. Depending on the choice of the common port, different duplexing schemes can be realized. Although this four-port device is not currently conceived for any specific application, the underlining concept of a generic multiport resonator network could be explored for circuit functions such as switchable diplexers or multi-input and multi-output filtering networks.

## ORCID

Eugene A. Ogbodo  <http://orcid.org/0000-0002-9798-723X>

## REFERENCES

- [1] Yang T, Chi PL, Itoh T. High isolation and compact diplexer using the hybrid resonators. *IEEE Microw Wirel Compon Lett.* 2010;20(10):551–553.
- [2] Wu KL, Meng W. A direct synthesis approach for microwave filters with a complex load and its application to direct diplexer design. *IEEE Trans Microwave Theory Tech.* 2007;55(5):1010–1017.
- [3] Cheng YL, Chen HW, Huang PD, Chang CY. A W-band quadrature hybrid coupled substrate integrated waveguide diplexer. In: 2015 Asia-Pacific Microwave Conference (APMC), Nanjing; 2015:1–3.
- [4] Skaik T, Lancaster M. Coupled resonator diplexer without external junctions. *J Electromagn Anal Appl.* 2011;3(6):238–241.
- [5] Saavedra CE. Diplexer using a circulator and interchangeable filters. In: 2008 7th International Caribbean Conference on Devices, Circuits and Systems, Cancun; 2008:1–5.
- [6] Ogbodo EA, Wu Y, Wang Y. Microstrip diplexers with dual-mode patch resonant junctions. In: 2016 46th European Microwave Conference (EuMC), London, United Kingdom; 2016: 1155–1158.
- [7] Guan X, et al. A novel microstrip diplexer with a common square ring resonator for WCDMA. In: 2016 IEEE International Workshop on Electromagnetics: applications and Student Innovation Competition (iWEM), Nanjing, China; 2016:1–3.
- [8] Wu Y, Wang Y, Ogbodo EA. Microstrip wideband diplexer with narrow guard band based on all-resonator structures. In: 2016 46th European Microwave Conference (EuMC), London, United Kingdom; 2016:1163–1166.
- [9] Macchiarella G. Synthesis of star-junction multiplexers. *IEEE Microwave Mag.* 2011;12(6):101–109.
- [10] Skaik TF, Tubail DA. Novel multiplexer topologies based on coupled resonator structures. In: 2015 IEEE 15th Mediterranean Microwave Symposium (MMS), Lecce; 2015:1–4.
- [11] Shang X, Wang Y, Wenlin X, Lancaster MJ. Novel multiplexer topologies based on all-resonator structures. *IEEE Trans Microwave Theory Tech.* 2013;61(11):3838–3845.
- [12] Chuang ML, Wu MT. Microstrip diplexer design using common T-shaped resonator. *IEEE Microwave Wirel Compon Lett.* 2011;21(11):583–585.
- [13] Guan X, Yang F, Liu H, Zhu L. Compact and high-isolation diplexer using dual-mode stub-loaded resonators. *IEEE Microwave Wirel Compon Lett.* 2014;24(6):385–387.
- [14] Chen CF, Huang TY, Chou CP, Wu RB. Microstrip diplexers with common resonator sections for compact size, but high isolation. *IEEE Trans Microwave Theory Tech.* 2006;54(5).
- [15] Hong J-S. *Microstrip Filters for RF/Microwave Applications.* Wiley, Hoboken, NJ; 2011.
- [16] Pozar DM. *Microwave Engineering.* 3rd ed. Wiley, New York, NY; 2005.

**How to cite this article:** Ogbodo EA, Wu Y, Callaghan P, Wang Y. Asynchronously coupled resonant junctions for diplexers and multiport filtering networks. *Microw Opt Technol Lett.* 2017;59:3046–3051. <https://doi.org/10.1002/mop.30877>

Received: 7 July 2017

DOI: 10.1002/mop.30870

# Cross-range target response analysis for extreme high-squint synthetic aperture radar

Matthew J. Burfeindt 

Air Force Research Laboratory, 306 W. Eglin Blvd., Bldg 432, Eglin AFB, Florida 32542

## Correspondence

Air Force Research Laboratory, 306 W. Eglin Blvd., Bldg 432, Eglin AFB, FL 32542.

Email: matthew.burfeindt.1@us.af.mil

## Abstract

We propose a formulation for predicting the cross-range characteristics of the synthetic aperture radar (SAR) point-spread function (PSF) for extremely high squints based on the concept of phased array factors. We demonstrate the validity of this approach by comparing theoretical predictions to PSF dimensions extracted from SAR images. The results show that the proposed approach is more robust than the conventional theory for extreme high-squint scenarios.

## KEYWORDS

phased arrays, synthetic aperture radar